Mechanism of action of GoSlo-SR-5-6 on $K_V7.4$ channels

A thesis submitted to the
School of Health & Science,
Dundalk Institute of Technology

For the degree of **Doctor of Philosophy**

By

Kaneez E Rabab M.Sc.

October 2021

Under the supervision of **Prof. Mark Hollywood** &
Co-supervision of **Prof. Gerard Sergeant**

Smooth Muscle Research Centre,
Dundalk Institute of Technology

Declaration

We, the undersigned declare that this thesis entitled "Mechanism of action of GoSlo-SR-5-6 on $K_v7.4$ channels" is entirely the author's own work and has not been taken from the work of others, except as cited and acknowledged within the text.

The thesis has been prepared according to the regulations of Dundalk Institute of Technology and has not been submitted in whole or in part for an award in this or any other institution.

Author Name: Kaneez E Rabab

Author Signature: K. Rabab

Date: 28th March 2022

Supervisor Name: Prof. Mark Hollywood

Supervisor Signature: Mark Hollywood

Date: 28th March 2022

Table of Contents

List of Figures

Figures Page No.

Chapter 1:

Chapter 2:

Chapter 3:

Chapter 4:

Chapter 5:

List of Tables

Tables Page No.

Acknowledgements

First of all, I would like to thank and express my sincere gratitude to my supervisor, Prof. Mark Hollywood. His support, guidance and encouragement have been invaluable throughout this study. I truly appreciate his time, patience and motivation which made this journey a smooth and enriching experience for me. His enthusiasm and overall insights had been inspiring as a young researcher. I would also like to thank Prof. Keith Thornbury and Prof. Gerard Sergeant for their valuable suggestions and encouragement during the running of this project. It was a great privilege and honour to work and study under their supervision.

I would like to say thank you to Billie McIlveen for her technical help and support, Roddy, Eamonn & Niki for always being very encouraging and helpful seniors in the lab. I would like to thank Srikanth for being a good friend and big support in the lab. I also would like to say a special thank you to all the past and present students in SMRC for truly making my time in the lab a very joyous and fruitful one.

This DCU-DkIT graduate programme was funded by the European Union (EU) Interreg funding for Borders and REgions in Airway Training Hub (BREATH). Thank you for providing me with the financial support for completing my research studies. I am also very grateful to the DkIT research office for its contributions.

I would also like to express my sincere gratitude and appreciation to Dr. Tushar Vaidya who instilled in me confidence as a researcher. I would be forever grateful for his guidance and encouragement at the beginning of my research journey and for continuing to be my mentor for life. My heartfelt thanks to all my friends and colleagues in CCMB for being so very supportive in my initial days as a researcher.

I dedicate this thesis to my very supportive and loving family Nanna, Mummy, Pappa, Aapu, Sofu baji, Ali bhai, Alvia, Syeda and Layla. Your unconditional love, understanding, prayers and continued support have got me through the good and tough times in this journey. I cannot thank enough for all your blessings and support. I am very blessed to have found Gianni as my partner in this journey who has supported me immensely and continue to be my strength. You are my family and I look forward to having a wonderful life ahead with you. I am also very thankful to all my friends and my extended family members whose support was invaluable and kept me going through this PhD.

Glossary

A	Alanine
(A)	Membrane surface area
Å	Angstrom
ANOVA	Analysis of variance
Aa	Amino acid
AC	Adenyl cyclase
AKAP	A-kinase anchoring protein
Arg	Arginine
Arnt	Aryl hydrocarbon receptor nuclear translocator protein
ASM	Airway smooth muscle
ASMC	Airway smooth muscle cell
ATP	Adenosine triphosphate
BK	Big potassium
BFNS	Benign familial neonatal seizures
βAR	β adrenoreceptor
bp	Basepair
C	Cysteine
(C)	Capacitance
Ca^{2+}	Calcium ion
cDNA	Complementary DNA
Cl^{-}	Chloride ion
CaM	Calmodulin
CaMBDs	Calmodulin binding domains
CTD	Cytoplasmic tail domain
C-ter	C-terminus
C-terminus	Carboxy terminus
CIP	Calf-intestinal phosphatase
CiVSP	Ciona intestinalis voltage sensor containing phosphatase
COPD	Chronic obstructive pulmonary disease
Cryo-EM	Electron cryomicroscopy
CHO	Chinese hamster ovary
CNS	Central nervous system
cADPR	Cyclic ADP ribose

cAMP	Cyclic adenosine monophosphate
COX	Cyclooxygenase enzymes
C_m	Membrane capacitance
(d)	membrane thickness
D	Aspartic acid
DAG	Diacylglycerol
DFNA2	Autosomal dominant type2 deafness
DHA	Docosahexaenoic acid
DNA	Deoxyribonucleic acid
diC8-PIP_2	Dioctanoyl PIP_2
ddH_2O	Double distilled water
dNTP	Deoxynucleoside triphosphate
dsDNA	double stranded DNA
dt^{sz}	Paroxysmal dystonic
DMEM	Dulbecco's Modified Eagle's medium
E	Glutamic acid
E.coli	Escherichia Coli
EC_{50}	Half maximal effective concentration
EDTA	Ethylenediaminetetraacetic acid
EGF	Epidermal growth factor
ECG	Electrocardiogram
F	Phenylalanine
FAF	Familial atrial fibrillation
FBS	Fetal bovine serum
G	Glycine
Gly	Glycine
(G)	Conductance
G-V	Conductance - Voltage
GPCR	G-protein coupled receptor
GFP	Green fluorescent protein
G_{max}	Maximal conductance
G/G_{max}	Normalized conductance
G_0	Gibb’s free energy of activation
$G_{-100\ mV}$	Conductane at -100 mV
GΩ	Gigaohm
H	Histidine
Hz	Hertz

HEK	Human embryonic kidney
hERG	Human ether-à-go-go-related genes
H^+	Hydrogen ion
I	Isoleucine
(I)	Current
IP_3	Inositol triphosphate
IHC	Inner hair cells
IK	Intermediate potassium
I-V	Current-Voltage
I_c	Capacitive current
I_{KM}	M-current
$I_{K,n}$	Non-inactivating current
I_{KS}	Cardiac slow activated potassium current
$I_{K,L}$	Large voltage gated K^+ current
IC_{50}	Half maximal inhibitory concentration
K	Lysine
K^+	Potassium ion
K_v	Voltage activated potassium
kb	Kilo basepair
kDa	Kilodaltons
kHz	Kilohertz
L	Leucine
Leu	Leucine
LB	Luria-Bertani
LQT	Long QT syndrome
Lys	Lysine
M	Methionine
Mg^{2+}	Magnesium ion
MLC	Myosin light chain
ml	Millilitre
mm	Millimeter
mM	Millimolar
ms	Millisecond
mV	Millivolt
MΩ	Megaohm
mAChR	Muscarinic acetylcholine receptor
mRNA	Messenger RNA

MDCK	Madin darby canine kidney cells
MEM	Minimum Essential Medium Eagle
MLCP	Myosin light chain phosphatase
MLCK	Myosin light chain kinase
mins	Minutes
MinK	Minimal K^+ channel
MiRP	MinK related protein
μ	Micro
μl	Microlitre
μm	Micrometer
μM	Micromolar
n	Number of experiments
N	Asparagine
nA	Nanoamperes
Na^+	Sodium ion
Na_v	Voltage-gated sodium channels
NH_4^+	Ammonium ion
ng	Nanogram
ns	Not significant
nM	Nanomolar
N_{ter}	N-terminal
N-terminus	Amino terminus
NEM	N-ethylmaleimide
NEB	New England Biolabs
OD	Optical density
OHC	Outer hair cells
P	Proline
pA	Picoamperes
Per	Period circadian protein
pEC_{50}	Absolute EC_{50}
pg	Picogram
P_o	Open probability
pS	Picosiemens
PIP_2	Phosphatidylinositol-(4,5)-bisphosphate
PD	Pore domain
PDE	Phosphodiester

PDB	Protein Data Bank
PKA	Protein kinase A
PKC	Protein kinase C
PL	Pore loop
PLA	Proximity ligation assay
PLC	Phospholipase C
PNK	Polynucleotide kinase
pH	Potential of hydrogen
PCR	Polymerase chain reaction
PUFA	Polyunsaturated fatty acids
Q	Glutamine
(Q)	Electric charge
Q_c	Charge under the capacitive transient
R	Arginine
(R)	Resistance
R_p	Pipette resistance
R_a	Access resistance
R_m	Membrane resistance
R_s	Series resistance
rpm	Revolutions per minute
RC	Resting closed state
RO	Resting open state
ROCK	Rho associated protein kinase
ROCC	Receptor-operated calcium channel
RT-PCR	Reverse transcriptase PCR
RyR	Ryanodine receptor
s	seconds
S	Serine
SAR	Structure-activity relationship
SCG	Superior cervical ganglion
SDM	Site directed mutagenesis
SEM	Standard error of the mean
SMP	Single-minded protein
SOC	Super optimal broth with catabolite repression
SOCC	Store-operated calcium channels
SQTS	Shot QT syndrome

SR	Sarcoplamsic reticulum
Src	non-receptor tyrosine kinases
ssDNA	Single stranded DNA
T	Threonine
τ	Time constant
τ_{act} (τ_a)	Time constant of activation
τ_{act_fast} (τ_{a_fast})	Fast component of activation
τ_{act_slow} (τ_{a_slow})	Slow component of activation
τ_{deact} (τ_d)	Time constant of deactivation
TM	Transmembrane
TA	Tannic acid
TEA	Tetraethylammonium
TRP	Transient receptor potential
V	Valine
(V)	Voltage
VSCC	Voltage sensitive calcium channels
VSD	Voltage sensor domain
VSP	Voltage sensor containing phsphatase
V_{com}	Command potential
V_m	Membrane voltage
V_p	Pipette potential
$V_{1/2}$	Half maximal activation voltage
VSP	Voltage sensitive phosphatase
W	Tryptophan
WT	Wildtype
Y	Tyrosine
ZnPy	Zinc pyrithione
$[Ca^{2+}]_i$	Intracellular calcium concentration
$[PIP_2]$	PIP_2 concentration
- F	Forward primer
- R	Reverse primer
º	Degree
ε_r	Dielectric constant
Ω	Ohm
%	Percentage
ºC	Celsius degrees

α	Alpha
β	Beta
Δ	Delta
$\Delta V_{1/2}$	Change in half maximal activation voltage
ΔV_m	Change in voltage
γ	Gamma

Abstract

Mechanism of action of GoSlo-SR-5-6 on $K_v7.4$ channels

Voltage-gated K^+ channels (K_v7) play important roles in a range of physiological functions such as sensory transduction, smooth muscle contraction, epithelial secretion and neuronal excitability (Soldovieri *et al.,* 2011). In the airway smooth muscle cells (ASMC), $K_v7.4$ and $K_v7.5$ are predominantly expressed and play an important role in the regulation of airway diameter and activators of K_v7 channels have been shown to induce relaxation of ASMC (Brueggemann *et al.,* 2018). In the lab previously, a family of compounds called the GoSlo-SR were developed (Roy *et al.,* 2012; Roy *et al.,* 2014). Among these, GoSlo-SR-5-6 (SR-5-6), was established as a potent and efficacious activator of $K_v7.1$, $K_v7.4$ and $K_v7.5$ channels and was less effective on $K_v7.2$ and $K_v7.3$. In $K_v7.4$ channels, SR-5-6 increased the G/G_{max} to ~1.6 and shifted the $V_{1/2}$ by ~-50 mV (Zavaritskaya *et al.,* 2020).

Phosphatidylinositol-(4,5)-bisphosphate (PIP_2) is a small membrane lipid known to be critical for K_v7 channel function (Gamper & Shapiro, 2007). PIP_2 is known to increase G_{max}, slow deactivation and negatively shift the $V_{1/2}$ and therefore has very similar effects to SR-5-6 on $K_v7.4$ channels. Given that PIP_2 could mimic the effects of SR-5-6, potential PIP_2 binding residues were mutated and the effect of each mutant was examined in the absence and presence of SR-5-6. Consequently, in this thesis, the data presented is aimed at:

1) Identifying potential residues in $K_v7.4$, important for the effect of SR-5-6 and assessing the state-dependent effect of SR-5-6 on $K_v7.4$ channels.
2) Assessing the effect of SR-5-6 on drug-sensitive $K_v7.4$ channels domain swapped with drug insensitive $K_v7.3$.
3) Examining the role of PIP_2 modulation and PIP_2 binding residues on SR-5-6 mediated activation of $K_v7.4$ channels.

The first results chapter investigated the role of drug binding residues of known activators, to look for potential binding sites for SR-5-6 in $K_v7.4$ channels. Although the effect of SR-5-6 was not abolished in any of the mutants studied in this chapter, a mutant (L249A) was found, which practically abolished the negative shift in activation $V_{1/2}$ of $K_v7.4$ channels. Although this mutant abolished

the effect of SR-5-6 on $\Delta V_{1/2}$, it failed to reduce its effect on G/G_{max}. In the later part of this chapter, the state-dependent activity of SR-5-6 on $K_v7.4$ channels was investigated. The findings suggested that the effects of this drug appeared to be greater than WT $K_v7.4$ when the VSDs were locked in the resting state (E136R). Also, with the partially activated state mutant (E136R/R207E), the channels were open at exceptionally negative potentials, but SR-5-6 could still enhance G/G_{max}. Overall, the results suggested that the effects of SR-5-6 were not state-dependent.

In the subsequent chapter, a chimeric approach was utilized between $K_v7.3$ and $K_v7.4$ channels and examined the effects of swapping each main domain of the $K_v7.3$ channel onto a $K_v7.4$ background. The rationale was based on the earlier demonstration by Dudem (2019) that $K_v7.3$ channels were substantially less sensitive to 10 μM SR-5-6 ($\Delta V_{1/2}$ ~-16 mV; G/G_{max} ~1) than $K_v7.4$ channels. However, when the S3-S4 linker, S4 domain, the S4-S5 linker, S5 domain, S6 domain, C-terminus, voltage-sensing domain (S1-S4), pore domain (S5-PL-S6) were swapped and mutated non-conserved residues between $K_v7.3$ and $K_v7.4$, none of these swap constructs or mutant channels mitigated the effects of SR-5-6. These data indicated that this approach was not effective at identifying a binding site for SR-5-6 in this channel.

The final results chapter examined whether interfering with PIP_2 altered the effects of SR-5-6. When PIP_2 was depleted using the voltage-sensitive phosphatase CiVSP, a clear reduction was observed in the effectiveness of SR-5-6 to shift $\Delta V_{1/2}$ and the change in G/G_{max} was significantly reduced. Similarly, when wortmannin was used to inhibit the replenishment of membrane PIP_2, it abolished the effect of SR-5-6 on G/G_{max}. These results demonstrated that PIP_2 may play an important role in mediating the effects of SR-5-6, particularly on G/G_{max}. Given the results of the above experiments, it was therefore surprising that the effects of SR-5-6 were not blocked when a number of PIP_2 binding mutant channels were studied. Furthermore, a number of these mutations in $K_v7.4$ channels did not result in loss-of-current mutations as reported in other K_v7 channels, which was surprising. This suggested that $K_v7.4$ may either have different PIP_2 binding residues or alternatively, more than one mutation was needed to reduce the binding PIP_2 in $K_v7.4$ channels.

Publications:

1) Zavaritskaya, O., Dudem, S., Ma, D., Rabab, K., Albrecht, S., Tsvetkov, D., Kassmann, M., Thornbury, K., Mladenov, M., Kammermeier, C., Sergeant, G., Mullins, N., Wouappi, O., Wurm, H., Kannt, A., Gollasch, M., Hollywood, M. and Schubert, R. (2020). Vasodilation of rat skeletal muscle arteries by the novel BK channel opener GoSlo is mediated by the simultaneous activation of BK and K_v7 channels. *British Journal of Pharmacology*, 177(5), pp.1164-1186.

Abstracts related to this thesis were communicated in different national and international scientific meetings:

1) K Rabab, S Dudem, IG Tikhonova, KD Thornbury, GP Sergeant and MA Hollywood. GoSlo-SR-5-6 activates K_v7 channels and its effects are reduced by a F322A mutant in $K_v7.4$. International K_v7 channels Symposium 2019, 12th - 14th September 2019.

2) K Rabab, S Dudem, SL Martin, IG Tikhonova, KD Thornbury, GP Sergeant and MA Hollywood. Assessing the state-dependent effects of SR-5-6 on $K_v7.4$ channels expressed in HEK cells. Irish Thoracic Society Annual Scientific Meeting 2018, 23rd and 24th November 2018.

3) K Rabab, KD Thornbury, GP Sergeant and MA Hollywood. Assessing the state-dependent effects of SR-5-6 on $K_v7.4$ channels expressed in HEK cells. BREATH Annual conference 2018. 19th and 20th June 2018.

4) K Rabab, KD Thornbury, GP Sergeant and MA Hollywood. Tracking down the binding site for GoSlo-SR-5-6 in $K_v7.4$ channels using $K_v7.4/7.3$ chimeras. BREATH Annual conferences 2019, 19th to 21st June 2019.

5) K Rabab, KD Thornbury, GP Sergeant and MA Hollywood. Utilizing chimeras and mutations to ascertain the binding site of GoSlo-SR-5-6 in

$K_v7.4$ channels. BREATH Annual conference 2020 - virtual, 15th to 17th June 2020.

6) K Rabab, KD Thornbury, GP Sergeant and MA Hollywood. Examining the role of PIP_2 modulation and PIP_2 binding residues for their effects on SR-5-6 mediated activation of $K_v7.4$ channels. BREATH Annual conference 2021 - virtual, 21st to 23rd June 2021.

Chapter 1

Literature Review

1.1 Introduction

The work presented in this thesis was made possible by the European Union (EU) Interreg funding for **B**orders and **RE**gions in **A**irway **T**raining **H**ub (BREATH) in the quest to better understand chronic obstructive pulmonary disease (COPD) and develop therapies for COPD patients. The focus of this thesis was to determine the molecular determinants involved in activation of K_v7 channels by GoSlo-SR-5-6 (SR-5-6).

1.2 Chronic Obstructive Pulmonary Disease (COPD)

COPD is one of the leading causes of morbidity and mortality in patients with lung diseases and is characterized by irregular function of the lung. The symptoms of COPD are persistent coughing, coupled to severe production of sputum and frequent breathlessness in response to exertion (Woolcock *et al.,* 1991). The pathology of COPD involves both the airways and the parenchyma of the lung and unfortunately, COPD patients respond poorly to bronchodilator or corticosteroid treatment (Woolcock *et al.,* 1991). The airway hyperresponsiveness observed in COPD is also associated with a reduced calibre of the airways, unlike that seen in asthma patients where the airway diameter was not significantly different when compared to healthy individuals (Scichilone *et al.,* 2006). Numerous COPD studies have examined the role of airway smooth muscle (ASM) in the pathology of the disease (Yan *et al.,* 2018; James & Wenzel, 2007) and found that irregular ASM function plays a major role in COPD pathogenesis. In 1968, Hogg *et al.,* in their breakthrough study showed that the density of smooth muscle tissue in the small airway increased significantly in patients with severe obstruction in airflow.

1.2.1 Role of Airway Smooth Muscle Cells (ASMCs) in COPD

The ASM lining the walls of the airways is critical for airway function and structure. In patients suffering from COPD, there is an increase in the density of ASMCs, which negatively impacts lung function (Hogg *et al.,* 2004). The most important pathology of COPD is airflow limitation which is progressive, irreversible and is mainly caused by a combination of airway remodelling, loss of small airways and emphysema (Chen *et al.,* 2014). The main factors responsible for reducing airflow are airway remodelling, inflammation (Hogg *et al.,* 2004) and smooth muscle

hypercontractility. Airway smooth muscle cells (ASMCs) not only contribute to the contractile function but also play a role in production of inflammatory factors, proteases and growth factors in lungs (Howarth *et al.,* 2004). When the contractile function and density of ASMCs is impaired it results in airway inflammation, hyperresponsiveness and remodelling (Hirota & Martin, 2013) which are the key characteristic features of lungs in COPD patients.

The contractile function of ASMCs is regulated by various mechanisms including the G-protein coupled receptor pathways (Billington & Penn, 2003), nonselective cation channels (Gosling *et al.,* 2005) and store-operated calcium channels (Ay *et al.,* 2004) (Figure 1.1). The ion channels that reside in the ASMC plasma membrane include voltage gated channels, receptor and store-dependent channels, stretch activated channels and Ca^{2+}-dependent K^+ channels, which all may play a crucial role in dysregulation of ASMC tone in COPD (Perez-Zoghbi *et al.,* 2009).

My thesis is focused on K_v7 channels and how they may be targeted pharmacologically. Given that these channels can modulate Ca^{2+} signalling in ASMC, the following sections will examine how Ca^{2+} signalling contributes to ASMC contraction and how K_v7 channels can modulate these cells.

1.2.2 Role of Ca^{2+} signalling in Airway Smooth Muscle Cell contraction

As shown in Figure 1.1, the mechanism of smooth muscle contraction is now well established and is governed by a variety of regulatory pathways. Important mechanisms include G_q and G_s-protein coupled receptor (GPCR) based pathways, nonselective cation channels especially transient receptor potential (TRP) channels (Gosling *et al.,* 2005) and store-operated calcium channels (SOCC).

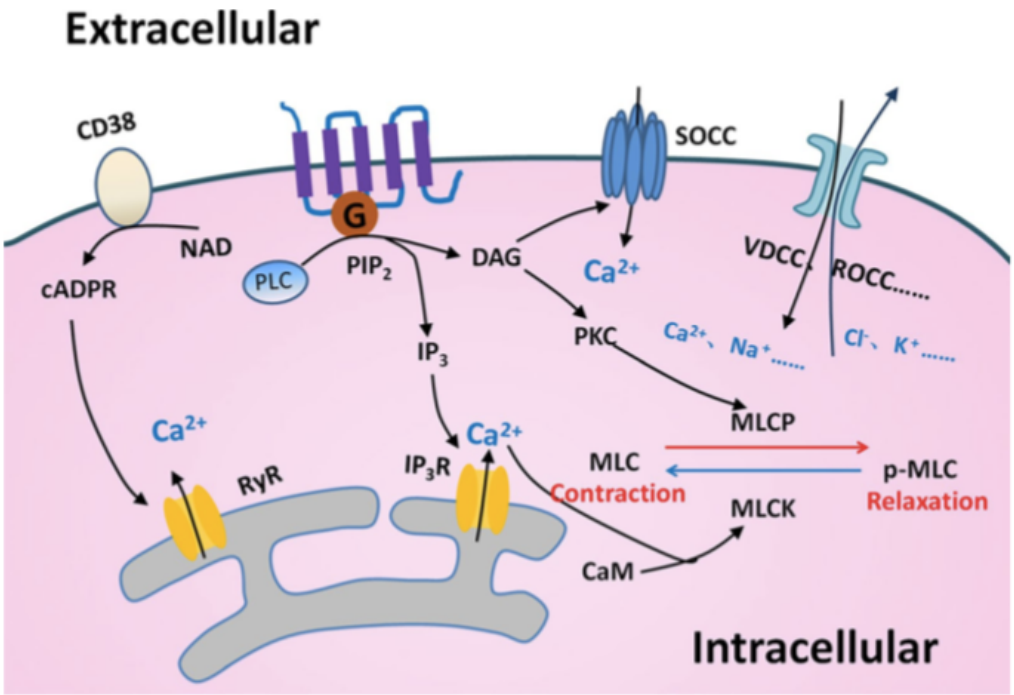

Figure 1.1: Mechanism of contraction of ASMC. *Different regulatory mechanisms in ASMC to control contraction and relaxation are indicated in the figure above. The G-coupled receptor activates phospholipase C (PLC) and converts phosphatidyl inositol 2 (PIP_2) into inositol triphosphate (IP_3) and diacylglycerol (DAG). The intracellular Ca^{2+} binds to calmodulin (CaM) to alter phosphorylation status of myosin light chain (MLC) and regulates ASMC function. They are other mechanisms that regulate the intracellular ion concentration and in turn the contractility of ASMCs (Adapted from Yan et al., 2018).*

The GPCR-based pathway activates phospholipase C (PLC) which converts phosphatidyl diphosphate inositol 2 (PIP_2) into inositol triphosphate (IP_3) and diacylglycerol (DAG). IP_3 binds to IP_3 receptors to cause the release of Ca^{2+} from the intracellular stores, called the sarcoplasmic reticulum (SR). Intracellular Ca^{2+} thus binds to the intracellular calmodulin (CaM) which alters the phosphorylation status of myosin light chain (MLC) and regulates the ASMC function (Billington & Penn, 2003). Also, CD38 ectoenzyme, which produces the second messenger cyclic ADP ribose (cADPR), causes Ca^{2+} release through ryanodine receptor (RyR) channels on the SR (Zhang & Li, 2006).

In ASMCs, increased cytosolic Ca^{2+} concentration ($[Ca^{2+}]_i$) results in airway contraction (Sanderson *et al.,* 2008). Thus, bronchoconstrictor agonists such as carbachol, histamine and endothelin activate $G_{q/11}$ - coupled receptors leading to increased levels of $[Ca^{2+}]_i$, which in turn elevates MLCK activity and/or decreases the MLCP activity (Horowitz *et al.,* 1996; Somlyo & Somlyo, 1994; Somlyo & Somlyo, 1998; Somlyo *et al.,* 1999; Somlyo & Somlyo, 2000; Penn & Benovic,

2008). The initial transient increase in the $[Ca^{2+}]_i$ results from the release of Ca^{2+} from the intracellular calcium stores. This transient increase in intracellular Ca^{2+} levels can be sustained by the influx of Ca^{2+} through Ca^{2+} channels in the plasma membrane. The sustained levels of Ca^{2+} play an important role in maintaining the contractile state in the ASMCs. As shown in Figure 1.1, various ion channels present on the plasma membrane are known to contribute to this and play a crucial role in maintaining the intracellular $[Ca^{2+}]$ levels during contraction of ASMCs.

The two main routes of Ca^{2+} entry are via voltage-dependent and voltage-independent calcium pathways (Hirota *et al.,* 2007). The voltage-independent increase in the cytosolic calcium is via store operated calcium channels (SOCCs), receptor-operated calcium channels (ROCCs) and/or non-selective cation channels such as TRP channels. The voltage-dependent increase of calcium is through voltage sensitive calcium channels (VSCCs). These two proposed mechanisms in ASMCs are similar to those observed in other smooth muscle cells (Perez-Zoghbi *et al.,* 2009).

There are two main types of voltage-dependent Ca^{2+} channels, called L and T channels, in smooth muscle and they can be distinguished on the basis of their electrophysiological and pharmacological properties. The 'low' voltage L-type channels open in response to membrane depolarization and the threshold for their activation in ASMC ranges from -45 mV to -25 mV, with maximal activation seen around 0 to +20 mV. These L-type VSCCs are blocked by dihydropyridine based compounds (Hirota *et al.,* 2007) which block L-type calcium channels. However, the resting membrane potential of ASMCs is around -60 mV to -45 mV (Liu & Xu, 2005), which suggests that at rest, the ASMC L-type VSCC would remain closed. Clearly then, the ASMC would need a depolarizing current to bring the membrane potential into the range where L-type VSCC could be activated. The currents responsible for this depolarization have been widely debated and various studies have implicated either low voltage T-type channels or TRP channels (Janssen, 1997; Yamakage *et al.,* 2001; Beech *et al.,* 2004; Dietrich *et al.,* 2006; Perez-Zoghbi *et al.,* 2009). The low voltage T-type currents were first identified at depolarizing potentials of -60 or -80 mV in bronchial smooth muscle (Janssen, 1997). They were noted to activate at -60 mV with maximal activation at ~-20 mV. This current was also blocked by nifedipine, although it was less

sensitive than L-type currents (Janssen, 1997). Sizable (~200 pA) T-type currents were also identified in porcine bronchial smooth muscle cells (Yamakage *et al.,* 2001). Thus, in addition to L-type Ca^{2+} currents, the T-type Ca^{2+} currents also played a central role in bronchial smooth muscle contraction and refilling of internal Ca^{2+} (Janssen, 1997).

However, given that K_v7 channels are activated at resting membrane potential, they could, if switched off, provide the depolarizing drive to bring the ASMC membrane potential into the range where L-type VSCC could be activated. Since these K_v7 channels have been shown to play an important role in ASMC contractility, the remainder of this review will focus on their potential contribution to ASMC contractility.

1.2.3 Role of K_v7 channels in ASMCs contractility

K_v7 channels are a family of plasmalemmal proteins which play a key role in maintaining the membrane potential in excitable cells. They are encoded by five genes, *KCNQ*1-5 which translate to the respective $K_v7.1$-$K_v7.5$ membrane proteins (a more detailed description of each subtype is described in Section 1.3). The K_v7 channels are known to activate at quite negative potentials (~-60 mV), which not only helps restore the resting membrane potential in cells following depolarization, but can act as a brake to prevent depolarization. These channels are expressed in a variety of tissues as illustrated in Figure 1.2.

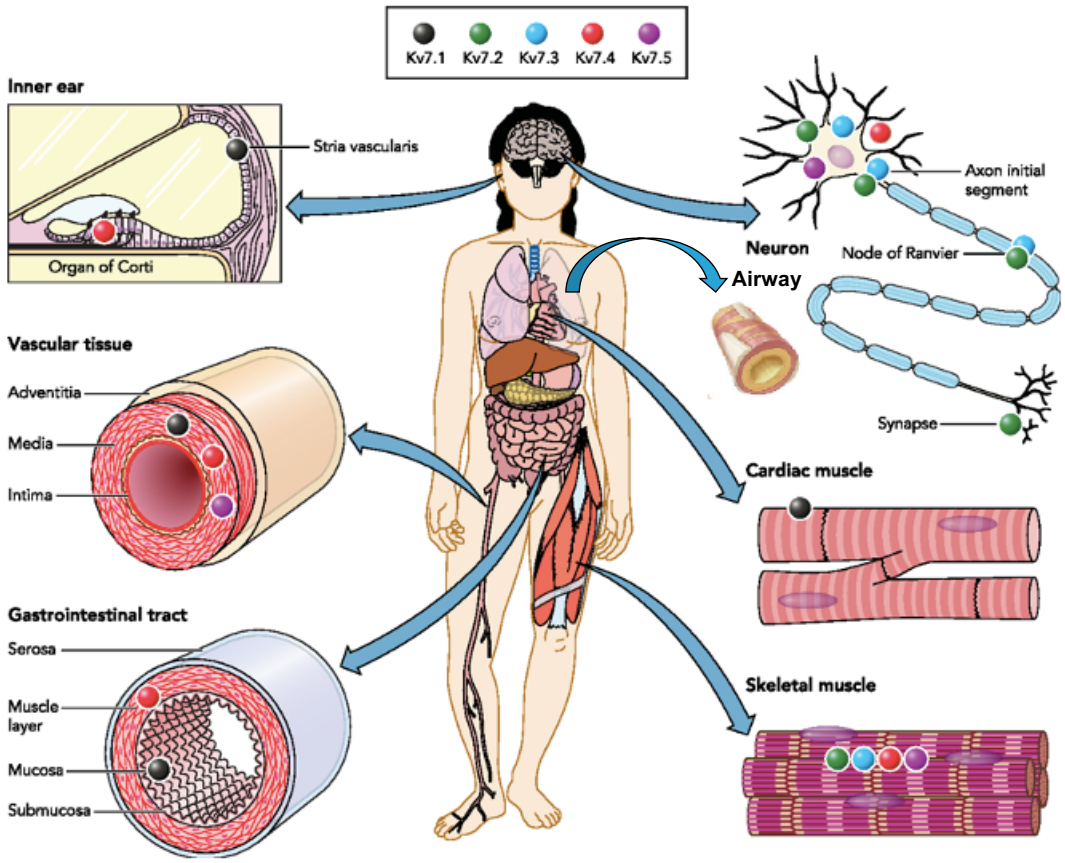

Figure 1.2: Distribution of K_v7 subtypes in tissues. *The different panels in the figure demonstrate some of the sites of expression of the K_v7 subtypes in a human body. In addition to those indicated, K_v7 expression has been detected also in epithelial cells from various other tissues like kidney, lung, pancreas, thymus, liver, adrenal glands and testis (Adapted from Soldovieri et al., 2011).*

Their roles were initially studied in heart, central nervous system (CNS) and auditory pathways (Jentsch, 2000; Robbins, 2001; Jespersen *et al.,* 2005), vascular system (Ohya *et al.,* 2003; Yeung *et al.,* 2007; Mackie *et al.,* 2008), uterine smooth muscle cells (McCallum *et al.,* 2009) and pulmonary epithelial cells (Greenwood *et al.,* 2009).

Many studies have emphasized how K_v7 channels can regulate the contractions of smooth muscle cells including ASMC. Brueggemann *et al.,* (2012) have shown the expression and function of K_v7 channels in ASMCs, where they found them responsible for keeping the internal $[Ca^{2+}]_i$ low in airway myocytes. They identified that, under resting, unstimulated conditions, ASMC K_v7 channel activity was essential to maintain the airways in a relaxed state. In addition, they found that the K_v7 currents were suppressed by $G_{q/11}$-coupled bronchoconstrictor agonists

and these effects could be reversed by activators of K_v7 channels (Brueggemann *et al.,* 2012). The expression pattern in ASMCs resembles that of vascular smooth muscle cells, where $K_v7.1$, $K_v7.4$ and $K_v7.5$ are significantly expressed, with little or no expression of $K_v7.2$ and $K_v7.3$ (Haick & Byron, 2016; Stott *et al.,* 2014). When electrophysiological experiments were carried out on fresh human tracheal myocytes, K_v7 currents were present and these were significantly enhanced by retigabine, a potent activator of $K_v7.2$-$K_v7.5$ (Tatulian *et al.,* 2001: Wickenden *et al.,* 2001). This was also observed in cultured ASM human cells (Brueggemann *et al.,* 2018) and was consistent with the idea that the K_v7 current expressed in ASMCs was due to the contribution of $K_v7.4$ and $K_v7.5$ channels rather than $K_v7.1$ channel (Brueggemann *et al.,* 2018).

In ASMC, relaxation of the constricted airways occurred through various pathways which also involve K_v7 channels. Activation of K_v7 channels can increase the outward potassium current, resulting in hyperpolarization of the membrane and a concomitant reduction in influx of Ca^{2+} into the cell by switching off L-type VSCCs (Byron *et al.,* 2014). Such a mechanism has been demonstrated in another study by Mani *et al.,* (2016), which showed that enhancement of $K_v7.5$ currents by the β adrenoceptor $\beta AR/G_s/cAMP/PKA$ pathway was due to phosphorylation of $K_v7.5$ channel subunits by PKA (Mani *et al.,* 2016). Several other studies reported various mechanisms through which K_v7 channels contributed to relaxation of ASMCs and these are summarized in Figure 1.3 below.

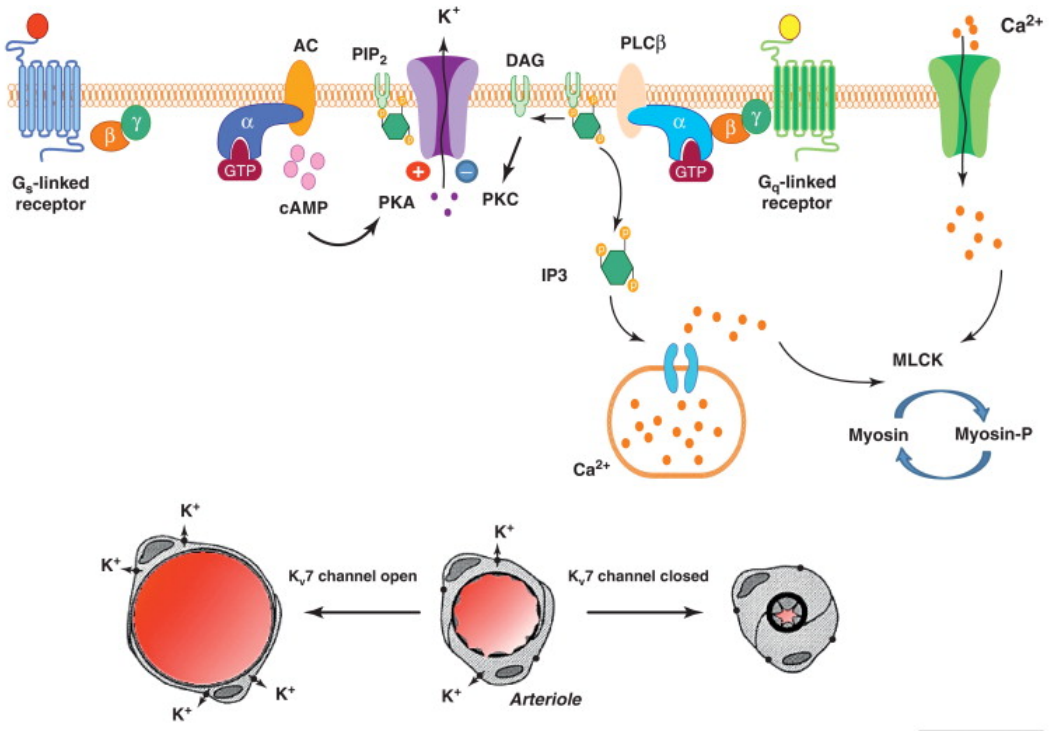

Figure 1.3: Endogenous signalling pathways coupling to voltage-gated potassium (K_v7) channels. *Endogenous signalling pathways activated via G_s- and G_q- coupled receptor signalling can regulate K_v7 channel activity. Increased activation of K_v7 channels results in relaxation and vasodilation whereas decreased activity results in contraction and vasoconstriction. Abbreviations; AC, adenylate cyclase; DAG, diacyl glycerol; IP_3, inositol triphosphate; MLCK, myosin light chain kinase; PLCβ, phospholipase C; PIP_2, phosphatidylinositol-(4,5)-bisphosphate (Adapted from Stott et al., 2014).*

As shown in the bottom panel of Figure 1.3, K_v7 channel activation causes relaxation and vasodilation, whereas decreasing K_v7 activity causes contraction and vasoconstriction. K_v7 channel activity can be regulated by endogenous signalling pathways stimulated by G_s- and G_q-coupled receptor signalling (Stott *et al.,* 2014). G_s-linked receptors are responsible for the relaxing effect, which is mediated in part by K_v7 channel-positive regulation via protein kinase A (PKA), which is triggered by the cyclic AMP pathway (Chadha *et al.,* 2012; Khanamiri *et al.,* 2013) (Figure 1.3). The effect of each of these mechanisms is the reduction in Ca^{2+} influx and/or the reduced release of Ca^{2+} from the intracellular store into the cytoplasm which finally results in ASMCs relaxation (Penn & Benovic, 2008; Johnson, 1998) (Figure 1.3). The constriction action is through G_q-linked receptors, which negatively regulate K_v7 channel activity via a protein kinase C (PKC)-mediated pathway (Brueggemann *et al.,* 2007; Mackie *et al.,* 2008) (Figure

1.3). In summary, it is now well established that both physiological and pharmacological stimulation of βARs promote relaxation of ASMCs and although the pathways involved in this are not yet fully understood, K_v7 channels appear to play an important role.

Given the effectiveness of K_v7 channel activation at inducing ASMC relaxation, it is not surprising that K_v7 channels have been targeted therapeutically. However, to selectively target specific tissues will require the development of K_v7 channel modulators that are not just specific for this channel but can differentiate between the different K_v7 family members.

1.3 K_v7 channels

The K_v7 channel family were cloned and re-expressed in heterologous expression systems in the 1990s (Wang *et al.,* 1996; Wang *et al.,* 1998; Kubisch *et al.,* 1999). There are five subtypes $K_v7.1$-$K_v7.5$ and these are encoded by five genes *KCNQ*1-5, respectively. Table 1.1 below summarizes the main biophysical properties of each of the five family members.

	$V_{1/2}$, mV	$\tau_{act+40mV\ (ms)}$	$\tau_{deact-60mV\ (ms)}$	Max P_o
$K_v7.1$	~ -20[a]	~90[b]	~450[b]	low[c*]
$K_v7.2$	~ -30[d]	~130[b]	~150[b]	low[e]
$K_v7.3$	~ - 40[d]	~60[b]	~100[b]	high[e]
$K_v7.4$	~ - 20[d]	~160[b]	~100[b]	low[e]
$K_v7.5$	~ - 40[d]	~150[b]	~120[b]	low[e]

Table 1.1: Summary of biophysical properties of K_v7 members. *Data in the above table are inferred from Refs. [a] Tristani-Firouzi & Sanguinetti, 1998; [b]Gamper & Shapiro, 2003; [c]Romey et al., 1997; [d]Miceli et al., 2009; [e]Li et al., 2004. *Low = p_o <20%; high = p_o >80%. Abbreviations: $V_{1/2}$ – voltage of half-maximum activation, τ_{act} - time constant of activation, τ_{deact} - time constant of deactivation, P_o - open probability.*

The first member to be identified was $K_v7.1$, which was initially named K_vLQT1, as it was identified in human heart from patients with long-QT condition (Sanguinetti *et al.*, 1996). It was shown that $K_v7.1$ channels were responsible for the slowly activating delayed K^+ rectifying current (I_{Ks}) in the heart (Osteen *et al.,* 2010). In a breakthrough study, Wang *et al.,* (1998), injected cDNA encoding

$K_v7.2$ and $K_v7.3$ in *Xenopus* oocytes and observed currents which were remarkably similar to the M-currents first recorded in neurons. Originally, M-currents were identified as non-inactivating K^+ currents, which activated slowly upon depolarization in frog and rat sympathetic neurons (Brown & Adams, 1980; Adams *et al.,* 1982). Later studies confirmed that $K_v7.2/K_v7.3$ heteromeric channels were responsible for conducting M-currents (Hadley *et al.,* 2003), which helps to repolarize the membrane towards its resting potential. It is a slowly activating current, which arises after an excitatory stimulus which depolarizes the neuron towards spike threshold. This process helps in limiting repetitive spike firing in neurons and is thought to suppress any epileptic activity (Soh *et al.,* 2014). The identification of K_v7 mediated M-current helped to explain the regulation of neuronal excitability by voltage-sensitive K^+ currents, which was identified previously in several studies in the 1960s and 1970s (Kobayashi & Libet, 1968; Krnjević *et al.,* 1971; Kuba & Koketsu, 1976; Weight & Votava, 1970). Through the various studies undertaken in the field of K_v7 channels, it has been reported that the channels formed by K_v7 subunits play critical roles in dozens of excitable tissues (Jentsch, 2000; Figure 1.2) and a description of each of the K_v7 subunits is provided below.

1.3.1 $K_v7.1$

The first human channelopathy in which a K_v7 gene defect was identified, was the Long QT Syndrome (LQTS) (Wang *et al.,* 1996). This arrhythmic disorder is characterized by a lengthening of the electrocardiogram's QT interval, which indicates prolonged action potential duration as a consequence of delayed cardiac action potential repolarization. In most cases, the LQTS is asymptomatic, unless some strenuous activity like exercise, stress, etc., leads to *torsades de pointes*, a distinctive re-entrant ventricular tachycardia, in which the QRS complex amplitude varies around an isoelectric line (Patoine *et al.,* 2011). Mutations in the gene encoding the $K_v7.1$ channel subunit (formerly known as K_vLQT1) were observed in the most common form (LQTS-1), accounting for over 50 percent of the LQTS instances (Wang *et al.,* 1996).

It was reported that $K_v7.1$ channels co-expressed with the β-subunit KCNE1, gave rise to potassium currents whose biophysical and pharmacological properties strongly resembled those of the $I_{K,slow}$ (I_{Ks}) component of the cardiac

delayed rectifier I_K current. During membrane depolarization and hyperpolarization, I_{Ks} activates and deactivates rather slowly (Sanguinetti & Jurkiewicz, 1990) (Table1.1).

The functional role of I_{Ks} in cardiac repolarization was debated extensively and in human ventricular cells, it contributed only marginally to repolarization under normal conditions. However, studies by Jost *et al.,* (2005; 2007) reported that I_{Ks} may provide a very important safety mechanism to prevent dangerous action potential lengthening. In a review by Peroz *et al.,* (2008) it has been reported that approximately 300 mutations have been associated with K_v7.1 in LQTS-1 patients. Several mutations in KCNE1 were also reported to have a crucial role in LQTS-1 (Vatta & Towbin, 2006). In patients suffering with LQTS-1 and LQTS-5, the pathogenesis was usually associated with impairment of I_{Ks} activity, due to loss-of-function mutations. A few gain-of-function mutations were also reported in both K_v7.1 and KCNE1 and these were associated with familial atrial fibrillation (FAF, Chen *et al.,* 2003) and short QT syndrome (SQTS, Bellocq *et al.,* 2004).

K_v7.1 has also been shown to play important roles in a variety of tissues outside the cardiovascular system. In epithelial cells for example, K_v7.1 channels in association with β-subunits KCNE2 and KCNE3 seem to underlie the open K^+ leak channels (Schroeder *et al.,* 2000). In gastric parietal cells, K_v7.1-KCNE2 channel complexes provided the apical recycling pathway needed for acidification by H^+ -K^+ and -ATPase (Heitzmann & Warth, 2007; Schubert, 2010). K_v7.1 and KCNE2 also form active K^+ channels in thyrocytes and control the normal biosynthesis of thyroid hormones (Roepke *et al.,* 2009).

1.3.2 K_v7.2 and K_v7.3

Mutations in K_v7.2 and K_v7.3 genes were demonstrated to result in many cases of Benign Familial Neonatal Seizures (BFNS), a rare autosomal-dominant idiopathic epilepsy of the new-born (Plouin, 1994). Although mutations in both K_v7.2 and K_v7.3 are associated with BFNS, they are 10 times more frequent in K_v7.2 than in K_v7.3 and are most commonly truncation mutants, splice site defects, missense mutations, non-sense mutations or frame-shift mutations (Soldovieri *et al.,* 2011). In contrast, the less frequent K_v7.3 mutations are mostly missense mutations (Soldovieri *et al.,* 2011). K_v7.2 mutations have also been implicated in rare cases of mild neonatal seizures (Bellini *et al.,* 2010). Many

studies on BFNS pathogenesis have suggested that mutations in $K_v7.2/K_v7.3$ mediate their effects by 1) altering steady-state levels and expression of channel subunits in the cell, 2) modifying intracellular trafficking of $K_v7.2/K_v7.3$ (Soldovieri *et al.,* 2007), 3) polarizing the surface distribution of the channels (Chung *et al.,* 2006) and 4) affecting channel function (Castaldo *et al.,* 2002; Dedek *et al.,* 2001; Soldovieri *et al.,* 2007).

Studies in heterologous expression systems demonstrated that the biophysical and pharmacological properties of $K_v7.2/K_v7.3$ hetero-multimers resembled those of the native M-current (I_{KM}, Wang *et al.,* 1998) first identified in sympathetic bullfrog neurons (Brown & Adams, 1980). I_{KM} was shown to be a non-inactivating, voltage-dependent K^+ current that activated at approximately -60 mV, in a time- and voltage-dependent manner and was suppressed by muscarinic receptor stimulation. I_{KM} was subsequently identified in rat superior cervical ganglion (SCG) cells by Constanti & Brown (1981) and in a variety of central neurons, including mammalian hippocampal and cortical pyramidal cells (Marrion, 1997). When I_{KM} current was active, it helped prevent cell depolarization in response to incoming excitatory stimuli, and thus reduced neuronal hyperexcitability. It also appears that $K_v7.2$ and $K_v7.3$ subunits mediate the slow K^+ current observed in nodes of Ranvier of mammalian peripheral myelinated fibres (Devaux *et al.,* 2004; Schwarz *et al.,* 2006). Recently, Tran *et al.,* (2020) reported two severe phenotypical variants of epileptic encephalopathy (A337T and A337G) in the HA helix of $K_v7.2$ that altered PIP_2 interactions and reduced current amplitude. Considering the important inhibitory role of I_{KM} in neuronal excitability, coupled to the fact that $K_v7.2$ and $K_v7.3$ subunits are widely distributed in the hippocampus, neocortex and cerebellar cortex, which are key sites for neuronal network oscillations and synchronization control, it is perhaps not too surprising that mutations in $K_v7.2$ or $K_v7.3$ genes cause epilepsy in humans. Thus, these two genes are studied extensively as therapeutic targets in treating neuronal hyperexcitability diseases in humans.

When $K_v7.2$ and $K_v7.3$ channels were expressed in mammalian cells or *Xenopus* oocytes, robust K^+ currents were generated (Wang *et al.,* 1998; Hadley *et al.,* 2003). $K_v7.2$ homomeric channels activated at ~-50 mV and these currents showed slow deactivation kinetics, as illustrated in Table 1.1. $K_v7.3$ homomeric channel currents activated at ~-60 mV, yet their amplitudes were rather small

compared to the other family members, despite the fact that they showed the highest open probability and unitary conductance (Li *et al.,* 2005) of all K_v7 channels. Interestingly, the heteromeric $K_v7.2/K_v7.3$ channels generate currents that are 10-fold greater in amplitude than homomeric $K_v7.2$ or $K_v7.3$ channels (Wang *et al.,* 1998; Yang *et al.,* 1998).

1.3.3 $K_v7.4$

The $K_v7.4$ gene was first identified as the gene responsible for autosomal dominant type 2 deafness (DFNA2), a progressive form of sensorineural hearing loss (Kubisch *et al.,* 1999). There are ~30 known mutations in this gene reported so far, all of which are linked to DFNA2 hearing loss (Dodson & Dominguez, 2012). Most of these mutations are missense changes in amino acids in or near the pore region and affect the assembly or functionality of the channels in the inner ear. Kubisch *et al.,* (1999) identified a non-functional mutation (G285S) in the pore region, which resulted in dominant negative effects on wildtype (WT) $K_v7.4$ channels associated with DFNA2. Some other DFNA2 mutations are deletions which cause haploinsufficiency and impair the interactions between the WT channels and the mutant channels. (Smith & Hildebrand, 2008).

The extensive distribution of $K_v7.4$ channels across the human body (Figure 1.2) illustrate the importance of these channels in many different processes. For example, in cochlear outer hair cells (OHCs), high $K_v7.4$ expression was reported and was shown to underlie $I_{K,n}$ currents in these cells (Housley & Ashmore, 1992). Interestingly, these currents activated near the resting potentials of -70 to -80 mV in OHC, and it appears that the role of $K_v7.4$ here, is to hold the cell near the equilibrium potential for K^+ ions. These K^+ currents have also been identified in mouse and rat inner hair cells (IHCs) using a combination of immunofluorescence, *in-situ* hybridization and RT-PCR studies. This overlap between $K_v7.4$ and $I_{K,n}$ provided solid evidence for $K_v7.4$ subunits contributing to $I_{K,n}$ also in IHC (Kimitsuki *et al.,* 2010). Similarly, in vestibular epithelia, type I hair cells display a high density of K^+ channels with a very negative voltage range of activation, which overlapped with the resting membrane potential (Rennie & Correia, 1994). Although $K_v7.4$ was described as the main K^+ current in the cochlear and vestibular epithelia, there were significant differences in the pharmacological and biophysical properties of native $I_{K,n}$ currents, compared to

those recorded in heterologous expression systems, suggesting that other regulatory subunits are present in native tissues. $K_v7.4$ channels also contribute to vascular smooth muscle cell function. For example, in penile arteries and the corpus cavernosum, $K_v7.4$ channels have been shown to regulate smooth muscle tone (Jepps *et al.,* 2016). Similarly, in ASMCs, $K_v7.4$ and $K_v7.5$ appear to contribute to the maintenance of airway diameter and also to the relaxation of the constricted airways (Brueggemann *et al.,* 2012). Thus, $K_v7.4$ can be exploited pharmacologically in the treatment of COPD and asthma, whereby activating the channels would induce relaxation of hyperconstricted airways in patients. Also, expression studies of C_2C_{12} cells, an *in vitro* model of skeletal muscle differentiation, revealed high expression of $K_v7.2$, $K_v7.3$ and $K_v7.4$ mRNAs (Iannotti *et al.,* 2010). A separate study revealed that K_v7 and more specifically $K_v7.4$ channels regulate the skeletal muscle proliferation, differentiation and responses to drug-induced myotoxic effects (Soldovieri *et al.,* 2011).

Electrophysiologically, the $K_v7.4$ channels are slightly different from the other K_v7 channels, whereby they activate slowly and deactivate rapidly (Kubisch *et al.,* 1999; Table 1.1). The homomeric $K_v7.4$ channels activate around -40 mV and have been reported to have the lowest unitary conductance (2.1pS) and also the smallest maximum open probability (0.07) of all the K_v7 channels (Li *et al.,* 2004). Despite having a small conductance and low open probability, expression of $K_v7.4$ channels gives rise to very large currents in heterologous expression systems. This may suggest that $K_v7.4$ channels are very efficiently trafficked and inserted into the plasma membrane (Zaika *et al.,* 2008), or that when they are inserted, the channel complex is remarkably stable. $K_v7.4$ channels have been shown to assemble with both $K_v7.3$ and $K_v7.5$ to form heteromeric channels, but they do not appear to co-assemble with either $K_v7.1$ and $K_v7.2$ subunits (Brueggemann *et al.,* 2011). $K_v7.4$ can also associate with the β ancillary subunits. KCNE1 associates with $K_v7.4$ and shifts the $V_{1/2}$ of activation by -10 mV compared to the $K_v7.4$ channels alone. Also, KCNE4 when co-expressed with $K_v7.4$ is reported to constitutively activate the $K_v7.4$ currents (Strutz-Seebohm *et al.,* 2006).

1.3.4 $K_v7.5$

$K_v7.5$ was the last member of the K_v7 gene family to be identified (Lerche *et al.,* 2000; Schroeder *et al.,* 2000a). The expression pattern of $K_v7.5$ largely overlaps with that of $K_v7.2$ and $K_v7.3$ and is therefore highly expressed in the brain and sympathetic ganglia (Schroeder *et al.,* 2000a). However, $K_v7.5$ channels are also expressed in skeletal (Iannotti *et al.,* 2010; Roura-Ferrer *et al.,* 2008; Yeung *et al.,* 2008) and smooth muscle cells (Yeung *et al.,* 2007). They have also been reported in the tunica media of various blood vessels, where they are thought to play an important role in vascular tone regulation (Brueggemann *et al.,* 2007).

The pathophysiological role of $K_v7.5$ is not well established, although some studies suggest that it may contribute to dystonia. For example, Sander *et al.,* (2016), observed aggravation of dystonia in the presence of a $K_v7.2$-$K_v7.5$ blocker XE-991 in a paroxysmal dystonic (dt^{sz}) hamster model. When they investigated transcriptional expression of the K_v7 subunit genes using RT-PCR, they observed that neither $K_v7.2$ or $K_v7.3$ were altered in motor and limbic structures of dystonic hamsters, but $K_v7.5$ mRNA levels were significantly reduced. In addition, they reported that ICA 27243, a more potent opener of $K_v7.2/7.3$ than $K_v7.5$, did not reduce the severity of dystonia in mutant hamsters. Overall, their experiments showed the functional relevance of $K_v7.5$ channels in paroxysmal dystonia (Sander *et al.,* 2016). Lehman *et al.,* (2017), also reported both loss-of-function (V145G, L341I and S448I) and gain-of-function (P369R) mutations in $K_v7.5$, which resulted in decreased depolarization reserve and increased excitability of neurons, resulting in intellectual disability and epileptic encephalopathy conditions (Lehman *et al.,* 2017).

When expressed in *Xenopus* oocytes, homomeric $K_v7.5$ channels generated K^+ currents which activated upon depolarization (~-40 mV) and exhibited very slow activation kinetics which required several seconds to activate completely (Brueggemann *et al.,* 2007, Table 1.1). $K_v7.5$ subunits co-assembled with $K_v7.3$ and $K_v7.4$ but did not co-assemble with $K_v7.2$ subunits (Brueggemann *et al.,* 2011). Interestingly, $K_v7.5$ has been shown to reduce heteromeric current density when co-expressed with $K_v7.2/K_v7.3$ subunit heteromers. It is thought that competitive binding of $K_v7.5$ with $K_v7.3$ reduces the number of $K_v7.3$ subunits available to form $K_v7.2/K_v7.3$ heteromers (Soldovieri *et al.,* 2011).

1.4 Structure of K_v7 channels

The structure of K_v7 channels resembles that of other K_v channels, with each functional channel forming homo or heterotetramers of six transmembrane (S1-S6) domains, as shown in Figure 1.4. The cryo-EM structure of $K_v7.1_{EM}$/CaM was recently resolved at a resolution of 3.7Å (Sun & MacKinnon, 2017). A more recent cryo-EM structure by Sun and MacKinnon (2020) of $K_v7.1_{EM}$-KCNE3-CaM is identical in dimensions and overlaps the configuration of $K_v7.1_{EM}$/CaM, except for the conformational changes observed in presence of KCNE3 and PIP_2 which will be discussed in subsequent sections. The $K_v7.1$ subunit studied in both of the above-mentioned papers was truncated at the N-terminal and the C-terminal regions to improve the biochemical and thermal stability. However, these truncated channels were fully functional (Sun & MacKinnon 2017; Sun & MacKinnon, 2020).

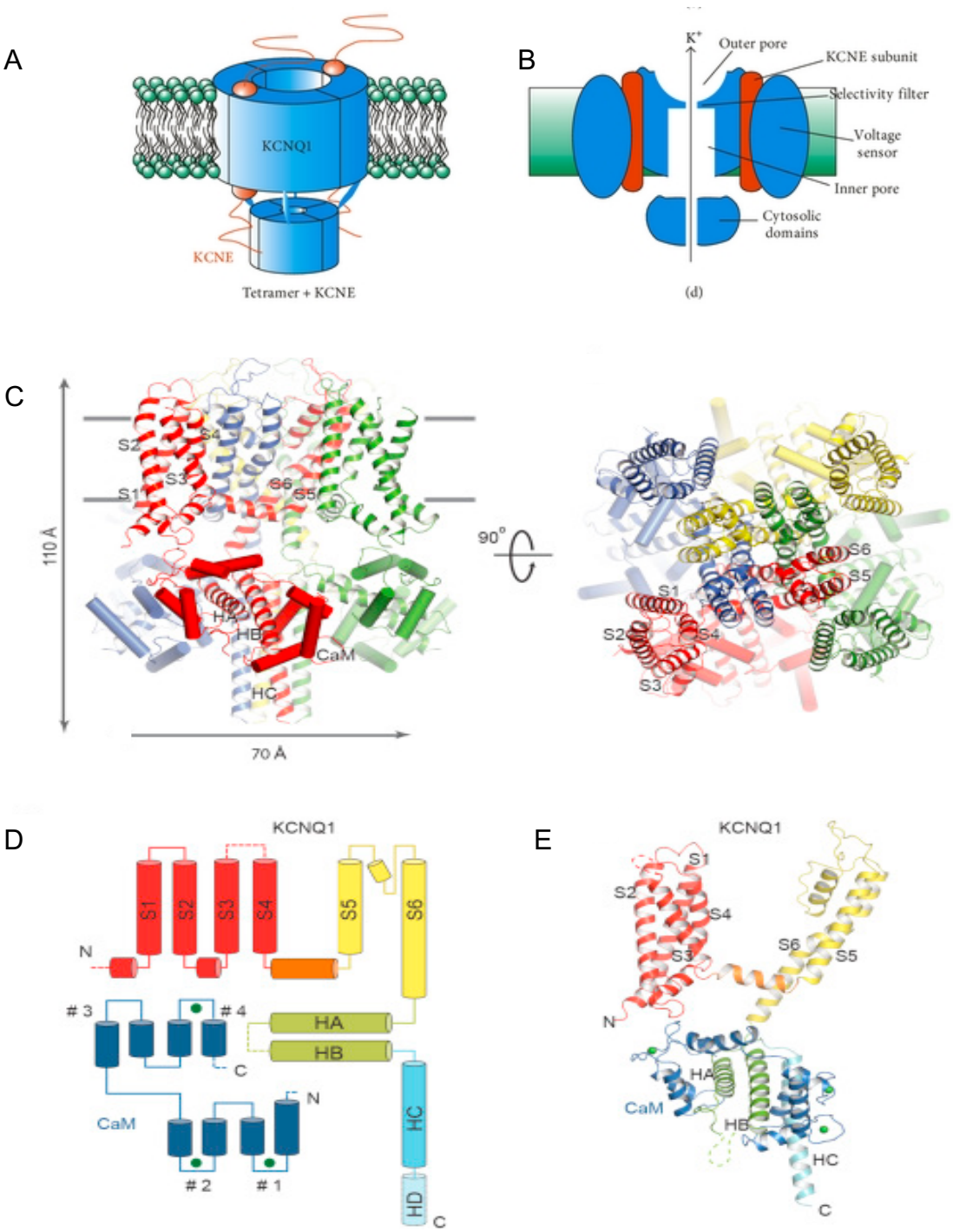

Figure 1.4: Structure of K_v7.1. A) *Assembly of K_v7.1-KCNE1 complex.* ***B)*** *View of section through the K_v7.1-KCNE1 complex highlighting main features.* ***C)*** *Top and side view of $K_v7.1_{EM}$/CaM complex, showing the different domains in the homotetramer, each monomer is highlighted in different colours.* ***D)*** *Domain organization of one subunit and* ***E)*** *Model of one subunit with domains coloured as in E (Adapted from Abbott, 2014; Sun & MacKinnon, 2017).*

The four-fold symmetrical structure (Figure 1.4C) of the $K_v7.1_{EM}$/CaM complex has approximate dimensions of ~ 70 Å 'wide' and 110 Å 'long'. Each monomer

has one $K_v7.1_{EM}$ subunit and one CaM molecule. The domain organization of a single subunit is depicted in Figure 1.4D, E where $K_v7.1_{EM}$ monomer contains six transmembrane helices (S1-S6) and four intracellular helices (HA-HD). In the same Figure 1.4D, the EF hands of CaM are shown as #1-#4, from the N-terminal to the C-terminal end. The first two EF hands (#1 and #2) form the N-lobe and the last two form the C-lobe of CaM molecule (Sun & MacKinnon, 2017). The S1-S4 transmembrane domains have regions that are responsible for sensing the voltage difference across the membrane, with S4 possessing many charged residues, which are essential for voltage sensing (Yellen, 1998; Li-Smerin *et al.,* 2000; Lu *et al.,* 2001; Bezanilla, 2002; Gandhi & Isacoff, 2002; Jiang *et al.,* 2003). The S5 and S6 domain, along with the pore loop region, form the ion conduction pathway, through which the ions pass when the channels are in an activated and open state (Figure 1.4B & D). In the tetrameric arrangement, the S6 domain forms the inner lining of the pore. Both the C and N-terminus are cytosolic in this channel. While all the subunits can combine to form homotetramers, the formation of hetero-tetramers is restricted to certain combinations as illustrated in Table 1.2 below:

	$K_v7.1$	$K_v7.2$	$K_v7.3$	$K_v7.4$	$K_v7.5$
$K_v7.1$	✓[1]				
$K_v7.2$		✓[1]	✓[2]		
$K_v7.3$		✓[2]	✓[1]	✓[1,3]	✓[4,5]
$K_v7.4$			✓[1,3]	✓[1]	✓[4,5]
$K_v7.5$			✓[4,5]	✓[4,5]	✓[1]

Table 1.2: Combinations of K_v7 members that can form heterotetramers. *Data in the above table are inferred from Refs. [1]Bal et al., 2008; [2]Wang et al., 1998; [3]Kubisch et al., 1999; [4]Bal et al., 2010; [5]Schroeder et al., 2000a.*

1.4.1 N-terminus

The N-terminus of K_v7 channels is believed to play an essential role in the localization of the channels to the membrane. There are two motifs identified as playing a crucial role in $K_v7.1$ protein trafficking to the membrane (Jespersen *et al.,* 2004). The first was the Leu-Glu-Leu motif at positions 38-40 in $K_v7.1$. A study by Jespersen *et al.,* (2004) on mammalian (MDCK) cell lines, reported that an

alanine substitution of leucines in this motif resulted in the protein being retained in the endosomal compartments. In the same study, they identified that tyrosine Y51 when replaced by an alanine, changed the localization of the channels from the basolateral to the apical membranes in the cell. This suggested that Y51 was a second important residue in N-terminus involved in channel trafficking (Jesperson *et al.,* 2004). However, Dahimène *et al.,* (2006) contradicted these findings, when they used a serial deletion approach to show that the first 106 residues in the N-terminus of $K_v7.1$ did not alter the surface expression of the channel. Instead, they demonstrated that removal of the first 114 residues significantly reduced $K_v7.1$ expression, suggesting that the residues between 106 and 114 played an important role in surface expression of the channel. This study was interesting particularly because it included two of the three residues (Y111C, L114P and P117L) implicated in Long-QT syndrome (Splawski *et al.,* 2000; Tester *et al.,* 2005; Schwartz *et al.,* 2001; Jongbloed *et al.,* 2002). When surface expression studies were carried out in CHO cells or cardiomyocytes, it was reported that none of the mutant channels expressed on the plasma membrane (Dahimène *et al.,* 2006). These three residues along with other residues in N-terminus, forming the motif YXXLERPXGW, are actually conserved across all the members of K_v7 family and hence may contribute as an export signal for all K_v7 subunits.

In another study, it was reported that the N-terminus contributed to the $K_v7.2/K_v7.3$ channel's open probability rather than to their trafficking (Etxeberria *et al.,* 2004). They used a chimeric approach, where they swapped the N-terminus of $K_v7.2$ with the N-terminus of $K_v7.3$. They found a 12-fold increase in current amplitude with this chimera co-expressed with $K_v7.3$, but they found no significant alteration in surface expression. When the chimeric approach was reversed and the $K_v7.3$ N-terminus was replaced with $K_v7.2$ N-terminus and co-expressed with $K_v7.2$, the current amplitude decreased (Etxeberria *et al.,* 2004), but this could not be explained by a change in membrane expression. Their results suggested that the N-terminus may play a role in regulating the open probability of the channel. The lack of conservation of the N-terminus sequence in K_v7 channels could explain the difference in N-terminus function between $K_v7.1$ and $K_v7.2/K_v7.3$ channels. However, it is conclusive that depending on the

channel, the N-terminus plays a role in either channel trafficking or in regulating the open-probability of the channel.

1.4.2 Voltage-Sensing Domain (VSD)

The S1-S4 transmembrane helices in the K_v7 channels constitute the voltage sensing domain (VSD) and shows a structural resemblance to the VSDs in the $K_v1.2$-2.1 chimera (Long *et al.,* 2007). Amongst these four transmembrane helices, the S4 domain is the primary voltage-sensing helix. Several studies in other K_v channels have shown that the S4 domain contains positively charged arginines (R1-R4) which serve as the main mobile charges responsible for sensing the voltage difference across the membrane (Aggarwal & MacKinnon, 1996; Seoh *et al.,* 1996; Gandhi & Isacoff, 2002). However, K_v7 channels lack one of these positively charged residues, corresponding to R3 in other K_v channels, and this is instead replaced by a glutamine (Panaghie & Abbott, 2007; see Figure 1.6B). In addition to the S4 domain, the negatively charged residues in the S2 domain and hydrophobic residues on S1, S2 and S3 have been shown to play an important role in voltage sensing (Yellen, 1998; Jiang *et al.,* 2002; Lu *et al.,* 2001; Long *et al.,* 2005). In $K_v7.1$, the negatively charged residues of S2 interact with the positive charged residues of the mobile S4 domain to attain different activation states (Wu *et al.,* 2010) and this is discussed in more detail below in Section 1.5.

The cryo-EM structure (PDB: 5VMS) of the voltage sensing domain of $K_v7.1$, as reported by Sun and MacKinnon (2017), retained some structural similarities to $K_v1.2$-2.1, although there were some notable differences too. The similarity was the presence of four positively charged (polar) residues in S4 helix extracellular to the phenylalanine residue (F157 in $K_v7.1$ and F233 in $K_v2.1$-1.2) and two positively charged S4 amino acids below the phenylalanine (F157 in $K_v7.1$ and F233 in $K_v2.1$-1.2) (Tao *et al.,* 2010; Sun & MacKinnon, 2017). The main differences between $K_v7.1$ ad $K_v1.2$-2.1 were: 1) the linker segment connecting S2 and S3 helices had a nine-amino acid insertion which was unique to $K_v7.1$) the S3 helix, was straight in the $K_v7.1_{EM}$ structure but in the $K_v1.2$-2.1 chimera possessed a ~ 25° bend. This bend is present in most K^+ channels and is due to the presence of a conserved proline residue that is absent in $K_v7.1$ channels (Long *et al.,* 2007) and 3) superimposition studies carried out by Sun and

MacKinnon (2017), showed a significant displacement of the hinge segment (K_v7.1-234-236) that connects S4 domain to the S4-S5 linker. In K_v1.2-2.1, there is a helical structure at this junction, but in $K_v7.1_{EM}$ it is replaced by a loop that is shifted by ~10.5 Å and, as a result, the S4-S5 linker is angled outward in $K_v7.1_{EM}$ (Sun & MacKinnon, 2017). This loop region coincides with the potential binding pocket of PIP_2 in K_v7.1 channels, suggesting that this region may form the binding pocket for PIP_2 in K_v7 channels (Zaydman *et al.,* 2014). Another important insight gained from the Sun and MacKinnon (2017) study was the identification of the S2-S3 loop as a potential alternative site for the interaction of calmodulin (CaM) with the K_v7 channels. In the same study, Sun and MacKinnon (2017), reported that CaM molecule binds to the C-terminus, but the secondary interaction is with the S2-S3 linker segment (Figure 1.4; Sun & MacKinnon, 2017). In the cryo-EM structure of $K_v7.1_{EM}$-KCNE3-CaM complex, it was shown that in the presence of KCNE3, the voltage sensors rotate ~7° counter-clockwise. This rotation moved the voltage sensor domain away from the pore and has been proposed to allow sufficient space for KCNE3 subunits to co-assemble in this region. The cryo-EM structure of $K_v7.1_{EM}$-KCNE3-CaM also showed binding of KCNE3 at the transmembrane interface to S6 from one subunit, S5 and pore helix in second subunit, and S1 and S4 from third subunit (Sun & MacKinnon, 2020). The extracellular half of KCNE3 lies between S1 and S6 helices in K_v7.1. This position of KCNE3 is said to stabilize the open conformation of K_v7.1 channel, which is reported to be the reason KCNE3 prevents voltage-dependent closure of K_v7.1 channels (Sun & MacKinnon, 2020).

1.4.3 Pore domain (PD)

The transmembrane helices S5 and S6 along with the pore loop (PL) form the pore domain. The pore domain is a K^+ selective aqueous pore with the pore loop containing the selectivity filter signature motif (TXXTXGYG), which is conserved across voltage-gated K^+ channels (Heginbotham *et al.,* 1992). When the channel is activated, the cytoplasmic lower halves of each S6 domain move apart, resulting in the open conformation in the channel (Yellen, 1998; Jiang *et al.,* 2002). In the cryo-EM structure study of K_v7.1, it was reported that the S6 helix was devoid of the conserved glycine and PXP motif, which was earlier reported to serve as a potential gating motif (Hackos *et al.,* 2002; Jiang *et al.,* 2002; Long

et al., 2005). In the closed conformation of the pore, the radius at the narrowest region of the pore (S339) is estimated to be ~0.8 Å, which is much less than the radius of K^+ ions. The narrowest restriction in the conduction path is formed by the GSG motif in $K_v7.1_{EM}$ (Sun & MacKinnon, 2017). The roles of the S6 domain and S4-S5 linker in the coupling of VSD activation and PD opening are elaborated upon in Section 1.5.2.

1.4.4 C-terminus

The cytosolic -COOH terminal of K_v7 channels comprises four helices (HA-HD), which have distinct binding motifs for regulators of K_v7 channels as shown below in Figure 1.5.

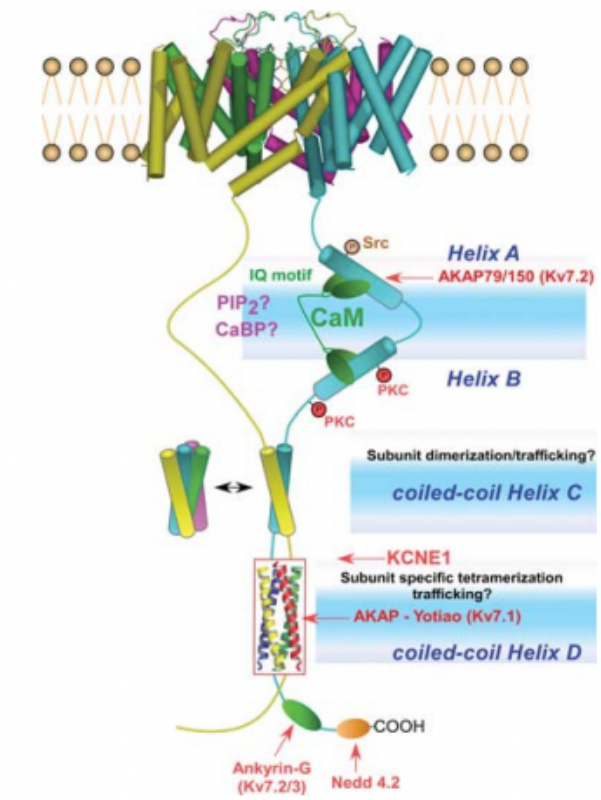

Figure 1.5: Structure of K_v7 channels and interaction sites on carboxy-terminal for different regulators. *The K_v7 C-termini helices exhibit conserved interaction sites for CaM, PIP_2, AKAP79/150, AKAP-Yotiao, Ankyrin-G and Nedd4.2 as indicated in this figure. The Helix B is endowed with PKC phosphorylation and Helix A contains a tyrosine kinase phosphorylation site. The coiled-coil Helix C and Helix D contribute to the dimerization and tetramerization of K_v7 subunits. (Adapted from Haitin & Attali, 2008).*

The helices HC-HD are crucial for the tetramerization of the channels and the helices HA-HB are important for CaM binding (Wen & Levitan, 2002; Yus-Nájera

et al., 2002; Gamper & Shapiro, 2003 & also see Figure 1.4). The HA helix has the CaM binding sequence similar to the highly conserved IQ motif (where IQ refers to the first two amino acids of the motif, isoleucine and glutamine), whereas the helix HB has two overlapping consensus 1-5-10 CaM-binding motifs (1-5-10 refers to the position of hydrophobic residues in this helix, Yus-Nájera *et al.,* 2002). The HA-HB helices (which are connected to the S6 domain) are also sandwiched between the N-terminus and C-terminus of the CaM molecule, as shown in Figure 1.4E (Sun & MacKinnon, 2017). In studies reporting long QT mutations in K_v7 channels (Haitin & Attali, 2008), a mutation was found close to this IQ motif in the $K_v7.1$ C-terminus. This mutation impaired CaM binding to the channel and significantly reduced current density (Ghosh *et al.,* 2006; Shamgar *et al.,* 2006). The C-terminus also forms the binding site for PIP_2 binding to the channel. A unique, positively charged pocket was identified in the cryo-EM structure of $K_v7.1$, which possibly could be the binding site for PIP_2 (Sun & MacKinnon, 2017). The pocket faces the inner leaflet of the membrane and consists of HB and the C terminus of S6 domain. The distal C-terminal helices HC-HD, (also known as the A-domain) are reported to play role in subtype-specific assembly (Schmitt *et al.,* 2000). More specifically, the HD helix, which is a poorly conserved region in the K_v7 family, confers significant differences between subtypes and is thought to play a key role in assembly specificity (Maljevic *et al.,* 2003; Schwake *et al.,* 2003; Schwake *et al.,* 2006). The binding of PIP_2 leads to a conformational change in S6 and HA helices wherein it changes from helix-loop-helix structure to single long helix (Figure 1.9A) (Sun & MacKinnon, 2020). This change in structure causes the CaM molecule to rotate 180 degrees and thus loses its interactions with voltage sensors, an important PIP_2-gating mechanism in K_v7 (Sun & MacKinnon, 2020). Other regulatory proteins like A-Kinase anchoring protein (AKAP) and KCNE1 are also known to bind to the C-terminal region of K_v7 channels to mediate their effects on channel kinetics. In an LQT mutation G589D (C-terminus), it was reported that the mutation disrupted the interactions of the I_{Ks} channel complex ($K_v7.1$/KCNE1) with AKAP (Marx *et al.,* 2002). Thus, the C-terminus of K_v7 channels plays a very important role in channel trafficking, tetramerization, forming complexes with other proteins and forms a binding domain for many signalling molecules involved in regulation of K_v7 channels.

1.5 Mechanism of gating in K_v7 channels

The K_v7 channels respond to cell depolarization by opening and this results in the movement of K^+ ions outwards across the membrane when recorded with normal physiological K^+ gradients. Channel activation and gating can be broadly be described in three steps, 1) activation of the voltage sensing domain (VSD), 2) coupling of the VSD to the pore domain (PD) and 3) opening of the pore ion conduction pathway allowing the passage of ions (Cui, 2016). In the sections below, each of these main steps is described and the factors and motifs proposed to play a role in each of these are discussed.

1.5.1 Activation of VSD by membrane depolarization

The location of the residues involved in the activation of voltage-gated channels

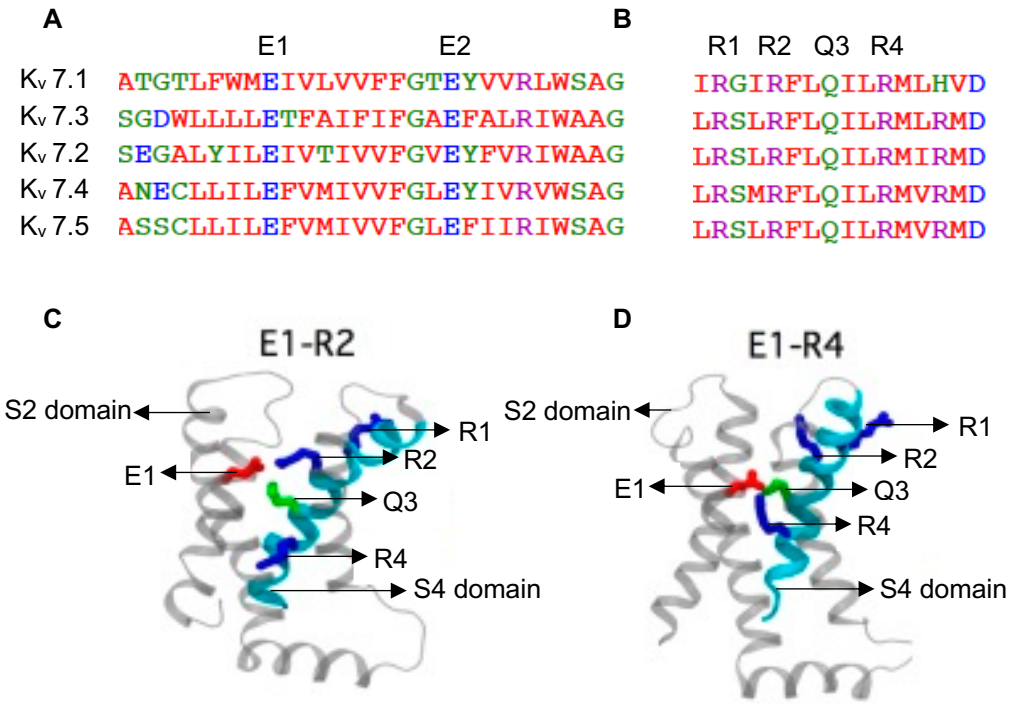

Figure 1.6: Voltage sensing domain of K_v7 channels. A) *and* ***B)*** *Protein sequence alignment of $K_v7.1$-$K_v7.5$ S2 and S4 domains, highlighting the E1 and E2 residues on S2 domain and R1, R2, Q3 and R4 residues on S4 domain.* ***C)*** *and* ***D)*** *Intermediate (E1-R2) and activated (E1-R4) states of K_v7 channels respectively (Adapted from Zaydman et al., 2014).*

was originally narrowed down to an unusual sequence of amino acids in the S4 helix of a cation channel by Noda *et al.,* (1984). They identified an alternating sequence of alternating Arg and Lys residues, which were highly conserved, and

proposed along with others, that these were involved in voltage sensing (Noda *et al.,* 1984; Greenblatt *et al.,* 1985; Catterall, 1986; Guy & Seetharamulu, 1986; Noda *et al.,* 1986). The density of positive charge varies in different voltage sensing K^+ channels, with the highest density found in Shaker K^+ channels (+7) compared to only 3 positive charges in the $K_v7.1$ channel (Panaghie & Abbott, 2007; see Figure 1.6).

In $K_v7.1$, Panaghie & Abbott (2007) used alanine scanning mutagenesis to establish that residues R228, R231 and R237 in S4 played a crucial role in voltage sensitive activation of the channels (Figure 1.6). Previous intragenic suppression studies of charged residues in the VSD indicated that electrostatic interactions between the third and fourth Arg in S4 (R3 and R4) and the first glutamate in S2 (E1) were essential for the activation of Shaker K^+ channels (Papazian *et al.,* 1995; Tiwari-Woodruff *et al.,* 1997; Zhang *et al.,* 2007). Similarly, studies by Long *et al.,* (2005; 2007) have shown that in the $K_v1.2$ channel crystal structure, the E1 residue in S2 is in close proximity to the R4 residue of the S4 segment when the channel is open.

Wu *et al.,* (2010), studied the charge reversal mutations in $K_v7.1$ associated with long QT syndrome (E1K in S2 domain) and reported that the mutation completely abolished K_v7 currents, but did not alter the trafficking of the protein to the plasma membrane. However, when this E1K mutant was paired with charge reversal mutations of S4 segment i.e., E1K-R4E, the currents were restored, which supported other findings suggesting the role of S2 residues in voltage sensing. They proposed that each of the three arginines in S4 lead to sequential activation of the VSD and resulted in resting, intermediate and activated states of VSDs (Figure 1.6). As a result, at each step, the VSD would translocate S4, in a stepwise fashion. This finding was further supported by a study from Osteen *et al.,* (2010), which used patch clamp fluorometry on $K_v7.1$ channels, to show that VSD activation had three distinct states - the resting, intermediate and fully activated states. They showed that in the resting state, the E1 residue interacted with the R1 residue, resulting in a stable closed state. When the E1 residue interacted with the R2 residue, this led to the intermediate state of the VSD activation. In the last state, the E1 residue is thought to interact with the R4 residue, leading to fully activated state where the channels are stabilized in an open conformation (Figure 1.6; Osteen *et al.,* 2010; Zaydman *et al.,* 2014). In

conclusion it is well established that when the membrane is depolarized these 'mobile' positively charged residues facilitate an outward shift of the S4 domain to an activated state, which in turn promotes channel opening (Papazian *et al.,* 1995; Larsson *et al.,* 1996; Silva *et al.,* 2009; Wu *et al.,* 2010; Delemotte *et al.,* 2011; Jensen *et al.,* 2012).

1.5.2 Coupling of VSD activation and PD

The VSD coupling to the pore gate domain (PD) is majorly attributed to 1) the interaction between S4-S5 linker and C-terminus (tail) of $S6_T$ domain, 2) the N-terminus and the S1 segment and 3) PIP_2 mediated coupling and each of these are discussed in more detail below.

1.5.2.1 S4-S5 linker (S4-S5L) and S6 terminal ($S6_T$)

Many studies investigating the VSD-PD coupling emphasized the interaction between the S4-S5 linker (S4-S5L) and the lower part of S6 segment, called the S6 tail or $S6_T$. The functional studies in Shaker and KcsA chimeras using mutagenesis approaches (Lu *et al.,* 2001; Lu *et al.,* 2002), alanine-scanning of S4-S5L and $S6_T$ in $K_v4.2$ (Barghaan & Bähring, 2009), cross-linking studies of S4-S5L and $S6_T$ in human ether-à-go-go-related genes (hERG; Ferrer *et al.,* 2006), all converge on the notion that the S4-S5 linker and S6 C-terminal play a significant role in coupling between VSDs and pore gate domain. This is further confirmed by the crystal structures of K_v and Na_v channels, which showed that the distance between S4-S5L and $S6_T$ fits with the hypothesis that these regions are in contact with one another (Long *et al.,* 2005; Payandeh *et al.,* 2011).

In Shaker-type K_v channels, substituted cysteine accessibility studies showed that the channel pore was formed by the lower part of the $S6_T$ (Liu *et al.,* 1997; del Camino & Yellen, 2001). In further studies by Bright & Sansom, (2004) and Grottesi *et al.,* (2005), it was suggested that the opening of the pore occurred as a result of kinking or swelling of the S6 helix, at the flexible gating hinge, which resulted in reorientation of residues around this region. This flexibility, in most K_v channels, is attributed to a highly conserved glycine residue in the middle of the S6 segment (Ding *et al.,* 2005), or by a further downstream PXP motif in the S6 segment (del Camino *et al.,* 2000; Labro *et al.,* 2003). The crystal structure of $K_v1.2$ shows that the S6 helix is actually bent at the PXP motif, thus orienting the

S6 cytoplasmic end towards the S4-S5 linker (Long *et al.,* 2005a). As a result, different interactions between $S6_T$ and the S4-S5L could provide a coupling mechanism between the S4 movement and the channel gate opening or closing (Long *et al.,* 2005). In K_v7 channels, the S6 segment structure differs from other K_v channels, as they lack the Gly in the middle of S6 and contain a PAG sequence instead of a PXP motif as shown by the red box in Figure 1.7.

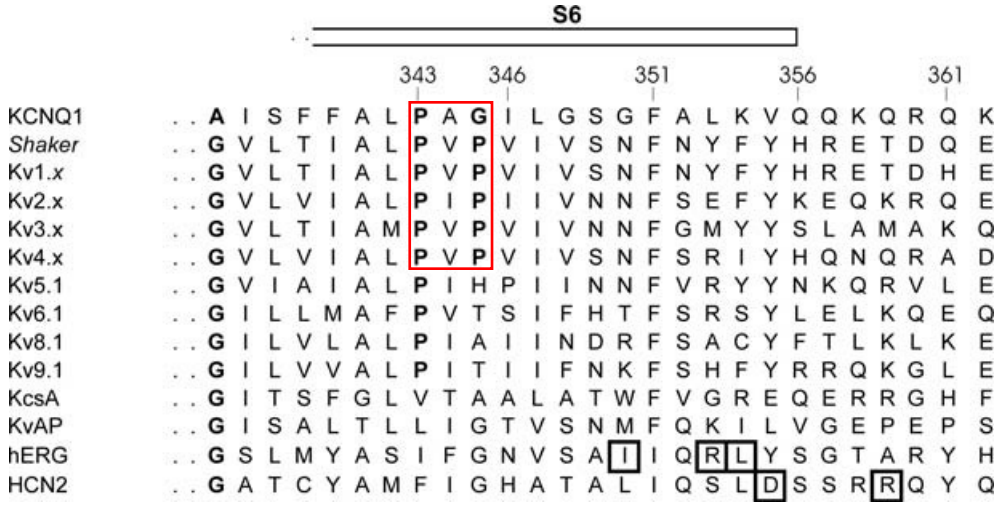

Figure 1.7: Sequence alignment of C-terminal part of S6 of several K_v channels. *Sequence alignment of the S6 C-terminal shows the conservation region amongst K_v channel members. In bold, the conserved glycine residue and the PXP motif is highlighted in red box. In $K_v7.1$ PXP motif is replaced by PAG sequence, and it does not possess the conserved glycine residue. Boxed residues in hERG and HCN2 have been shown to interact with S4-S5 linker and are critical in gating and molecular coupling (Tristani-Firouzi et al., 2002; Decher et al., 2004; Ferrer et al., 2006). (Adapted from Boulet et al., 2007).*

However, the PAG motif in $K_v7.1$ is still thought to form a similar hinge region, which is essential for coupling of the VSD to the pore gate of the channel. Alanine and tryptophan perturbation scanning of the $S6_T$ region in K_v7, revealed several other residues to be important for channel gating (Boulet *et al.,* 2007). Many $K_v7.1$ mutations including G348A, S349A, G350A, F351A, A352W and V355W were graded as high impact, based on the stable open and closed states of the channels measured by $\Delta\Delta G_0$ (Boulet *et al.,* 2007). For example, the mutant G348A in the above study showed a negative $\Delta\Delta G_0$ value, which indicated that the mutation caused the open state to be stabilized. In contrast, the S349A, G350A, F351A, A352W and V355W mutants all showed a positive $\Delta\Delta G_0$ indicating that these mutations caused the closed state to be stabilized over the

open state (Li-Smerin *et al.,* 2000). The mutations F351A and V355W have been shown to generate an I_{Ks}- like phenotype (Boulet *et al.,* 2007). This suggested that these mutations could mimic the action of KCNE1 on K_v7.1 channels, by producing a local conformational change in K_v7.1 comparable to that generated by KCNE1, or by modifying the transitional states that KCNE1 might affect during the channel gating process (Boulet *et al.,* 2007). In addition, the introduction of an alanine or a charged amino acid in place of a leucine at position 353 resulted in a constitutively conducting phenotype, which emphasized the crucial role of L353 in stabilizing the closed conformation of the K_v7.1 channels (Boulet *et al.,* 2007).

1.5.2.2 N-terminus and the S1 segment - Role in VSD-pore coupling

Other regions outside of S4-S5L and $S6_T$ also clearly influence voltage-dependent channel activity. The N-terminus (N_{ter}) is one such region which, in three K_v channel families, namely K_v10, K_v11 and K_v12, a PAS domain is present and has been shown to be essential for VSD-pore coupling (Choveau *et al.,* 2012). The PAS domain functions as a signal sensor and spans from residues 1-135 in K_v11.1a channels (Ke *et al.,* 2014). It is named after the transcription factors in which it was first discovered: period circadian protein (Per), aryl hydrocarbon receptor nuclear translocator protein (Arnt), and single-minded protein (SMP) (Ke *et al.,* 2014). The delayed deactivation of hERG channels is thought to be caused by an interaction between the PAS domain and S4-S5L (Wang *et al.,* 1998; Chen *et al.,* 1999). A disruption of the hypothesized link between the PAS domain and S4-S5L was also reported to accelerate the deactivation rate in some LQT patients, which resulted in a decrease in the repolarizing current (Chen *et al.,* 1999). Alonso-Ron *et al.,* (2008) found that channels lacking the PAS domain, or with mutations in the S4-S5L, had similar slower deactivation and a positive change in the voltage dependency of activation, indicating that these two regions interact. A study by de la Peña *et al.,* (2011) also demonstrated a close proximity between N_{ter} and S4-S5L in hERG. Taken together, it these studies suggest that N_{ter} can bind to S4-S5L and may be important for channel gating (Choveau *et al.,* 2012).

Coupling between the VSD and the pore may also occur via transmembrane domain (TMD) interactions (Choveau *et al.,* 2012). Cross-linking experiments in

the Shaker channel (Broomand *et al.,* 2003; Gandhi *et al.,* 2003) demonstrated the connection between the S4 and S5 segments and indicated that interactions could be involved in the coupling between the VSD and the pore (Broomand *et al.,* 2003; Gandhi *et al.,* 2003). Furthermore, statistical analysis of K_v channels sequences, as well as mutagenesis studies, suggest that this coupling often involves a strongly conserved interface between the S1 domain and the pore helix, both highly conserved in K_v channels (Lee *et al.,* 2009). In summary, a network of interactions appears to be involved in coupling VSD and pore, including N_{ter}, S1, S4-S5L, and $S6_T$.

1.5.2.3 PIP_2 mediated coupling of VSD and the PD

PIP_2 is a small lipid found mainly in the plasma membrane's inner leaflet. It modulates a variety of ion channels, including some voltage-gated channels (Suh & Hille, 2008). In general, PIP_2 is involved in coupling K_v7 channel opening following membrane depolarization (Zhang *et al.,* 2003) and stabilizes its open conformation, leading to increased current amplitude, slower deactivation kinetics and a negative shift in the steady state activation curve (Choveau *et al.,* 2012). Studies by Zaydman *et al.,* (2013) on PIP_2 regulation of K_v7 channels, suggested that it enhances communication between the VSD and the PD. Zaydman *et al.,* (2013) also suggested that PIP_2 binding affected the electrostatic repulsion between the VSD and PD and thus helps to potentiate the coupling between these two domains. Through site-directed mutagenesis studies and homology modelling, Zaydman *et al.,* (2013) also identified 16 basic residues in the VSD-PD interface that were highly conserved among K_v7 channels and were necessary for PIP_2 binding in K_v7 channels. Among these 16 residues, eight mutations (see red & blue shading in Figure 1.8A) severely decreased the whole-cell current amplitude (R190Q, R195Q, H258N, R259Q, K354N, R360Q, H363N, R366Q) and four mutations (see green shading in Figure 1.8A) mildly decreased the current amplitude (R192Q, R243Q, K358N, K362N). In the above study the effects of each the mutants were studied on K_v7 channel surface expression, time course of current rundown and VSD-PD coupling strength. The results of these studies strongly suggested that these mutations disrupt VSD-PD coupling and decreased channel current by directly affecting PIP_2 binding.

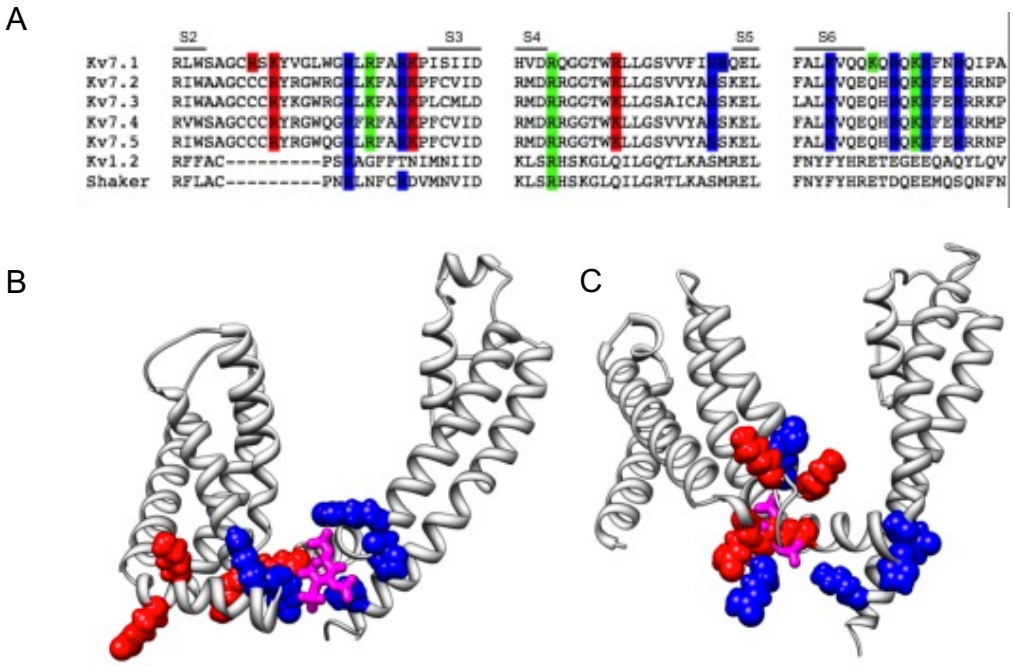

Figure 1.8: PIP$_2$ binding site and VSD-PGD coupling. A) *Protein sequence alignment of the S2-S3 linker, S4-S5 linker and end S6 residues. Highlighted blue and green residues were PIP$_2$ binding residues, charge neutralization of these residues reduced the current amplitudes of the channels. The highlighted red residues charge neutralization mutations increased the current amplitudes.* ***B)*** *Activated open* ***C)*** *Resting closed models with PIP$_2$ binding. Magenta-PIP$_2$ head group, blue-PIP$_2$ binding residues (Adapted from Zaydman et al., 2013).*

Such mutations replicated the effects of PIP$_2$ depletion on WT channels, where they strongly inhibited ionic current, prevented VSD activation and significantly reduced VSD-PD coupling. Sun and MacKinnon, (2020) have recently published the cryo-EM structure of human $K_v7.1_{EM}$-KCNE3-CaM complex in the presence of PIP$_2$ and have identified binding residues for PIP$_2$ near a loop connecting S4 helix to S4-S5 linker (R181, K183, Y184, R195, K196, Q244, W248 and R249). This structure also confirmed the binding of PIP$_2$ to basic amino acid residues in S1, the S2-S3 and S4-S5 linkers, which is consistent with previous studies (Choveau *et al.,* 2018; Eckey *et al.,* 2014; Kasimova *et al.,* 2015; Telezhkin *et al.,* 2013; Zaydman *et al.,* 2013). This cluster of basic residues was thus established as a crucial interaction site for PIP$_2$-mediated coupling.

1.5.3 Opening of pore domain to allow passage of ions

The pore domain is comprised of the S5 and S6 helices as well as the pore loop segment of the channel. The S6 domain forms the internal lining of the K_v pore,

and its residues have been explored in an attempt to understand the mechanisms underlying pore opening. It has been established that the PVP motif in S6 of Shaker channels is involved in S6 movement during pore opening (Yellen, 1998). This PVP motif aligns to P343, A344 and G345 in K_v7.1 channels (see Figure 1.7). Mutagenesis studies by Seebohm *et al.,* (2005) and Panaghie *et al.,* (2006), also identified a cluster of mutations in the S6 domain of K_v7.1 channels that affected the current amplitude and/or shifted the activation voltage. Amongst this cluster were three mutations P343A, G345A and I346A, which rendered the channel non-functional (Seebohm *et al.,* 2005; Seebohm *et al.,* 2006). F340W was another important mutation that resulted in constitutively activated channels (Panaghie *et al.,* 2006). The glycine residue (G366) in the S6 domain in Shaker K_v channels is well conserved in most of the K^+ channels and is shown to act as a critical hinge in S6, during pore opening (Jiang *et al.,* 2002). In K_v7.1 channels, the equivalent residue is A336, which when mutated, increased current amplitude, and shifted the voltage dependence of activation to more negative potentials (Seebohm *et al.,* 2006). Also reported are the studies on K_v7.1 where mutations associated with LQT (F339S, A341V, A341E, and G345E) are said to suppress current amplitude significantly (Wang *et al.,* 1999; Hoosien *et al.,* 2013). A large conformational change in the $K_v7.1_{EM}$-KCNE3-CaM cryo-EM structure in presence of PIP_2 was reported by Sun and MacKinnon (2020). They demonstrated that binding of PIP_2 in the S6 and HA helix of C-terminus changed the helix-loop-helix structure to a single, continuous long helix (Figure 1.9A). This shift caused the CaM molecule to rotate 180 degrees and disassociate from the VSD. Also, the linker connecting S6 to the HA helices called “RQKH” motif (which is conserved in K_v7.1-7.5), undergoes structural rearrangement from a loop to helix in presence of PIP_2 (Figure 1.9A), suggesting a PIP_2-dependent gating mechanism in K_v7 channels. The cryo-EM structure showed a PIP_2 induced, outward bend in the C-terminal half of S6 at the conserved “PAG” motif (Figure 1.9B), which causes the cytoplasmic pore entrance to dilate (Figure 1.9C). Consequently, the amino acids that usually restrict the pore (S349, G345 and L353, Figure 1.9D), expand in presence of PIP_2, leading to the open conformation of the channel.

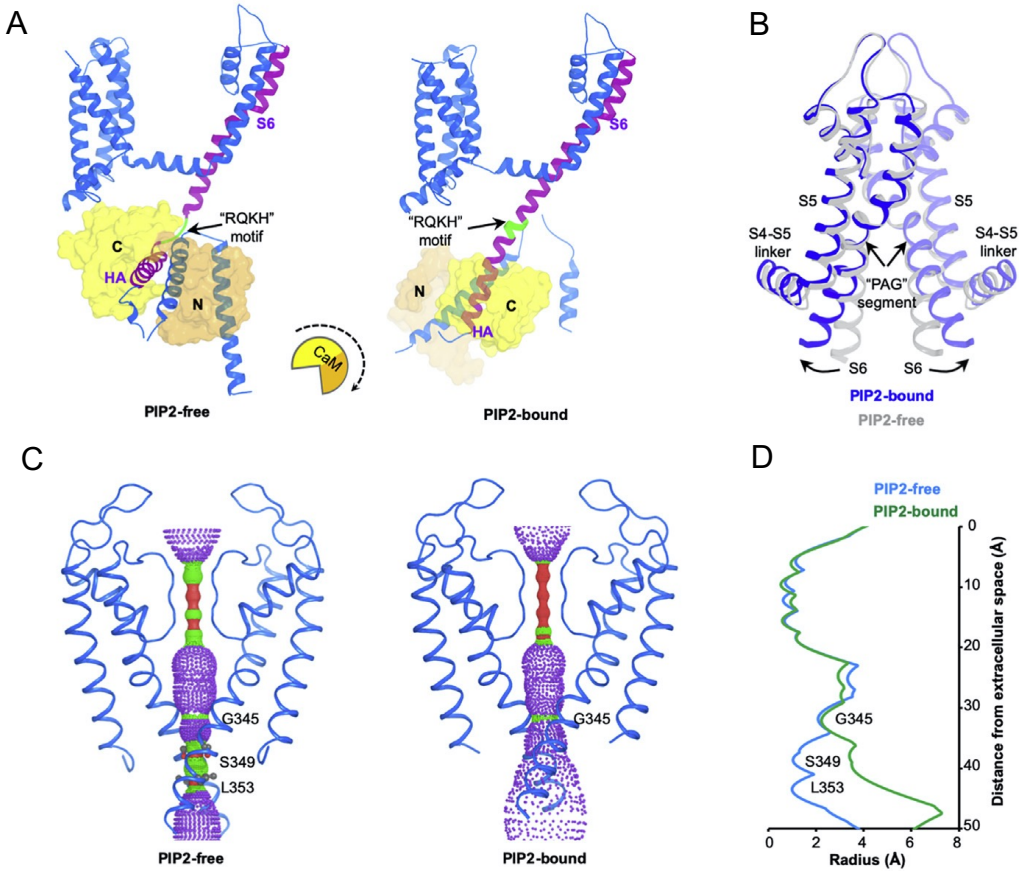

Figure 1.9: PIP_2 induced conformational changes in $K_v7.1$-CaM. A) *Conformational change of one $K_v7.1$-CaM channel protomer. The "RQKH" motif is shown in green, S6 and HA helixes of $K_v7.1$ are colored in purple, CaM is shown as surface with its N-lobe in orange and C-lobe in yellow.* ***B)*** *Overlay of pore domains of PIP_2-free and PIP_2-bound structures indicating conformational changes in the ion-conduction pathway.* ***C)*** *Ion-conduction pathways for PIP_2-free and PIP_2-bound state showing important residues lining the pore.* ***D)*** *Radius of the pore calculated using the HOLE program showing increase in pore radius in PIP_2-bound state (Adapted from Sun & MacKinnon, 2020).*

1.6 Regulation of K_v7 channels

K_v7 channels are regulated by a number of accessory proteins and some of the best-characterized modulatory proteins are discussed below.

1.6.1 Calmodulin (CaM)

CaM binding to the C-terminus of K_v7 channels is necessary to produce functional channels (Gamper & Shapiro, 2003; Ghosh *et al.,* 2006; Shamgar *et al.,* 2006; Wen & Levitan, 2002; Yus-Nájera *et al.,* 2002). In ion channels, CaM often mediates its effects through IQ/CaM binding domains (CaMBDs). Secondary structure studies have shown the C-terminus has four helical regions (helices A-D), a feature which is conserved in all the family members of K_v7 channels (Yus-

Nájera *et al.,* 2002). Amongst these four helices, Helix A and Helix B are known to encode the binding site for CaM (Wen & Levitan, 2002; Yus-Nájera. *et al.,* 2002; Gamper & Shapiro, 2003). Helix A is said to have the CaM binding motif that is partially consistent with the IQ (isoleucine and glutamine) motif, and Helix B has the overlapping 1-5-10 motif which is conserved across K_v channels (1-5-10 motif termed based on the position of hydrophobic residues, Yus-Nájera *et al.,* 2002). In parallel to these findings was another finding in $K_v7.4$, where a structural study of C-terminus constructs clearly showed Helix B was essential for Ca^{2+}/CaM binding and Helix A and Helix B were critical for apo-CaM binding (Xu *et al.,* 2013). CaM is also known to modulate trafficking of the protein from the endoplasmic reticulum to the plasma membrane (Ghosh *et al.,* 2006; Shamgar *et al.,* 2006). In a study by Gamper *et al.,* (2005), it was established that CaM functions as a Ca^{2+} sensor and binds to low affinity CaM binding sites in K_v7 channels. In the same study, they showed that when CaM was over-expressed along with K_v7 channels in CHO cells, it reduced current density in $K_v7.2$, $K_v7.4$ and $K_v7.5$ but not in $K_v7.1$ and $K_v7.3$ channels (Gamper *et al.,* 2005). Gamper and Shapiro (2003), showed that increased $[Ca^{2+}]_i$ suppressed the neuronal M-current generated by $K_v7.2/K_v7.3$ channels, via CaM modulation. However, CaM modulation also has been shown to play a role in stimulation of I_{Ks} current in cardiac myocytes with increase in $[Ca^{2+}]_i$ (Shamgar *et al.,* 2006).

Other studies (Sihn *et al.,* 2016) have suggested that in human $K_v7.4$ channels, CaM binds to two $K_v7.4$ isoforms in a Ca^{2+} independent manner. This binding of CaM to the human $K_v7.4$ isoform *a* in particular decreased the channel open probability and altered the activation kinetics (Sihn *et al.,* 2016). In the same study, the G321S mutation in S6, upstream of the CaMBD, altered CaM binding and had a reduction in the inhibitory effect of Ca^{2+}/CaM on the $K_v7.4$ channel. Their model suggested that in WT $K_v7.4$, the native G321 permitted the side chain of H234 in the S4-S5 linker to come in direct contact with S6 and potentially stabilize a conformation of the C-terminus, that was suitable for CaM binding. In the mutant however, the S321 residue displaced the side chain of H234 (S4-S5 linker) from interacting with the S6. This decoupling of S4-S5 linker with S6 segment was reported to affect the conformation of the C-terminus which interfered with CaM binding (Sihn *et al.,* 2016).

Another important function of CaM on K_v7 channels is its involvement in folding of the K_v7 channels. It was established by a structural study of C-terminus/CaM complex that an LQT-mutation, S373P leads to misfolding and misassembly of the channel (Shamgar *et al.,* 2006). This residue was previously established to be the CaM binding residue (Shamgar *et al.,* 2006). It was suggested that the S373P mutation may perturb the helical bundle and CaM C lobe interactions. Point mutation studies in Helix A (I375D) and Helix B (V516D) also altered the CaM binding, reduced protein expression, and decreased current density. This suggested that C-terminal/CaM interactions were essential for proper biosynthesis and channel assembly (Shamgar *et al.,*2006). Thus, in conclusion, the CaM-binding module present at the C-terminal of the K_v7 channels has a dual function, 1) it acts as a Ca^{2+} sensor and modulates channel current and 2) it is involved in channel trafficking and folding.

1.6.2 Phosphatidylinositol-(4,5)-Bisphosphate (PIP_2)

PIP_2 is a phospholipid component of cell membranes known to act as substrate for a number of signalling proteins. In K_v7 channels, the plasma membrane levels of PIP_2 modulate the channel (Delmas & Brown, 2005; Suh & Hille, 2005; Gamper and Shapiro, 2007). A decrease in [PIP_2], as a result of $G_{q/11}$-coupled receptor stimulation, is a key biochemical signal that controls the function of K_v7 channels in both native and recombinant channels (Hughes *et al.,* 2007). Elevations in PIP_2 have been shown to increase the open probability (P_o) by stabilizing the open state of homomeric and heteromeric $K_v7.2$-$K_v7.5$ channels, (Li *et al.,* 2005) although it does not appear to affect the unitary conductance of the channel (Li *et al.,* 2005). The apparent order of affinity of K_v7 channels to PIP_2 aligns with their maximal open probability (P_o), $K_v7.3 > K_v7.2/K_v7.3 > K_v7.2 > K_v7.4$ (Li *et al.,* 2004). The study by Li *et al.,* (2004), suggested that the differential open probability observed between the K_v7 subtypes may be governed by variations in their affinity to PIP_2. Brueggemann *et al.,* (2019), identified unique sites in N and C-terminals of $K_v7.5$ which altered the affinities of the channel to PIP_2. Their findings suggested that PKA-dependent phosphorylation of S53 in the N-terminus increased PIP_2 affinity, whereas PKC-dependent phosphorylation of the C-terminus reduced the PIP_2 affinity in $K_v7.5$ channels in smooth muscle cells (Brueggemann *et al.,* 2019).

When PIP_2 was applied cytosolically, it decreased the rundown of I_{Ks} currents, slowed their deactivation kinetics and shifted the activation $V_{1/2}$ negatively, suggesting it played a role in modulating voltage sensitivity of $K_v7.1$ channels (Loussouarn *et al.,* 2003). Various studies attempted to locate possible PIP_2 binding sites and have concluded that it required a cluster of basic residues interspersed between hydrophobic aromatic or acidic residues. A number of these clusters have been identified in S2-S3 and S4-S5 linker regions and also in the C-terminus region of channels. However, a number of studies have questioned the contribution of either the S2-S3 or S4-S5 linkers to PIP_2 binding in K_v channels (Aivar *et al.,* 2012; Telezhkin *et al.,* 2013).

It has been established that in $K_v7.2$-4, PIP_2 interacts in a region between the Helix A and Helix B, within a conserved cluster of basic residues - K452, R459 and R461 (Hernandez *et al.,* 2008; see Figure 1.5). However, although this cluster of basic residues is not present in $K_v7.1$, two other groups of basic residues (proximal C-terminus – K354, K358, R360, K362; distal C-terminus R539 and R555) have been identified as a potential PIP_2 interaction site (Park *et al.,* 2005; Thomas *et al.,* 2011). Tobelaim *et al.,* (2017) showed in their study that residues K526 and K527 in $K_v7.1$ Helix B form a critical site where CaM competes with PIP_2 to stabilize $K_v7.1$ channel open state. Interestingly, the LQT mutation K526E showed severely impaired channel function, as evidenced by a rightward shift in the voltage dependence of activation, a decrease in current amplitude and decreased Ca^{2+}/CaM sensitivity. The most recent cryo-EM structure of $K_v7.1_{EM}$+KCNE3+CaM complex (Sun & MacKinnon, 2020) suggests that PIP_2 opens the channel by inducing a very significant conformational change in the channel which is described in Section 1.5.3 (see Figure 1.10 A & B).

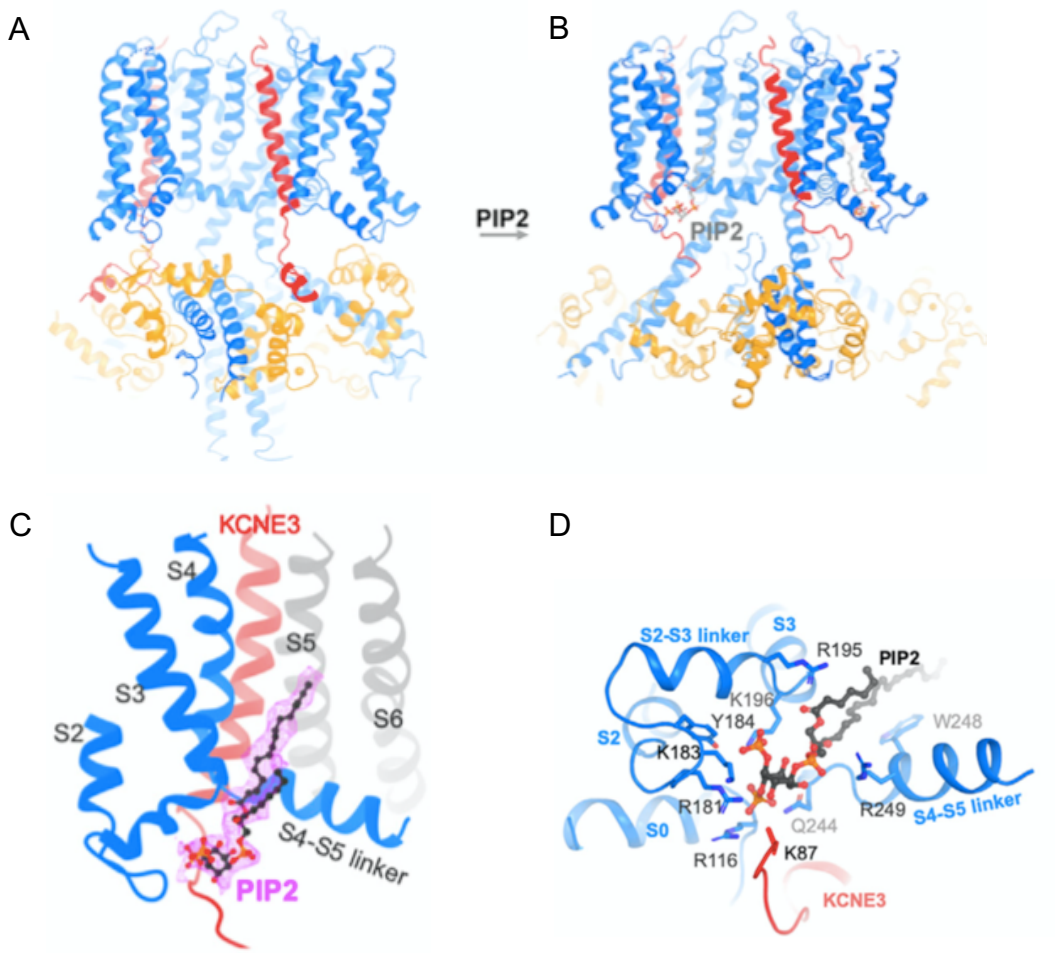

Figure 1.10: Conformational changes induced by PIP$_2$ and PIP$_2$ binding site in K$_v$7.1$_{EM}$+KCNE3+CaM complex: A) *Cryo-EM derived structural model of K$_v$7.1$_{EM}$-KCNE3-CaM complex in the absence and (blue - K$_v$7.1; red - KCNE3; orange - CaM)* ***B)*** *in the presence of PIP$_2$.* ***C)*** *Cryo-EM density of PIP$_2$ in K$_v$7.1$_{EM}$-KCNE3-CaM complex (red - KCNE3; blue & grey - K$_v$7.1 subunits; balls and sticks - PIP$_2$).* ***D)*** *side chains of residues in K$_v$7.1$_{EM}$-KCNE3-CaM complex that bind with PIP$_2$. (Adapted from Sun & MacKinnon, 2020).*

The above cryo-EM study also demonstrated the involvement of the S1, S2-S3 and S4-S5 linkers of K$_v$7.1, as well as the adjacent membrane region of KCNE3, in PIP$_2$ binding (Figure 1.10C & D; Sun & MacKinnon, 2020). Additionally, in a study by Tobelaim *et al.,* (2017), the conservation of homologous residues in helix B of K$_v$7.2 and K$_v$7.3 was reported, which conferred similar competition of Ca^{2+}/CaM with PIP$_2$ binding for their proximal C-termini. This calmodulin and PIP$_2$ binding site overlap confers more complexity to the regulation of K$_v$7 channels, where they might functionally cooperate to have an effect on the channel properties. Physiologically, the function of K$_v$7.2 and/or K$_v$7.3 channels was suppressed by enhanced calmodulin binding and was activated by PIP$_2$, whereas

$K_v7.1$ and I_{Ks} channels were enhanced by both PIP_2 and calmodulin (Brown *et al.,* 2007; Tobelaim *et al.,* 2017).

1.6.3 Phosphorylation

The K_v7 C-terminus also houses the modulatory sites for various protein kinases, including AKAP79/150, which forms a protein kinase C (PKC) trimeric complex (Hoshi *et al.,* 2003). PKC's direct involvement in K_v7 channels and how this interferes with CaM and PIP_2 mediated effects has been well established. Hoshi *et al.,* 2003 demonstrated that elimination of two putative PKC phosphorylation sites in Helix B of $K_v7.2$, lead to the inhibition of these currents. This was suggested to occur because removal of PKC phosphorylation prevented agonists from acting on $G_{q/11}$ coupled receptors (Hoshi *et al.,* 2003). Interestingly, in $K_v7.1$ channels the formation of AKAP79/150 complexes has not been demonstrated. However, these channels do interact with a separate Yotiao anchoring protein, which binds to protein kinase A (PKA) (Marx *et al.,* 2002).

The K_v7 C-terminus also acts as a substrate for tyrosine phosphorylation, via receptor- and non-receptor tyrosine kinases (Gamper *et al.,* 2003a). It was shown that the non-receptor tyrosine kinase Src, suppressed native M-currents as well as K_v7 channels in subunit-specific manner (Gamper *et al.,* 2003a). $K_v7.3$-$K_v7.5$ subunits were phosphorylated by Src kinase, which decreased the current amplitude and slowed activation kinetics by 2-fold (Gamper *et al.,* 2003a). In $K_v7.3$, Src recognized two tyrosine residues in the channel, one in the N-terminus (Y67) and one in the C-terminus at Helix A (Y349) (Li *et al.,* 2004a). Their data also indicated that Src kinase did not alter channel density at the plasma membrane but decreased the open probability of the channel (Li *et al.,* 2004a).

1.6.4 Regulation by ancillary subunits KCNE's

KCNE genes encode 5 single transmembrane domain proteins (KCNE1-5) which possess an extracellular N-terminus. These subunits were originally called *mink*, which stood for "minimal K^+ channel"). However, the KCNE subunits are non-conducting proteins, but do modulate K_v7 channels significantly (Takumi *et al.,* 1988; Abbott *et al.,* 1999) by altering their plasmalemma expression, biophysical properties and pharmacology (McCrossan & Abbott, 2004; Li *et al.,* 2006; Kanda & Abbott, 2012).

1.6.4.1 KCNE1

Co-expression of KCNE1 with $K_v7.1$ channel increased $K_v7.1$ current density, induced a positive shift in the voltage activation threshold, and slowed both activation and deactivation (Splawski *et al.,* 1997). Studies by Seebohm *et al.,* (2003) found that co-expression of KCNE1 with $K_v7.1$ stabilized the open conformation of the $K_v7.1$ pore by altering an interaction between the pore helix, the selectivity filter and the S5/S6 domain. Other studies have suggested that direct physical interactions between the S6 domain and KCNE proteins was the basis for KCNE-mediated modulation of $K_v7.1$ (Melman *et al.,* 2004), but this remains to be determined. KCNE1 was also suggested to alter the function of I_{Ks} by modulating the interaction between PIP_2 and the $K_v7.1$/KCNE1 complex (Li *et al.,* 2011). In the same study, four basic residues (R67, K69, K70 and H73) were identified in KCNE1 that play an important role in increasing the PIP_2 sensitivity of I_{Ks}. Structural studies have shown that for KCNE1, KCNE3 and KCNE5, a triplet of amino acids located in transmembrane domain of KCNE was crucial for modulation of $K_v7.1$ (Melman *et al.,* 2000; Angelo *et al.,* 2002).

1.6.4.2 KCNE2

KCNE2 was originally described as a modulator of the potassium current (Abbott *et al.,* 1999) encoded by the ether-à-go-go-related gene 1 (ERG1). Later it was also found to alter the gating mechanism dramatically in $K_v7.1$ channels (Tinel *et al.,* 2000). The $K_v7.1$/KCNE2 complex *in vivo* played an essential role in establishing the resting membrane potential in parietal cells of the gastric glands and in the intestines (Dedek & Waldegger, 2001; Jesperson *et al.,* 2004). KCNE2 makes the $K_v7.1$ channels constitutively open (Jespersen *et al.,* 2004). Mutations related to Long-QT syndrome have been associated with KCNE2 (Splawski *et al.,* 2000; Abbott *et al.,* 1999). A number of studies have documented that the expression of KCNE2 overlaps completely in the brain with $K_v7.1$ and also ERG1 channels (Splawski *et al.,* 2000; Abbott *et al.,* 1999). Given that both of these channels play an important role in the CNS, there was a possibility that KCNE2 could contribute to neuronal function significantly (Splawski *et al.,* 2000; Abbott *et al.,* 1999; Balijepalli *et al.,* 2007; Abbott, 2012).

1.6.4.3 KCNE3

In mammalian cells, co-expression of KCNE3 with $K_v7.1$, does not have any obvious effect on the I-V relationship of these channels, although it does accelerate activation and deactivation of the channels (Jespersen *et al.,* 2004; Mazhari *et al.,* 2002). However, when *Xenopus* oocytes are used as the expression system (Schroeder *et al.,* 2000), $K_v7.1$/KCNE3 co-expression resulted in currents with near-instant activation and an almost linear current-voltage (I-V) relationship. The altered current-voltage relationship has since been attributed to the structural binding of KCNE3 subunits to $K_v7.1$ in cryo-EM structure of $K_v7.1_{EM}$-KCNE3-CaM complex (Sun & MacKinnon, 2020). Four KCNE3 molecules bind to one $K_v7.1$ tetramer, thus supporting 4:4 stoichiometry. The interaction between KCNE3 and $K_v7.1$ occurs at two main sites. The first interaction site is in the cytosolic region, close to the CaM binding site and the second is where it binds to the transmembrane domains of $K_v7.1$ (Sun & MacKinnon, 2020). The binding of KCNE3 (also described in Section 1.3.2) shown in the cryo-EM structure of $K_v7.1_{EM}$+KCNE3+CaM indicates direct binding of KCNE3 to the bottom of S4 helix when the voltage sensors are in the depolarized (open) conformation. It stabilizes this contact in the depolarized state and, as a result, makes it more difficult for S4 to move downward at hyperpolarizing potentials. Thus, KCNE3 stabilizes and favours the depolarized conformation of the voltage sensors, effectively locking the channels in an open configuration (Sun & MacKinnon, 2020).

1.6.4.4 KCNE4

The KCNE4 subunit dramatically inhibits $K_v7.1$ current at physiologically relevant potentials when co-expressed in either *Xenopus* oocytes or mammalian cells. However, slowly activated currents can still be recorded, although potentials >50 mV are required to activate the channels (Bendahhou *et al.,* 2005; Grunnet *et al*., 2002; Grunnet *et al*., 2005). These effects of KCNE4 were attributed to effects on K_v7 channel gating, rather than altered surface expression (Grunnet *et al.,* 2002). Although the physiological function of KCNE4 is unclear, KCNE4 mRNA is expressed in significant levels in several tissues, including brain, that also contain $K_v7.1$ channels (Abbott, 2016). It is thought to interact with $K_v7.1$ primarily via its C-terminus (Manderfield & George, 2008; Manderfield *et al.,* 2009).

Interestingly, Strutz-Seebohm *et al.,* (2006), demonstrated that KCNE4 increased $K_v7.4$ current amplitude and negatively shifted the $V_{1/2}$ of activation, in stably transfected HEK cells. The PLA experiments by Jepps *et al.,* (2015), have shown that KCNE4 subunits co-localize with $K_v7.4$ and $K_v7.5$ in freshly isolated mesenteric smooth muscle cells. In the same study, it was proposed that KCNE4 was an important regulator of cell surface density and $K_v7.4$ function. Hence, the modulation of $K_v7.4$ by KCNE4 may have implications in various vascular diseases, such as hypertension.

1.6.4.5 KCNE5

$K_v7.1$/KCNE5 channels activate at potentials >40 mV in heterologous expression systems, suggesting that they are usually closed under physiological conditions (Angelo *et al.,* 2002; Bendahhou *et al.,* 2005). Piccini *et al.,* (1999) showed that KCNE5 mRNA is expressed in the developing embryo of the mouse and in several adult human tissues such as the brain, skeletal muscle and heart. However, later studies by Bendahhou *et al.,* (2005) contradicted this and suggested that KCNE5 expression in brain tissues was low.

1.7 Pharmacology of K_v7 channels

A variety of fairly selective synthetic small molecule K_v7 channel blockers and activators have been developed over the years (Tatulian *et al.,* 2001; Wickenden *et al.,* 2001; Wang *et al.,* 2001; Martire *et al.,* 2004; Xiong *et al.,* 2008; Wickenden *et al.,* 2008; Padilla *et al.,* 2009; Blom *et al.,* 2010). Potentiation of K_v7 channels by synthetic compounds is beneficial in treating diseases involving neuronal hyperexcitability, such as epilepsy and neuropathic pain (Lawson & McKay, 2006; Surti & Jan, 2005) and as mentioned earlier, may play an important role in helping to treat 'hypercontractile' smooth muscle as is the case in overactive bladder and ASM in COPD (Svalø *et al.,* 2011; Brueggemann *et al.,* 2012). The following section briefly describes the pharmacological properties of K_v7 channels blockers and activators.

1.7.1 K_v7 Inhibitors

Linopirdine [DuP 996, 1,3-dihydro-1-phenyl-3,3-bis(4-pyridinylmethyl)-2(H)-indol-2-one], is a derivative of phenylindolinone, which was originally developed

as a cognitive enhancer and a neurotransmitter release enhancer (Nickolson *et al.,* 1990). Aiken *et al.,* (1995) later found that it was an effective M-channel blocker (Aiken *et al.,* 1995). Linopirdine appears to be selective for K_v7 channels and does not affect other K_v channels substantially (Wang *et al.,* 1998). The IC_{50} for pan-K_v7 channel linopirdine block varies from 1.2 to 36 μM, depending on the heterogeneity of the molecular composition of the channels (Brown *et al.,* 2002; Wickenden *et al.,* 2001). In contrast, the linopirdine analog, **XE991** [10,10-bis(4-pyridinylmethyl)-9(10H)-anthracenone] was more effective and can block neuronal M current with an IC_{50} of about 1 μM, as well as $K_v7.2/K_v7.3$ currents and $K_v7.1$ currents with IC_{50}'s of 0.6 μM and 0.7 μM respectively (Wang *et al.,* 2001). Co-expression of K_v7 with KCNE1 appeared to alter the affinity of the K_v7 channel for XE991, since $K_v7.1$-KCNE1 channels were about 14-18 times less sensitive to XE991 than $K_v7.1$ alone (Wang *et al.,* 2001). Although these compounds appear relatively selective and have been utilised widely in laboratory based experiments (Schnee & Brown, 1998; Wladyka & Kunze, 2006), they are epileptogenic (Wang *et al.,* 2001; Brown & Passmore, 2009) and this rules out any clinical or therapeutic use (Zaczek *et al.,* 1998). Although XE991 was initially thought to be selective, Zhong *et al.,* (2010) demonstrated that it also blocked other K_v channels, albeit at voltages more positive than 20 mV. **Chromanol 293B** [trans-6-cyano-4-(N-ethylsulfonyl-N-methylamino)-3-hydroxy-2,2-dimethyl-chroman] has been shown to be an effective blocker of $K_v7.1$ channels (Gerlach 2003; Gerlach *et al.,* 2001). Likewise, the heteromultimer encoded $K_v7.1$-KCNE1 is inhibited by **JNJ282, L-768-673** and **HMR 1556** (Seebohm *et al.,* 2003; Towart *et al.,* 2009). The pharmacological selectivity of these inhibitors is modified by various KCNE isoforms (Lerche *et al.,* 2007). Hadley *et al.,* (2000) demonstrated that **tetraethylammonium** (TEA), also inhibited $K_v7.1$, $K_v7.2$ and $K_v7.4$ channels but had little effect on $K_v7.3$. The IC_{50} for TEA inhibition of $K_v7.2$ and $K_v7.2/3$ currents was 0.3 ± 0.02 mM and 3.8 ± 0.2 mM respectively, and these inhibitory effects had been attributed to the presence of a tyrosine residue (Y284) just downstream of GYG pore motif in $K_v7.2$ channels (Kavanaugh *et al.,* 1991; Hadley *et al.,* 2000). However, in TEA-sensitive $K_v7.1$ and $K_v7.4$ channels, there is no tyrosine at the same position, suggesting that other residues are important in determining TEA block of K_v7 channels (Hadley *et al.,* 2000).

1.7.2 K_v7 Activators

Flupirtine (D-9998; trade name Katadolon1) belongs to the triaminopyridine class and since 1984, has been used successfully in clinical practice in Europe, as a centrally active, non-opioid analgesic with muscle relaxing properties. Flupirtine was shown to enhance the activity of I_{KM} channels formed by homomeric assembly of $K_v7.2$ subunits close to the therapeutic concentration (2-6 μM, Martire *et al.,* 2004).

Retigabine (D-23129; N-(2-amino-4-(4-fluorobenzylamino)-phenyl) carbamic acid ethyl ester) is a potent activator of neuronal $K_v7.2$-$K_v7.5$ channels, which was derived from Flupirtine (Rostock *et al.,* 1996; Tatulian *et al.,* 2001). It was initially developed as an antiepileptic drug to specifically activate K_v7 channels and has been demonstrated to have clear anticonvulsant effects (Rundfeldt, 1997; Rundfeldt and Netzer, 2011). Retigabine affects each of the $K_v7.2$-$K_v7.5$ isoforms, with an EC_{50} of ~5 μM (Tatulian *et al.,* 2001; Wickenden *et al.,* 2001). It has three main effects on these channels (Tatulian *et al.,* 2001; Tatulian & Brown, 2003). Firstly, it caused a hyperpolarizing shift in the voltage of half-maximum activation ($V_{1/2}$). Secondly, retigabine affected the kinetics of the currents by accelerating the activation and delaying the deactivation, both of which are typical characteristics of open-state stabilization (Tatulian *et al.,* 2001). Thirdly, retigabine enhanced the maximal conductance (G_{max}) of K_v7 channels and this effect was due to an increase in maximum open probability of the channels (Tatulian & Brown, 2003). From chimera based studies between retigabine sensitive $K_v7.3$ and retigabine insensitive $K_v7.1$, Schenzer *et al.,* (2005) identified a single amino acid, tryptophan (W265) in the S5 domain to be a critical determinant of retigabine sensitivity (Schenzer *et al.,* 2005; Wuttke *et al.,* 2005). Mutational studies at the equivalent residue in other retigabine sensitive channels, $K_v7.2$ (W236L), $K_v7.4$ (W242L) and $K_v7.5$ (W235L) also exhibited loss of retigabine sensitivity (Schenzer *et al.,* 2005). Interestingly however, the introduction of a tryptophan in $K_v7.1$ in the equivalent position (L266W) did not result in retigabine sensitivity, although it changed other channel properties. This indicated that other residues were involved in retigabine binding to the channel. Wuttke *et al.,* (2005) showed that the highly conserved G301, a gating hinge residue within the $K_v7.2$ S6 segment (equivalent to G340 in $K_v7.3$), which is generally crucial for K_v7 channel gating (Seebohm *et al.,* 2006), is also critical to

the sensitivity of retigabine. This residue presumably permits flexibility of the S6 helix and may allow retigabine to access its binding site. Lange *et al.,* (2008), used homology modelling (based on $K_v1.2$) to reveal that residues W265 and L314 likely represent the outer limits of a well-defined retigabine binding pocket. Additionally, the same study suggested that T271 and L272, in the S5 helix, were likely to be important residues delineating the retigabine pocket (Lange *et al.,* 2008). Both L314 and L338, which are located in the pore loop and the S6 domain respectively, were shown to be critical for retigabine binding in heteromeric K_v7 subunit assemblies (Lange *et al.,* 2008).

ML213 (N-mesitybicyclo[2.2.1]heptane-2-carboxamide), was identified as an activator for $K_v7.2$, $K_v7.4$, $K_v7.5$ and $K_v7.4/K_v7.5$ heteromeric channels (Brueggemann *et al.,* 2014). It is a potent activator of $K_v7.2$ and $K_v7.4$ with EC_{50} values of 230 nM and 510 nM, respectively (Yu *et al.,* 2011). Brueggemann and co-workers (2014) found that the tryptophan residue W242L in $K_v7.4$ and W235L in $K_v7.5$, equivalent to retigabine binding residue in $K_v7.3$, was also critical for ML213 sensitivity. The same tryptophan residue has also been shown to be crucial for other activators including **(S)-1** [(S)-*N*-[1-(3-morpholin-4-yl-phenyl)-ethyl]-3-phenyl-acrylamide) and **BMS-204352** [(3S)-(1)-(5-chloro-2-methoxyphenyl)-1,3-dihydro-3-fluoro-6-(trifluoromethyl)-2H-indol-2-one], although these drugs have greater efficacy in activating $K_v7.4$ and $K_v7.5$ rather than $K_v7.2$ and $K_v7.3$ (Dupuis *et al.,* 2002; Bentzen *et al.,* 2006).

SF0034 is an activator of K_v7 channels which showed the highest affinity and efficacy for $K_v7.2/3$ channels. For example, although retigabine shifted the $V_{1/2}$ of $K_v7.2/3$ currents with an EC_{50} of 6.5 μM, SF0034 shifted the $V_{1/2}$ with an EC_{50} of 1.3 μM, which suggests that SF0034 is five times more potent than retigabine. It is another retigabine derivative and was developed by incorporating a fluorine substituent in the 3-position of the aminophenyl ring of retigabine. However, unlike retigabine, SF0034 did not alter the voltage dependence of either $K_v7.4$ or $K_v7.5$ homomeric channels. This selective activity of SF0034 suggested that it is a specific modulator of a subset of K_v7 and may therefore cause fewer side effects than retigabine. SF0034 appears to mediate its effects, rather like retigabine, through the intracellular end of the S5 helix, since both W236 in $K_v7.2$ and W265 in $K_v7.3$ appear important for mediating the channel's sensitivity to this compound (Kalappa *et al.,* 2015).

The acrylamide **(S)-2** activated K_v7.2-5 (Blom *et al.,* 2009), but its effects were quite complex. Although (S)-2 activated both K_v7.4 and K_v7.5, it had a bimodal effect on homomeric K_v7.2 and on K_v7.2/3 channels. In K_v7.2, (S)-2 caused a negative shift in the voltage-dependence of activation, slowed deactivation kinetics (τ_{deact}) and accelerated the fast component of the activation kinetics (τ_{act_fast}) (Blom *et al.,* 2009). The effect of (S)-2 on K_v7.2 can be divided into two main components: 1) the activating effect, which was visible as a voltage-dependent shift in activation $V_{1/2}$ and 2) an inhibitory effect, which could be observed as a decrease in current amplitude and an increased τ_{act_slow}. (S)-2 also increased the current amplitude at voltages below -10 mV and accelerated the slow activation kinetics portion (τ_{act_slow}). Nevertheless, the compound had a secondary inhibitory effect at voltages above -10 mV. The effect on the current amplitude and τ_{act_slow} crosses over at these depolarized voltages and becomes inhibitory. The excitatory effects of (S)-2 on K_v7.2 were lost when a leucine (K_v7.2-W236L) replaced the tryptophan residue in S5, but the inhibitory effects remained (Blom *et al.,* 2009).

SMB-1 is an analog of (S)-2, in which the amide group was methylated. Interestingly, it acted as an inhibitor of K_v7.2 channels but activated K_v7.4 channels (Blom *et al.,* 2014). The inhibitory effects of SMB-1 on K_v7.2 (IC_{50}=7.4 μM) was similar to the effect of (S)-2 on the W236L mutant channel. The excitatory effects on K_v7.4 relied on the tryptophan residue in S5 (Blom *et al.,* 2014). In addition, the K_v7.4-L305V mutant was insensitive to SMB-1, supporting the idea that SMB-1 causes activation via the retigabine binding site. On the other hand, SMB-1's inhibitory effect on K_v7.2 was not significantly dependent on the tryptophan residue in S5. However, the L275V mutation in K_v7.2 decreased 10 μM SMB-1 inhibitory efficacy, suggesting that its binding to K_v7.2 may occur close to this residue (Blom *et al.,* 2014).

Another group of K_v7 channel activators are called gating modifiers. These compounds appear to interact with the S1-S4 voltage sensing domain instead of the S5-S6 pore domain segment (Peretz *et al.,* 2010). This group of compounds includes the two structurally unrelated group of compounds: N-pyridyl and pyrimidine benzamides (ICA-27243, ICA-069673, and ztz240) and N-phenylanthranilic acid derivatives (diclofenac, meclofenamic acid (2-[2,6-

dichloro-3-methylphenyl) amino]benzoic acid) and NH29 (2-[(2, 6-dichloro-4-nitrophenyl)amino]-N-(hydroxymethyl)-3,5-dinitrobenzamide) (Peretz *et al.,* 2007; Wickenden *et al.,* 2008; Padilla *et al.,* 2009; Peretz *et al.,* 2010; Gao *et al.,* 2010; Amato *et al.,* 2011; Li *et al.,* 2013).

ICA-27243 (N-(6-chloropyridine-3-yl)-3,4-difluorobenzamide) was found to be 20 times more effective as an activator on heteromeric K_v7.2/7.3 channels (EC_{50}=0.4 μM) than homomeric K_v7.4 channels (EC_{50}=9.7 μM, Wickenden *et al.,* 2008; Padilla *et al.,* 2009). It was unable to activate homomeric K_v7.3 and only weakly activated K_v7.3/7.5 channels (EC_{50} of >10 mM) (Wickenden *et al.,* 2008; Padilla *et al.,* 2009; Blom *et al.,* 2010). **ICA-069673 (ICA73)**, which is a structural analogue of ICA-27243, appeared to be a relatively selective activator of K_v7.4 over K_v7.5 channels. Although it increased the current amplitude of K_v7.4 channels, 30 μM of the compound failed to enhance K_v7.5 current amplitude. In fact, when 100 μM ICA73 was applied to cells expressing K_v7.5 currents, it actually inhibited them in a voltage-dependent manner at potentials positive to -20 mV (Brueggemann *et al.,* 2014). Padilla *et al.,* (2009) utilised a chimeric approach with drug-sensitive and drug-insensitive subunits to demonstrate a novel binding site for ICA73, within the S1-S4 voltage sensor domain of K_v7 channels (Padilla *et al.,* 2009). More recently, Wang and co-workers (2018), have demonstrated different state-dependent actions of pore versus voltage-gated activators of K_v7 channels and also identified two point mutations, A181P and F168A in K_v7.2, that altered the sensitivity to ICA73. They found that the rate of ICA73 association with K_v7.2 closely tracked the voltage dependence of channel activation. Thus, the ICA73 association during the resting state was very slow until the channel is depolarized and presumably this 'opened' access to the binding site (Wang *et al.,* 2018). **Ztz240**, which is also structurally related to ICA-27243 and ICA73, was initially identified through the screening of approximately 20,000 compounds in the quest a K_v7.2-specific activator (Gao *et al.,* 2010). Ztz240 (10 μM) shifted the $V_{1/2}$ of K_v7.2 by -47 mV, K_v7.4 by -20 mV and K_v7.5 channels by -11 mV, but failed to have an effect on either K_v7.1 or K_v7.3 channels at same concentration (Gao *et al.,* 2010). Li *et al.,* (2013), later identified crucial residues in S2 and S4 domain that were proposed to form the binding pocket for ztz240 (E130, I134, F137, G138, R207 and R210). The S1 residue S105 and S3

residue M174 were also proposed to play important roles in the ztz240 binding pocket, in $K_v7.2$ channels (Li *et al.,* 2013).

The N-phenylanthranilic acid derivatives (fenamates), **diclofenac** and **meclofenamic** acid (2-[2,6-dichloro-3-methylphenyl) amino]benzoic acid, which are well known blockers of the cyclooxygenase enzymes COX-1 and COX-2 and used clinically as nonsteroidal anti-inflammatory drugs, have been identified as $K_v7.2$ and $K_v7.3$ activators with EC_{50} values of 25 μM and 2.6 μM respectively. They also exert robust antiepileptic properties *in vivo* (Peretz *et al.,* 2005). These compounds caused a hyperpolarizing shift in $V_{1/2}$ and slowed deactivation in $K_v7.2$ and $K_v7.3$ channels. Peretz and co-workers (2007) reported that **NH6**, (another fenamate) also had effects similar to that of meclofenamic acid and diclofenac.

A unique diphenylamine carboxylate derivative **NH29** was first identified to increase $K_v7.2$ currents with an EC_{50}=14 ± 2 μM (Peretz *et al.,* 2010). At -40 mV, NH29 (25 μM) enhanced $K_v7.2$ current amplitude by ~3.5 fold. However at positive potentials, the effects of NH29 became weaker and little change in maximal conductance was observed. In addition, NH29 significantly reduced both activation and deactivation rates. It also increased current amplitude of heteromeric $K_v7.2/K_v7.3$ with a similar potency to $K_v7.2$ homomeric channels. It weakly increased the homomeric $K_v7.4$ channel current (1.3 fold at -40 mV) but was ineffective on homomeric $K_v7.3$, homomeric $K_v7.1$ and heteromeric $K_v7.1$/KCNE1 channels (Peretz *et al.,* 2010). In the same study, it was established that NH29 did not interact with the retigabine site on $K_v7.2$, since it could potently stimulate W236L mutant channels, as evidenced by the negative shift in activation $V_{1/2}$. Through mutagenesis, chimera constructs and docking studies, Peretz *et al.,* (2010), identified several important residues; L197, L200, R198, R207 and R214 in S4, K120 in the S1-S2 loop and Y127 and E130 in the S2 subunit were all suggested to contribute to the effects of NH29 on $K_v7.2$.

Fasudil, the only clinically available RhoA/Rho kinase (ROCK) inhibitor was found to selectively activate only $K_v7.4/K_v7.5$ channels (Zhang *et al.,* 2016). 30 μM Fasudil was also found to slightly inhibit $K_v7.1$+KCNE1 currents but did not have any effect on $K_v7.2/K_v7.3$ currents. The selective effect of Fasudil on the vascular ($K_v7.4/K_v7.5$) versus neuronal K_v7 ($K_v7.2/K_v7.3$) made it a potentially

selective vascular relaxant (Zhang *et al.,* 2016). When applied to $K_v7.4$ and $K_v7.4/K_v7.5$ currents, Fasudil augmented the currents with EC_{50} of ~13 μM and 16 μM respectively. It increased the conductance of the channel and Fasudil also modestly shifted the G-V curves to more negative potentials (<-10 mV; Zhang *et al.,* 2016). In the same study, docking and mutational experiments helped identify two residues, namely V248 in S5 and I308 in the S6 helix of $K_v7.4$ which were critical for the selective activation by Fasudil in $K_v7.4$ channels (Zhang *et al.,* 2016).

Polyunsaturated fatty acids (PUFAs) and PUFA analogs are activators of $K_v7.1$ channels (Liin *et al.,* 2015). They modestly shifted the voltage dependence of channel opening negatively and also increased the maximal conductance of the channels (G_{max}). The EC_{50} for the PUFA analog, docosahexaenoic acid (DHA) was reported to be 50 μM in $K_v7.1$ channels and 70 μM DHA shifted the G-V curve by ~-10 mV (Liin *et al.,* 2015). Electrophysiology and molecular biology experiments have concluded that PUFA binds to both the voltage sensor domain and the pore domain to bring about its effects on $K_v7.1$ channels (Liin *et al.,* 2016; Liin *et al.,* 2018). The R218 residue in the S4 helix was important for the shift in $V_{1/2}$ and residue K316 in the S6 helix was critical for PUFA's effect on G_{max} (Liin *et al.,* 2016; Liin *et al.,* 2018). Those studies argued that the negatively charged PUFA head group was stabilized by electrostatic interactions with R218, R221 and K316 and the hydrophobic tail was reported to selectively bind to cassettes of hydrophobic residues. Further studies by Yazdi *et al.,* (2021) identified that the rigid saturated tail of stearic acid prevented close contacts with $K_v7.1$, whereas the mobile tail in linoleic acid bound to a hydrophobic pocket. In the same study, residue Y268 was identified as a critical PUFA binding residue important for fatty acid selectivity (Yazdi *et al.,* 2021).

Zinc pyrithione (ZnPy) also activates K_v7 channels and causes a substantial hyperpolarizing shift in voltage sensitivity as well as a pronounced decrease in the deactivation rate (Xiong *et al.,* 2007; Li *et al.,* 2004). The effects of ZnPy are primarily achieved by increasing open channel probability (P_o) and its efficacy follows the sequence $K_v7.5>K_v7.4>K_v7.2>K_v7.1$. ZnPy failed to activate $K_v7.3$ (Xiong *et al.,* 2007; Li *et al.,* 2004). ZnPy augments K_v7 activity at a site distinct from the retigabine binding site, as it is fully effective in potentiating the $K_v7.2$

(W236L) mutant. With respect to molecular determinants, Xiong *et al.,* (2007) proposed L249, L275 and A306 ($K_v7.2$) as important residues affecting ZnPy interaction with K_v7 channels. They found that the L249A:L275A double mutant and the A306T mutant reduced the effect of ZnPy on $V_{1/2}$ and G_{max} respectively.

R-L3 ([(3-*R*)-1,3-dihydro-5-(2-fluorophenyl)-3-(1*H*-indol-3-ylmethyl)-1-methyl-2*H*-1,4-benzodiazepin-2-one] is a benzodiazepine, that acts as a partial $K_v7.1$ channel agonist. It induces activation at concentrations up to 1 μM but block occurs when it is applied at 10 μM (Salata *et al.,*1998). In addition to altering the $K_v7.1$ current amplitude, R-L3 slowed channel activation and deactivation. In the presence of KCNE1 co-expressed with $K_v7.1$, the effects of R-L3 were reduced, suggesting that the presence of KCNE1 reduced R-L3 binding. Seebohm *et al.,* (2003) found a putative binding site for R-L3 near the S5 and S6 helices in $K_v7.1$ and suggested that residues Y267, I268, L271 and G272 (S5 domain), as well as F335 and I337 (S6 domain) were important. Additionally, molecular docking analysis identified G269 (S5 helix), V230 (S4 helix), F332 and A336 (S6 helix) in $K_v7.1$ as important residues which may help form the putative binding pocket for R-L3 (Seebohm *et al.,* 2003).

NS1643 [1,3-bis-(2-hydroxy-5-trifluoromethyl-phenyl)-urea] was discovered in 2006 as an activator that potentiated both recombinant and native hERG channels (Casis *et al.,* 2006; Hansen *et al.,* 2006) making it a promising candidate for treating LQT2 (Hansen *et al.,* 2006; Diness *et al.,* 2006). Li *et al.,* (2014), found that NS1643 also activated $K_v7.2$, $K_v7.4$ and $K_v7.2$/ $K_v7.3$ channels, but not $K_v7.1$ or $K_v7.3$ channels. It also had an inhibitory effect on the outward currents of $K_v7.1$/KCNE1 complex (Hansen *et al.,* 2006). The EC_{50} value of NS1643 on $K_v7.2$ channels was 2.44 ± 0.25 μM and its effects resemble those of retigabine (Li *et al.,* 2014). NS1643 is structurally similar to ztz240, which explains the same subtype selectivity pattern of these two compounds on K_v7 channels. It was also reported that the effects of both ztz240 and NS1643 involve residue F137 in $K_v7.2$ channels (Li *et al.,* 2014). Interestingly, the substitution of smaller hydrophobic side chains at F137 failed to alter NS1643 sensitivity, but substitution with a tryptophan (F137W) at this position completely abolished the effect of NS1643 (Li *et al.,* 2014). This suggested that ztz240 and NS1643 may interact differently on the residue to mediate their effects on K_v7 channels (Li *et al.,* 2014).

In sympathetic neurons and cloned $K_v7.2$ channels, the cysteine-modifying reagent **N-ethylmaleimide (NEM)** is known to have an excitatory effect (Shapiro *et al.,* 2000). At saturating voltages, whole-cell currents of $K_v7.2$, $K_v7.4$, and $K_v7.5$ but not $K_v7.3$ were increased by three to four-fold, and their voltage dependencies were shifted negatively ~ -20 mV in 50 μM NEM. The dose-response relationship of NEM on $K_v7.2$ channels yielded an EC_{50} of approximately 14 μM and shifted the $V_{1/2}$ of $K_v7.2$ and $K_v7.3$ channels by ~-15 and -10 mV respectively (Roche *et al.,* 2002). NEM also shifted the activation $V_{1/2}$ for $K_v7.4$ and $K_v7.5$ by ~-10 mV and ~-20 mV. Li *et al.,* (2004) also demonstrated that NEM increased the maximal open probability (P_o) of $K_v7.2$, $K_v7.4$, and $K_v7.5$ by ~4 fold, but had no effect on single channel conductance, consistent with the idea that the increase in current amplitude was due to an increase in P_o. $K_v7.3/4$ chimeras helped narrow down the site of NEM's action to the C-terminus (Li *et al.,* 2004). Furthermore, the C519A mutant in $K_v7.4$ was insensitive to NEM, supporting the idea that NEM mediated its effects via this residue (Li *et al.,* 2004).

Tannic acid (TA), enhances $K_v7.4$ and $K_v7.3/7.5$ K^+ currents approximately 3-fold (Zhang *et al.,* 2016a). The effects of TA on these channels is concentration dependent and the EC_{50} for both $K_v7.4$ and $K_v7.3/7.5$ was ~25 μM. Tannic acid also induced a significant negative shift in the *G-V* curve of the $K_v7.4$ and $K_v7.3/7.5$ currents (Zhang *et al.,* 2016a).

1.7.3 GoSlo-SR Compounds

Our lab has developed and patented a family of compounds called the GoSlo-SR compounds. These compounds are known to activate BK channels at physiological membrane potentials (Roy *et al.,* 2012; Roy *et al.,* 2014). Of all the members of GoSlo family, the effects of SR-5-6 and SR-5-130 have been most extensively examined by our group (Large *et al.,* 2015; Zavaritskaya *et al.,* 2020; Webb *et al.,* 2015; Hannigan *et al.,* 2016). SR-5-6 is a potent BK channel activator, which can shift the activation $V_{1/2}$ of BK channels by ~-100 mV in the presence of 100 nM Ca^{2+} (Roy *et al*., 2012). The related carboxylic acid derivative SR-5-130 has a similar efficacy to SR-5-6 (Roy *et al*., 2012) but requires β1 subunits to mediate its maximal effects on BK channels (Large *et al.,* 2015). In collaboration with Dr. Rudolf Schubert (University of Mannheim), it has

been shown that these two compounds induced vasodilation in rat *Gracilis* arteries (Zavaritskaya *et al.,* 2020), but this effect was not blocked by BK channel blockers. This suggested that vasodilation observed in the presence of GoSlo-SR-5-6 and GoSlo-SR-5-130 was due to other K^+ channels and not BK channels alone. This led to investigation of these two compounds on each of the K_v7 family members (Dudem, 2019). The effects of GoSlo-SR-5-6 and GoSlo-SR-5-130 on WT $K_v7.1$-$K_v7.5$ channels were successfully demonstrated. The figure below shows the maximal conductance (G/G_{max}) and activation $V_{1/2}$ summary data from this work (Figure 1.11 A & B).

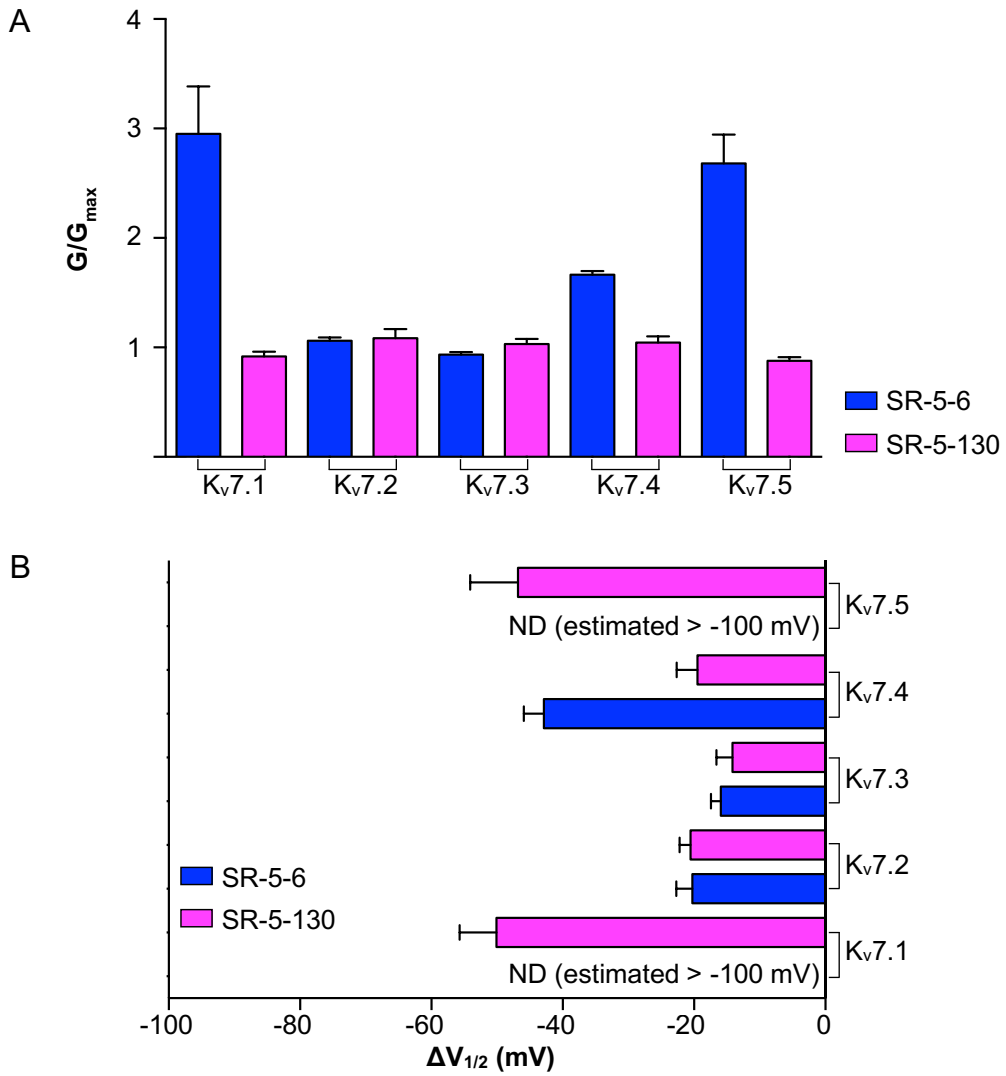

Figure 1.11: Comparison effects of SR-5-6 and SR-5-130 on K_v7 channels. A) *The effects of SR-5-6 on the maximal conductance of K_v7 channel subtypes. Compared to other K_v7 channels SR-5-6 increased the G_{max} of $K_v7.1$, $K_v7.4$ and $K_v7.5$. SR-5-130 failed to increase the maximal conductance of the K_v7 channel subtypes.* ***B)*** *The negative shift of the activation curve ($\Delta V_{1/2}$) of SR-5-6 and SR-5-130 on the K_v7 subtypes. SR-5-6 constitutively activated $K_v7.1$ and $K_v7.5$ channels. (Adapted from Dudem S. - PhD thesis, 2019).*

Thus, SR-5-6 appeared to activate all K_v7 channels but its efficacy followed the sequence $K_v7.1>K_v7.5>K_v7.4>K_v7.2>K_v7.3$. However, the effects of SR-5-6 were to constitutively activate $K_v7.1$ and $K_v7.5$, which made it difficult to study its effects on the kinetics of activation, etc. In $K_v7.2$ and $K_v7.3$, SR-5-6 failed to increase the maximal conductance (G/G_{max}) of the channels, however it did cause a small negative shift in $V_{1/2}$ (~ -20 mV). In $K_v7.4$ channels, SR-5-6 increased the G/G_{max} and shifted the $V_{1/2}$ by ~ -50mV without constitutively activating the channels and making it more suitable to examine its effects on current kinetics. It was reported that SR-5-6 slowed $K_v7.4$ deactivation and accelerated activation, characteristics typically associated with drugs that stabilize channels in the open state. Tables 1.3 & 1.4 below summarize these effects of SR-5-6 on the K_v7 subtypes.

	Activation $V_{1/2}$ in mV		**$\Delta V_{1/2}$**	**G_{max}**	
	Control	**SR-5-6**		**Control**	**SR-5-6**
$K_v7.1$	-26 ± 3	-	> 100	0.98 ± 0.01	2.95 ± 0.43
$K_v7.2$	-17 ± 3	-39 ± 5	-20 ± 3	0.98 ± 0.01	1.06 ± 0.02
$K_v7.3$	-45 ± 2	-61 ± 1	-16 ± 1	0.93 ± 0.02	0.93 ± 0.02
$K_v7.4$	-19 ± 2	-62 ± 2	-43 ± 3	0.98 ± 0.01	1.67 ± 0.03
$K_v7.5$	-29 ± 6	-	> 100	0.99 ± 0.01	2.87 ± 0.21

Table 1.3: SR-5-6 effects on $K_v7.1$-$K_v7.5$ channels. *The effects of 10 μM SR-5-6 on the activation $V_{1/2}$ and the maximal conductance of K_v7 channel subtypes. SR-5-6 constitutively activated $K_v7.1$ and $K_v7.5$ channels. (Adapted from Dudem S. - PhD thesis, 2019).*

	$\tau_{activation}$ at +40 mV		**$\tau_{deactivation}$ at -120 mV from +40 mV**	
	Control	**SR-5-6**	**Control**	**SR-5-6**
$K_v7.1$	12 ± 1	-	53 ± 4	-
$K_v7.2$	70 ± 6	55 ± 7	12 ± 1	21 ± 2
$K_v7.3$	21 ± 3	18 ± 2	17 ± 2	132 ± 25
$K_v7.4$	126 ± 8	71 ± 6	14 ± 1	45 ± 5
$K_v7.5$	105 ± 12	-	27 ± 3	-

Table 1.4: SR-5-6 effects on kinetics of K_v7 subtypes. *The effects of 10 μM SR-5-6 on the $\tau_{activation}$ at +40 mV and the $\tau_{deactivation}$ at -120 mV of K_v7 channel subtypes. (Adapted from Dudem S. - PhD thesis, 2019).*

The GoSlo-SR compounds are anilino-anthraquinone derivatives (Figure 1.12) and structure-activity studies carried out in our lab demonstrated that the sulfonate group on the C-ring was essential for maximal activity on $K_v7.4$ channels.

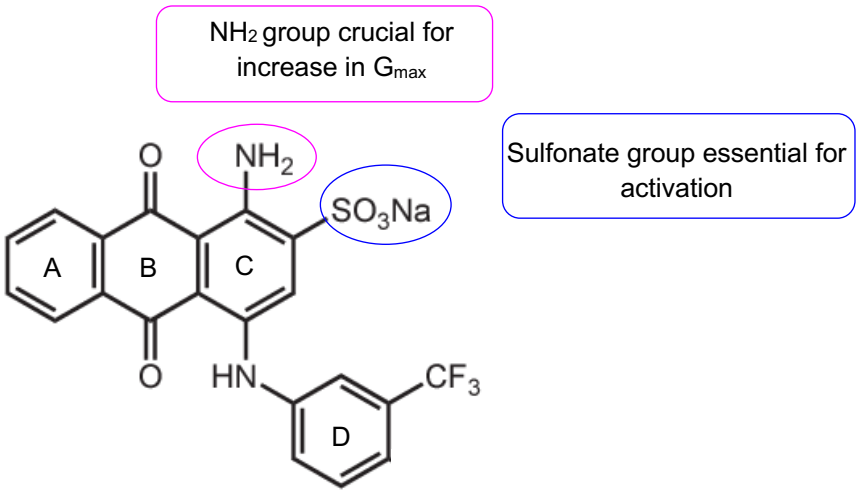

Figure 1.12: Structure of GoSlo-SR-5-6. *Representation of the structure of GoSlo-SR-5-6. Structure-activity relationship (SAR) of SR-5-6 on K_v7.4 channels, demonstrated that the sulfonate group on C-ring and the hydrophobic D-ring were essential for K_v7.4 activity (Adapted from Roy et al., 2014).*

As the SAR of GoSlo-SR compounds indicated that SR-5-6 was an efficacious activator of K_v7.4 channels, Dudem (2019) investigated which residues could contribute to the effects of SR-5-6. Through mutational studies, it was found that the retigabine binding mutation W242L in K_v7.4 did not abolish the effects of SR-5-6. The most effective mutation that reduced the effects of 10 μM SR-5-6 on K_v7.4 channels was F322A on the S6 helix. Further studies in collaboration with Dr. Irina Tikanova (Queen's University, Belfast) identified a hydrophobic binding pocket close to F322A. Although this docking study identified a number of residues around this pocket, none of these mutations reduced the drug effect, suggesting that this proposed hydrophobic pocket was not involved in SR-5-6 binding to K_v7.4. Therefore, the location of the binding site for SR-5-6 and other GoSlo family members remains to be determined.

1.8 Aim and objective of the project

This thesis aims to elucidate the molecular mechanisms underlying the effect of SR-5-6 on the activation of K_v7.4 channels, in an attempt to identify a binding site for K_v7 openers which may be useful for future drug development studies. It was decided to examine the effects of SR-5-6 on K_v7.4 because these channels expressed robustly when transfected in HEK cells and SR-5-6 caused

reproduceable changes in G/G_{max} and $\Delta V_{1/2}$. Therefore, the experiments presented in this thesis focused on three main objectives:

1) Determining the residues important for SR-5-6 activity in $K_v7.4$ channels.

2) Investigating if domain swap chimeras of $K_v7.3$ and $K_v7.4$ channels altered the effects of SR-5-6.

3) Establishing if mutations of putative PIP_2 binding residues reduced the effects of SR-5-6 on $K_v7.4$ channels.

Chapter 2

Materials and Methods

2.1 $K_v7.3$ - $K_v7.4$ plasmid constructs

The human $K_v7.3$ and $K_v7.4$ plasmid constructs were a kind gift from Dr. Nicole Schmitt and Prof. SP Olesson, University of Copenhagen. $K_v7.3$ (NM_004519.3) and $K_v7.4$ (NM_004700.3) genes with the mentioned accession number were cloned into pcDNA3.1 vector.

2.2 Preparation of competent cells

The calcium chloride method was used for competent cells preparation. Prior to the start of the procedure, 0.1 M $CaCl_2$, 0.1 M $MgCl_2$ and LB broth was prepared and autoclaved for competent cells preparation. At first the *E. coli* DH5α bacterial strain was streaked onto a LB agar plate and incubated at 37ºC overnight to get single isolated colonies. The following day, a single colony was picked and inoculated in 10 ml of LB media (starter culture). This was incubated again for overnight growth at 37ºC at 220 rpm in a shaker incubator. The next day, subcultured from the starter culture, 0.1-0.5% of the bacterial cells in 200 ml LB broth. This was incubated in the shaker incubator (37ºC, 220 rpm) until the OD reached 0.6. Cell growth was arrested by incubating on ice for 30 mins, followed by pelleting the culture at 3000 rpm for 10 mins. The pellet was then resuspended and pelleted sequentially firstly with ice cold 0.1 M $MgCl_2$ and then with ice cold 0.1 M $CaCl_2$. Finally the cells were resuspended in ice cold 1200 µl 0.1 M $CaCl_2$ with 20% glycerol. This resuspension was aliquoted (30-50 µl) and stored at -80ºC for future use.

2.3 Transformation

The transformation was carried out with *E. coli* (DH5α) chemical competent cells. The protocol was as follows: 50 µl of competent cells were incubated with the plasmid construct, on ice for 30 mins, which allowed the plasmid DNA to attach to the cells. Next, cells were heat shocked for 30 secs in a 42ºC water bath, which shifted the polar heads in the plasma membrane, allowing the entry of the plasmid into cells. Subsequently, the cells were incubated on ice for 2 mins in order to restore the polar heads of the membrane lipids back to their native state. Immediately after this, 200 µl of SOC (Super Optimal broth with Catabolite repression) media was added to the cells and incubated at 37ºC in a shaker

incubator for 1 hour to permit cell recovery. Finally, cells were plated on agar plates for overnight incubation.

2.4 Mutagenesis

2.4.1 Point mutations with the Phusion method

K_v7.4 point mutations were carried out using Phusion Hot Start II DNA polymerase method (Xia *et al.,* 2015). The mutagenesis protocol consists of 3 main steps: 1) PCR amplification of template DNA, 2) DpnI digestion of PCR product and 3) Ligation of PCR product, as illustrated in Figure 2.1 below.

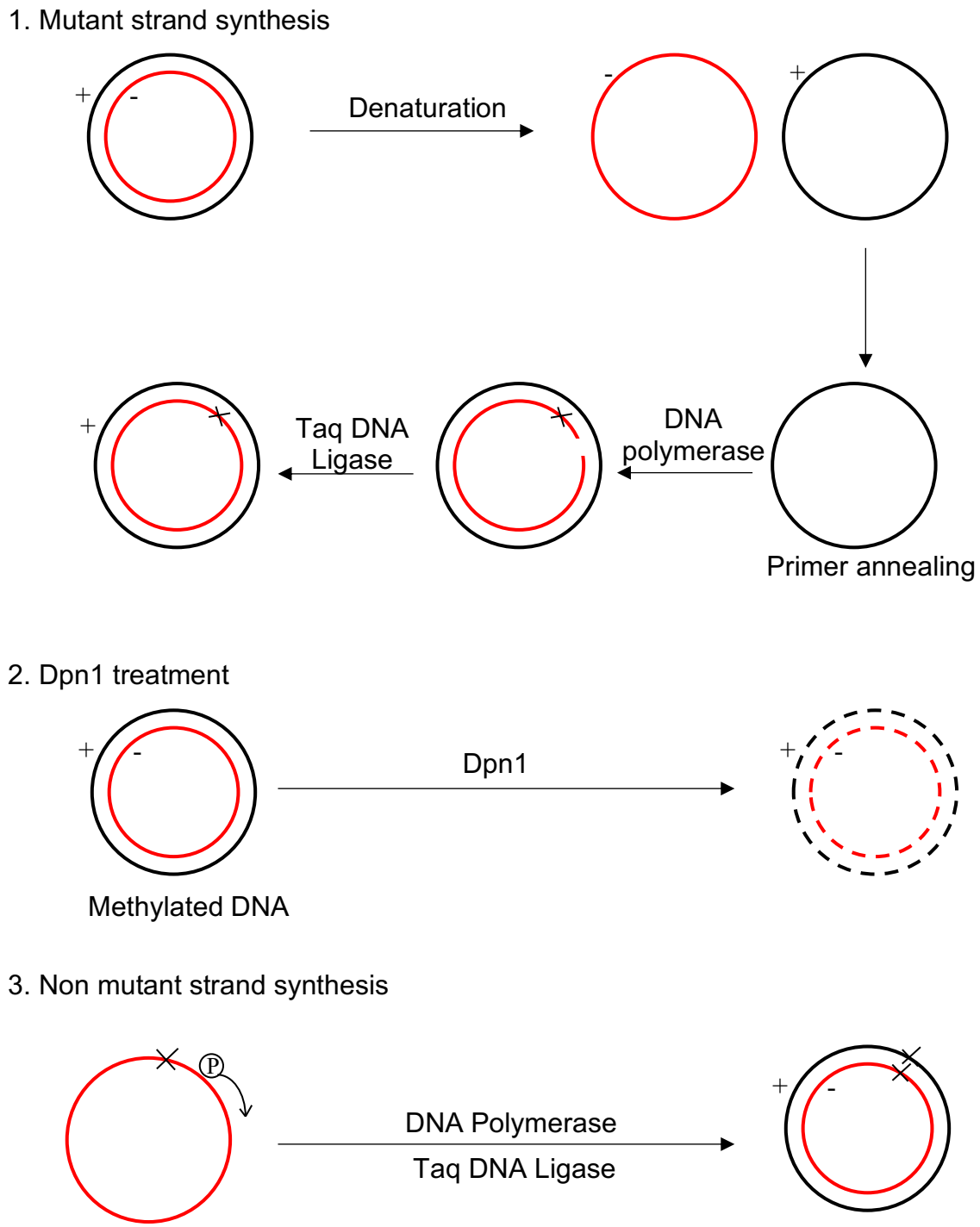

Figure 2.1: Schematic representation of Site Directed Mutagenesis (SDM). *The mutagenic primer was designed on a minus strand. The DpnI digested methylated template DNA strands are shown by dotted lines. The PCR based synthesized DNA strands are indicated by solid lines. X indicates introduced mutations.*

2.4.1.1 PCR amplification of template DNA

100 pg - 1 ng template DNA was used for each 50 µl PCR reaction. In this method, two primers (Forward and Reverse) were utilized for PCR amplification.

Point mutations were designed in the middle of the forward primer with 10-15 perfectly matched nucleotides on each side as shown in Figure 2.1. Primers were designed on both sides of the deleted segment for deletion mutants as shown in Figure 2.1. The forward primer was designed on the sense strand and the reverse primer was designed on anti-sense strand of plasmid DNA. Primers were phosphorylated with T4 polynucleotide kinase on the 5' end before PCR amplification. The 50 µl PCR reaction contained the following components:

Template DNA	100 pg - 1 ng
Forward primer	0.5 µM
Reverse primer	0.5 µM
10mM dNTP	1 µl (10 mM)
5x Phusion buffer	10 µl
Phusion DNA polymerase	0.5 µl
ddH_2O	to 50 µl

The temperature program of PCR is shown below:

Step	Temperature	Time	Cycles
Initial Denaturation	98ºC	10 secs	1
Denaturation Annealing Extension	98ºC 65-72ºC 72ºC	10 secs 30 secs 3 - 5 mins	25
Final extension	72ºC	10 mins	1

By the end of the PCR cycle, the reaction mixture contained the amplified PCR product either with a deleted region or a point mutation introduced at the site of interest. The amplified PCR product was analyzed with agarose gel electrophoresis.

2.4.1.2 Dpn1 treatment

After the PCR amplification, the reaction mixture will contain the native template and the mutated, hemi-methylated dsDNA (a hybrid of mutant strand and the template sense strand), which both have a high efficiency for transformation. In order to eliminate unmutated methylated DNA, a DpnI restriction enzyme

digestion was carried out at 37ºC for 1 hour. This enzyme detects the methylated adenines in the dsDNA and cleaves them.

2.4.1.3 Ligation of PCR product

The amplified PCR product was then circularized using T4 DNA ligase. A 20 µl ligation reaction consisting of the following components was performed at room temperature for 2 hours:

PCR product	3 µl (approximately 10 - 20 ng DNA)
10x T4 DNA ligase buffer	2 µl
T4 DNA ligase	1 µl
dd H_2O	15 µl

T4 DNA ligase catalyzes the phosphodiester (PDE) bond between 5' phosphate and 3' hydroxyl of juxtaposed DNA. The PCR primers were initially phosphorylated with T4 PNK. The ligated PCR product was then transformed into *E. coli* cells (section 2.3). A BIOLINE Isolate II Plasmid Mini Kit (BIO-52057) was used to isolate the mutant protein-containing plasmid after transformation. The mutant plasmids were then sequenced, which was outsourced to Source BioScience (results not shown).

2.5 Chimera cloning method

The production of $K_v7.4$:$K_v7.3$ domain swap chimeras involved the following five steps –

- Insertion of restriction sites - site directed mutagenesis (PCR)
- Restriction digestion
- CIP treatment and PCR purification
- Ligation and Transformation
- Restriction site removal via site directed mutagenesis (PCR)

Figure 2.2 summarizes the method used for chimera production and each step is described in more detail below.

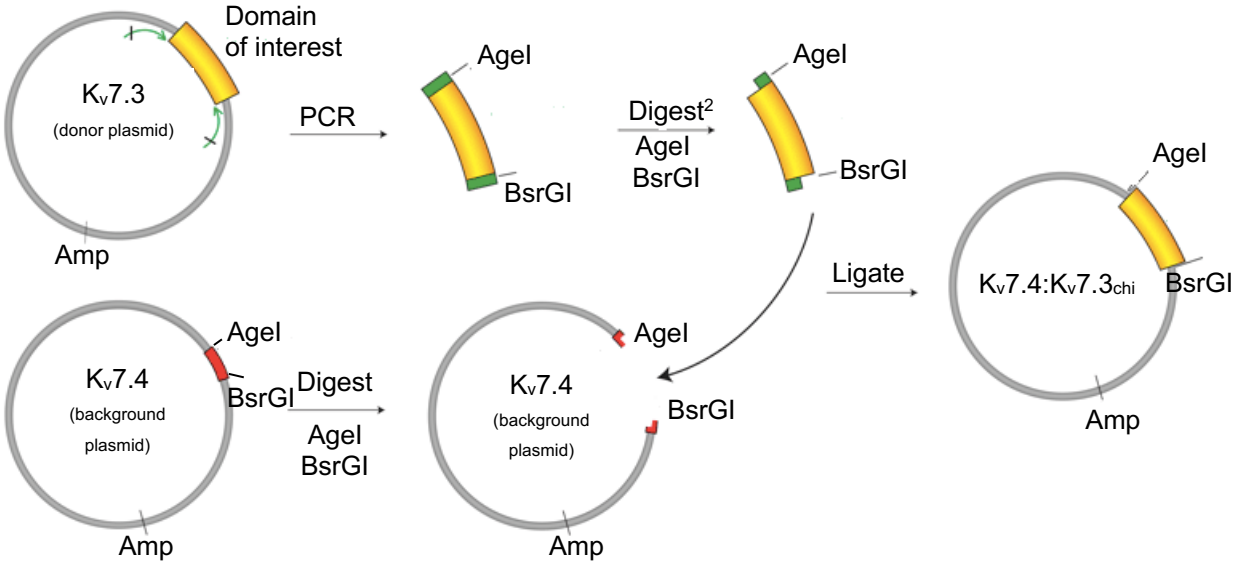

Figure 2.2: Representative diagram for the construction of chimeras through molecular cloning method. *Step1 – insertion of the restriction sites (AgeI and BsrGI) in both K_v7.4 and K_v7.3 using site directed mutagenesis. Step 2 – digestion of both donor plasmid and background plasmid with AgeI and BsrGI restriction enzymes to get sticky ends. Step3 – Ligation of the domain of interest and the background K_v7.4 plasmid. The circles represent the plasmids carrying K_v7.3 and K_v7.4 genes as labelled. The yellow rectangle is the domain we were interested to clone from K_v7.3 into K_v7.4. After the ligation, the chimeras cloning involved the removal of the restriction site through PCR which is not shown in the above figure (Adapted from Addgene).*

2.5.1 Insertion of restriction sites - site directed mutagenesis (PCR)

The first step in the chimera cloning method was to identify unique restriction sites that were not already present in the K_v7.4, K_v7.3 and pcDNA3.1 plasmid sequences. SnapGene Viewer (https://www.snapgene.com/snapgene-viewer/) was used to identify the already present restriction sites. Then, the NEB catalogue of restriction sites (https://international.neb.com/products/restriction-endonucleases) was utilized to identify two unique restriction sites - AgeI and BsrGI. The insertion of AgeI at the 5' end of the domain of interest and BsrGI at the 3' end of the domain was carried out using the site directed mutagenesis method with Phusion Hot Start polymerase. The restriction sites were added at the start of the forward primers for both insertions. The protocol for this step was same as described in Section 2.4.

2.5.2 Restriction digestion

Once $K_v7.4$ and $K_v7.3$ clones were generated with the restriction sites at the 5' and 3' end of the domain of interest, next the product was digested using the following digestion mixture:

PCR product	20 µl (approximately 10 µg DNA)
AgeI	4 µl
BsrGI	4 µl
10x CutSmart buffer	5 µl
dd H_2O	17 µl
Total	50 µl

The digestion mix was incubated at 37ºC for an hour followed by 20 mins at 65ºC to inactivate the enzyme. Once inactivated, the digestion mix was run on a 0.7% agarose gel to separate the backbone and insert. The backbone ($K_v7.4$/ $K_v7.3$ plasmid) and the insert (domain of interest) were then gel purified using the QIAGEN gel purification kit.

2.5.3 Alkaline Phosphatase, Calf Intestinal Phosphatase (CIP) Treatment

The backbone was next treated with phosphatase to remove the phosphate group in order to prevent background colonies being transformed post ligation. The CIP treatment reaction mixture contained the following components:

DNA	1 µg DNA
10x CutSMart Buffer	2 µl
CIP	1 µl
dd H_2O	to 20 µl

The backbone was incubated at 37ºC for 30 minutes, prior to purification with a PCR purification kit (QIAGEN PCR Purification Kit). The product was then used for ligation with the insert of interest.

2.5.4 Ligation and transformation

The backbone (vector) and the insert were then ligated using the T4 DNA ligase. The concentration of insert (ng insert) was calculated using the formula given below:

$$\frac{Insert\ size(kb)}{vector\ size(kb)} \times \frac{insert}{vector} = \frac{ng\ insert}{ng\ vector}$$

(mass ratio) (desired molar ratio)

100 ng of vector and 1:10 desired molar ratio were used, to calculate the amount of insert to be used for chimera cloning ligation. For example; if the insert size = 132 bp and vector size = 7414 bp, then using the above formula for 100 ng of vector and 1:10 molar ratio, the concentration of insert can be calculated as -

ng insert = (132/7414) x (10/1) x 100

= 17.8 ng

The ligation protocol is same as described in the Section 2.4.1.3, except that the ligation mix was incubated overnight at 16ºC. The no-ligase control and the no-insert control were also set up along with a full ligation mixture. This was to avoid false positive clones in the full reaction plate. The ligation mix after overnight incubation was transformed using *E. coli* (DH5α) chemical competent cells. The protocol is described in Section 2.3.

2.5.5 Removal of restriction sites

Once the positive clone was identified through sequencing, the restriction sites were removed by a site directed mutagenesis protocol using the Phusion Hotstart polymerase enzyme as detailed in Section 2.4. The primers were designed for deletion of the restriction sites from both 5' and 3' end of the domain of interest.

2.6 Cell culture

Human embryonic kidney 293 (HEK293) and Chinese hamster ovary (CHO) cells are commonly utilized as hosts for expressing recombinant ion channel proteins

in order to investigate their structural, biophysical, and pharmacological properties (Baldi *et al.,* 2007; Dalton & Barton, 2014). HEK293 cells are an ideal heterologous system for membrane protein expression as they feature the post-translational modification machinery essential for target protein folding and/or biological activity. They also have higher transfection efficiency, faithful translation, and protein processing (Wurm, 2004) than other mammalian cells, such as CHO cells, resulting in higher protein yields (Backliwal *et al.,* 2008; Bollin *et al.,* 2011). These characteristics, along with cell size, morphology, rapid division rate, ease of maintenance, and the ability to express transgenic receptor proteins and ion channels with high fidelity (Thomas & Smart, 2005), have made HEK293 cells the host of choice for transient heterologous expression of membrane proteins for electrophysiology applications (Lemtiri-Chlieh & Ali, 2013; Ooi *et al.,* 2016). Studies from the SMRC in DKIT have demonstrated that HEK293 cells offer a robust platform for ion channel expression (Webb *et al*., 2015; Dudem 2019; Dudem *et al*., 2021), with little contamination from endogenous currents (Dudem, 2019) and stable gigaseals (Ponce *et al.,* 2018), which permits the continuous recording of overexpressed channels over many minutes. As a result, HEK293 cells were chosen as the expression system in this investigation.

HEK293 cells were cultured in DMEM+MEM media containing 10% FBS and 1% penicillin, streptomycin antibiotics at 37ºC and 95% humidifying incubator containing 5% CO_2. Subculturing was carried out after treatment with 0.05% Trypsin-EDTA (Gibco, Thermo Fisher Scientific) solution for 2 - 3 mins after rinsing with sterile 1X PBS. Initially, HEK293 cells were cultured in 100 mm dishes. The confluent 100 mm dish had 9 x 10^6 cells. While subculturing, the confluent 100 mm dish was trypsinised and dissolved in 9 ml of growth media. Then, these cells were seeded in 35 mm dishes (2 ml growth media) with 1 x 10^5 cell density in each dish. After 18-24 hours of seeding, each 35 mm dish contained 40- 50% of cell density ($4x10^5$), at this stage dishes were transfected with the desired mutated clone.

For storage of cells, 10% DMSO containing growth medium was added to an equal volume of cells after trypsinisation and allowed to freeze slowly at -80ºC for 30 min. Cell vials were stored in liquid nitrogen for long term storage. For cell

revival, the HEK293 cell vial from liquid nitrogen was immediately thawed at 37ºC and suspended in falcon tube containing 5 ml of growth media. These falcon tubes were centrifuged at 2000 rpm for 3 min to collect the cell pellet. The DMSO content was also removed by this process. Later the cell pellet was dissolved in 5 ml of fresh growth media and plated in a T25 flask.

2.7 Transfection methods

All K_v7.4 WT, K_v7.3 WT, K_v7.4 mutant and chimera plasmids were co-transfected into HEK293 cells with GFP encoding plasmids using the lipofectamine method (Xia *et al*., 2015) as detailed below.

2.7.1 Lipofectamine transfection

The day before transfection, cells were plated in 35 mm dishes at 30-40% density. Plasmid construct (K_v7.1-K_v7.5) complexes were diluted in 100 µl serum free media. In another tube, lipofectamine reagent (0.3 µl for 100 ng DNA) was diluted in 100 µl serum free media. These two solutions were mixed together and incubated for 30 mins at room temperature. Cells were replaced with serum and antibiotic free media before transfection. Following 30 mins of incubation at room temperature, the 200 µl transfection mixture was added to the dish, drop by drop. After a further 4 hours, the transfection was stopped by replacing the media in each dish with fresh growth media.

2.8 Electrophysiology

The voltage clamp technique was invented by Hodgkin and Huxley (1952) and later the patch-clamp technique was described by Neher and Sakmann (1976). The current clamp and voltage clamp are the two configurations of the patch clamp technique most commonly used. In this study, the voltage clamp method was employed throughout to permit the cell voltage across the membrane to be controlled and the resultant currents from voltage steps to be measured.

To carry out voltage clamp recording on HEK cells in this study, a glass pipette was filled with whole-cell K^+ pipette solution (see Section 2.11.2) and inside the glass pipette, a chlorided silver electrode was present. A similar silver electrode was present in the bath which acts as an earth electrode. The pipette was then steered towards the surface of the HEK cell under study and an attempt was

made to form a gigaseal between the cell membrane and the glass pipette. To help promote gigaseal formation, gentle suction was applied after the tip of the pipette touched the surface of the HEK cell. Typically, these gigaseals had an electrical resistance of more than 10 gigaohms (GΩ), prior to breaking into the cell. The formation of such a high resistance seal not only isolates the membrane patch from the external solution and thus allows the experimenter to record ionic currents across the cell membrane, but it also ensures that background noise is reduced.

In this study, the whole cell configuration of the patch clamp technique (Hamill *et al.,* 1981) was used to study K_v7 channel currents in WT and mutant K_v7 channels. Strong suction was also used to rupture the cell membrane after generating a gigaseal in this configuration, thus allowing the pipette to have direct contact with the cytoplasm and permitting the flow of currents across the cell membrane to be recorded.

The electrode and pipette are electrically continuous and were linked to the amplifier's negative input (-), while the experimenter's voltage, also known as command potential (V_{com}), was attached to the positive input (+). The presence of a feedback resistor between the output and negative input permitted the comparison of the pipette (V_p) and V_{com} voltages. When V_p and V_{com} differ, a compensatory current is injected into the cell via the feedback loop, in order to ensure that $V_p = V_{com}$ at all times. This compensatory current represents the ionic flux across the membrane and effectivelty permits the recording of curents flowing across the cell membrane.

The bath was constantly perfused with Hanks and, as illustrated in Figure 2.3, drugs were delivered to the bath via a custom-built gravity-fed, drug-perfusion system. A number of 20 ml syringes were elevated above the bath and small bore tubing delivered drugs to a central 1 ml syringe. The small bore tubing terminated in this syringe and these were secured in place using silicon sealant which was hardened overnight, prior to use. A glass pipette ~ 200-300 µm in diameter was attached to the 1 ml syringe via appropriately sized silicon tubing and placed roughly 300 µm away from the cell to allow direct delivery of a drug or solution to the cell under study. This could be switched, with a dead-space time of around five seconds to a solution containing a drug.

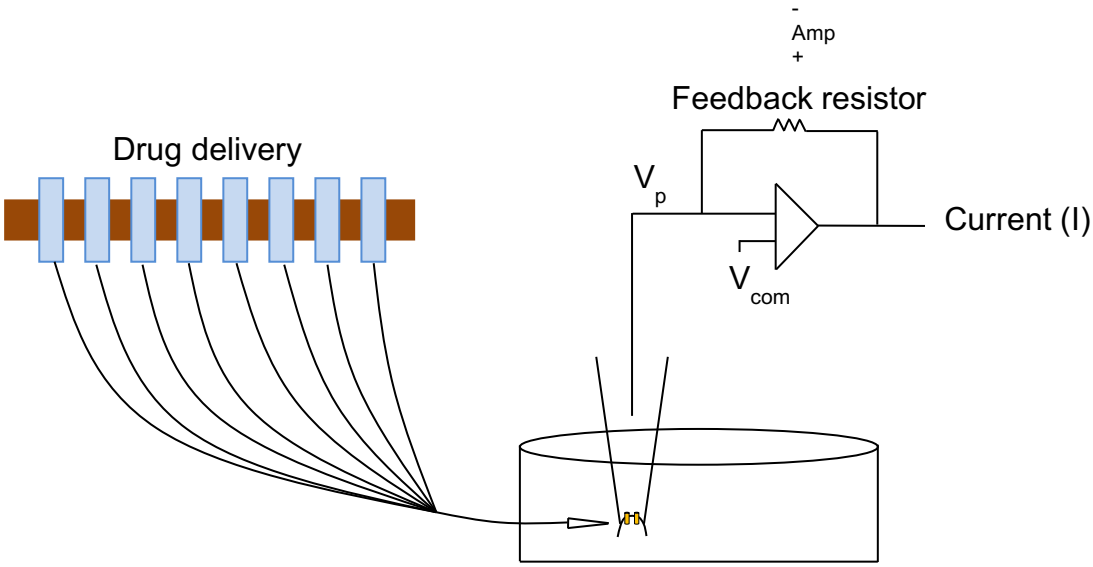

Figure 2.3: Diagrammatic representation of the patch clamp setup. *An electrolyte solution is filled in the glass pipette and a tight seal is formed with the cell membrane. The current flowing through the channels is recorded by a silver electrode which is connected to an amplifier. The intracellular environment can be altered by a gravity fed drug delivery system.*

2.8.1 Patch clamp recordings

Electrophysiology recordings were made from single HEK cells expressing human $K_v7.4$, $K_v7.3$ and $K_v7.4$ mutant channels, 24-48 hours post transfection. Throughout the experiments, the dish with HEK cells was superfused with Hanks solution in addition to the drug delivery system described in Section 2.8. All experiments were carried out at room temperature. The patch pipettes were pulled from thin walled borosilicate glass (1.5 mm OD x 1.17 mm ID.; Clark Medical Instruments) to a tip of diameter approximately 1-1.5 µm and a resistance of 2.5 MΩ, using a Sutter P-97 micropipette puller. Voltage clamp commands were delivered via an Axopatch 200A amplifier (Axon Instruments) and digitized using a Digidata 1322A AD/DA converter (Axon Instruments). The leak currents were subtracted offline, by manual leak subtraction. pCLAMP software (Clampex and Clampfit 10) was utilized for stimulus generation, data acquisition and analysis. The data was acquired at 10 kHz and filtered at 2 kHz. Excess 50 Hz electrical noise was eliminated using a HumBug (Quest Scientific) which was

inserted between the amplifier and digitizer. Attempts to compensate for series resistance using the Axon 1D amplifier series resistance compensation circuitary were fruitless, since the circuitry continually began to 'ring' and seals were continuously lost. Consequently, series resistance was not routinely compensated for, but the series resistance errors were estimated to be <15 mV, as detailed in Section 2.8.5.

2.8.2 Current, voltage and resistance

The electrical activity of a cell is determined by the movement of charged ions such as Na^+, Ca^{2+}, K^+, and Cl^- across the cell membrane. Current is the movement of ions across the cell membrane, which is controlled by the driving force. Voltage (V, measured in millivolts) is the energy required to move ions, and current is the flow of ions (I, measured in amperes). Ions travel through ion channels embedded in the cell membrane because the cell membrane does not enable them to freely permeate across it.

The relationship between current, voltage, and resistance (R, measured in ohms, Ω) is defined by Ohm's law:

$$V = IR \qquad \text{(Eq 2.1)}$$

Rearranging this equation yields:

$$I = V/R \qquad \text{(Eq 2.2)}$$

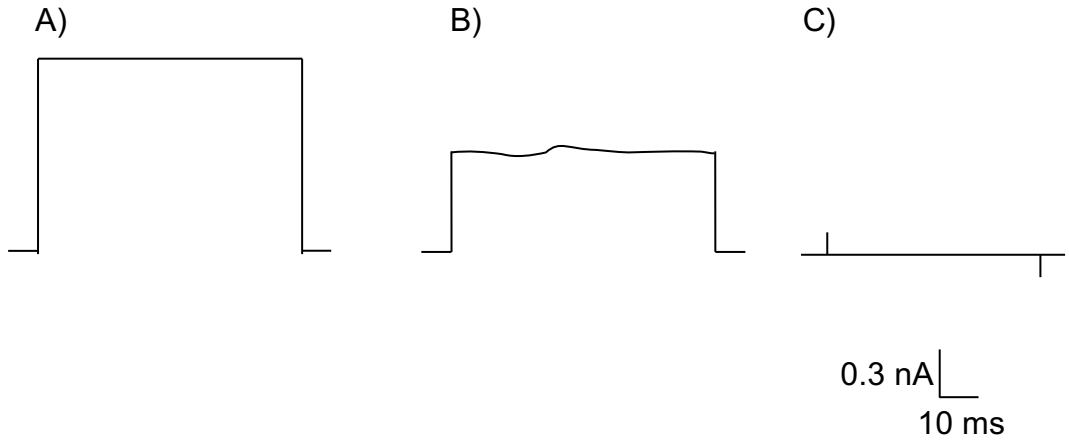

Figure 2.4: Diagrammatic representation of a gigaseal formation. A*) A voltage pulse of 5 mV applied for 50 ms results in a current flowing through the patch pipette immersed in the bath solution of 2.0 nA.* ***B****) When the tip of the pipette touches the HEK cell the current is approximately reduced by half due to the increase in resistance.* ***C****) A gigaseal is formed following the application of negative pressure, which decreases current flow dramatically, as a result of gigaseal formation.*

Thus, voltage is directly proportional to current in the preceding equation, whereas resistance is inversely proportional to current. This is exemplified in Figure 2.4, where a constant voltage (5 mV) was applied to a pipette and a current of roughly 2.0 nA was recorded, prior to forming a seal. When the pipette contacted the cell, the resistance increased and this caused the current to drop. When negative pressure was applied, a seal formed between the pipette glass and the cell membrane, increasing resistance even further, resulting in only a small amount of current passing across the pipette tip at this level of high resistance.

The resistance of the pipette, prior to seal formation (Figure 2.4A) can be calculated using the Ohm's law since R = V/I

$$R = (5 \times 10^{-3})\ V / (2.0 \times 10^{-9})\ A \qquad \text{(Eq 2.3)}$$
$$= 2.5\ M\Omega$$

However, when the seal was formed (Figure 2.4C), although the same voltage step was applied, the recorded current was less than 5 pA and the calculated seal resistance was in excess of 1 GΩ.

2.8.3 Leak subtraction

The current recorded from a membrane patch with channels is made up of several components:

i) Leakage current - A passive current flowing through membrane resistance and capacitance. This current is usually linear to the voltage.

ii) Non-linear gating current - Caused by gating charges moving across the electric field.

iii) Non-linear ionic current - This current represents the opening of ion channels as a result of voltage fluctuations.

The ionic current must be distinguished from the passive linear components, and this can be accomplished using leak subtraction. In this study, the manual leak subtraction method was employed. The leak current was calculated from the current at the end of the repolarization step to -120 mV and this was digitally subtracted from the recorded ionic currents.

2.8.4 Membrane capacitance

The cell membrane is ideally suited to acting as a capacitor, which can store charge in response to a change in voltage. The quantity of charge stored is determined by the following formula:

$$Q = C.V \qquad \text{(Eq 2.4)}$$

Where electrical charge (Q) is equal to the capacitance (C) multiplied by the voltage (V) across the membrane. Since capacitance is directly related to membrane surface area (A), a larger membrane will accumulate more charge. Because the electromagnetic field strength that attracts ions on both sides of the membrane decreases with distance, capacitance is inversely related to membrane thickness (d), as shown in the equation below. Finally, the electromagnetic field is influenced by the substance that separates the two conductors (intracellular and extracellular media). The dielectric constant ε_r is a quantity that defines the capacitance qualities of the membrane.

$$C = A\varepsilon_r/d \qquad \text{(Eq 2.5)}$$

Electrical charges on the inside and outside of the membrane also migrate

towards or away from the membrane, causing current to flow through the capacitor. This current is known as the capacitive current (I_c), and it only flows when the voltage across the membrane varies over time. The capacitive current equation can be derived from the capacitance equation above, as shown below.

$$Q = C.V \qquad \text{(Eq 2.4)}$$

Dividing by time into both sides of the equation yields

$$Q/t = C.V/t \qquad \text{(Eq 2.6)}$$

Introducing differential terms on both sides of the equation

$$dQ/dt = C.(dV/dt) \qquad \text{(Eq 2.7)}$$

Since capacitive current, $I_c = dQ/dt$ (Eq 2.8)

$$I_c = C\,(dV/dt) \qquad \text{(Eq 2.9)}$$

The capacitative current is therefore proportional to the magnitude of the voltage shift, shown in the above equation. In the whole-cell configuration, the amplifier whole-cell capacitance compensation was utilized to reduce the capacitive transients.

2.8.5 Series resistance

During whole cell patch clamp, a “series circuit” is formed which consists of the pipette resistance (R_p), access resistance (R_a) and membrane resistance (R_m). The sum of R_p and R_a is known as the series resistance (R_s). Ogden & Stanfield (1994) demonstrated experimentally that significant voltage errors can arise when series resistance is high, especially when large currents are recorded. They determined series resistance by running a depolarizing protocol of successive 10 mV step increases from the holding potential at -80 mV while measuring the passive current responses. The calculation for determining the time constant (τ) of decay for the initial capacitance transient is described in Eq 2.10, where R_s is the series resistance and C_m is the membrane capacitance.

$$\tau = R_s \times C_m \text{ or } R_s = \tau / C_m \qquad \text{(Eq 2.10)}$$

C_m can be determined from Eq 2.11, where Q_c is the charge under the capacitive transient obtained by integrating the capacitative current, thus causing a change in voltage (ΔV_m), evoking the capacitative transient.

$$C_m = Q_c / \Delta V_m \qquad \text{(Eq 2.11)}$$

In the present study with the whole cell patch clamp technique, the series resistance for HEK cells was ~4 MΩ (since R_a=~1.5 MΩ and R_p=~2.4 MΩ). The resultant voltage error obtained was ~13 mV and was uncompensated as discussed above. To help minimise voltage errors, cells expressing currents with an amplitude greater than 4 nA at +50 mV under control conditions were discarded.

2.9 Data analysis

All the experiments were carried out in the whole-cell configuration (Hamill *et al.,* 1981). Cells were routinely held at -80 mV and stepped from -100 mV to +50 mV for 1 second in 10 mV increments, with a 10 second interval between steps. Activation curves were constructed from the tail currents generated by repolarization back to -120 mV following the depolarization voltage steps. The expressed summary data was in mean ± SEM. G-V relationships were fitted with the Boltzmann equation below,

$$\frac{G}{G_{max}} = \frac{1}{1 + \exp\left[\frac{V_{1/2} - V_m}{Slope}\right]1} \qquad \text{(Eq 2.12)}$$

where G was the conductance at test potential, G_{max} was the maximal conductance, $V_{1/2}$ was the membrane potential at which there was half maximal activation and V_m was membrane potential. The change in activation $V_{1/2}$ ($\Delta V_{1/2}$) induced by the drug was obtained by subtracting the $V_{1/2}$ in control from that in the presence of the drug under investigation. The leak current calculated was described in Section 2.8.3.

The Hill equation was used to fit the concentration effect curves and determine the EC_{50} or IC_{50} of the drugs. In the experiments, the above-mentioned drug concentrations were tested on the channels at a specified voltage. To produce an EC_{50} or IC_{50}, the concentration effect of each drug on the channels was normalized to the maximal current obtained in the experiment, and this was fitted with the Hill equation of the form:

$$Y = \frac{(1.0)}{\left(1 + 10^{(([Drug] - pEC_{50}) * H)}\right)} \qquad \text{(Eq 2.13)}$$

where: [Drug]= concentration of drug, H=Hill slope and pEC_{50}= absolute EC_{50} – concentration of agonist required to increase the response to half or 50% of its maximal value.

2.10 Statistical analysis

All experimental data sets were obtained from a minimum of 5 cells, and these were obtained from at least two transfections. The size of each respective data set was detailed as 'n'. All summary data, including EC_{50} values were represented as the mean ± SEM. Statistical analysis was performed in GraphPad Prism software, using a two-tailed student's unpaired t-tests, paired t-tests, Mann-Whitney non-parametric test and analysis of variance (ANOVA), as appropriate. A Bonferroni *post-hoc* multiple comparison test was used for ANOVA where required. A p value <0.05 was taken as significant and represented with *, whereas $p<0.01$, $p<0.001$ and $p<0.0001$ were represented with **, *** and **** respectively.

2.11 Recording solutions

All recording solutions were made up with double distilled H_2O (Milli-Q Millipore). All salt concentrations are in millimolar (mM).

2.11.1 Hanks solution:

NaCl (140), KCl (5.36), Glucose (10), Sucrose (2.9), $NaHCO_3$ (4.17), KH_2PO_4 (0.44), Na_2HPO_4 (0.33), $MgCl_2.6H_2O$ (1.8), $CaCl_2.2H_2O$ (1.8), $MgSO_4.7H_2O$ (0.4), HEPES (10). pH adjusted to 7.4 with 3 M NaOH.

2.11.2 Whole-cell K^+ pipette solution:

KCl (133), $MgCl_2.6H_2O$ (1), EGTA (0.5), HEPES (10), Na_2ATP (1), NaGTP (0.1), Na_2 phosphocreatine (2.5). pH adjusted to 7.2 with 1 M KOH

2.12 List of Primers used in this study

Primer Name	**Primer Sequence**
L249A - F	5’ GTTCCTGGTGGCCATCTTCGCC 3’
L249A - R	5’ CAGGTAGACCAGGAAGGA 3’
L305A - F	5’ GGCTTCGCCGGACTGGGCATC 3’
L305A - R	5’ GGATGCCGGCAGGCAGGG 3’
F174L - F	5’ CAGAAAGCCCTTATGTGTCATCG 3’
F174L - R	5’ GCAAAGCGGAAGCGACCC 3’
A187P - F	5’ GCCTCGGTGCCCGTCATCGCC 3’
A187P - R	5’ CACGAACACGATGAAGTC 3’
C519A - F	5’ GAGCTACCAGGCTGAGCTCACG 3’
C519A - R	5’ TTCTCCTCTGCTACTTCCTC 3’
F254A - F	5’ CTTCGCCTCCGCCCTGGTCTAC 3’
F254A - R	5’ ATGAGCACCAGGAACCCGATG 3’
R297A - F	5’ GCTGGGCGCGGTCCTGGCT 3’
R297A - R	5’ CATGTGTGCGGTGTCTTGTCACCATAG 3’
E136R - F	5’ CTCATCTTGCGCTTCGTGATG 3’
E136R - R	5’ GAGACACTCGTTGGCAAG 3’
R204E - F	5’ GTCCGCGCTGGAAAGCATGCGCTTC 3’
R204E - R	5’ GTGGCGAAGATGTTGCCCT 3’
R207E - F	5’ GCGCAGCATGGAATTCCTGCAGATC 3’
R207E - R	5’ GCGCAGCATGGAATTCCTGCAGATC 3’
R213E - F	5’ GCAGATCCTGGAAATGGTGCGCATGGACC 3’
R213E - R	5’ AGGAAGCGCATGCTGCGC 3’

S6 AgeI insertion K_v7.3 - F	5' ACCGGTTGGGAAGGCCGTCTGATT 3'
S6 AgeI insertion K_v7.3 - R	5' CGTTTTGGGTGTCTTGTC 3'
S6 BsrGI insertion K_v7.3 - F	5' TGTACACTCAAGGTGCAGGAGCAA 3'
S6 BsrGI insertion K_v7.3 - R	5' GGCCAGCCCGGACCCCAG 3'
S6 AgeI insertion K_v7.4 - F	5' ACCGGTTGGCTGGGCAGGGTCCTG 3'
S6 AgeI insertion K_v7.4 - R	5' TGTGTGCGGTGTCTTGTC 3'
S6 BsrGI insertion K_v7.4 - F	5' TGTACACTGAAGGTCCAGGAGCAG 3'
S6 BsrGI insertion K_v7.4 - R	5' GGCAAAGCCGGAGCCTAG 3'
S6 AgeI deletion K_v7.4 - F	5' TGGCTGGGCAGGGTCCTGGCT 3'
S6 AgeI deletion K_v7.4 - R	5' TGTGTGCGGTGTCTTGTC 3'
S6 BsrGI deletion K_v7.4 - F	5' CTGAAGGTCCAGGAGCAGCAC 3'
S6 BsrGI deletion K_v7.4 - R	5' GGCAAAGCCGGAGCCTAG 3'
S5 V248T - F	5' CATCGGGTTCCTGACGCTCATCTT 3'
S5 V248T - R	5' TACCAGGCGGTGATCAGC 3'
S5 F251L&A252S - F	5' GGTGCTCATCTTATCCTCCTTCCTGG 3'
S5 F251L&A252S - R	5' AGGAACCCGATGTACCAG 3'
S5 A259V - F	5' GTCTACCTGGTCGAGAAGGACG 3'
S5 A259V - R	5' CAGGAAGGAGGATAAGATG 3'
S4 M206L - F	5' GCTGCGCAGCCTGCGCTTCCTG 3'
S4 M206L - R	5' GCGGACGTGGCGAAGATG 3'
S4 V215L - F	5' CTGCGCATGCTGCGCATGGACCG 3'
S4 V215L - R	5' GATCTGCAGGAAGCGCATGC 3'
S3-S4$_L$ T193N, I197V&F198L- F	5' GCCGCGGGTAACCAGGGCAACGTCTTA 3'
S3-S4$_L$ T193N, I197V&F198L- R	5' GGACGTGGCTAAGACGTTG 3'

S3-S4$_L$ A202 deletion - F	5’ CTGCGCAGCATGCGCTTCCTG 3’
S3-S4$_L$ A202 deletion - R	5’ GGACGTGGCGAAGACGTTG 3’
S1-S4 AgeI insertion K_v7.3 - F	5’ ACCGGTTGGGCGCTGCTTTACCAC 3’
S1-S4 AgeI insertion K_v7.3 - R	5’ GCCCCGCGGTCTCTCCAG 3’
S1-S4 BsrGI insertion K_v7.3 - F	5’ TGTACACGGAGAGGTGGCACCTGG 3’
S1-S4 BsrGI insertion K_v7.3 - R	5’ GTCCATCCGCAGCATGCG 3’
S1-S4 AgeI insertion K_v7.4 - F	5’ ACCGGTTGGGCCTTCGTCTACCAC 3’
S1-S4 AgeI insertion K_v7.4 - R	5’ GCCGCGGGGCCGCTCCAG 3’
S1-S4 BsrGI insertion K_v7.4 - F	5’ TGTACACGCCGCGGCGGCACCTGG 3’
S1-S4 BsrGI insertion K_v7.4 - R	5’ GTCCATGCGCACCATGCG 3’
S1-S4 AgeI deletion K_v7.4 - F	5’ TGGGCCTTCGTCTACCACGTC 3’
S1-S4 AgeI deletion K_v7.4 - R	5’ GCCGCGGGGCCGCTCCAG 3’
S1-S4 BsrGI deletion K_v7.4 - F	5’ CGCCGCGGCGGCACCTGGAAG 3’
S1-S4 BsrGI deletion K_v7.4 - R	5’ GTCCATGCGCACCATGCG 3’
C-ter AgeI insertion K_v7.3 - F	5’ ACCGGTCAGAAGCACTTTGAGAAA 3’
C-ter AgeI insertion K_v7.3 - R	5’ ACGGTGTTGCTCCTGCAC 3’
C-ter BsrGI insertion K_v7.3 - F	5’ TGTACAAAGAGGTCACTGGCTGACCCC 3’
C-ter BsrGI insertion K_v7.3 - R	5’ TTAAATGGGCTTATTGGAAGGG 3’
C-ter AgeI insertion K_v7.4 - F	5’ ACCGGTCAGAAGCACTTCGAGAAG 3’
C-ter AgeI insertion K_v7.4 - R	5’ CCGGTGCTGCTCCTGGAC 3’
C-ter BsrGI insertion K_v7.4 - F	5’ TGTACAGGATCCTGGAATTAATTCGCTGTC 3’
C-ter BsrGI insertion K_v7.4 - R	5’ TCAGTCCATGTTGGTGCTG 3’
C-ter AgeI deletion K_v7.4 - F	5’ CAGAAGCACTTCGAGAAGCGG 3’
C-ter AgeI deletion K_v7.4 - R	5’ CCGGTGCTGCTCCTGGAC 3’

C-ter BsrGI deletion K_v7.4 - F	5’ GGATCCTGGAATTAATTCGCT 3’
C-ter BsrGI deletion K_v7.4 - R	5’ TCAGTCCATGTTGGTGCTG 3’
V230A - F	5’ GCTGGGCTCAGCGGTCTACGCG 3’
V230A - R	5’ AGCTTCCAGGTGCCGCCG 3’
V231I - F	5’ GCTGGGCTCAGTGATCTACGCGCAT 3’
V231I - R	5’ AGCTTCCAGGTGCCGCCG 3’
Y232C - F	5’ GCTGGGCTCAGTGGTCTGCGCGCATAGC 3’
Y232C - R	5’ AGCTTCCAGGTGCCGCCG 3’
S265E - F	5’ GACGCCAACGAAGACTTCTCCTC 3’
S265E - R	5’ CTTCTCAGCCAGGTAGACCAG 3’
D266E - F	5’ GCCAACTCCGAGTTCTCCTCCTAC 3’
D266E - R	5’ GTCCTTCTCAGCCAGGTAG 3’
S268E - F	5’ CAACTCCGACTTCGAATCCTACGCC 3’
S268E - R	5’ GCGTCCTTCTCAGCCAGG 3’
S269T - F	5’ CGACTTCTCCACCTACGCCGAC 3’
S269T - R	5’ GAGTTGGCGTCCTTCTCAGC 3’
S273A - F	5’ CTACGCCGACGCGCTCTGGTGG 3’
S273A - R	5’ GAGGAGAAGTCGGAGTTGGCG 3’
T278L - F	5’ CTGGTGGGGGTTGATTACATTG 3’
T278L - R	5’ CTGGTGGGGGTTGATTACATTG 3’
T282A - F	5’ GATTACATTGGCAACCATCGGC 3’
T282A - R	5’ GTCCCCCACCAGAGCGAGTC 3’
R166A - F	5’ GATGGCAGGGTGCCTTCCGCTTTG 3’
R166A - R	5’ CTCGGTAGCGGCAGCAGC 3’

R171A - F	5’ CGCTTTGCCGCAAAGCCCTTC 3’
R171A - R	5’ GAAGCGACCCTGCCATCC 3’
H234N - F	5’ GTCTACGCGAATAGCAAGGAGC 3’
H234N - R	5’ CACTGAGCCCAGCAGCTTC 3’
S235A - F	5’ GTCTACGCGCATGCCAAGGAGCTG 3’
S235A - R	5’ CACTGAGCCCAGCAGCTTC 3’
H334A - F	5’ GCCTTCGAGAAGCGGAGGATG 3’
H334A - R	5’ CTTCTGCCGGTGCTGCTC 3’
K337A - F	5’ CACTTCGAGGCGCGGAGGATG 3’
K337A - R	5’ CTTCTGCCGGTGCTGCTC 3’
K481A - F	5’ GCGAGCTGGAGCTTCAATGAC 3’
K481A - R	5’ TTGCACCTTGGTGGGGCTG 3’
R488A - F	5’ CTTCAATGACGCCACCCGCTTC 3’
R488A - R	5’ CTCCAGCTCTTTTGCACCTTG 3’
R490A - F	5’ GCCTTCCGGGCATCTCTGAGAC 3’
R490A - R	5’ GGTGCGGTCATTGAAGCTCC 3’
K546N - F	5’ CTGGTGGCCAACAGGAAATTCAAG 3’
K546N - R	5’ GAACTTGAGAATCCTGATGGAGCGG 3’
R547A - F	5’ CTGGTGGCCAAAGCGAAATTCAAG 3’
R547A - R	5’ GAACTTGAGAATCCTGATGGAG 3’
K559A - F	5’ GTACGACGTGGCGGACGTCATTG 3’
K559A - R	5’ GGTCGCAGTGTCTCCTTGAATTTC 3’

Table 2.1: Shows the sequence of each primer set used in this study. The yellow highlighted region indicates the restriction sites used for cloning.

Chapter 3

Identifying potential residues in $K_V7.4$ important for the effect of SR-5-6 and assessing the state-dependent effect of SR-5-6 on $K_V7.4$ channels

3.1 Introduction

Voltage-gated potassium channels are key regulators of cellular membrane potential (V_m). Amongst the potassium channels, the K_v7 family of voltage-gated potassium channels are widely studied as they can be targeted pharmacologically and play various important physiological roles. The expression and function of K_v7 channels is dependent on the subtype distribution in the body. The K_v7 (*KCNQ*) family is comprised of five members ($K_v7.1$-$K_v7.5$), where $K_v7.1$ is mainly expressed in cardiac cells (Brown & Adams, 1980; Barhanin *et al.,* 1996) and $K_v7.2$ - $K_v7.5$ are widely distributed in neuronal, primary sensory cells, smooth muscle cells and skeletal muscle cells (Brown & Adams, 1980; Singh *et al.,* 1998; Charlier *et al.,* 1998; Kubisch *et al.,* 1999; Kharkovets *et al.,* 2000).

Pharmacological targeting of K_v7 channels has provided a wealth of information into the role of these ion channels. In our lab, a group of novel anthraquinone derivatives called the GoSlo-SR compounds were synthesized and patented ((Thornbury *et al.,* 2018; Roy *et al.,* 2012; Roy *et al.,* 2014). Although these compounds are potent BK channel openers (Roy *et al.,* 2012; Roy *et al.,* 2014), their proposed site of action on the S6/S4-S5L of BK channels suggested they may also have effects on other channels. Subsequently, Dudem (2019) found that GoSlo-SR-5-6 activated the K_v7 family of ion channels. The order of efficacy of SR-5-6 on K_v7 channels expressed in HEK cells was $K_v7.1>K_v7.5>K_v7.4>K_v7.2>K_v7.3$. SR-5-6 constitutively activated $K_v7.1$ and $K_v7.5$ but had little effect on either $K_v7.3$ or $K_v7.2$ channels. In $K_v7.4$ channels, SR-5-6 had 3 main effects which were a negative shift in the activation $V_{1/2}$, an increase in the maximal conductance and a slowing of deactivation. However, little is known about where SR-5-6 interacts with K_v7 channels to mediate these effects. Consequently, the main objectives of this chapter were to use a mutagenesis approach to:

1. Establish if retigabine binding site mutations (L249A, L281A, L305A in $K_v7.4$) altered the effects of SR-5-6 on $K_v7.4$ channels.
2. Establish if the effects of SR-5-6 were altered by the $K_v7.4$ residues implicated in mediating the effects of ICA73.
3. Examine the effects of SR-5-6 on NEM binding mutation C519A in $K_v7.4$ channels.

4. Investigate the role of PUFA binding residues F254A and R297A in SR-5-6 mediating effects in $K_v7.4$ channels.
5. Investigate the state dependency of SR-5-6 effects by locking the voltage sensors of the channels in different states.

3.2 Results

3.2.1 Effect of SR-5-6 on wildtype $K_v7.4$ channels

The first experiment was sought to confirm if SR-5-6 had similar effects on $K_v7.4$ channels to those first observed by Dudem (2019). $K_v7.4$ channels were transiently overexpressed in HEK cells, and all experiments were carried out with the whole-cell configuration of the patch-clamp technique. Cells were held at -80 mV and 1 second voltage pulses from -100 mV to +50 mV were applied to the cell with 10 mV increments (inset Fig 3.1A) to elicit steady-state currents, before stepping back to -120 mV to generate tail currents. Figure 3.1A shows a typical family of currents obtained from wildtype (WT) $K_v7.4$ channels overexpressed in HEK cells and evoked using the protocol detailed above. The currents were activated at potentials positive to -60 mV in the absence of any drugs. Previously, the EC_{50} for SR-5-6 on $K_v7.4$ at -40 mV was determined to be ~6 μM (Dudem, 2019). Therefore, in all experiments 10 μM SR-5-6 was used on K_v7 channels, to quantify the drug effects. As Figure 3.1B suggests, application of 10 μM SR-5-6 activated $K_v7.4$ currents, as evidenced by the increased amplitude of currents. SR-5-6 also increased the rate of activation as the time constant (τ) of activation at +50 mV decreased from 126.4 ± 9.9 ms to 74.3 ± 4.7 ms ($p<0.01$; paired t-test; Figure 4.10A). It also increased the amplitude and decreased the rate of decay of tail currents. The deactivation was slowed from 13.6 ± 1.1 ms in control to 43.6 ± 5 ms in SR-5-6, following a step from +50 mV to -120 mV ($p<0.01$; paired t-test; Figure 4.10B). The conductance-voltage (G-V) curves shown in Fig 3.1C were obtained from the tail currents and fitted with the Boltzmann equation. The current amplitudes at each potential were normalized to the maximum tail current recorded following a step to +50 mV to generate the G-V curves in both absence (open symbols) and presence of SR-5-6 (blue circles). Application of 10 μM SR-5-6 increased the maximal conductance (G/G_{max}) to 1.58 ± 0.1 and shifted the activation $V_{1/2}$ from -19 ± 2 mV to -65 ± 5 mV ($p<0.0001$; paired t-test; n=7; Figure 3.1C), resulting in a shift in $V_{1/2}$ ($\Delta V_{1/2}$) of -47 ± 4 mV. These effects were practically identical to those recorded previously by Dudem (2019). Similarly, the conductance (G) at -100 mV ($G_{-100\ mV}$) increased markedly from 0.03 in control to 0.36 in presence of SR-5-6 (Figure 3.16). Taken together, these results confirmed the findings of Dudem (2019) that application of SR-5-6 to $K_v7.4$ channels

activated the currents at all voltages tested, shifted the activation $V_{1/2}$ to more negative potentials and slowed current deactivation.

3.2.2 The effect of SR-5-6 on untransfected HEK cells

Given that the SR-5-6 effects were examined on $K_v7.4$ channels expressed in HEK cells, it was important to establish the effects of SR-5-6 on the endogenous K^+ currents in HEK cells. In these experiments, untransfected HEK cells were subjected to the same voltage protocol described in Figure 3.1, following break-in and dialysis. Figure 3.2 shows the currents obtained in absence of drug (panel A) and in presence of 10 μM SR-5-6 (panel B). The G-V curve shown in panel C was plotted from the outward currents for this set of experiments and fitted with the Boltzmann equation. The key differences between endogenous currents and WT $K_v7.4$ channels were - i) the endogenous currents were of smaller magnitude, (the mean value at +50mV = 600 ± 86.5 pA) and SR-5-6 actually decreased current amplitude, as evidenced by a slight reduction in G/G_{max} to 0.86 ± 0.1 in SR-5-6 (n=6; blue circles; Figure 3.2C), ii) the time constant of activation at +50 mV was 6.4 ± 0.4 ms in control and it barely changed to 10 ± 2 ms in presence of SR-5-6 indicating the endogenous currents activated much more rapidly compared to WT $K_v7.4$ channels (126 ± 9.9 ms in control and 74.3 ± 4.7 ms in SR-5-6), and iii) SR-5-6 caused a rightward shift in the activation $V_{1/2}$ of the endogenous current from 9 ± 1 mV under control conditions to 21 ± 1 mV resulting in a $\Delta V_{1/2}$ of 13 ± 2 mV, which was significantly different from the effects of SR-5-6 seen in WT $K_v7.4$ channels ($\Delta V_{1/2}$ = -46 ± 3 mV; $p<0.0001$; unpaired t-test; Figure 3.1C & 3.2C). These results clearly demonstrated that SR-5-6 had minimal effects on the endogenous HEK currents, compared to its effects on WT $K_v7.4$ channels.

3.2.3 The effect of SR-5-6 on retigabine binding mutations L249A, L281A and L305A in $K_v7.4$

Retigabine is known to activate $K_v7.2$-$K_v7.5$ channels (Tatulian *et al.,* 2001) and it was important to test if SR-5-6 mediated its effects through the same residues as retigabine, given the similarity of their effects on wildtype $K_v7.4$ channels (negative shift in the activation curve and slowed deactivation of the channels). Lange *et al.,* (2008) described the potential binding pocket for retigabine and

identified Leu-272, Leu-338 and Leu-314 in the S5 domain, pore loop and S6 domain of $K_v7.3$ respectively, to be important residues delineating the retigabine binding pocket. The role of these residues in mediating the effect of SR-5-6 on $K_v7.4$ channels was examined. Therefore, the equivalent residues on $K_v7.4$ (L249, L281 and L305) were mutated to alanine using site-directed mutagenesis. The voltage clamp protocol was identical to that used for the WT $K_v7.4$ channel (Figure 3.1). Figure 3.3A shows a family of currents recorded from **L249A** mutation. These currents started to activate from -50 mV and the $V_{1/2}$ derived from the G-V curve was shifted positively compared to WT $K_v7.4$, with a $V_{1/2}$ of -3 ± 2 mV (Figure 3.3C), which was significantly different from that observed in WT $K_v7.4$ channels (-19 ± 2 mV; $p<0.001$; unpaired t-test; Figure 3.1). In presence of 10 μM SR-5-6 on the same cell (Figure 3.3B), the amplitude of the current was enhanced at all voltages with G/G_{max} increased from 1 to 2.2 ± 0.1 (n=10; $p<0.05$; non-parametric test; Figure 3.15B). Also, the $G_{-100\ mV}$ increased from 0.05 in control to 0.1 in SR-5-6, which was significantly less than that observed with the WT $K_v7.4$ channels ($p<0.05$; non-parametric test; Figure 3.15C). Importantly, the activation $V_{1/2}$ was not shifted significantly in the presence of the drug as the $V_{1/2}$ in 10 μM SR-5-6 in L249A mutation of $K_v7.4$ was -8 ± 5 mV. In 10 similar experiments, the $\Delta V_{1/2}$ induced by SR-5-6 in this mutant was only -7 ± 5 mV (n=10; Figure 3.3C), which was significantly reduced when compared to WT $K_v7.4$ ($p<0.01$; one-way ANOVA; Figure 3.15A) (Note: If not stated otherwise, the Mann-Whitney non-parametric test to evaluate significant differences in the effects of SR-5-6 on G/G_{max} & $G_{-100\ mV}$ and one-way ANOVA for $\Delta V_{1/2}$ between the mutant channels and WT $K_v7.4$ was utilized in all of the experiments).

The second retigabine binding residue equivalent in $K_v7.4$ - **L281A** was non-functional and failed to produce any currents, other than endogenous HEK currents, therefore, it was difficult to establish if this residue played any role in SR-5-6 binding to the $K_v7.4$ channel. However, the **L305A** mutant (equivalent to L338 in $K_v7.3$) was functional and produced slowly activating currents, typical of $K_v7.4$ channels, as shown in Figure 3.4A. The L305A mutant currents began to activate around -60 mV and had a $V_{1/2}$ of -22 ± 2 mV, which was similar to WT $K_v7.4$ channels. In the same cell, in the presence of 10 μM SR-5-6, the mutant

channels activated more negatively as shown in Figure 3.4B. The current was enhanced at all voltages in the presence of SR-5-6. When the G-V relationship was plotted from the tail currents, the maximal conductance G/G_{max} was increased from 1 to 1.9 ± 0.2, which was not significantly greater than that observed with WT $K_v7.4$ channels (n=6; Figure 3.15B). The $G_{-100\ mV}$ also increased from 0.01 in control to 0.75 in SR-5-6 in the L305A mutant, but, as summarized in Figures 3.16 and 3.15C, this was not significantly different from the effect observed with SR-5-6 on WT $K_v7.4$. The activation $V_{1/2}$ was also shifted from -22 ± 2 mV to -82 ± 7 mV (Figure 3.4C) in this mutant, resulting in a $\Delta V_{1/2}$ of -66 ± 11 mV (n=6), but this was not significantly different from that observed in the WT $K_v7.4$ channels in presence of 10 μM SR-5-6 (Figure 3.4C and 3.15A).

3.2.4 Mutation of F174L and A187P (ICA73 binding mutation) failed to reduce the effect of SR-5-6 on $K_v7.4$ channels

ICA-069673 (ICA73) is a structural analog of ICA-27243 and ztz240, which are Icagen compounds and will be referred to as 'Icagens' here. These drugs are thought to mediate their effects by interacting with the voltage-sensing domain (S1-S4) (Padilla *et al.,* 2009; Wang *et al.,* 2018), unlike retigabine and its derivatives, which mediate their effects through the pore domain (Padilla *et al.,* 2009; Wang *et al.,* 2018). As the effects of SR-5-6 were not abolished in the retigabine binding residue mutants in $K_v7.4$, the next approach was to examine if the SR-5-6 mediated its effects through voltage-sensing domains, like the Icagens. Wang *et al.,* (2018) identified two residues, A181P and F168 in $K_v7.2$, which abolished the effects of ICA73. The equivalent residues (F174L and A187P) were mutated in $K_v7.4$ and the effect of SR-5-6 on these mutant channels was examined. First, the phenylalanine (F) was mutated in the S3 domain to leucine (**F174L**). As Figure 3.5A shows, when the mutant channels were subjected to different voltages of -100 mV to +50 mV in 10 mV increments, the channels activated more negatively (~-70 mV) than WT $K_v7.4$. When 10 μM SR-5-6 was applied to the same cell, the mutant channels were activated at all potentials and the current amplitude was enhanced significantly (Figure 3.5B). In the G-V curve summary data, it is clearly seen that the maximal conductance (G/G_{max}) increased from 1 to 2.18 ± 0.2 (n=8; Figure 3.5C), which was not significantly greater than its effect on wildtype channels (Figure 3.15B). The

conductance at -100 mV ($G_{-100\ mV}$) increased from 0.04 in control to 0.64 in SR-5-6, but this was not significantly different than observed in WT $K_v7.4$ (Figure 3.16 and 3.15C). The voltage-dependent activation also shifted negatively in the presence of SR-5-6 as can be seen in Figure 3.5C. The mean activation $V_{1/2}$ in the mutant channels was -28 ± 2 mV and shifted to -75 ± 5 mV in the presence of SR-5-6, resulting in a $\Delta V_{1/2}$ of -49 ± 6 mV (n=8; Figure 3.5C), but this effect was not significantly different to the effect of SR-5-6 on WT $K_v7.4$ (Figure 3.15A). Since the F174L mutation failed to alter the SR-5-6 effects, the focus was next shifted to the other ICA73 binding mutation, **A187P** (equivalent to A181P in $K_v7.2$), which was identified by Wang *et al.,* (2018) and is located in the S3 domain of K_v7 channels. The Wang *et al*., (2018) study showed that although many A181 mutations were sensitive to ICA73, the A181P substitution diminished the effects of ICA73 in $K_v7.2$ (Wang *et al.,* 2018). With this information in hand, the equivalent position (A187) was mutated to proline in $K_v7.4$. As Figure 3.6A suggests, the A187P mutant channels were functional and generated currents upon depolarization at potentials positive to -80 mV. In the presence of 10 μM SR-5-6 (Figure 3.6B) on the same cell, the currents activated at even more negative potentials and inward currents were seen at potentials negative to -80 mV. Figure 3.6C shows the summary G-V relationship curve in this mutant channel in the absence (open circles) and presence of the drug (blue circles). As seen in the summary data, SR-5-6 enhanced the maximal conductance (G/G_{max}) from 1 to 1.8 ± 0.1 (n=7) which was not significantly different from that seen in WT $K_v7.4$ channels (Figure 3.15B). The activation $V_{1/2}$ also shifted negatively in the presence of SR-5-6 to -89 ± 5 mV compared to -24 ± 3 mV in its absence. This resulted in a mean $\Delta V_{1/2}$ of -67 ± 10 mV (n=7), which was not significantly different to that observed in WT $K_v7.4$ channels (Figure 3.6C and 3.15A). The $G_{-100\ mV}$ also increased from 0.04 in control to 0.78 in presence of SR-5-6, which was significantly greater than the effect of SR-5-6 on WT $K_v7.4$ channels ($p<0.05$; Figure 3.15C & 3.16).

Taken together, the data from the above two ICA73 binding mutations clearly suggested that SR-5-6 does not mediate its effects on the channel through the same binding pocket as ICA73.

3.2.5 The effect of SR-5-6 on C519A mutation, a NEM binding residue

The cysteine-modifying reagent N-ethylmaleimide (NEM) was also found to augment currents in $K_v7.2$, $K_v7.4$ and $K_v7.5$ channels (Li *et al.,* 2004). Li *et al.,* 2004 utilized chimera and mutagenesis approaches to demonstrate that the C519A mutant in $K_v7.4$ was sufficient to abolish the effects of NEM. To investigate the role of this residue in SR-5-6 mediating effects on $K_v7.4$, a C519A mutant channel was generated. When expressed in HEK cells, the C519A mutant channels produced currents that activated at potentials positive to -60 mV (Figure 3.7A). When 10 μM SR-5-6 was applied, three main effects were observed, i) an increase in current amplitude at all voltages, ii) a huge increase in tail current amplitude and iii) tail current deactivation was slowed (Figure 3.7B). When the G-V relationship was plotted from the tail currents at -120 mV and fitted with Boltzmann's equation in the absence (open symbols) and presence (blue symbols) of SR-5-6 (Figure 3.7C), SR-5-6 increased the G/G_{max} in this mutant to 1.9 ± 0.2 (ns compared to WT $K_v7.4$, Figure 3.15B). There was also a significant shift in $V_{1/2}$ from -29 ± 1 mV in control to -91 ± 4 mV in SR-5-6, resulting in a $\Delta V_{1/2}$ of -61 ± 9 mV (n=6, ns compared to WT $K_v7.4$, Figure 3.15A). Although the $G_{-100\ mV}$ increased from 0.02 in control to 0.87 upon application of SR-5-6, this was also not significantly different from that observed in WT $K_v7.4$ channels (Figure 3.16 and 3.15C). From the results mentioned above, it was clear that SR-5-6 effects were not eliminated in this mutant channel either and suggested that this compound can activate $K_v7.4$ even when a C519A mutation is present.

3.2.6 The effect of SR-5-6 on PUFA binding residue mutations, F254A and R297A in $K_v7.4$ channels

PUFA is a polyunsaturated fatty acid that acts as a potent activator of K_v7 channels (Liin *et al.,* 2015) by increasing their G_{max} and shifting their $V_{1/2}$ negatively in $K_v7.1$, $K_v7.1$/KCNE1 and $K_v7.2$/$K_v7.3$ channels (Liin *et al.,* 2015; Doolan *et al.,* 2002; Liin *et al.,* 2016). In $K_v7.1$ channels, K316 in the S6 helix has been identified as an important residue that contributed to the increased G_{max} (Liin *et al.,* 2018). Additionally, Y268 in the S5 helix was found to be a critical anchoring point for PUFA in $K_v7.1$ (Yazdi *et al.,* 2021). Earlier studies suggested that the negative shift in $V_{1/2}$ was attributed to R218 and R221 in the S4 helix (Liin *et al.,* 2015, 2018). In this section, the effects of SR-5-6 on F254A and R297A

mutations in $K_v7.4$, which correspond to Y268 and K316 residues found to be critical for PUFA binding in $K_v7.1$ channels were examined. The effects of the R218 (R204 in $K_v7.4$) and R221 (R207 in $K_v7.4$) mutations are described in the next section (3.2.7) which examined if the effects of SR-5-6 were state-dependent.

First, **F254** was mutated in the S5 helix to alanine and tested the effects of SR-5-6. Figure 3.8A and 3.8B shows the typical currents recorded from HEK cells expressing F254A mutant channels in the absence and presence of SR-5-6 respectively. The mutant channels started to activate from -70 mV and the $V_{1/2}$ was -21 ± 2 mV, which was not different to WT $K_v7.4$ channels. In presence of 10 μM SR-5-6, large outward currents, inward currents at potentials negative to -80 mV and massive, slowly deactivating tail currents were present. The G/G_{max} increased to 1.58 ± 0.1 (n=10; Figure 3.8C), but this was not significantly different from WT $K_v7.4$ channels (Figure 3.15B). SR-5-6 also shifted the $V_{1/2}$ to -73 ± 5 mV from -21 ± 2 mV, resulting in a $\Delta V_{1/2}$ of -53 ± 7 mV for this mutant, suggesting that the F254A residue did not reduce the SR-5-6 mediated activation in $K_v7.4$ channels.

When an attempt was made to record currents from the **R297A** mutant, only small outward currents were observed (Figure 3.9A), which was assumed to be endogenous K^+ currents as the activation $V_{1/2}$ was 15 ± 3 mV in control (Figure 3.9C; white circles) and the rate of activation was 7.4 ± 1.8 ms, both of which were remarkably similar to those of endogenous K^+ currents ($V_{1/2}$ = 9 ± 1 mV; τ_{act} = 6.4 ± 0.4 ms; Figure 3.2). This suggested that the R297 residue played an important role in channel function since it did not produce large K_v7-like currents in these cells. It is possible that the mutation may have hampered protein folding, transportation, localization and/or membrane expression, which could explain the small amplitude currents. Surprisingly, however, when 10 μM SR-5-6 was applied onto these cells, an increase in current amplitude at potentials positive to +30 mV was observed. This was in contrast to the effect of SR-5-6 on the endogenous currents shown in Figure 3.2. When the G-V relationship was plotted from the outward currents and the data was fitted with a Boltzmann, the activation $V_{1/2}$ was 15 ± 3 mV in control (n=6; Figure 3.9C), which is positively shifted by ~30 mV compared to WT $K_v7.4$. In presence of SR-5-6, it was difficult to accurately

determine the $V_{1/2}$, since the channels did not reach their maximal conductance even at +50 mV. However, the G/G_{max} did increase to 1.5 ± 0.1 in the presence of SR-5-6. Interestingly, there was no change in $G_{-100\ mV}$ when SR-5-6 was applied (Figure 3.9C), which was significantly different from that observed in WT $K_v7.4$ channels ($p<0.001$; Figure 3.15C & 3.16). The control current traces were also digitally subtracted from the drug traces to obtain 'SR-5-6-sensitive' currents and their conductance was plotted as light blue symbols in Figure 3.9C. Although the $V_{1/2}$ could not be deduced for these SR-5-6 sensitive currents, it was clear from Figure 3.9C that SR-5-6 enhanced the currents, but only at potentials positive to +30 mV. It was presumed that the currents recorded in SR-5-6 at very positive potentials were $K_v7.4$ currents, given their sensitivity to SR-5-6. However, although the rate of activation of these SR-5-6-sensitive currents at +50 mV was slower (17.2 ± 3 ms) than the endogenous currents (10 ± 2 ms; $p<0.05$; unpaired t-test), it was significantly faster than that observed in WT $K_v7.4$ channels (74.3 ± 4.7 ms; $p<0.0001$, unpaired t-test). These data suggested that the R297 residue present in the proximal end of the S6 helix may play an important role in channel function, given its effects on the biophysical properties of the channel. Furthermore, although SR-5-6 was able to stimulate the channels, it only did this at very positive potentials.

3.2.7 The state-dependent effects of SR-5-6 on $K_v7.4$ channels

Given that the effects of SR-5-6 were not abolished by mutations of binding site residues of known K_v7 channel activators, the next approach was to examine if the effects of SR-5-6 were modified as a result of state-dependent activation of K_v7 channels. Previous work in the lab (Dudem, 2019) demonstrated that the F322A mutation in $K_v7.4$ abolished the effect of 10 μM SR-5-6, but the mutation of any residues in a hydrophobic pocket surrounding this residue failed to alter the effects of SR-5-6 (Dudem, 2019). However, as previously demonstrated by Zaydman *et al.,* (2014), the F322A in $K_v7.4$ was equivalent to mutation F351A in $K_v7.1$ and plays an important role in VSD-PD coupling. This F351A mutant prevented the channel from entering an intermediate open state and altered both the pharmacological and permeation properties of the channel (Zaydman *et al.,* 2014). Thus, it was hypothesized that the F322A mutant locked the channels in a state where SR-5-6 binding was reduced. To examine if SR-5-6 mediated

effects were state-dependent, charge reversal mutants were used in the voltage sensor regions, in an attempt to lock the $K_v7.4$ channels' voltage sensors in different states, using the approach of Zaydman *et al.,* (2014).

As shown in the inset of Figure 3.10A, the first $K_v7.4$ channel mutation examined with this approach was the E136R mutant. This negatively charged glutamic acid in the S2 helix was mutated to a positively charged arginine and should hold the channel voltage sensors in the resting state. This should occur because the mutant S2 and normal S4 helices now have positively charged residues, which should result in electrostatic repulsion and presumably prevent VSD activation, as shown in the cartoon inset in Figure 3.10A. The **E136R** (E1R) channel currents were much more difficult to activate using the standard IV protocol, as shown in Figure 3.10A. Thus, even at +50 mV, only small currents were recorded. These were presumably $K_v7.4$ rather than endogenous currents, as they had rapid deactivating kinetics ($\tau_{\mathbf{deact}}$ = 19.4 ± 1 ms) resembling those of WT K_v7 channels (13.6 ± 1.1 ms), but the rate of activation at +50 mV was 29 ± 0.8 ms which was not slow when compared to WT $K_v7.4$ channels ($\tau_{\mathbf{act}}$ = 126.4 ± 9.9 ms). However, in the presence of 10 μM SR-5-6 (Fig 3.10B), the channels were massively activated at all potentials. As Figure 3.10C suggests, the G/G_{max} increased from 1 to 8.3 ± 1.4 (n=10), which was approximately 5-fold greater than its effects on WT $K_v7.4$ channels ($p<0.001$; Figure 3.15B). Similarly, the conductance at -100 mv ($G_{-100\ mV}$) also increased massively from 0.1 in control to 3.6, upon application of SR-5-6 (Figure 3.16), which was significantly higher than that observed in WT $K_v7.4$ channels ($p<0.001$; Figure 3.15C & 3.16). Unfortunately, the activation $V_{1/2}$ could not be determined in either control or in the presence of the drug, as it was difficult to evoke maximum tail currents under either recording condition, but it was clear that the drug had a large excitatory effect, even though the channels were unable to activate their VSD, because of a presumed electrostatic repulsion between S2 and S4 in this mutant.

The concentration-dependent effects of SR-5-6 on this mutant were then examined in the absence and presence of 300 nM, 1 μM, 3 μM,10 μM and 30 μM SR-5-6, in an attempt to determine if the affinity of the channel for this drug was altered. In the experiment shown in Figure 3.11A, the cells expressing the E136R $K_v7.4$ mutant were held at -80 mV for 50 ms, then stepped to -40 mV for 500 ms

to generate steady-state currents and repolarized back to -120 mV to generate the tail currents. The amplitude of current was measured at -40 mV for each concentration of SR-5-6 and was plotted in Fig 3.11B, where the EC_{50} of 9.4 ± 1.03 μM (n=10) was estimated by fitting the data with the Hill-Langmuir equation. The EC_{50} was significantly higher than WT $K_v7.4$ (6.4 ± 0.5 μM; $p<0.05$; unpaired t-test).

The effects of the charge reversal mutations **E136R & R204E** (E1R/R1E), in which the E136 residue in S2 was mutated to arginine and the first arginine R204 in S4, was mutated to glutamic acid in $K_v7.4$ channels, were examined next. This presumably locked the channels VSD in a partially activated state - I (intermediate state) as shown in Figure 3.12 inset. Panel A of Figure 3.12 shows a family of currents from this mutant in control conditions. Although currents could be evoked even at negative potentials, they were slower to activate (τ_{act} = 93.1 ± 20 ms) and the rate of deactivation (τ_{deact} = 32.2 ± 10 ms) was slower than the WT (τ_{deact} = 13.6 ± 1 ms; $p<0.01$; unpaired t-test). However, it is clear from the tail currents that the currents had not maximally activated, even following a pulse to +50 mV in control conditions since no plateau was reached in the G-V curve. Even in the presence of 10 μM SR-5-6 (Figure 3.12B), the channels were clearly activated at all voltages but, as seen in the summary G-V relationship curve, the currents still failed to maximally activate even at +50 mV (Figure 3.12C). In the summary G-V relationship (Figure 3.12C), it can be seen clearly that the maximal conductance G/G_{max} increased from 1 to 1.8 ± 0.1 (n=12) in the presence of SR-5-6, indicating that SR-5-6 still activated these channels. The conductance at -100 mV increased from 0.1 in control to 0.3 in presence of SR-5-6, which was not significantly different from that seen in WT $K_v7.4$ (Figures 3.15C and 3.16). The activation $V_{1/2}$ could not be calculated in either the control or in the presence of SR-5-6 as in both cases the activation of channels did not reach a maximum. Nevertheless, it was clear that the drug effect was not abolished in these constructs.

The intermediate - open state mutant **E136R & R207E** (E1R/R2E) was then studied, as seen in the inset in Figure 3.13. In this, the E136 was mutated to arginine in S2 and R207 in S4 to glutamic acid, in an attempt to lock the channel VSD in another intermediate-open state. As expected, in this mutant, under control conditions the channels were clearly activated, even at very negative

potentials (Figure 3.13A). There were large inward tail currents observed, even from potentials as negative as -100 mV, consistent with the idea that these channels were locked in an intermediate activated state. Figure 3.13B shows the family of currents from the same cell in the presence of 10 μM SR-5-6 and illustrates that current amplitude was increased at all potentials in the presence of SR-5-6. When the summary G-V relationship was plotted from the tail currents, the maximal conductance G/G_{max} increased from 1 to 1.37 ± 0.08 (n=5; ns when compared to WT $K_v7.4$; Figure 3.13C & 3.15B). The $G_{-100\ mV}$ increased from 0.59 in absence of SR-5-6, to 1 in its presence ($p<0.05$ compared to WT $K_v7.4$; Figure 3.15C Figure 3.16). The activation $V_{1/2}$ could not be calculated as the channels in either the absence or presence of SR-5-6 were activated at all voltages tested. Nevertheless, the data suggested that SR-5-6 could still activate $K_v7.4$ channels, even when the voltage sensors were locked in intermediate states.

The last charge reversal mutant produced in this experimental series was the **E136R & R213E** (E1R/R4E) mutant, which locked the VSD in a fully activated - open state. As shown in the inset of Figure 3.14, the E136 residue was mutated in S2 to arginine and the R213 residue was mutated in S4 of $K_v7.4$ to glutamic acid. Figure 3.14A shows a family of currents recorded from the mutant channels in the control condition. As predicted the channel was activated at all given potentials, as evidenced by the large tail currents evoked following steps as negative as -100 mV. In the presence of 10 μM SR-5-6 on the same cell, the current amplitude was still enhanced at all voltages. The channels were constitutively activated in the presence of 10 μM SR-5-6 (Figure 3.14B). When the G-V relationship was summarized from the tail currents generated at -120 mV, in the absence and presence of SR-5-6, the maximal conductance increased from 1 to 1.56 ± 0.1 (n=8), an effect which was not significantly different from the effect observed in WT $K_v7.4$. The conductance at -100 mV ($G_{-100\ mV}$) showed only a very small increment from 0.70 in control to 0.78 in SR-5-6, although this was from a significantly elevated baseline, compared to WT $K_v7.4$ in the absence of the SR-5-6 (Figure 3.16). The activation $V_{1/2}$ again could not be calculated because the channels were significantly activated at all potential tested.

3.3 Discussion

The aim of this chapter was to attempt to identify any residues in the $K_v7.4$ channel which could potentially contribute to the activating effects of SR-5-6. The major conclusions from this chapter were as follows:

1. The L249A mutant was substantially less responsive to the effects of SR-5-6, as evidenced by the reduced shift in activation $V_{1/2}$.
2. Mutation of the equivalent residues in $K_v7.4$ for the retigabine, ICA73, NEM and PUFA binding sites failed to alter the effects of SR-5-6.
3. The effect of SR-5-6 on $K_v7.4$ was not state-dependent, as it activated the channels irrespective of the state in which the VSD was held.

The initial results of this chapter confirm the earlier findings of Dudem (2019) that SR-5-6 is an effective activator of $K_v7.4$ channels, with an EC_{50} of 6.3 ± 0.5 μM (n=5, Zavaritskaya *et al.,* 2020). The SR-5-6 induced shift in activation $V_{1/2}$ ($\Delta V_{1/2}$) in WT channels (-47 mV, Figure 3.1) was considerably greater than that observed with other potent activators of K_v7 channels. For example, the $\Delta V_{1/2}$ observed with retigabine was -14 mV (Tatulian *et al.,* 2001), with ICA73 was -15 mV (Yu *et al.,* 2011) and with ML213 was only -20 mV (Brueggemann *et al.,* 2014) and suggests that SR-5-6 is a more efficacious activator than other K_v7 channel openers.

As mentioned earlier in the literature review, the K_v7 channel openers can be broadly classified into two types, based on their quite diverse mechanism of action: 1. Activators that mediate their effects through the pore domain so-called Pore Domain Activators (PDA) and 2. Voltage Sensor Domain Activators (VSDA). The proposed binding pocket for the PDA is situated in the S5 and S6 helix in the pore domain (Lange *et al.,* 2008), where T265 and L314 ($K_v7.3$) were defined to be the outer limits of the retigabine binding pocket. Along with these two residues, L272, L314, L338 and T271 were proposed to line the retigabine binding pocket (Lange *et al.,* 2008). Many other retigabine derivatives (ML213) and a few other activators like SF0034 (Kalappa *et al.,* 2015), acrylamide (S)-2 (Blom *et al.,* 2009) and SMB-1 (Blom *et al.,* 2014) are known to mediate their effects through this pocket.

The second proposed site for drugs activation on K_v7 channels is in the voltage-sensing domain (VSD). Drugs that mediate their effects here are called gating modifiers, as they bind to the S1-S4 voltage-sensing domain (Peretz *et al.,* 2010). Icagens such as ICA-27243, ICA-069673 (ICA73) (Padilla *et al.,* 2009), N-phenylanthranilic acid derivatives (Peretz *et al.,* 2005; Peretz *et al.,* 2007; Abitbol *et al.,* 1999) and NH29 (Peretz *et al.,* 2010) are all thought to mediate their excitatory effects via binding to voltage-sensing domains (Peretz *et al.,* 2007; Wickenden *et al.,* 2008; Padilla *et al.,* 2009; Peretz *et al.,* 2010; Gao *et al.,* 2010; Amato *et al.,* 2011; Li *et al.,* 2013). As the main aim of my work was to find the binding site for SR-5-6 on K_v7 channels, mutations were carried out on both of these activator binding sites in $K_v7.4$, to see if the mutations altered the effects of SR-5-6.

Retigabine is a very well-studied activator of K_v7 channels, which like SR-5-6, shifted $V_{1/2}$ negatively, increased G_{max} and slowed deactivation. Therefore, looked at the putative retigabine binding pocket to examine if SR-5-6 interacted with residues here. Previous studies had suggested that W265 in S5 of $K_v7.3$ was a crucial residue involved in retigabine binding (Schenzer *et al.,* 2005; Wuttke *et al.,* 2005). Another study by Lange *et al.,* (2008) expanded on this work and identified a putative retigabine binding pocket involving L272, L338, L314 and T271 as critical residues in this binding pocket in $K_v7.3$. Previous studies from the lab mutated the equivalent W265 residue in $K_v7.4$ (W242L) and found that although it blocked the effect of ML213 (a retigabine analogue), it failed to reduce the effect of SR-5-6 (Zavaritskaya *et al.,* 2020). When the other retigabine binding pocket residues equivalent to L272, L314 and L338 were mutated on the $K_v7.4$ channel (L249A, L281A and L305A), the effects of SR-5-6 were either unchanged (L305A, Figure 3.4) or moderately reduced (L249, Figure 3.3).

However, it is interesting to note that the L249A mutant only showed a small shift in $V_{1/2}$ ($\Delta V_{1/2}$ = -7 ± 5 mV) in response to SR-5-6, compared to the ~-50 mV shift in $V_{1/2}$ observed in the WT $K_v7.4$ under the same conditions. However, although it practically abolished the effect of SR-5-6 on $\Delta V_{1/2}$, it failed to reduce the effects on G/G_{max}. This suggested that perhaps SR-5-6 mediated its two main effects (shift in activation and increase in G/G_{max}) through different residues and that L249A in the S5 helix is a potential residue involved in mediating the negative shift in activation $V_{1/2}$. This potential involvement of independent, distinct sites

which modify different K_v7 channel biophysical properties, had already been proposed for the effects of zinc pyrithione (ZnPy) and polyunsaturated fatty acids (PUFA) on K_v7 channels (Xiong *et al.,* 2007; Liin *et al.,* 2018; Yazdi *et al.,* 2021). Although the L249A mutant significantly reduced the effects of SR-5-6 on $\Delta V_{1/2}$, the change in G/G_{max} (to 2.2 ± 0.1) was not reduced, suggesting that only one component of the SR-5-6 effect was altered by this mutant. Unfortunately, the L281A mutant formed non-functional channels and we could not determine its role in SR-5-6 binding to the K_v7 channels. Interestingly, however, the other retigabine binding mutation (L305A) failed to reduce the effect of SR-5-6 on $K_v7.4$ channels. This suggests that although SR-5-6 and retigabine may bind to at least one common residue, their binding pockets appear to differ.

SR-5-6 also does not appear to interact with the residues involved in ICA73 binding (Wang *et al.,* 2018), since when A187P and F174L in $K_v7.4$ were mutated, they failed to reduce the effects of SR-5-6 (Figure 3.5 and Figure 3.6), in contrast to the effects of these mutations on ICA73.

Similarly, the effects of SR-5-6 could not be altered when a mutant was produced which was previously shown to abolish the effect of N-ethylmaleimide (NEM) on native $K_v7.2$ channels (Li *et al.,* 2004). Their study recorded whole-cell currents of $K_v7.2$, $K_v7.4$ and $K_v7.5$ and demonstrated that they were increased approximately fourfold and their activation shifted by ~-20 mV by 50 μM NEM. Li *et al.,* (2004) found that a single mutation C519A in the C-terminus region of $K_v7.4$ abolished the effects of NEM. However, this mutation failed to significantly alter the effects of SR-5-6 and suggested that SR-5-6 does not exert its effects via this residue.

The residues involved in the effects of PUFAs were then examined to see if they potentially played a role in mediating the effects of SR-5-6. It has been proposed two different sites in S4 and S6 act independently to bring about an increase in G_{max} and a negative shift in $V_{1/2}$ with PUFAs (Liin *et al.,* 2015, 2018; Yazdi *et al.,* 2021). The electrostatic interaction between the carboxylic acid head group in PUFA with the positively charged R218 and R221 in the S4 helix has been demonstrated to contribute to the negative shift in $V_{1/2}$ in $K_v7.1$ (Liin *et al.,* 2015, 2018; Yazdi *et al.,* 2021). In contrast, the increase in G_{max} with PUFAs was attributed to an interaction with the positively charged S6 residue K326 in $K_v7.1$ channels (Liin *et al.,* 2018). Yazdi *et al.,* (2021) also identified Y268 in the S5

helix in $K_v7.1$ as a critical PUFA binding residue important for fatty acid selectivity in K_v7 channels. When the two PUFA binding residues F254 and R297 corresponding to Y268 and K316 in $K_v7.1$ were mutated in $K_v7.4$, it did not abolish the effects of SR-5-6 with the F254A mutant. With the R297A mutant, however, the biophysical properties of the channel appeared to be massively altered. Indeed the biophysical properties of the channels appeared to be altered as the current amplitude was very small, the activation $V_{1/2}$ was shifted positively and the channels had a rapid rate of activation. Interestingly, these biophysical properties were typical of endogenous K^+ currents shown in Figure 3.2 and initially led us to believe that the R297A was non-functional or that the mutant altered protein transport, localisation or membrane expression. However, in contrast to its effects on endogenous currents (Figure 3.2), application of 10 μM SR-5-6 to this R297A mutant did activate currents, albeit only at very positive potentials (Figure 3.9). Also, the currents recorded in SR-5-6 at very positive potentials resembled $K_v7.4$ current characteristics, as evidenced by the slowly activating currents. This suggested that the R297 mutant was functional, but its biophysical properties were hugely affected such that the channels only activated at very positive potentials, in the absence of drugs. Presumably, in presence of SR-5-6, the channels were able to activate, as a result of SR-5-6 shifting the activation $V_{1/2}$ of the channels negatively. The use of fluorescent tagged K_v7 channels or immunocytochemistry with $K_v7.4$ selective antibodies would allow help to confirm if the R297 mutant is efficiently trafficked to and expressed in the membrane of HEK cells.

In the final experiments in this chapter, examined if the efficacy of SR-5-6 was altered when the VSD were locked in different states, by utilizing the approach of Wu *et al.,* (2010). The rationale was that Dudem (2019) had shown that SR-5-6 effects were abolished by a single mutation in S6 (F322A), other mutations around this residue had no effect on the ability of SR-5-6 to activate K_v7 channels. Also, F322 was equivalent to one of the three residues (L227, S317 and I326 in BK) identified by Webb *et al.,* (2015) to be involved in SR-5-6 binding in BK channels. It was reasoned that the F322 mutant could lock the channels in a state where SR-5-6 binding was reduced. Indeed, previous studies by Zaydman *et al.,* (2014) demonstrated that the F351A mutant in $K_v7.1$ (equivalent to F322A in $K_v7.4$), altered VSD-PD coupling to prevent the intermediate open state from

occurring. This resulted in changes to both the pharmacology and permeation of $K_v7.1$ channels.

Interestingly, Dudem (2019), carried out preliminary experiments to examine if there were state-dependent effects of SR-5-6 on $K_v7.4$ channels. An example of one of his experiments is shown in Figure 3.0, in which the effects of SR-5-6 on currents evoked by a depolarization from -80 mV to +40 mV (Figure 3.0A), were compared with its effects when SR-5-6 was applied during a continuous depolarization to +40 mV (Figure 3.0B). It was clear from these experiments that SR-5-6 was much less effective at increasing current amplitude when applied during a depolarizing pulse.

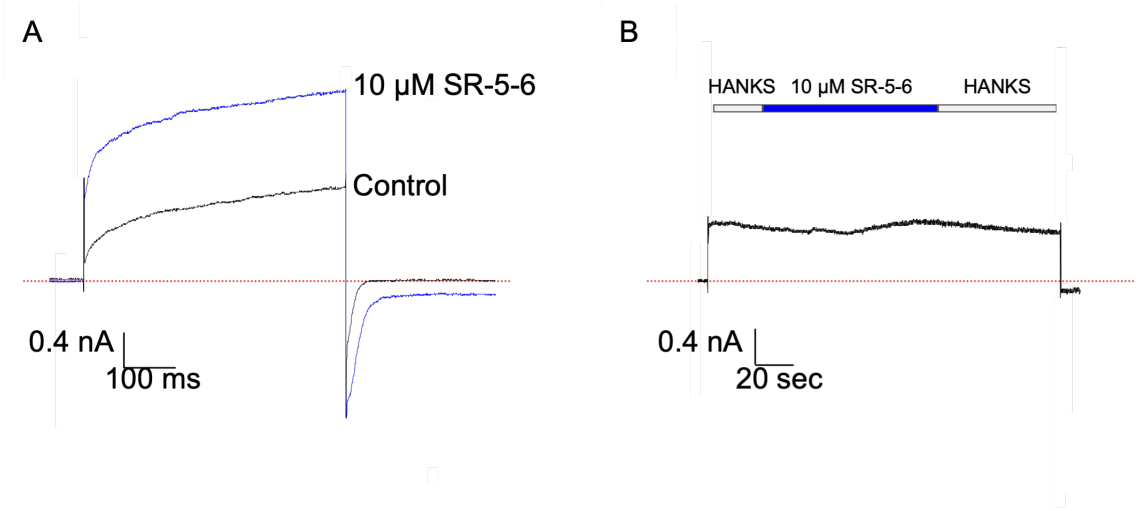

Figure 3.0: *Effect of SR-5-6 on the step and continuous recording at +40 mV of $K_v7.4$ channels.* ***A)*** *The effect of 10 µM SR-5-6 at depolarization step to +40 mV.* ***B)*** *The effect of 10 µM SR-5-6 at +40 mV continuous recording in $K_v7.4$ channels. (Adapted from Dudem S. - PhD thesis, 2019)*

This suggested that the effects of SR-5-6 were state-dependent and, therefore, the effects of SR-5-6 were examined on mutations where the K_v7 channels remained locked in the resting, intermediate and activated states.

It is known that VSD activation occurs through stepwise transitions due to salt bridge interactions between the basic residues on S4 and acidic residues on S1 and S2, defining the resting, intermediate and activated states (Papazian *et al.,* 1995; Tiwari-Woodruff *et al.,* 1997; Wu *et al.,* 2010; Delemotte *et al.,* 2011; Jensen *et al.,* 2012; Lacroix *et al.,* 2012). Wu *et al.,* (2010) identified these interactions in $K_v7.1$ where S4 arginines interacted with E1 in S2 leading to state-dependent electrostatic interactions and activation of the channels. In the same

study, the K_v7 channels were locked in resting, intermediate and activated states by reversing the charged residues in S2 and S4.

When a similar approach was used to lock $K_v7.4$ channels in resting, intermediate, and activated configurations, it was found that SR-5-6 could greatly enhance currents in the resting state mutant, E1R (Figure 3.10), implying that it could bind even when the VSD was resting. The channels were activated by SR-5-6 in partially active states (E1R:R1E and E1R:R2E) and completely activated state (E1R:R4E), as demonstrated by the increase in G/G_{max} in the presence of the drug in each case. Unfortunately, the activation $V_{1/2}$ in any of these mutants could not be quantified. There was no statistically significant reduction in G/G_{max} in SR-5-6 compared to WT, with the exception of a slight reduction in G/G_{max} in the E1R:R2E mutant. The results of the state-dependent mutant studies, combined, demonstrated that SR-5-6 could activate $K_v7.4$ channels regardless of the VSD activation state. This was in contrast to Wang *et al.,* (2018) findings, which showed that the pore and voltage sensor targeting K_v7 activators exhibit state-dependent actions. Also, these results are inconsistent with the initial findings of Dudem (2019), which showed SR-5-6 was not as effective when cells were held at depolarizing potentials of +40 mV (Figure 3.0) and perhaps suggests that the apparent state-dependent effects of SR-5-6 recorded by Dudem (2019) were not mimicked by the mutations produced in our study.

The summary data shown in Figure 3.15 compares the SR-5-6 effects on $\Delta V_{1/2}$, G_{max} and $G_{-100\ mV}$ of the mutants utilized in this chapter. This summary $\Delta V_{1/2}$ data suggests that the Icagen binding mutants (A187P and F174L), the retigabine binding mutant (L305A), the NEM binding mutant (C519A) and the PUFA binding mutant (F254A) failed to alter the efficacy of SR-5-6. Interestingly, however, L249A, another retigabine binding site mutant, showed a significantly reduced shift in $V_{1/2}$ in the presence of SR-5-6 (Figure 3.15A). This suggested that L249 in the S5 helix may act as a binding residue that brings about the negative shift in activation in the presence of SR-5-6. Alternatively, it may alter the binding pocket at a different site, through an allosteric mechanism. Interestingly, although SR-5-6 was less effective at altering $\Delta V_{1/2}$ in the L249A mutant, the tail currents were still slowed in presence of SR-5-6 (Figure 3.3) and the SR-5-6 effect on G/G_{max} was retained (Figure 3.15B), suggesting that different residues and,

potentially, different binding sites may be responsible for mediating these two effects of SR-5-6 on $K_v7.4$ channels. When the G/G_{max} was summarized, it became apparent that no single mutation reduced the G/G_{max} in the presence of SR-5-6. In fact, SR-5-6 greatly enhanced G/G_{max} in the E136R mutant channels and increased G/G_{max} in L249A mutant channels, compared to WT $K_v7.4$ channels. Taken together, these results suggest that SR-5-6 may mediate its effect on $\Delta V_{1/2}$ by interacting with L249, but its effects on G/G_{max} occur via different, elusive residues.

3.4 Future directions

Given the results from this chapter, future directions that could be explored include:

1) Mutational studies of individual pore domain residues implicated in the increase in G/G_{max}, since these residues are primarily engaged in the channel's ion conduction.

2) Membrane expression investigations using an immunocytochemistry/confocal microscopy approach, which could confirm if any mutant channels had altered membrane expression and help ascertain if this could contribute to the lack of effect of SR-5-6 on these channels.

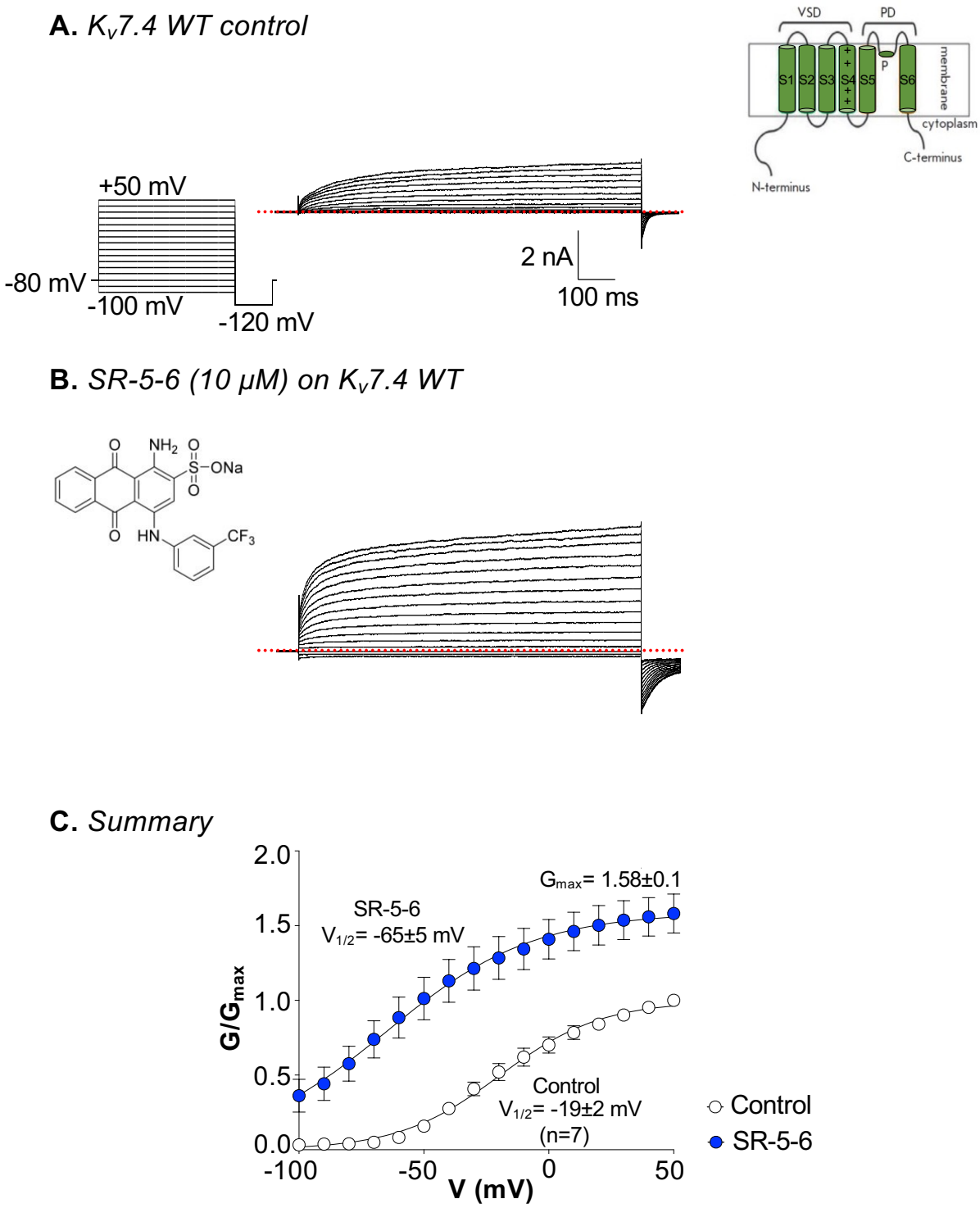

Figure 3.1: Effect of SR-5-6 on wildtype K_v7.4 channels. A) A typical family of currents obtained from wildtype K_v7.4 channels expressed in HEK cells. Voltage clamp protocol is described in the inset. Dotted lines represent the zero current level. **B**) The effect of 10 μM SR-5-6 on currents from the same cell. **C**) Summary activation curves obtained by measuring tail currents in seven cells before (open circles) and during (blue circles) application of SR-5-6 (n=7). The curves were fit with the Boltzmann equation.

A. *Untransfected HEK cells - control*

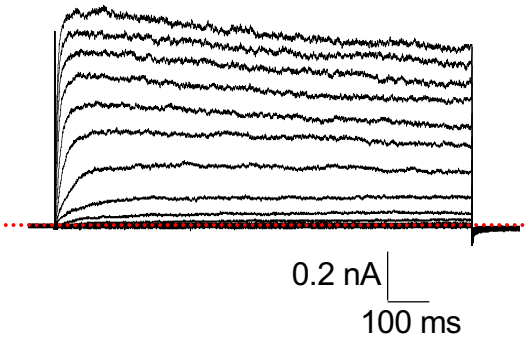

B. *SR-5-6 (10 μM) on Untransfected HEK cells*

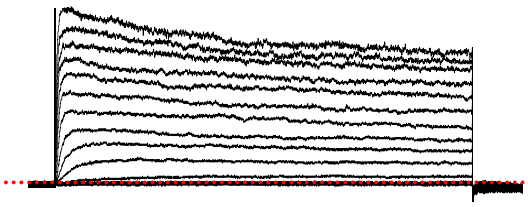

C. *Summary*

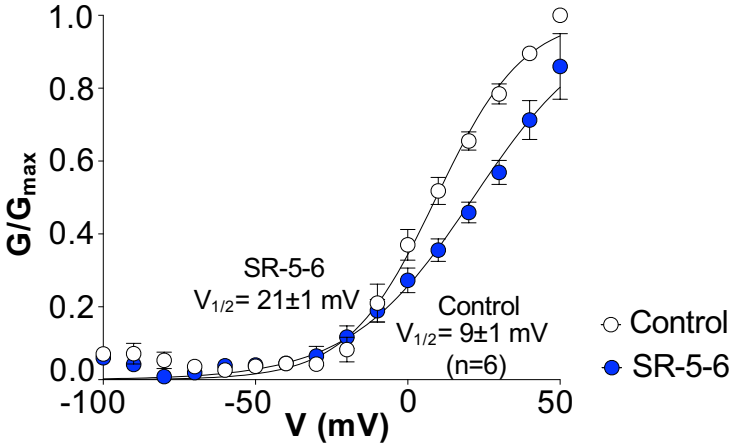

Figure 3.2: Effect of SR-5-6 on Untransfected HEK cells. A) A typical family of currents obtained from untransfected HEK cells. Voltage clamp protocol as described in Figure 3.1. Dotted lines represent the zero current level. **B**) The effect of 10 μM SR-5-6 on currents from the same cell. **C**) Summary activation curves obtained by measuring outward currents in six cells before (open circles) and during (blue circles) application of SR-5-6 (n=6). The curves were fit with the Boltzmann equation.

A. *L249A mutant control*

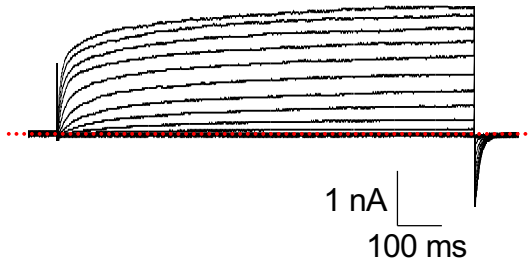

B. *SR-5-6 (10 μM) on L249A mutant*

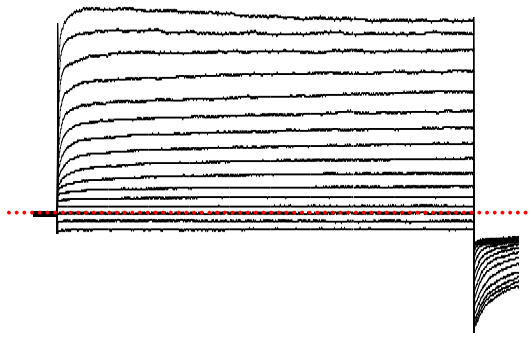

C. *Summary*

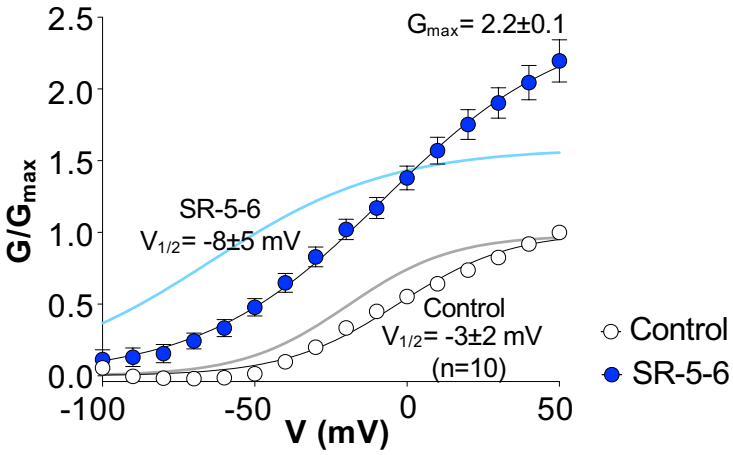

Figure 3.3: Effect of SR-5-6 on retigabine binding site mutation L249A of K_v7.4 channels. A) A typical family of currents obtained from L249A mutation of K_v7.4 channels expressed in HEK cells. Voltage clamp protocol as described in Figure 3.1. Dotted lines represent the zero current level. **B**) The effect of 10 μM SR-5-6 on currents from the same cell. **C**) Summary activation curves obtained by measuring tail currents in ten cells before (open circles) and during (blue circles) application of SR-5-6 (n=10). The continuous grey and light blue lines in the background represent the activation curves of control and the effect of the SR-5-6 on WT K_v7.4 channels respectively The curves were fit with the Boltzmann equation.

A. *L305A mutant control*

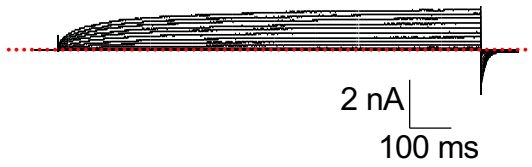

B. *SR-5-6 (10 μM) on L305A mutant*

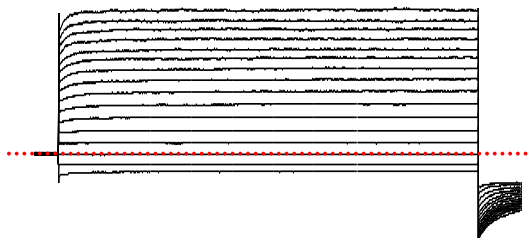

C. *Summary*

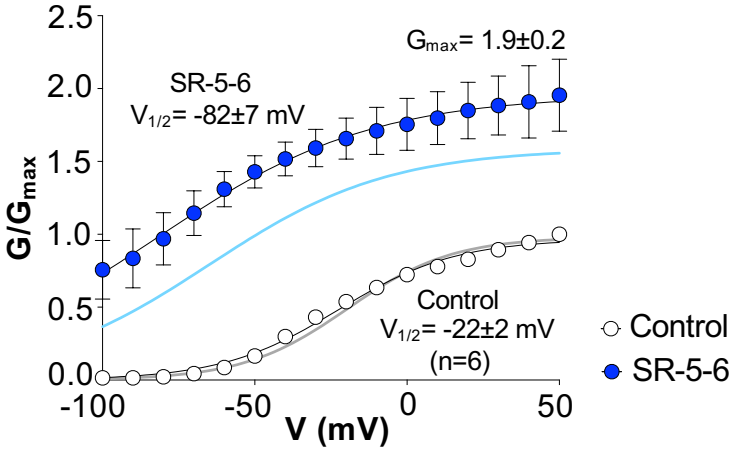

Figure 3.4: Effect of SR-5-6 on retigabine binding site mutation L305A of K_v7.4 channels. A) A typical family of currents obtained from L305A mutation of K_v7.4 channels expressed in HEK cells. Voltage clamp protocol as described in Figure 3.1. Dotted lines represent the zero current level. **B**) The effect of 10 μM SR-5-6 on currents from the same cell. **C**) Summary activation curves obtained by measuring tail currents in six cells before (open circles) and during (blue circles) application of SR-5-6 (n=6). The continuous grey and light blue lines in the background represent the activation curves of control and the effect of the SR-5-6 on WT K_v7.4 channels respectively. The curves were fit with the Boltzmann equation.

A. *F174L mutant control*

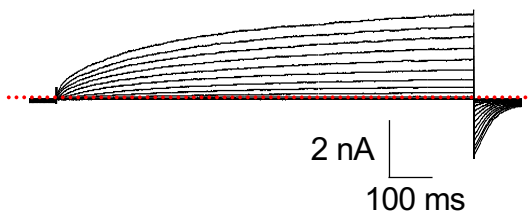

B. *SR-5-6 (10 μM) on F174L mutant*

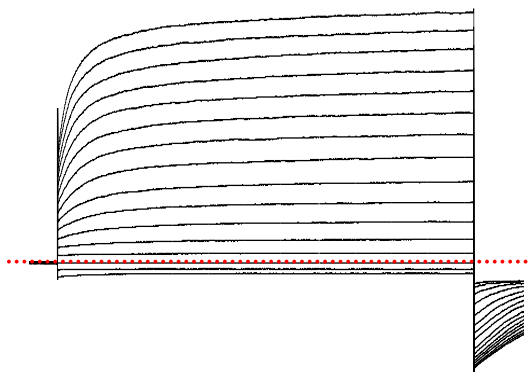

C. *Summary*

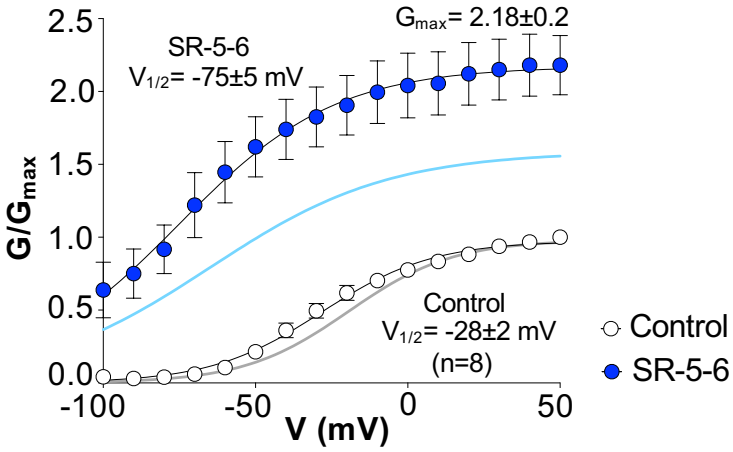

Figure 3.5: Effect of SR-5-6 on ICA73 binding site mutation F174L of K_v7.4 channels. A) A typical family of currents obtained from F174L mutation of K_v7.4 channels expressed in HEK cells. Voltage clamp protocol as described in Figure 3.1. Dotted lines represent the zero current level. **B**) The effect of 10 μM SR-5-6 on currents from the same cell. **C**) Summary activation curves obtained by measuring tail currents in eight cells before (open circles) and during (blue circles) application of SR-5-6 (n=8). The continuous grey and light blue lines in the background represent the activation curves of control and the effect of the SR-5-6 on WT K_v7.4 channels respectively. The curves were fit with the Boltzmann equation.

A. *A187P mutant control*

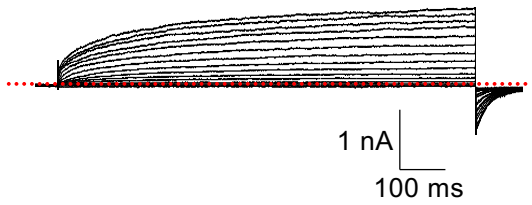

B. *SR-5-6 (10 μM) on A187P mutant*

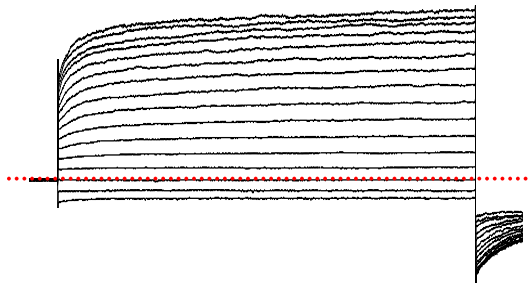

C. *Summary*

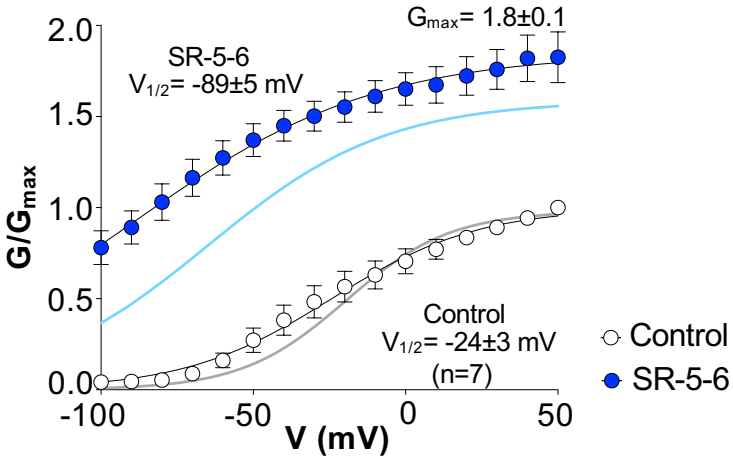

Figure 3.6: Effect of SR-5-6 on ICA73 binding site mutation A187P of K_v7.4 channels. A) A typical family of currents obtained from A187P mutation of K_v7.4 channels expressed in HEK cells. Voltage clamp protocol as described in Figure 3.1. Dotted lines represent the zero current level. **B**) The effect of 10 μM SR-5-6 on currents from the same cell. **C**) Summary activation curves obtained by measuring tail currents in seven cells before (open circles) and during (blue circles) application of SR-5-6 (n=7). The continuous grey and light blue lines in the background represent the activation curves of control and the effect of the SR-5-6 on WT K_v7.4 channels respectively. The curves were fit with the Boltzmann equation.

A. *C519A mutant control*

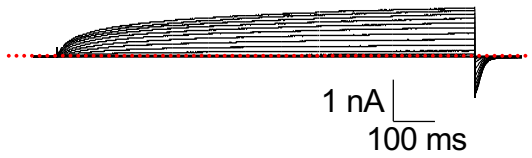

B. *SR-5-6 (10 μM) on C519A mutant*

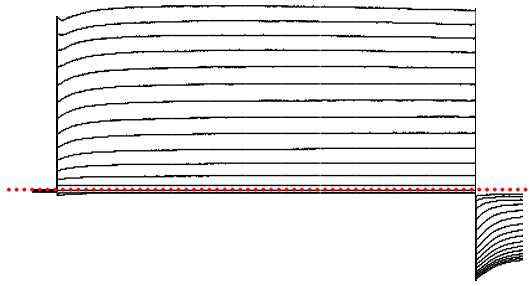

C. *Summary*

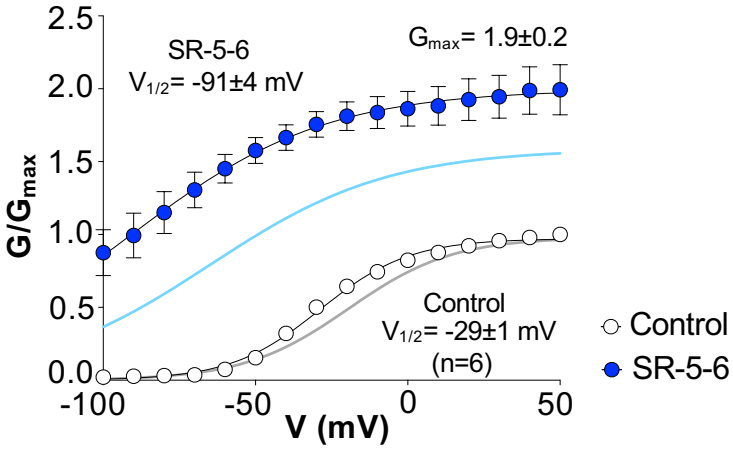

Figure 3.7: Effect of SR-5-6 on C519A mutation of K_v7.4 channels. A) A typical family of currents obtained from C519A mutation of K_v7.4 channels expressed in HEK cells. Voltage clamp protocol as described in Figure 3.1. Dotted lines represent the zero current level. **B**) The effect of 10 μM SR-5-6 on currents from the same cell. **C**) Summary activation curves obtained by measuring tail currents in six cells before (open circles) and during (blue circles) application of SR-5-6 (n=6). The continuous grey and light blue lines in the background represent the activation curves of control and the effect of the SR-5-6 on WT K_v7.4 channels respectively. The curves were fit with the Boltzmann equation.

A. *F254A mutant control*

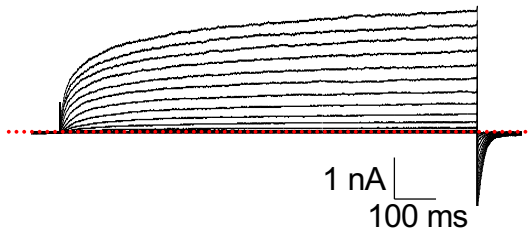

B. *SR-5-6 (10 μM) on F254A mutant*

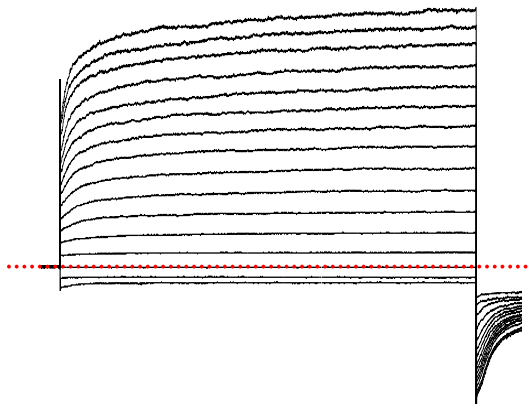

C. *Summary*

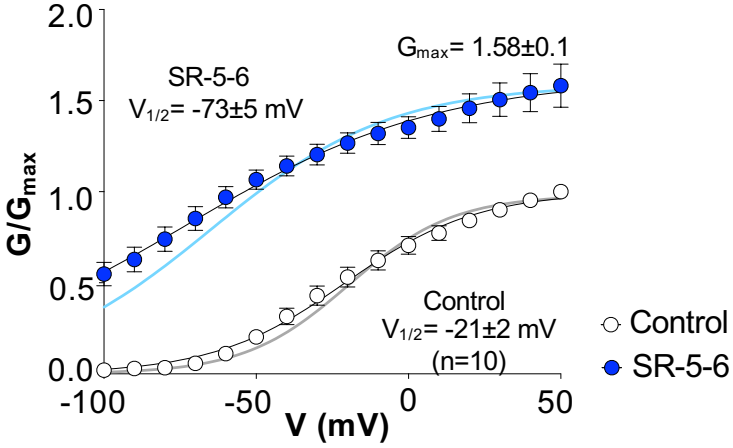

Figure 3.8: Effect of SR-5-6 on PUFA binding site mutation F254A of K_v7.4 channels. A) A typical family of currents obtained from F254A mutation of K_v7.4 channels expressed in HEK cells. Voltage clamp protocol as described in Figure 3.1. Dotted lines represent the zero current level. **B**) The effect of 10 μM SR-5-6 on currents from the same cell. **C**) Summary activation curves obtained by measuring tail currents in ten cells before (open circles) and during (blue circles) application of SR-5-6 (n=10). The continuous grey and light blue lines in the background represent the activation curves of control and the effect of the SR-5-6 on WT K_v7.4 channels respectively. The curves were fit with the Boltzmann equation.

A. *R297A mutant control*

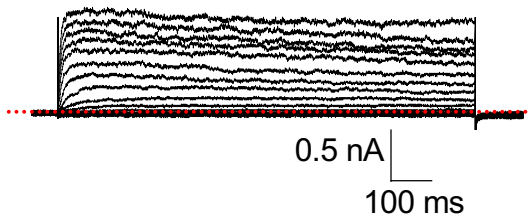

B. *SR-5-6 (10 μM) on R297A mutant*

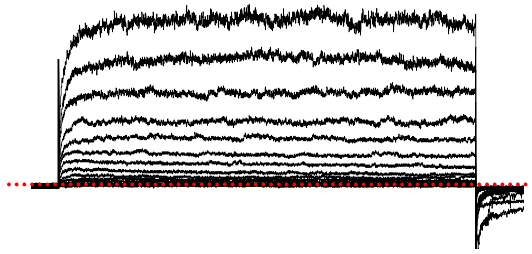

C. *Summary*

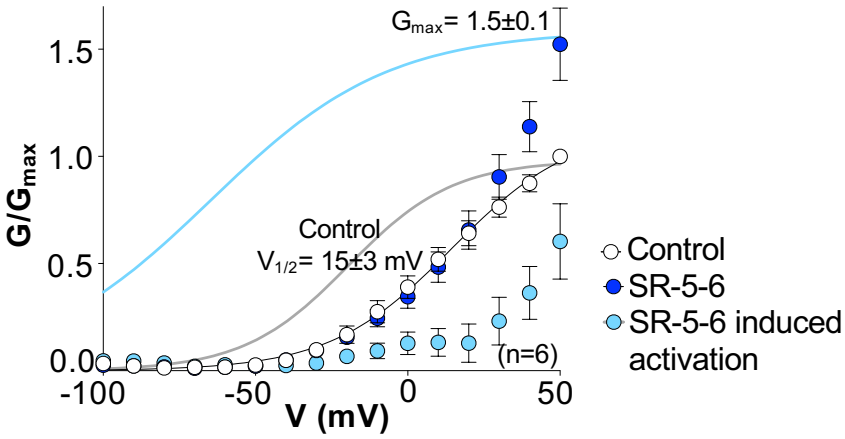

Figure 3.9: Effect of SR-5-6 on PUFA binding site mutation R297A of K_v7.4 channels. A) A typical family of currents obtained from R297A mutation of K_v7.4 channels expressed in HEK cells. Voltage clamp protocol as described in Figure 3.1. Dotted lines represent the zero current level. **B**) The effect of 10 μM SR-5-6 on currents from the same cell. **C**) Summary activation curves obtained by measuring outward currents in six cells before (open circles) and during (blue circles) application of SR-5-6 (n=6). The continuous grey and light blue lines in the background represent the activation curves of control and the effect of the SR-5-6 on WT K_v7.4 channels respectively. The curves were fit with the Boltzmann equation.

A. *E1R (E136R) - resting state mutant control*

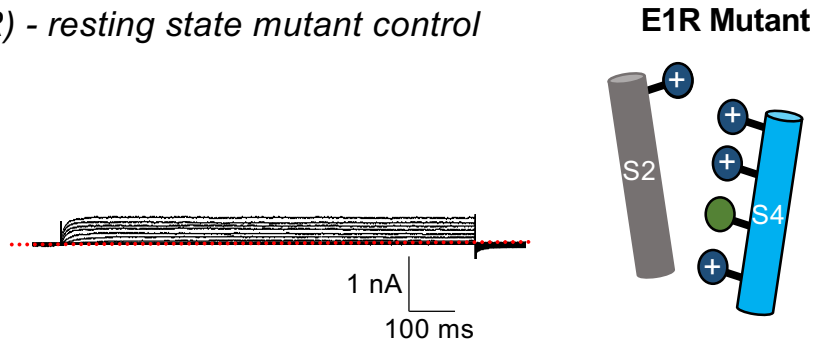

B. *SR-5-6 (10 μM) on E1R mutant*

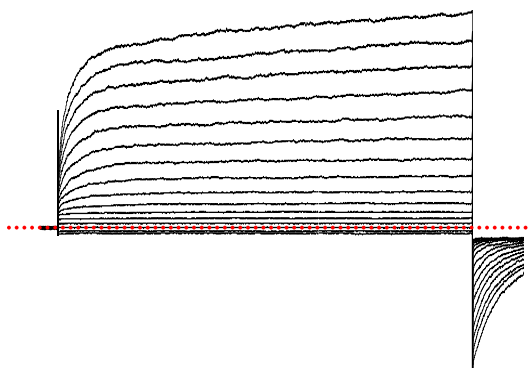

C. *Summary*

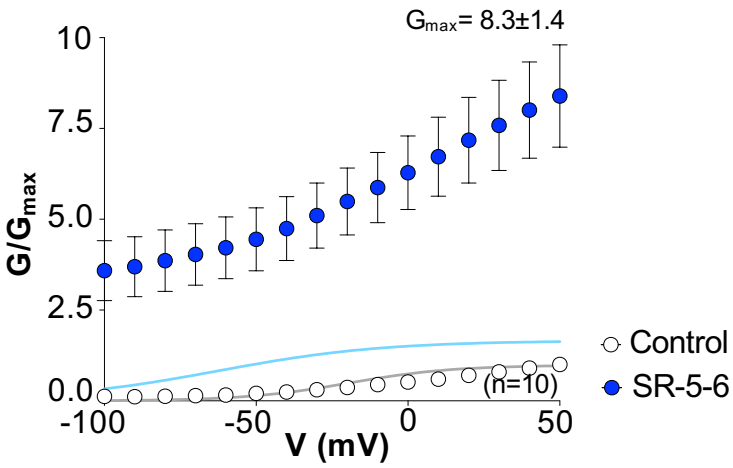

Figure 3.10: Effect of SR-5-6 on state dependent mutation E136R of K_v7.4 channels. A) A typical family of currents obtained from E136R mutation of K_v7.4 channels expressed in HEK cells. Voltage clamp protocol as described in Figure 3.1. Dotted lines represent the zero current level. **B**) The effect of 10 μM SR-5-6 on currents from the same cell. **C**) Summary activation curves obtained by measuring tail currents in ten cells before (open circles) and during (blue circles) application of SR-5-6 (n=10). The continuous grey and light blue lines in the background represent the activation curves of control and the effect of the SR-5-6 on WT K_v7.4 channels respectively. The curves were fit with the Boltzmann equation.

A. *Concentration effect of SR-5-6 on E1R (E136R) mutant*

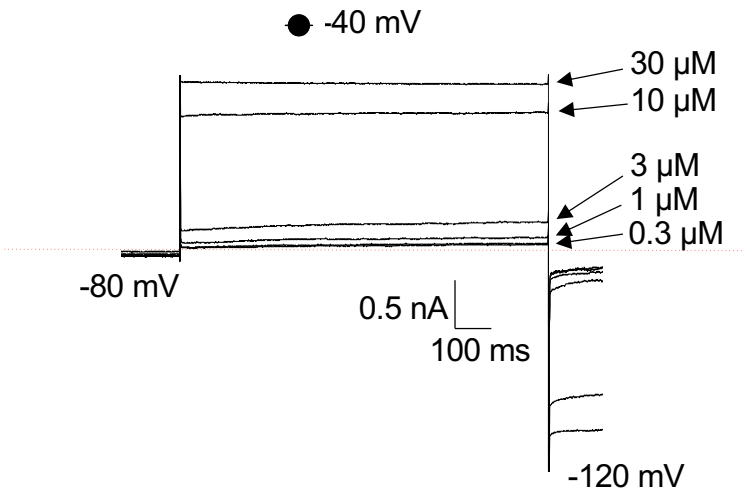

B. *Summary EC_{50}*

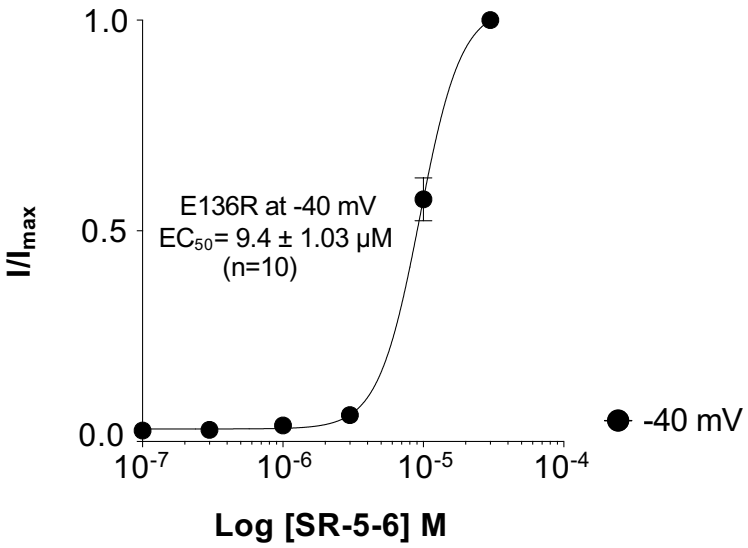

Figure 3.11: Concentration effects of SR-5-6 on E136R mutant channels. A) A typical family of currents obtained from E136R mutant channels expressed in HEK cells. Cells were held at -80 mV before evoking currents by stepping to -40 mV and stepped back to -120 mV to evoke tail currents. On the same cell 0.3 μM, 1 μM, 3 μM, 10 μM and 30 μM SR-5-6 effects were investigated and estimated the EC_{50} at -40 mV, Dotted lines represent the zero current level. **B**) Summary concentration effect curve of the SR-5-6 at -40 mV on E136R mutant (n=10). The curves were fit with the Hill-Langmuir equation.

A. *E1R;R1E (E136R;R204E) – partially activated state mutant control*

E1R/R1E Mutant

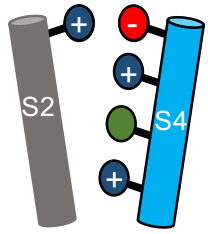

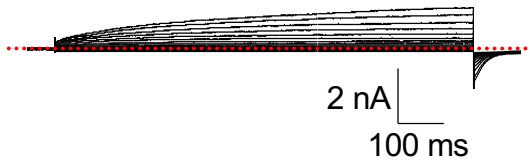

B. *SR-5-6 (10 μM) on E1R;R1E mutant*

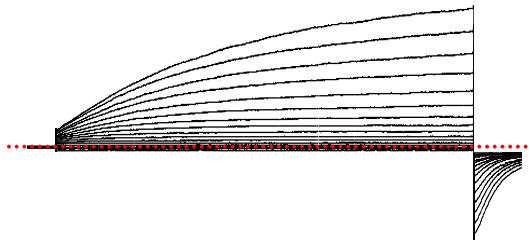

C. *Summary*

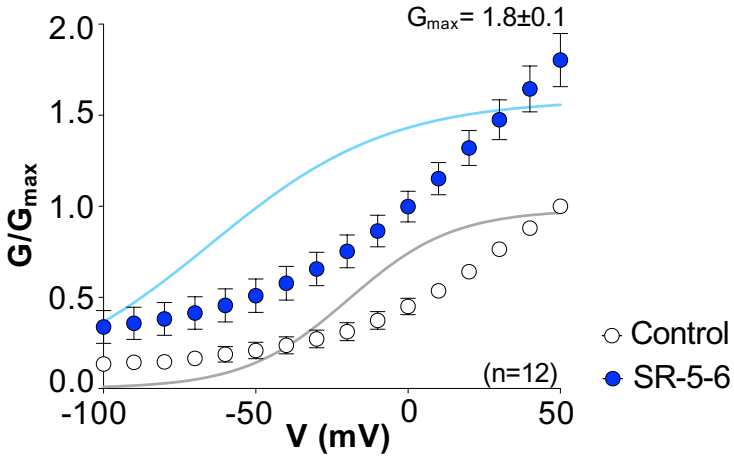

Figure 3.12: Effect of SR-5-6 on state dependent mutation E136R;R204E of K_v7.4 channels. A) A typical family of currents obtained from E136R;R204E mutation of K_v7.4 channels expressed in HEK cells. Voltage clamp protocol as described in Figure 3.1. Dotted lines represent the zero current level. **B**) The effect of 10 μM SR-5-6 on currents from the same cell. **C**) Summary activation curves obtained by measuring tail currents in twelve cells before (open circles) and during (blue circles) application of SR-5-6 (n=12). The continuous grey and light blue lines in the background represent the activation curves of control and the effect of the SR-5-6 on WT K_v7.4 channels respectively. The curves were fit with the Boltzmann equation.

A. *E1R;R2E (E136R;R207E) – partially activated state mutant control*

E1R/R2E Mutant

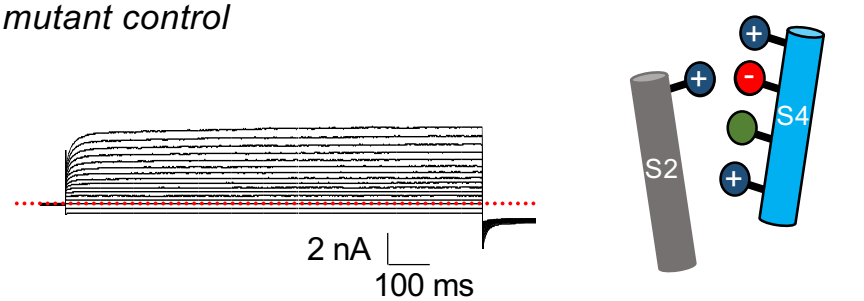

B. *SR-5-6 (10 μM) on E1R;R2E mutant*

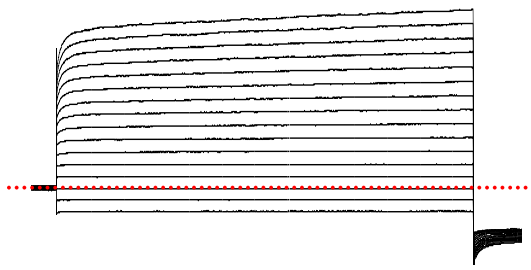

C. *Summary*

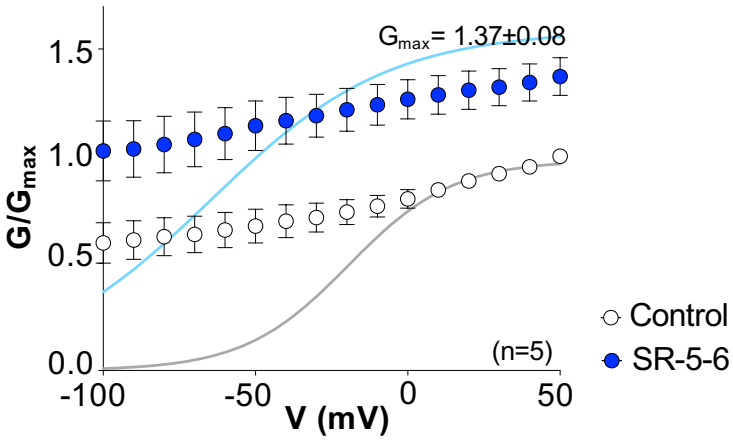

Figure 3.13: Effect of SR-5-6 on state dependent mutation E136R;R207E of K_v7.4 channels. A) A typical family of currents obtained from E136R;R207E mutation of K_v7.4 channels expressed in HEK cells. Voltage clamp protocol as described in Figure 3.1. Dotted lines represent the zero current level. **B**) The effect of 10 μM SR-5-6 on currents from the same cell. **C**) Summary activation curves obtained by measuring tail currents in five cells before (open circles) and during (blue circles) application of SR-5-6 (n=5). The continuous grey and light blue lines in the background represent the activation curves of control and the effect of the SR-5-6 on WT K_v7.4 channels respectively. The curves were fit with the Boltzmann equation.

A. *E1R;R1E (E136R;R213E) – fully activated state mutant control*

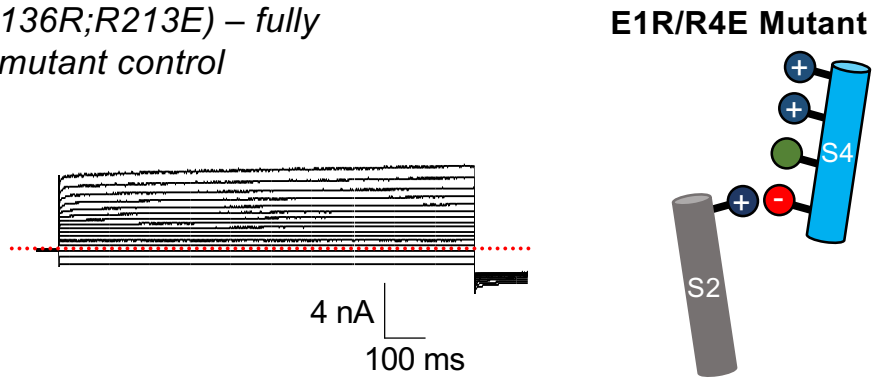

B. *SR-5-6 (10 μM) on E1R;R4E mutant*

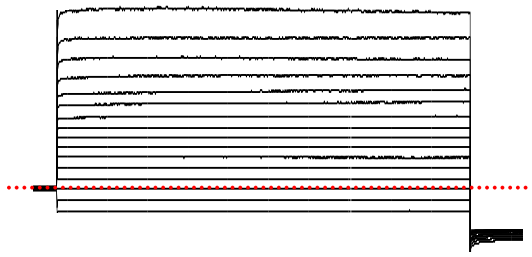

C. *Summary*

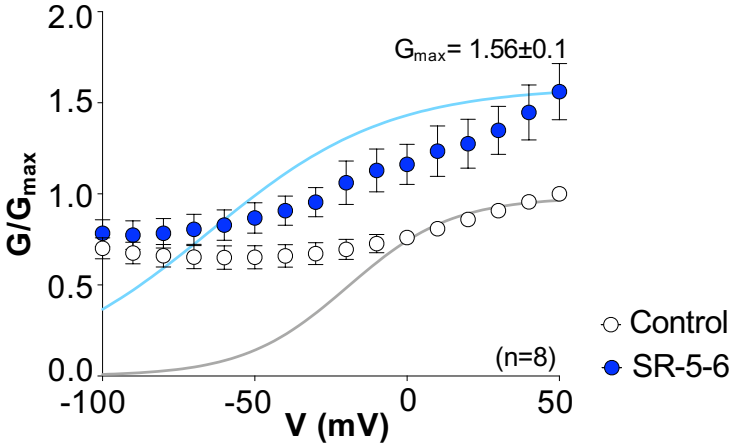

Figure 3.14: Effect of SR-5-6 on state dependent mutation E136R;R213E of K_v7.4 channels. A) A typical family of currents obtained from E136R;R213E mutation of K_v7.4 channels expressed in HEK cells. Voltage clamp protocol as described in Figure 3.1. Dotted lines represent the zero current level. **B**) The effect of 10 μM SR-5-6 on currents from the same cell. **C**) Summary activation curves obtained by measuring tail currents in eight cells before (open circles) and during (blue circles) application of SR-5-6 (n=8). The continuous grey and light blue lines in the background represent the activation curves of control and the effect of the SR-5-6 on WT K_v7.4 channels respectively. The curves were fit with the Boltzmann equation.

A. *Effect of SR-5-6 (10 μM) on $\Delta V_{1/2}$ of K_v7.4 mutants*

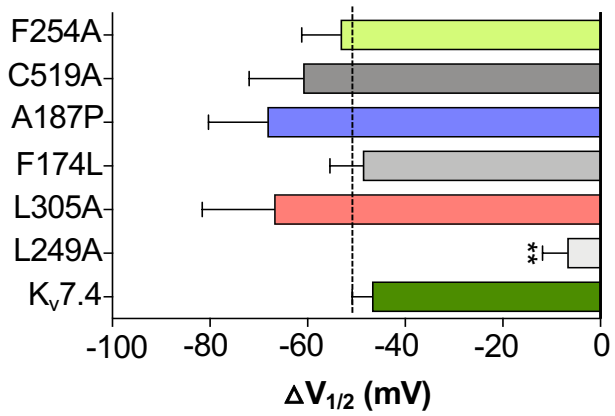

B. *Effect of SR-5-6 (10 μM) on G/G_{max} of K_v7.4 mutants*

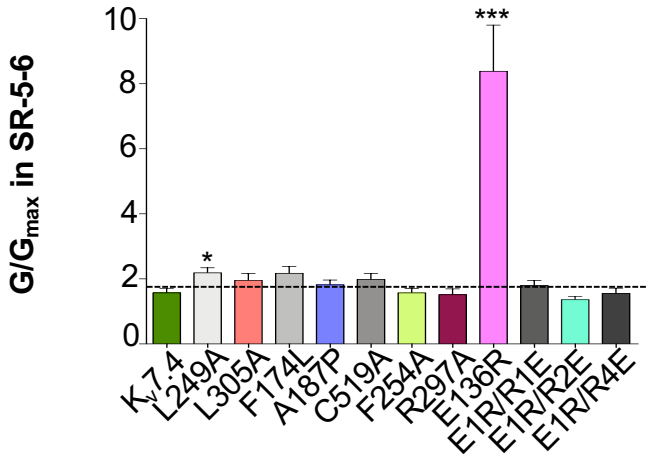

C. *Effect of SR-5-6 (10 μM) on $G_{-100\ mV}$ of K_v7.4 mutants*

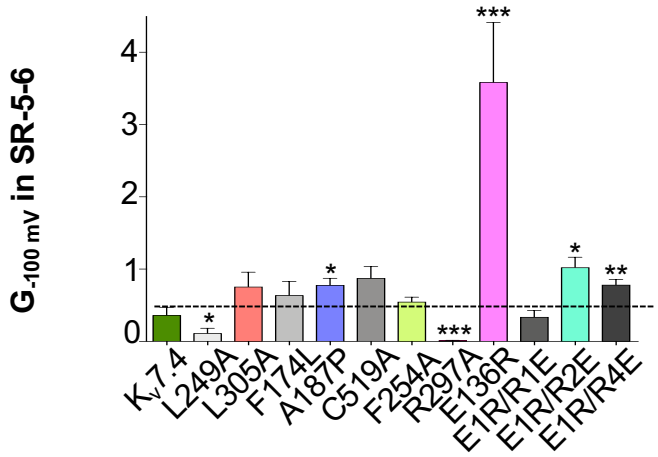

Figure 3.15: Effect of 10 μM SR-5-6 on $\Delta V_{1/2}$, G/G_{max} and $G_{-100\ mV}$ of K_v7.4 mutants. A) SR-5-6 mediated negative shift of the activation curve ($\Delta V_{1/2}$) on various mutants of K_v7.4 channels. A one-way ANOVA was performed with K_v7.4 as the control **B)** The effects of SR-5-6 on maximal conductance (G/G_{max}) of various mutants of K_v7.4 channels. **C)** SR-5-6 mediated change in conductance (G) at -100 mV on mutants of K_v7.4 channels. A Mann-Whitney, non-parametric test was used for G/G_{max} and $G_{-100\ mV}$ to compare K_v7.4 with other groups. *p<0.05, **p<0.01, ***p<0.001, ****p<0.0001.

A. *Effect of SR-5-6 (10 µM) on $G_{-100\ mV}$ of $K_v7.4$ mutants*

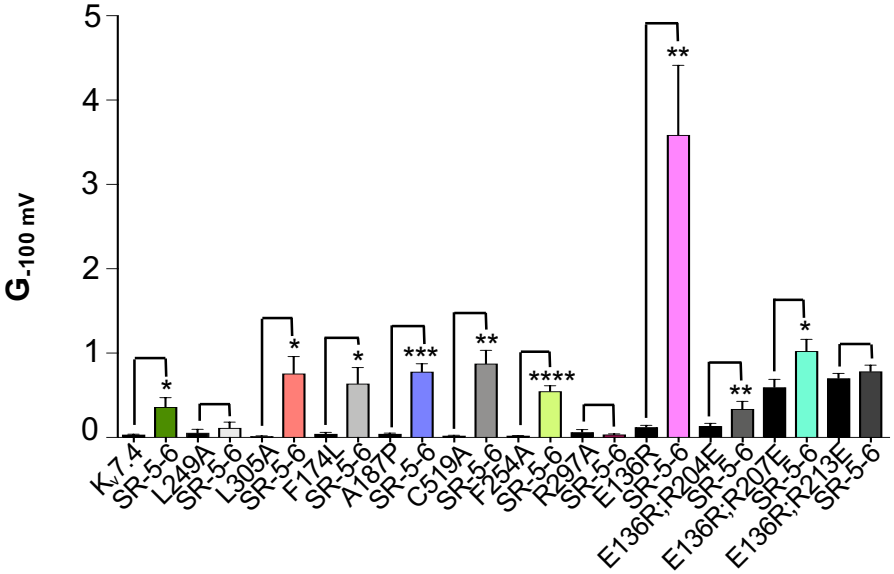

Figure 3.16: Effect of 10 µM SR-5-6 on $G_{-100\ mV}$ of $K_v7.4$ mutants.
The above data depicts the change in conductance (G) at -100 mV in HEK cells expressing the wildtype and the mutant channels. The black bars represent the control condition and the respective colored bars indicate the effect of SR-5-6 as labelled in the figure. Paired t tests, *p<0.05, **p<0.01, ***p<0.001, ****p<0.0001.

Chapter 4

Assessing the effects of SR-5-6 on $K_v7.4$ domain swap constructs and mutant channels expressed in HEK cells

4.1 Introduction

The results presented in Chapter 3 demonstrated that SR-5-6 was a very effective $K_v7.4$ channel opener, but they failed to identify the residues which, when mutated, abolished the excitatory effects of SR-5-6. Interestingly, from a screen of mutants that had previously been shown to contribute to the effects of other K_v7 activators, the L249A mutant was found to be effective at reducing the ability of SR-5-6 to shift $V_{1/2}$ negatively. However, the identification of other mutants that also blocked the effects of SR-5-6 on G/G_{max} was unsuccessful. Consequently, it was decided to take a different approach to help determine which regions of the channel might contribute to these excitatory effects. In this chapter, the chimeric channels between $K_v7.3$ and $K_v7.4$ were examined, given that Dudem (2019) previously showed that $K_v7.3$ channels were much less sensitive to 10 μM SR-5-6 ($\Delta V_{1/2}$ = -16 ± 1 mV; G/G_{max} = 1.04 ± 0.04) than $K_v7.4$ channels ($\Delta V_{1/2}$ = -46 ± 1.2; G/G_{max} to 1.58 ± 0.1). Consequently, the $K_v7.4$ channel was divided into a series of structural units and swapped with the corresponding region from $K_v7.3$ channels (Figure 4.0), in an attempt to ascertain which regions of the channel were responsible for the differential sensitivity to SR-5-6 to $K_v7.3$ and $K_v7.4$.

The main objectives of this chapter were to examine the effects of SR-5-6 on:

1. S4, S5, S6 transmembrane helix and S3-S4 linker $K_v7.4$:$K_v7.3$ swap constructs.
2. $K_v7.3$/$K_v7.4$ pore loop chimera.
3. S1-S2-S3-S4 voltage-sensor domain and S5-PL-S6 pore domain swap constructs.
4. C-terminus swap construct.
5. S4-S5 linker and pore loop mutations.

Figure 4.0 overleaf shows a diagrammatic representation of each domain swapped construct compared to WT $K_v7.4$ (panel A) and WT $K_v7.3$ (panel B).

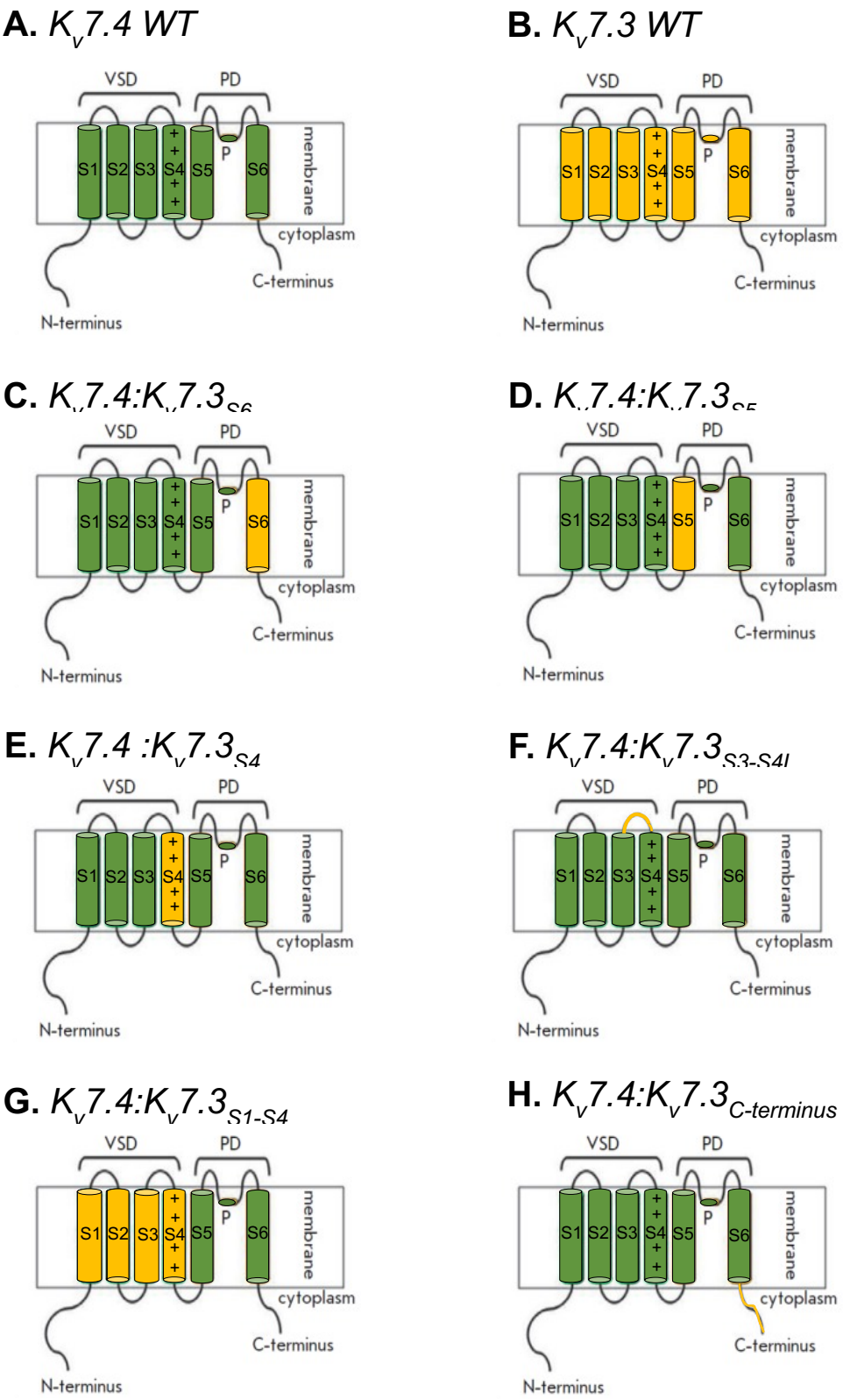

Figure 4.0: Cartoon representation of K_v7 single subunit for the wildtype and swap constructs examined in this chapter. A) *Wildtype $K_v7.4$ channels with helices coloured in green.* ***B)*** *WT $K_v7.3$ representative cartoon with helices coloured in yellow.* ***C, D, E, F, G & H)*** *Swap constructs showing the $K_v7.4$ background in green and the yellow helices represent the helices/C-terminus from $K_v7.3$.*

4.2 Results

4.2.1 SR-5-6 was not effective in K_v7.3 wildtype channels

In the first set of experiments for this chapter, the effects of 10 μM SR-5-6 on the wildtype (WT) K_v7.3 channels was re-examined, to confirm that they were less responsive than K_v7.4. Figure 4.1A shows a family of currents from WT K_v7.3 channels expressed in HEK293 cells. The whole-cell patch configuration was used to record the currents and, as shown inset in Figure 4.1, the cells were held at -80 mV and then were stepped from -100 mV to +50 mV in 10 mV increments to evoke steady-state currents. The cells were then repolarized to -120 mV to generate tail currents, which were used to generate the G-V summary data. As has been reported previously, the amplitude of K_v7.3 current was much smaller compared to wildtype K_v7.4 channels (see Figure 3.1), even though the concentration of cDNA used for transfection was 10 times higher for K_v7.3 channels (K_v7.4 - 25 ng/ml and K_v7.3 - 250 ng/ml). When the G-V data for the K_v7.3 channels was fitted with a Boltzmann equation (Figure 4.1C, solid lines), the activation $V_{1/2}$ was -42 ± 1 mV (n=5). In the presence of 10 μM SR-5-6 (Figure 4.1B) the current amplitude was not significantly enhanced, but it was clear that it slowed deactivation (from 17 ± 1.6 ms to 81.8 ± 17.5 ms; $p<0.05$; paired t-test; Figure 4.10B) as measured following a step from +50 mV to -120 mV. The time constant of activation at +50 mV was not affected by SR-5-6 since it was 24.2 ± 2.4 ms in control compared to 24.7 ± 3.1 ms in SR-5-6 (Figure 4.10A). When the G-V relationship was summarized from the tail currents, there was no significant increase in G/G_{max} in presence of SR-5-6 (G/G_{max} = 1.02 ± 0.05; n=5; $p<0.01$ when compared to WT K_v7.4; Figure 4.1C & 4.9B), but the activation $V_{1/2}$ shifted from -42 ± 1 mV to -57 ± 2 mV which was significantly less when compared to WT K_v7.4 channels ($\Delta V_{1/2}$ = -15 ± 2 mV, $p<0.05$; Figure 4.9A). The conductance at -100 mV ($G_{-100\ mV}$) was 0.06 in control and 0.08 in presence of SR-5-6 (Figure 4.11), which was significantly reduced compared to WT K_v7.4 ($p<0.01$; Figure 4.9C & 4.11). These data were consistent with the previous findings of Dudem (2019) where the SR-5-6 effects were much less pronounced in K_v7.3 than in K_v7.4. This suggested that using K_v7.3/7.4 chimeras may help to narrow down the regions of the channel that bind SR-5-6.

4.2.2 SR-5-6 effects were not altered with the S6 helix swap construct: $K_v7.4$:$K_v7.3_{S6}$

In contrast to $K_v7.3$ WT channels, SR-5-6 effects on $K_v7.4$ WT (Figure 3.1) provided very different results, as evidenced by i) a substantial rise in G/G_{max} to ~1.6, ii) a much more negative shift in the activation $V_{1/2}$ (~50 mV), and iii) a significant increase in $G_{-100\ mV}$ to 0.36. As a result, it was important to explore what effects SR-5-6 would have if the different helices were swapped. Figure 4.2 shows a multiple sequence alignment of $K_v7.1$-$K_v7.5$ in which the 6 transmembrane helices are shaded in yellow. In the first helix swap experiment, the $K_v7.3$ S6 helix replaced the S6 helix on an otherwise normal, $K_v7.4$ background, as shown in panel C of Figure 4.0. In all subsequent experiments, the background channel is listed first ($K_v7.4$) and the helix swapped into it from the donor ($K_v7.3_{S6}$) is listed after the colon. The resultant $K_v7.4$:$K_v7.3_{S6}$ chimeric construct was then overexpressed in HEK cells and studied under voltage clamp in whole-cell mode, using the same protocol as that shown in Figure 4.1 (inset). Figure 4.3A shows a family of currents for the $K_v7.4$:$K_v7.3_{S6}$ chimera in control conditions. This construct produced currents which resembled $K_v7.4$. However, the currents only activated at voltages more positive to -50 mV. When 10 μM SR-5-6 was applied to the same cell (Figure 4.3B), three main effects were noticed. Firstly, the current amplitude was increased. Secondly, the channels activated more rapidly than under control conditions, as the kinetics of activation at +50 mV were significantly increased by the application of SR-5-6 (81.7 ± 13.3 ms before and 61.6 ± 14.9 ms in SR-5-6; n=8; $p<0.05$; paired t-test; Figure 4.11A). Thirdly, the tail currents were larger and slower than those recorded under control conditions. The deactivation time constant was 8.9 ± 1.2 ms in control, compared to 37.8 ± 6 ms in SR-5-6, following a step from +50 mV to -120 mV ($p<0.01$; paired t-test; Figure 4.11B). When the control G-V data (open symbols) was plotted from the tail currents, we observed a positive shift in the control activation $V_{1/2}$ compared to WT $K_v7.4$ (WT shown as a grey line, Figure 4.3C). In these experiments, prior to application of SR-5-6, the activation $V_{1/2}$ of the $K_v7.4$:$K_v7.3_{S6}$ channels was -0.5 ± 2 mV and in the presence of SR-5-6, it shifted to -39 ± 4 mV, resulting in a $\Delta V_{1/2}$ of -38 ± 4 mV (n=8). The $\Delta V_{1/2}$ was not significantly different to that observed in WT $K_v7.4$ channels (Figure 4.9A). The G/G_{max} in presence of SR-5-6 was clearly enhanced as well, to 2.1 ± 0.2 (n=8), though it did not read

significance when compared to WT $K_v7.4$ channels (Figure 4.9B). The conductance at -100 mV ($G_{-100\ mV}$) was not significantly increased (0.015 ± 0.005 in control compared to 0.04 ± 0.01 in presence of 10 μM SR-5-6; ns; paired t-test; Figure 4.11) which was different from that observed in WT $K_v7.4$ channels ($p<0.01$; Figure 4.9C), where $G_{-100\ mV}$ changed from 0.03 in control to 0.36 in SR-5-6 (n=7; $p<0.05$; paired t-tests; Figure 4.11). This indicated that in this chimeric construct, SR-5-6 did not activate the channels at very negative potentials. However, the above results suggested that the replacement of the $K_v7.4$ S6 helix with the $K_v7.3$ S6 helix did not abolish the effects of SR-5-6 on either G/G_{max} or $\Delta V_{1/2}$.

4.2.3 $K_v7.4$ channels S5 helix chimera ($K_v7.4$:$K_v7.3_{S5}$) construct failed to reduce the effects of SR-5-6

Next, the substitution of the S5 helix was examined if it altered the response of the SR-5-6. The S5 helix along with the S6 and pore loop form the main ion conduction pathway or the pore domain and is critical in the gating mechanism for several other modulators (Heginbotham *et al.,* 1992; Yellen, 1998; Lange *et al.,* 2008; Tatulian *et al.,* 2001). It was technically more efficient to utilize site-directed mutagenesis of the four non-conserved residues between $K_v7.3$ and $K_v7.4$ (V248T, F251L, A252S and A259V, Figure 4.2) to produce the $K_v7.4$:$K_v7.3_{S5}$ construct, which is shown in cartoon form in Figure 4.0D. This construct was functional and, as can be seen in Figure 4.4, the $K_v7.4$:$K_v7.3_{S5}$ currents activated at potentials positive to -60 mV. When 10 μM SR-5-6 was applied, it significantly increased current amplitude at all potentials and massive tail currents were observed upon repolarisation (Figure 4.4B). The activation kinetics resembled those of WT $K_v7.4$ channels where the time constant of activation at +50 mV was faster in the presence of SR-5-6 (70.3 ± 6.2 ms compared to control of 146.5 ± 15.8; $p<0.01$; paired t-test; Figure 4.10A). Also, the time constant of deactivation at -120 mV, following step to +50 mV was almost 5 fold slower (71.8 ± 4.9 ms, compared to control 16.9 ± 2.6 ms; $p<0.001$; paired t-test; Figure 4.10B). When the G-V relationship was plotted, G/G_{max} increased in presence of SR-5-6 to 1.3 ± 0.03 (n=5) which was significantly less than that observed in WT $K_v7.4$ ($p<0.05$; Figure 4.9B). The conductance at -100 mV (G_{-100}

$_{mV}$) was significantly increased from 0.02 in control to 0.3 in SR-5-6 ($p<0.05$; paired t-test; Figure 4.11), which was similar to that observed in WT $K_v7.4$ channels, in the presence of SR-5-6 (Figure 4.9C). The activation $V_{1/2}$ under control conditions was -10 ± 2 mV and in the presence of SR-5-6, it significantly shifted to -73 ± 2 mV, resulting in a $\Delta V_{1/2}$ for SR-5-6 in this swap construct of -58 ± 4 mV, which was not significantly different to WT $K_v7.4$ channels (n=5; Figure 4.9A). These results suggested that the only obvious effect of substituting the $K_v7.3$ S5 residues into a $K_v7.4$ background was a smaller increase in the G/G_{max} compared to WT $K_v7.4$ in the presence of SR-5-6.

4.2.4 Effects of SR-5-6 on the voltage sensing helix S4 chimera ($K_v7.4$:$K_v7.3_{S4}$)

The S4 helix was examined next and, as shown in Figure 4.2, this region differs from the $K_v7.3$ S4 helix region only at two amino acid positions (M206L and V215L). Given these were the only differences, used mutagenesis to create the construct, which is referred to as $K_v7.4$:$K_v7.3_{S4}$ (Figure 4.0E). This construct was functional and as shown in Figure 4.5A, produced outward currents at potentials positive to -70 mV. In the presence of 10 μM SR-5-6 (Figure 4.5B), the current amplitude was increased significantly at all potentials and also observed large inward currents at potentials negative to -80 mV. The G-V relationship was plotted in Figure 4.5C, the G/G_{max} was enhanced from 1 to 1.96 ± 0.2 in the presence of SR-5-6 (ns when compared to WT $K_v7.4$; Figure 4.9B). The $G_{-100\ mV}$ also increased significantly from 0.04 in control to 0.5 in SR-5-6 ($p<0.001$, paired t-test; Figure 4.11). The activation $V_{1/2}$ shifted from -11 ± 4 mV in control to -54 ± 8 mV (n=7) resulting in a $\Delta V_{1/2}$ of -43 ± 8 mV. These effects were very similar to those observed in the WT $K_v7.4$ channels before (grey line) and in the presence of SR-5-6 (blue line). It also slowed deactivation (recorded at -120 mV, following a step to +50 mV) from 14.4 ± 2.2 ms in control to 38.8 ± 5.8 ms in the presence of SR-5-6 ($p<0.001$; paired t-test; Figure 4.10B). The activation was also faster as evidenced by the change in the activation time constant at +50 mV, from 138.6 ± 15.8 ms in control, compared to 55.1 ± 11.8 ms in SR-5-6 ($p<0.01$; paired t-test; Figure 4.10A). The overlap in the activation curves of the $K_v7.4$:$K_v7.3_{S4}$ chimeric

channel with the $K_v7.4$ WT channels, clearly shows that effects of SR-5-6 were not abolished in this construct.

4.2.5 The S3-S4 linker swap did not reduce the effects of SR-5-6 in $K_v7.4$ channels

Next, produced a construct in which the S3-S4 linker of $K_v7.3$ was added in place of the same region in $K_v7.4$, as illustrated in Figure 4.6A (inset). Sequence alignment of this region (Figure 4.2) showed three non-conserved residues (T193N, I197V, F198L) and one deletion (A202) when the $K_v7.4$ and $K_v7.3$ S3-S4 linkers were compared. Given this, used a mutagenesis approach to generate this construct, which is referred to as $K_v7.4$:$K_v7.3_{S3\text{-}S4L}$ and is shown diagrammatically in Figure 4.0F. Currents evoked from this construct again looked similar to WT $K_v7.4$ currents, although the currents activated at more positive potentials. When the activation curve was constructed, these currents had a $V_{1/2}$ of 11 ± 3 mV which was significantly different to the WT $K_v7.4$ ($p<0.0001$; unpaired t-test). However, as Figure 4.6B suggests, SR-5-6 still increased the current amplitude and slowed deactivation. The G/G_{max} in the presence of SR-5-6 was increased to 1.68 ± 0.1 (n=8). The deactivation slowed from 20.4 ± 4.1 to 55.1 ± 6.3 ms following a step from +50 mV to -120 mV ($p<0.0001$; paired t-test; Figure 4.10B). As shown in the blue symbols of Figure 4.6C, SR-5-6 shifted activation negatively to -48 ± 5 mV, resulting in a $\Delta V_{1/2}$ of -58 ± 6 mV (n=8). Interestingly, the time constant of activation at +50 mV did not change significantly in this swap construct in SR-5-6, as it was 91.3 ± 8.7 ms in control and 97.4 ± 15.2 in presence of SR-5-6 (Figure 4.10A). This was unlike what was observed in WT $K_v7.4$, where a significant enhancement of the rate of activation in presence of SR-5-6 was observed (Figure 3.1 & 4.10A). Also, the $G_{-100\ mV}$ increased from 0.03 in control to 0.2 in presence of SR-5-6 ($p<0.05$, paired t-test; Figure 4.11). Overall, the above results suggested that, with the exception of a lack of effect on activation tau, the remaining SR-5-6 effects were not reduced in the $K_v7.4$:$K_v7.3_{S3\text{-}S4L}$ chimeric channel.

4.2.6 Pore loop region swap between $K_v7.4$ and $K_v7.3$ yielded non-functional channels

As both S6 and S5 helix of the pore domain were swapped and examined the SR-5-6 effects on the chimeric channels, the results suggested that neither helix from $K_v7.3$ abolished the effect of SR-5-6. The pore loop region from $K_v7.3$ was then swapped into the $K_v7.4$ background, but unfortunately, this $K_v7.4$:$K_v7.3_{PL}$ mutant did not appear to form functional channels. Consequently, it was not possible to deduce if the differential effects of SR-5-6 in $K_v7.4$ and $K_v7.3$ was due to its binding in the pore loop of the channel.

4.2.7 Effects of SR-5-6 on voltage domain swap construct S1-S4 chimera ($K_v7.4$:$K_v7.3_{S1-S4}$)

As the individual helices examined through the chimeric approach so far did not reduce the effects of SR-5-6, it was next hypothesized if a combination of two or more helices contributed to the effects of SR-5-6. To test this, larger chimeras were generated, whereby the whole voltage-sensing domain (S1-S4), pore domain (S5-PL-S6) and the C-terminus was swapped between $K_v7.4$ and $K_v7.3$. The first set of larger chimeras was the S1-S4 voltage sensor domain swap construct ($K_v7.4$:$K_v7.3_{S1-S4}$, Figure 4.0G), which was generated using the cloning method (Section 2.5 in methods). The resultant domain swap construct was overexpressed in HEK cells and studied using whole-cell patch configuration, using the protocol described in Figure 4.1. The $K_v7.4$:$K_v7.3_{S1-S4}$ construct produced currents which were activated at around -80 mV, as shown in Figure 4.7A and summarised in the open symbols of Figure 4.7C. On addition of 10 μM SR-5-6 to the same cell, the current amplitude increased at all voltages and large inward currents were apparent at potentials negative to -80 mV (Figure 4.7B). The activation and deactivation kinetics could not be determined for this set of experiments, as the channels appeared to be constitutively active in the presence of SR-5-6. However, when the G-V relationship was plotted for five cells under control conditions (open circles) and in presence of SR-5-6 (blue circles), an increase in G/G_{max} to 1.2 ± 0.06 was observed in presence of SR-5-6 (n=5). The increase in G/G_{max} was significantly reduced when compared to WT $K_v7.4$ channels ($p<0.05$; Figure 4.9B). In contrast, the conductance at -100 mV ($G_{-100\ mV}$) increased from 0.03 in control to 0.74 in the presence of SR-5-6, which was

significantly more than that observed in WT $K_v7.4$ channels ($p<0.05$; Figure 4.9C). The activation $V_{1/2}$ under control was -34 ± 1 mV, but in the presence of SR-5-6, it was not possible to fit the data with a Boltzmann equation to accurately determine the $V_{1/2}$. Nevertheless, it was clear that an increase in G/G_{max} and a large increase in $G_{-100\ mV}$ was still observed in presence of SR-5-6 in the $K_v7.4$:$K_v7.3_{S1-S4}$ construct. These data demonstrated that the effects of SR-5-6 were not abolished when the entire voltage-sensing domain (S1-S4) was swapped between $K_v7.3$ and $K_v7.4$.

4.2.8 Pore domain swap (S5-PL-S6) between $K_v7.3$ and $K_v7.4$ could not be examined as it yielded a non-functional protein

The next chimera generated had the pore domain (S5-PL-S6) from $K_v7.3$ swapped into the $K_v7.4$ background. Molecular cloning was used to generate this construct and the resultant $K_v7.4$:$K_v7.3_{S5-PL-S6}$ channels were expressed in HEK cells, prior to electrophysiological characterization. Unfortunately, this $K_v7.4$:$K_v7.3_{S5-PL-S6}$ construct, just like the pore loop swap construct ($K_v7.4$:$K_v7.3_{PL}$), failed to generate any currents in response to the standard voltage-clamp protocols. This suggested that the non-functionality of the channel was mainly attributed to the pore loop region.

4.2.9 C-terminus chimera between $K_v7.3$ and $K_v7.4$ also did not abolish the effects of SR-5-6

Since substitution of either the voltage-sensing domain or the pore domain failed to abolish the effects of SR-5-6, the contribution of the C-terminus to the response to SR-5-6 was next examined. The C-terminus in $K_v7.4$ is 365 amino acids long, has a CaM binding pocket, a PIP_2 binding pocket and a number of phosphorylation sites that play a key role in the regulation of the channel (Haitin & Attali, 2008; Sun & MacKinnon; 2020; Marx *et al.,* 2002). Therefore, a C-terminus swap construct was generated between $K_v7.3$ and $K_v7.4$ using molecular cloning. The resultant $K_v7.4$:$K_v7.3_{C-terminus}$ construct was overexpressed in HEK cells and studied using the protocol shown in Figure 4.1. Under control conditions, the $K_v7.4$:$K_v7.3_{C-terminus}$ currents were similar to WT $K_v7.4$ channels and activated at potentials positive to -60 mV (Figure 4.8A). When 10 μM SR-5-6 was applied to the same cell, as seen in Figure 4.8B, a very large

increase in current amplitude was observed at all potentials and the tail currents were bigger and slower than in control. The time constant of deactivation slowed from 9.9 ± 1 ms in control to 32.6 ± 7 ms in SR-5-6 ($p<0.05$; paired t-test; Figure 4.10B). The activation kinetics could not be fit in this set of experiments, as the channels appeared to activate instantaneously, in response to each voltage step, presumably as a result of the channels being activated at much more negative potentials, in the presence of SR-5-6. In six similar cells (Figure 4.8C) G/G_{max} increased to 1.76 ± 0.2 in presence of SR-5-6 (n=6; ns compared to WT $K_v7.4$; Figure 4.9B) and $V_{1/2}$ shifted from -29 ± 1 mV to -102 ± 6 mV in presence of SR-5-6, resulting in a $\Delta V_{1/2}$ of -71 ± 10 mV (n=6, ns compared to WT $K_v7.4$; Figure 4.9A). The conductance at -100 mV ($G_{-100\ mV}$) also increased from 0.01 in control to 0.9 in presence of SR-5-6 (Figure 4.11) which was significantly higher than that in WT $K_v7.4$ channels ($p<0.05$; Figure 4.9C). These results suggested that the effects of SR-5-6 were not reduced in $K_v7.4$:$K_v7.3_{C\text{-terminus}}$ channels.

4.2.10 The effects of SR-5-6 on S4-S5 linker mutations V230A, V231I and Y232C in $K_v7.4$ channels

As the sequence of S4-S5 linker (S4-S5L) shown in Figure 4.2 demonstrated, there are only three non-conserved residues in this region of $K_v7.3$ (V230A, V231I and Y232C) compared to $K_v7.4$. Therefore, site-directed mutagenesis was used to change the $K_v7.4$ S4-S5L segment into a $K_v7.3$ linker segment. Unfortunately, this triple mutant (V230A:V231I:Y232C) failed to generate functional channels when expressed in HEK cells and studied under a voltage clamp. Consequently, each of these three residues was mutated individually in $K_v7.4$, to the corresponding $K_v7.3$ residues before examining the effects of SR-5-6 on these.

4.2.10.1 S4-S5 linker mutant $V230A_{S4\text{-}S5L}$ did not abolish the effect of SR-5-6 in $K_v7.4$ channels

The first mutation examined in the S4-S5 linker region was $K_v7.4$:$V230A_{S4\text{-}S5L}$ and Figure 4.12 shows a typical family of currents recorded from this mutant channel in control conditions (Figure 4.12A) and in the presence of SR-5-6 respectively (Figure 4.12B). Interestingly, this mutant activated at much more negative potentials. When the activation curves were constructed from tail currents and summarized data for seven cells under control conditions (open circles) and in

the presence of SR-5-6 (blue circles), it was clear that SR-5-6 appeared even more effective at activating these negatively activating channels. In control, the activation $V_{1/2}$ was -47 ± 4 mV (n=7; Figure 4.12C), but it was not possible to fit the data obtained in the presence of SR-5-6 with the Boltzmann function, as the activation curve was approximately linear over the entire voltage range recorded. However, in this mutant, the G/G_{max} increased to 1.4 ± 0.2 (n=7; Figure 4.12C) in the presence of SR-5-6. In the presence of SR-5-6, the channels appeared to be constitutively active, as evidenced by a large increase in $G_{-100\ mV}$ to 1.2 ± 0.1 ($p<0.01$ compared to WT $K_v7.4$; Figure 4.21C and 4.22). The results thus suggest that mutating the V230 residue in $K_v7.4$ to alanine not only failed to reduce the effect of SR-5-6 but actually appeared to enhance its effects.

4.2.10.2 $K_v7.4$ channels S4-S5 single mutant channel $V231I_{S4\text{-}S5L}$ did not reduce the effect of SR-5-6

V231 in $K_V7.4$ was the next residue to be mutated and it was changed to isoleucine, which is present at the equivalent position in $K_v7.3$ ($K_v7.4$:$V231I_{S4\text{-}S5L}$). In contrast to the effects of the V230A mutant, the $K_v7.4$:$V231I_{S4\text{-}S5L}$ mutant did not shift the activation $V_{1/2}$, as shown in Figure 4.13A, where it activated at around -70 mV, which was very similar to WT $K_v7.4$ channels. When 10 μM SR-5-6 was applied to this mutant, it significantly enhanced the currents at all potentials (Figure 4.13B). When the data was summarized and fitted with Boltzmann equation to generate a G-V curve, it was clear that SR-5-6 enhanced the G/G_{max} from 1 to 1.47 ± 0.08 (n=7; ns vs WT $K_v7.4$; Figure 4.13C) and shifted the activation $V_{1/2}$ from -16 ± 2 mV in control to -63 ± 4 mV, resulting in a $\Delta V_{1/2}$ of -50 ± 5 mV (n=7; Figure 4.13C). The conductance at -100 mV ($G_{-100\ mV}$) also increased from 0.05 in the control to 0.27 in presence of SR-5-6 (Figure 4.22). These effects were practically identical to the effects on the WT $K_v7.4$ (see solid grey and blue lines for comparison) and it is clear that the V231I mutant did not reduce the effects of SR-5-6 in $K_v7.4$ channels.

4.2.10.3 The effects of SR-5-6 on $Y232C_{S4\text{-}S5L}$ mutation in $K_v7.4$ channels

The final, non-conserved residue in the S4-S5 linker segment between $K_v7.4$ and $K_v7.3$ was Y232. Y232 was mutated to cysteine which is present in $K_v7.3$ at the equivalent position ($K_v7.4$:$Y232C_{S4\text{-}S5L}$). These mutant currents also activated

from -70 mV (Figure 4.14A) and as can be seen from the summary data (Figure 4.14C), the $K_v7.4$:Y232C_{S4-S5L} control currents were also very similar to wildtype $K_v7.4$ channels (solid grey line). 10 μM SR-5-6 (Figure 4.14B) enhanced the currents at all voltages, although it appeared to be a little less effective than on the WT $K_v7.4$ (see solid blue line). From the summary G-V curve obtained from six cells, the G/G_{max} was increased from 1 to 1.4 ± 0.06 in SR-5-6 (n=6; Figure 4.14C), which was not significantly different than what was observed in WT $K_v7.4$ channels (Figure 4.21B). The activation also shifted negatively from -22 ± 1 mV in control to -61 ± 2 mV in SR-5-6, resulting in a $\Delta V_{1/2}$ for this mutant of -40 ± 2 mV (n=6; Figure 4.14C), which was not significantly different to that observed in WT channels (Figure 4.21A). From the above data, we conclude that none of the non-conserved residues in the S4-S5 linker were essential for mediating the effects of SR-5-6 in $K_v7.4$ channels.

4.2.11 The effects of SR-5-6 on pore loop mutations in $K_v7.4$ channels

Having failed to generate a functional swap construct of either the pore loop region or the bigger pore domain (S5-PL-S6), the individual residues that were non-conserved between $K_v7.3$ and $K_v7.4$ in this region were next targeted, before mutating them and examining if they altered the response to SR-5-6.

4.2.11.1 The effects of SR-5-6 on pore loop mutation $K_v7.4$:S265$E_{(PL)}$ in $K_v7.4$ channels

The first mutation examined was $K_v7.4$:S265$E_{(PL)}$ and under control conditions, appeared quite similar to WT $K_v7.4$ channels (Figure 4.15A). When 10 μM SR-5-6 was applied to the same cell, the typical three main effects of SR-5-6 were observed, namely i) an increase in current amplitude at all voltages, ii) rapid activation of the currents and iii) slowed deactivation kinetics (Figure 4.15B). When the data from five cells were summarized and the G-V curve was generated from the tail currents, an increase in G/G_{max} to 2.3 ± 0.3 was observed in presence of SR-5-6 (n=5) and a $\Delta V_{1/2}$ of -60 ± 9 mV in this mutant channel (Figure 4.15B), both of which were not significantly different to the effects of SR-5-6 on WT $K_v7.4$ channels (Figure 4.21A & B). The conductance at -100 mV ($G_{-100\ mV}$) also shifted from 0.02 in control to 0.97 ± 0.07 in SR-5-6 which was a significant increase

from WT $K_v7.4$ channels ($p<0.05$; Figure 4.21C). These data suggested that the S265E mutation does not affect the response to SR-5-6.

4.2.11.2 The effects of SR-5-6 on pore loop mutation $K_v7.4$:D266E$_{(PL)}$ in $K_v7.4$ channels

The next non-conserved residue in the pore loop region studied was D266 where it was mutated to the corresponding glutamic acid (E) in $K_v7.3$. The mutant channel currents resembled those of $K_v7.4$ WT channels, with slow activation and rapid deactivation kinetics (Figure 4.16A). When 10 μM SR-5-6 was applied on the same cell, as shown in Figure 4.16B, current amplitude increased at all voltages. Summary G-V curve generated from the tail currents showed an increase in G/G_{max} to 2.4 ± 0.2 in presence of SR-5-6 (n=5; Figure 4.16C) which was significantly greater than WT $K_v7.4$ channels ($p<0.01$; Figure 4.21B). SR-5-6 also shifted the activation $V_{1/2}$ from -25 ± 1 mV in control to -80 ± 4 mV, resulting in a $\Delta V_{1/2}$ of -54 ± 10 mV for this mutant (n=5; Figure 4.16C, ns when compared to WT $K_v7.4$). The $G_{-100\ mV}$ also increased from 0.03 in control to 0.74 in presence of SR-5-6 and this was not significantly different from that observed in WT $K_v7.4$ (Figure 4.21C). All of these results demonstrated that SR-5-6 effects were, if anything, enhanced in the $K_v7.4$ D266E mutant channel.

4.2.11.3 The effects of SR-5-6 on pore loop mutation $K_v7.4$:S268E$_{(PL)}$ in $K_v7.4$ channels

The S268E mutation was the next mutant channel examined in the pore loop region. Figure 4.17A and B show a typical family of currents from HEK cells expressing the $K_v7.4$:S268E$_{(PL)}$ mutant channel in the absence and presence of SR-5-6 respectively. Like the other mutants in this region, the currents under control conditions were very similar to WT $K_v7.4$ ($V_{1/2}$ =-25 ± 1 mV, n=6; Figure 4.17A and C) and 10 μM SR-5-6 (Figure 4.17B) appeared to be more effective on this mutant compared to WT $K_v7.4$. Thus, SR-5-6 increased G/G_{max} to 2.2 ± 0.3 (n=6; ns vs WT $K_v7.4$; Figure 4.21B), shifted the $V_{1/2}$ to -102 ± 10 (blue circles; Figure 4.16C) and the $\Delta V_{1/2}$ was -85 ± 11 mV, which was significantly higher than that observed in WT $K_v7.4$ channels ($p<0.05$; Figure 4.21A). The conductance at -100 mV was also increased from 0.01 in control to 1.2 in the presence of SR-5-

6 (ns when compared to WT $K_v7.4$; Figure 4.21C) further supporting the idea that the S268E mutant enhanced, rather than reduced the effects of SR-5-6 in $K_v7.4$ channels.

4.2.11.4 The effects of SR-5-6 on pore loop mutation $K_v7.4$:S269T$_{(PL)}$ in $K_v7.4$ channels

A $K_v7.4$:S269T$_{(PL)}$ mutant was also produced and its activation $V_{1/2}$ measured in control conditions was -36 ± 2 mV as shown in Figures 4.18A and C. These mutant channels appeared slower to activate but the rate of activation at +50 mV was 89.17 ± 17 ms which was not significantly slower than WT $K_v7.4$ channels (126.4 ± 9.9 ms; unpaired t-test; Figure 3.1A) When SR-5-6 was applied an increase in current amplitude was observed at all potentials and $G_{-100\ mV}$ increased from 0.04 in control to 0.7 in SR-5-6 ($p<0.05$ compared to WT $K_v7.4$; Figure 4.18C & Figure 4.21C). The activation $V_{1/2}$ in the presence of SR-5-6 was -98 ± 4 mV which makes the shift in $V_{1/2}$ ($\Delta V_{1/2}$) of -64 ± 10 mV for this mutant channel (n=6; Figure 4.18C, ns compared to WT $K_v7.4$; Figure 4.21A). The G/G_{max} was increased to 1.5 ± 0.1 by SR-5-6 which was not significantly different from that observed in WT $K_v7.4$ channels (1.58; n=7; Figure 4.21B). These results suggested that the effects of SR-5-6 were not altered in this pore loop mutant.

4.2.11.5 The effects of SR-5-6 on pore loop mutation $K_v7.4$:S273A$_{(PL)}$ in $K_v7.4$ channels

The $K_v7.4$:S273A$_{(PL)}$ pore loop mutant also produced currents that resembled those of $K_v7.4$ WT channels, as shown in Figure 4.19. When 10 μM SR-5-6 was applied on the same cell, it clearly activated the channels, as evidenced by the large tail currents and slowed deactivation kinetics (Figure 4.19B). In six cells, G/G_{max} increased to 1.75 ± 0.3 in presence of SR-5-6 (n=6; Figure 4.19C). The activation $V_{1/2}$ in control was -31 ± 1 mV (open circles) and in presence of SR-5-6, it shifted to -97 ± 9 mV (blue circles; Figure 4.19C). Thus, the $\Delta V_{1/2}$ for this mutant was -66 ± 9 mV, which was higher than the WT $K_v7.4$ channels but it did not read significance when compared to WT $K_v7.4$ (Figure 4.21A). The conductance (G) at -100 mV also increased significantly from 0.01 in control to 0.8 in presence of SR-5-6 (Figure 4.22), and this was significantly greater to its

effects on WT $K_v7.4$ channels ($p<0.05$; Figure 4.21C). These data support the idea that the effects of SR-5-6 were not altered massively in the $K_v7.4$:S273A mutant.

4.2.11.6 The $K_v7.4$ pore loop double mutation $K_v7.4$:T278L:T282A did not abolish the effects of SR-5-6

In our final set of pore loop mutations, the polar hydrophilic threonine residues at positions 278 and 282 were changed to their $K_v7.3$ equivalents, which were the hydrophobic residues leucine and alanine (Figure 4.2). This double mutant channel ($K_v7.4$:T278L:T282A) was expressed in HEK cells and as shown in Figure 4.20, activated at -3 ± 2 mV (n=7, Figure 4.20C), which was more positive potentials than observed in WT $K_v7.4$ channels. However, application of 10 μM SR-5-6 (Figure 4.20B), activated the channels, even at negative potentials, as significant inward current was observed at potentials negative to -80 mV. The summary G-V relationship curve clearly indicated the activation of this mutant channel in presence of SR-5-6, as the G/G_{max} increased from 1 to 2.9 ± 0.2 (n=7; $p<0.01$ compared to WT $K_v7.4$; Figure 4.21B) and the $V_{1/2}$ shifted to -47 ± 10 mV in presence of 10 μM SR-5-6 (blue circles, Figure 4.21C), whereas the mean $\Delta V_{1/2}$ was -42 ± 11 mV, which was not different to the effect on WT $K_v7.4$ channels (Figure 4.21A). From this double mutant experiment, it was concluded that these threonine residues in the pore loop do not contribute to the sensitivity of $K_v7.4$ channels to SR-5-6.

4.3 Discussion

This chapter aimed to narrow down the search for the potential binding site for SR-5-6 on $K_v7.4$ channels, using swap constructs between $K_v7.3$ and $K_v7.4$. The major conclusions of this chapter are as follows:

1. SR-5-6 was less efficacious on $K_v7.3$ channels compared to $K_v7.4$ channels.
2. The effects of SR-5-6 were not abolished in any of the chimeric and swap constructs.
3. The non-conserved residue mutants between $K_v7.3$ and $K_v7.4$ in S4-S5 and pore loop also failed to inhibit the effects of SR-5-6.

The initial results of this chapter confirmed the previous finding (Dudem, 2019) that SR-5-6 was a less efficacious activator on $K_v7.3$ channels compared to $K_v7.4$ channels. Thus, SR-5-6 failed to increase the G/G_{max} significantly (1.02 ± 0.05; n=5) in $K_v7.3$ channels and the activation $V_{1/2}$ was only shifted negatively by -15 ± 2 mV, which was significantly less compared to its effect on $K_v7.4$ channels (-47 ± 4 mV). However, SR-5-6 massively slowed the deactivation of both $K_v7.3$ and $K_v7.4$ channels. Previously in the lab, Dudem (2019) established that SR-5-6 appeared to activate all K_v7 channels, but its efficacy varied with the following sequence - $K_v7.1>K_v7.5>K_v7.4>K_v7.2>K_v7.3$. A chimeric approach was used to exploit this differential efficacy of SR-5-6 on different K_v7 isoforms and identify the molecular mechanisms mediating the effects of SR-5-6 on K_v7 channels.

A similar approach has previously been successful, since Schenzer *et al.,* (2005), identified the W265 residue in the S5 domain of $K_v7.3$ to be critical for retigabine binding, by constructing different chimeras of $K_v7.1$ (immune to retigabine effects) and $K_v7.3$ (susceptible to retigabine effects). Similarly, Padilla *et al.,* (2009), used a chimeric approach with drug-sensitive and drug-insensitive isoforms, to determine the boundaries of the novel site within S1-S4 VSDs of K_v7 channels to be the site of action of ICA-27243 and ICA-73.

In this chapter, a similar approach was undertaken, and domain swap chimeras and constructs were generated between $K_v7.3$ and $K_v7.4$ channels. The first domain targeted was the S6 domain since it, along with the S5 domain and the pore loop, form the ion conduction path. This ion conduction path is known to be

operated by the reorientation of the intracellular portions of S6 helices (Webster *et al.,* 2004; del Camino & Yellen, 2001; Jiang *et al.,* 2002). When the effects of SR-5-6 on the $K_v7.4$:$K_v7.3_{S6}$ chimeric construct were examined, similar effects were observed as seen for the WT $K_v7.4$ channels where: 1) It significantly enhanced the conductance of the channel at all voltages in presence of SR-5-6 (G/G_{max} = 2.1 ± 0.2), 2) It slowed deactivation more than fourfold and 3) The activation $V_{1/2}$ was shifted to hyperpolarized potentials by ~-40 mV. The only observed difference was that $K_v7.4$:$K_v7.3_{S6}$ chimeric channels activated at more positive potentials than the wildtype $K_v7.4$ channels, but, clearly the effects of SR-5-6 were not reduced in this $K_v7.4$:$K_v7.3_{S6}$ chimeric channel.

As the S6 chimeric channel did not alter the effect of SR-5-6, the S5 domain was next targeted to examine the SR-5-6 effects. The S5 domain also forms part of the ion conduction path along with the S6 and the pore loop (Webster *et al.,* 2004; del Camino & Yellen, 2001; Jiang *et al.,* 2002). It had been identified as an important domain as retigabine and its derivatives have their binding residues in this domain (W265, L272, T271; Lange *et al.,* 2008). Although these residues are well conserved across the K_v7 channel family, there are a number of non-conserved residues in the S5 domain between $K_v7.3$ and $K_v7.4$. For example, T271 in $K_v7.3$ is said to be an important residue delineating the retigabine binding pocket (Lange *et al.,* 2008). This residue is represented by V248 in $K_v7.4$ at the equivalent position. Thus, the S5 domain swap construct ($K_v7.4$:$K_v7.3_{S5}$) was next examined in our next experimental set. However, the $K_v7.4$:$K_v7.3_{S5}$ construct in the presence of SR-5-6 showed similar effects to those observed in WT $K_v7.4$ channels. Thus, it enhanced the conductance at all voltages in the presence of SR-5-6 (G/G_{max} = 1.3 ± 0.03), significantly slowed deactivation and shifted the activation $V_{1/2}$ negatively by 58 ± 4 mV. These results demonstrated that the S5 domain swap construct did not alter the effects of SR-5-6.

The pore loop (PL), which is the third important segment of the ion conduction path, was then targeted. The non-conserved residues in this region between $K_v7.4$ and $K_v7.3$ are highlighted in Figure 4.2. As this region has a high percentage of non-conserved residues, the $K_v7.4$:$K_v7.3_{PL}$ chimeric channel was generated through a cloning strategy. When these chimeric channels ($K_v7.4$:$K_v7.3_{PL}$) were transfected and overexpressed in HEK cells, the patch-clamp recording produced endogenous currents only, even though the protocol

used was the same as for other mutants and swap constructs. This suggested that when the pore loop of $K_v7.3$ was inserted in the place of the pore loop of $K_v7.4$, the channels were non-functional. Interestingly, the protein alignment shown in Figure 4.2 demonstrated that there is an insertion of an extra 10 residues in the $K_v7.3$ pore loop compared to $K_v7.4$. It was hypothesized that the presence of these additional 10 residues on the $K_v7.4$ background may have rendered the $K_v7.4$:$K_v7.3_{PL}$ channel non-functional. It could possibly hamper the protein folding or trafficking of the channel. To test this directly, an attempt was also made to delete these 10 residues from the $K_v7.4$:$K_v7.3_{PL}$ channel, to see if we could generate a functional protein. But as in the case of the $K_v7.4$:$K_v7.3_{PL}$ chimeric channel, this deletion construct also produced a non-functional channel and hence the data was not included in the results. Thus, the above experiment suggested that the pore loop is probably critical for channel folding and function. This is supported by various findings which have shown that mutations in the pore region resulted in misfolding, leading to loss of trafficking and expression of K_v channels on the cell surface (Gajewski *et al.,* 2011; Delaney *et al.,* 2014; Benson *et al.,* 1996; Huang *et al.,* 2001).

As the SR-5-6 effects were retained in both S6 and S5 domain swap constructs, our focus was then shifted to the voltage-sensing domains. The first voltage domain swap construct generated was the S4 domain swap ($K_v7.4$:$K_v7.3_{S4}$). It was observed that in this construct, the SR-5-6 effects were, again, very similar to the wildtype $K_v7.4$ channels (Figure 4.5). The data from this appears to rule out any role for the S4 helix in mediating the effects of SR-5-6 on $K_v7.4$ channels. A swap construct was next generated where the $K_v7.4$ S3-S4 linker segment was changed into $K_v7.3$ S3-S4 linker segment ($K_v7.4$:$K_v7.3_{S3\text{-}S4L}$). This chimeric construct produced functional channels but no significant reduction was observed in the effects of SR-5-6 on $V_{1/2}$ or conductance. Interestingly, however, SR-5-6 failed to enhance the activation time constant in this construct, which is markedly different to that seen in WT $K_v7.4$ channels with SR-5-6. One potential explanation for this was that the voltage sensors were perhaps not shifted as much in this mutant. If this were the case, the presence of SR-5-6 might have also resulted in a reduction in the $\Delta V_{1/2}$. However, in this mutant, the shift observed with SR-5-6 was clearly not reduced, as shown in Figure 4.6C. This perhaps suggested that the effect was not on the voltage sensors but perhaps it

was affecting the coupling between the pore and the voltage sensors. Nonetheless, it was concluded that the presence of the $K_v7.3$ S3-S4 linker does not affect the binding of SR-5-6 on $K_v7.4$ channels.

Since none of the individual domains examined so far reduced the effects of SR-5-6, it was next decided to construct bigger chimeras of $K_v7.4$ and $K_v7.3$. The goal was to examine if SR-5-6 brought about its effects by binding to multiple helices/domains of $K_v7.4$ channels. To investigate this, swapped (i) the entire voltage sensor domain (S1-S4) from $K_v7.3$ into the $K_v7.4$ background ($K_v7.4$:$K_v7.3_{S1-S4}$), (ii) the pore domain ($K_v7.4$:$K_v7.3_{S5-PL-S6}$) and (iii) the cytosolic C-terminus ($K_v7.4$:$K_v7.3_{C-terminus}$). When the entire voltage sensor domain was swapped, a small, but significant reduction was observed in G/G_{max} compared to the WT $K_v7.4$ response to SR-5-6. However, a significant increase in $G_{-100\ mV}$ was also seen as illustrated in Figures 4.7C and 4.9C). Furthermore, although it was difficult to deduce the $\Delta V_{1/2}$ in the presence of the drug from Figure 4.7, it was clear that the effects of SR-5-6 remained when the voltage-sensing domain was swapped between $K_v7.3$ and $K_v7.4$.

The next larger chimera generated was the pore domain chimera, $K_v7.4$:$K_v7.3_{S5-PL-S6}$ which consisted of the $K_v7.3$ S5 segment, pore loop and the S6 domain. The pore gate forms the K^+ selective aqueous pore and in K_v7 channels, the pore loop contains the signature selectivity filter motif TXGYG, which is conserved among K_v7 channels (Strutz-Seebohm *et al.,* 2013). The S5 and S6 domains also play a very important role in coupling between voltage-sensing domain and pore opening in K_v7 channels (Li-Smerin *et al.,* 2000; Broomand *et al.,* 2003; Gandhi *et al.,* 2003; Boulet *et al.,* 2007). Unfortunately, only endogenous HEK currents were recorded when this chimera was transfected, suggesting that these channels were rendered non-functional when the pore domain was swapped between $K_v7.3$ and $K_v7.4$. The non-functionality of this chimera is likely to be attributable to the pore loop region, as both S5 and S6 individual swap constructs gave functional channels (Figure 4.3 and 4.4). Thus, any swap construct or deletion involving the pore loop in $K_v7.4$ rendered the channel non-functional, implying that the sequence of the pore loop is critical to channel function, as has been demonstrated in a number of studies (Gajewski *et al.,* 2011; Delaney *et al.,* 2014; Benson *et al.,* 1996; Huang *et al.,* 2001).

The final chimera generated in this part of the study was the C-terminus chimera ($K_v7.4$:$K_v7.3_{C\text{-terminus}}$) The C-terminus in K_v7 channels is a long intracellular chain that plays a vital role in channel trafficking, tetramerization, forming complexes with other modulators and proteins, including phosphatidylinositol-4,5-bisphosphate (PIP_2), calmodulin (CaM), syntaxin, A-kinase-anchoring proteins, protein kinase C, and ankyrin-G (Haitin & Attali, 2008; Sun & MacKinnon, 2020; Marx *et al.,* 2002; Barrese *et al.,* 2018). The C-terminus is ~350 residues long and consists of both conserved and non-conserved regions among the K_v7 family. Hence, it was of interest to examine if differences in this region were responsible for the differential effects of SR-5-6 on $K_v7.3$ and $K_v7.4$. When the C-terminus was swapped from $K_v7.3$ in the background of $K_v7.4$ ($K_v7.4$:$K_v7.3_{C\text{-terminus}}$), it was observed that the SR-5-6 effect on both G/G_{max} (Figure 4.9C) and $\Delta V_{1/2}$ was more pronounced in these $K_v7.4$:$K_v7.3_{C\text{-terminus}}$ chimeric channels.

The summary data for $\Delta V_{1/2}$, G/G_{max} and $G_{-100\ mV}$ from each of the different swap constructs, support the idea that the efficacy of SR-5-6 was not significantly decreased in any of these constructs. In fact, in the $K_v7.4$:$K_v7.3_{C\text{-terminus}}$ chimeric channels, the efficacy of SR-5-6 was enhanced, although it did not read significance, when compared to WT $K_v7.4$ channels (see Figure 4.9A). The maximal conductance (G/G_{max}) was unaltered ($K_v7.4$:$K_v7.3_{S6}$, $K_v7.4$:$K_v7.3_{S4}$, $K_v7.4$:$K_v7.3_{S3\text{-}S4L}$ and $K_v7.4$:$K_v7.3_{C\text{-terminus}}$). Only a modest, albeit significant reduction in the SR-5-6 mediated enhancement of G/G_{max} compared to WT $K_v7.4$ channels (Figure 4.10B), in two constructs ($K_v7.4$:$K_v7.3_{S5}$ and $K_v7.4$:$K_v7.3_{S1\text{-}S4}$) was observed. Although the increase in G/G_{max} was reduced in both $K_v7.4$:$K_v7.3_{S5}$, and $K_v7.4$:$K_v7.3_{S1\text{-}S4}$ channels, the shift in $V_{1/2}$ was not significantly reduced, clearly ruling out that these mutants or domains contribute significantly to this effect of SR-5-6 on $K_v7.4$ channels.

The conductance at -100 mV ($G_{-100\ mV}$) was also summarized and this summary data is shown in Figure 4.9C. As in WT $K_v7.4$ channels, the conductance was increased, in presence of SR-5-6 at -100 mV, in the vast majority of the constructs. However, it is important to note that in the $K_v7.4$:$K_v7.3_{S6}$ channel, SR-5-6 did not significantly enhance the conductance at -100 mV. This indicated that the effect of SR-5-6 was reduced at very negative potentials in this construct. This may be explained by the S6 swap construct's rightward shift in activation $V_{1/2}$ (Figure 4.3C), which indicated that the channels when swapped with the

$K_v7.3$ S6 helix, required more positive potentials to activate it and that currents at very negative potentials, could not be elicited even in the presence of SR-5-6. Other findings showing the S6 domain is critical in coupling between VSDs and the pore domain in K_v7 channels corroborate the observations (Lu *et al.,* 2001; Lu *et al.,* 2002; Barghaan & Bähring, 2009; Ferrer *et al.,* 2006; Long *et al.,* 2005; Payandeh *et al.,* 2011).

When the time constants of activation and deactivation were summarized (Figure 4.10), it was observed that SR-5-6 increased the rate of activation in WT $K_v7.4$ and in all swap construct channels, except for the $K_v7.4$:$K_v7.3_{S3\text{-}S4L}$. However, the activation rate of this construct, in the absence of SR-5-6, was faster (~1.4 fold) than that observed in WT $K_v7.4$, but much slower than WT $K_v7.3$ channels (see Figure 4.10A). When the rate of activation across all voltages was looked at, it was similarly unaltered in the presence or absence of SR-5-6. The lack of apparent voltage dependence of the activation time constant could be a feature of this ($K_v7.4$:$K_v7.3_{S3\text{-}S4L}$) construct and may suggest that this is the maximal rate at which these channels can open at, irrespective of the presence of SR-5-6. Despite any change in the rate of activation of this mutant, a shift in activation $V_{1/2}$ was still observed in presence of SR-5-6, which perhaps implied that this unaltered rate of activation could be due to an alteration in coupling between the pore domain and voltage sensors, rather than the voltage sensors' activation range being shifted.

The S4-S5 linker was also targeted since it, along with the C-terminus and the S6 domain, are major contributors to the coupling of VSD to the pore domain opening (Lu *et al.,* 2001; Lu *et al.,* 2002; Barghaan and Bähring, 2009; Ferrer *et al.,* 2006; Prole & Yellen, 2006; Long *et al.,* 2005; Payandeh *et al.,* 2011). Keeping this in mind, the sequence dissimilarity was checked between $K_v7.3$ and $K_v7.4$ in this region and three non-conserved residues were identified. Unfortunately, when this $K_v7.4$:$K_v7.3_{S4\text{-}S5L}$ swap construct was overexpressed in HEK cells, it could only generate endogenous HEK cell currents in patch-clamp recordings, suggesting that this construct was non-functional. Therefore, individual three residues were mutated that differed in this region between $K_v7.3$ and $K_v7.4$ (V230A, V231I and Y232C). However, the results from these experiments suggested that none of these three alterations in the S4-S5 linker region reduced the effects of SR-5-6 (Figure 4.12; Figure 4.13; Figure 4.14). In fact, it was pretty

clear that the V230A mutant channel was actually more responsive to SR-5-6 since the channels were constitutively activated at negative potentials, in its presence. The above data clearly ruled out the three non-conserved residues in the S4-S5 linker segment in mediating the effects of SR-5-6 effects on $K_v7.4$ channels.

As the pore domain and pore loop swap constructs gave non-functional proteins, the individual residues non-conserved in the pore loop region between $K_v7.3$ and $K_v7.4$ were next investigated through a mutational approach, as illustrated in the sequence alignment shown in Figure 4.2. When these residues were mutated in $K_v7.4$ to the corresponding residues in $K_v7.3$ and examined the effects of SR-5-6, it was observed that the mutated channels (S265E, D266E, S268E, S269T, S273A, T278L & T282A) were as responsive as WT $K_v7.4$ to SR-5-6, as shown in Figure 4.21. These results clearly suggested that these residues in the pore loop did not play an important role in the differential effects of SR-5-6 on $K_v7.3$ and $K_v7.4$. However, as the deletion construct of the 10 residues in $K_v7.4$:$K_v7.3_{PL}$ and the other non-conserved residue N264K gave non-functional channels, it could not definitively be ruled out the role of the pore loop in mediating the excitatory effects of SR-5-6 on $K_v7.4$ channels. However, from the data shown in this chapter, it was clear that none of the domain swap constructs or mutations reduced the SR-5-6 effects in $K_v7.4$ channels.

4.4 Future directions

Even though the results of this chapter did not reveal any major domain or specific residues that eliminated the effects of SR-5-6, significant reductions in G/G_{max} were observed in the S5 domain swap and S1-S4 domain swap between $K_v7.3$ and $K_v7.4$. The L249A residue was found to be involved in mediating the negative shift in $V_{1/2}$ in $K_v7.4$ channels in the presence of SR-5-6 in the previous chapter. Future experiments based on these findings could focus on:

1) Investigating the effects of SR-5-6 in the $K_v7.4$:$K_v7.3_{S5}$ and $K_v7.4$:$K_v7.3_{S1-S4}$ swap constructs with the L249A mutation.

2) Using an immunocytochemical/confocal microscopy approach to examine if the ‘non-functional’ pore domain and pore loop swap constructs were trafficked and inserted into the cell membrane.

3) Collaborating with laboratories with expertise in ion channel cryo-EM would pinpoint the precise residues involved in the binding of SR-5-6.

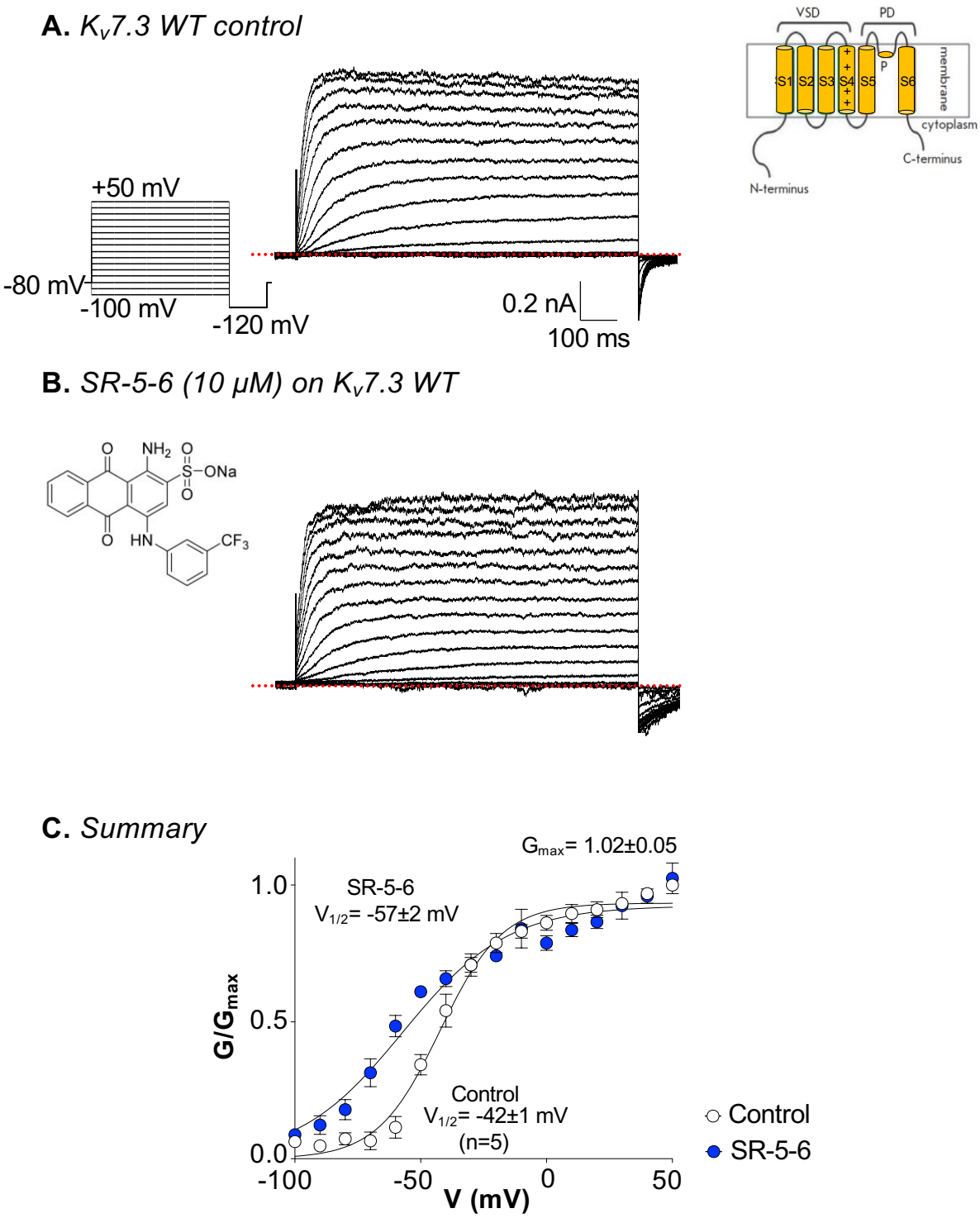

Figure 4.1: Effect of SR-5-6 on wildtype K_v7.3 channels. A) A typical family of currents obtained from wildtype K_v7.3 channels expressed in HEK cells. Voltage clamp protocol is described in the inset. Dotted lines represent the zero current level. **B**) The effect of 10 μM SR-5-6 on currents from the same cell. **C**) Summary activation curves obtained by measuring tail currents in five cells before (open circles) and during (blue circles) application of SR-5-6 (n=5). The curves were fit with the Boltzmann equation.

```
Kv7.1  --PAAPAAPPVA--SDLGPRPPVSLDPRVSIYSTRRPVLARTHVQGRVYNFLERPTGWKC 122
Kv7.3  GGGRDEGQRRTPQGIGLLAKTPL------S-RPVKRNNAKYRRIQTLIYDALERPRGWA- 122
Kv7.2  GSEAPKRGSI-LSKPR--AGGAG------A-GKPPKRNAFYRKLQNFLYNVLERPRGWA- 92
Kv7.4  -SPLPP-GAP-LPGPGSGSGSAC------G-QRSSAAHKRYRRLQNWVYNVLERPRGWA- 98
Kv7.5  -KPLSY----------------T------S-SQSCRRNVKYRRVQNYLYNVLERPRGWA- 126
                                     .           ::*  :*: **** **
                 S1                                S2
Kv7.1  FVYHFAVFLIVLVCLIFSVLSTIEQYAALATGTLFWMEIVLVVFFGTEYVVRLWSAGCRS 182
Kv7.3  LLYHALVFLIVLGCLILAVLTTFKEYETVSGDWLLLLETFAIFIFGAEFALRIWAAGCCC 182
Kv7.2  FIYHAYVFLLVFSCLVLSVFSTIKEYEKSSEGALYILEIVTIVVFGVEYFVRIWAAGCCC 152
Kv7.4  FVYHVFIFLLVFSCLVLSVLSTIQEHQELANECLLILEFVMIVVFGLEYIVRVWSAGCCC 158
Kv7.5  FIYHAFVFLLVFGCLILSVFSTIPEHTKLASSCLLILEFVMIVVFGLEFIIRIWSAGCCC 186
       ::**  :**:*: **:::*::*: ::   :   *  :* . :..** *: :*:*:*** .
                                S3                                S4
Kv7.1  KYVGLWGRLRFARKPISIIDLIVVVASMVVLCVGSKGQVFATSAIRGIRFLQILRMLHVD 242
Kv7.3  RYKGWRGRLKFARKPLCMLDIFVLIASVPVVAVGNQGNVLATS-LRSLRFLQILRMLRMD 241
Kv7.2  RYRGWRGRLKFARKPFCVIDIMVLIASIAVLAAGSQGNVFATSALRSLRFLQILRMIRMD 212
Kv7.4  RYRGWQGRFRFARKPFCVIDFIVFVASVAVIAAGTQGNIFATSALRSMRFLQILRMVRMD 218
Kv7.5  RYRGWQGRLRFARKPFCVIDTIVLIASIAVVSAKTQGNIFATSALRSLRFLQILRMVRMD 246
       :* *  **::*****:.::* :*.:**: *:.. .:*:::*** :*.:********:::*
                                   S5
Kv7.1  RQGGTWRLLGSVVFIHRQELITTLYIGFLGLIFSSYFVYLAEKDAVN-----ESGRVEFG 297
Kv7.3  RRGGTWKLLGSAICAHSKELITAWYIGFLTLILSSFLVYLVEKDVPEVDAQGEEMKEEFE 301
Kv7.2  RRGGTWKLLGSVVYAHSKELVTAWYIGFLCLILASFLVYLAEKGE----------NDHFD 262
Kv7.4  RRGGTWKLLGSVVYAHSKELITAWYIGFLVLIFASFLVYLAEKDA----------NSDFS 268
Kv7.5  RRGGTWKLLGSVVYAHSKELITAWYIGFLVLIFSSFLVYLVEKDA----------NKEFS 296
       *:****:****.:  * :**:*: ***** **::*::***.**.          . .*
                                                 S6
Kv7.1  SYADALWWGVVTVTTIGYGDKVPQTWVGKTIASCFSVFAISFFALPAGILGSGFALKVQQ 357
Kv7.3  TYADALWWGLITLATIGYGDKTPKTWEGRLIAATFSLIGVSFFALPAGILGSGLALKVQE 361
Kv7.2  TYADALWWGLITLTTIGYGDKYPQTWNGRLLAATFTLIGVSFFALPAGILGSGFALKVQE 322
Kv7.4  SYADSLWWGTITLTTIGYGDKTPHTWLGRVLAAGFALLGISFFALPAGILGSGFALKVQE 328
Kv7.5  TYADALWWGTITLTTIGYGDKTPLTWLGRLLSAGFALLGISFFALPAGILGSGFALKVQE 356
       :***:**** :*::******* * ** *: ::: *::::.:*************:*****:

Kv7.1  KQRQKHFNRQIPAAASLIQTAWRCYAAENPD---SSTWKIYIRKAPRSHTLLSP------
Kv7.3  QHRQKHFEKRRKPAAELIQAAWRYYATNPNRIDLVATWRFYESVVSFPFFRK--------
Kv7.2  QHRQKHFEKRRNPAAGLIQSAWRFYATNLSRTDLHSTWQYYERTVTVPMYRLIPPLNQ-L
Kv7.4  QHRQKHFEKRRMPAANLIQAAWRLYSTDMSRAYLTATWYYYDSILP--SFRELALLFEHV
Kv7.5  QHRQKHFEKRRNPAANLIQCVWRSYAADEKSVS-IATWKPHLK--------A--------
       ::*****:::   ** *** .** *:::       :**  :
```

Figure 4.2: Multiple sequence alignment of K_v7.1 - K_v7.5 channels.
Protein sequence alignment of K_v7 channels subtypes from K_v7.1 (NP_000209.1), K_v7.2 (NP_004509.2), K_v7.3 (NP_004510.1), K_v7.4 (NP_004691.2) and K_v7.5 (NP_062816.2). The K_v7 channel S1-S6 transmembrane helices were highlighted with yellow. The transmembrane helices represented based on the cryo-EM structure of K_v7.1 (Sun & MacKinnon, 2017).

A. *$K_v7.4$:$K_v7.3_{S6}$ control*

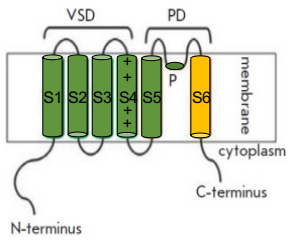

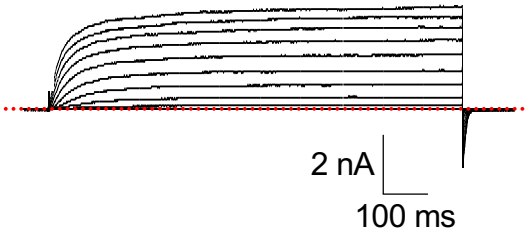

B. *SR-5-6 (10 μM) on $K_v7.4$:$K_v7.3_{S6}$*

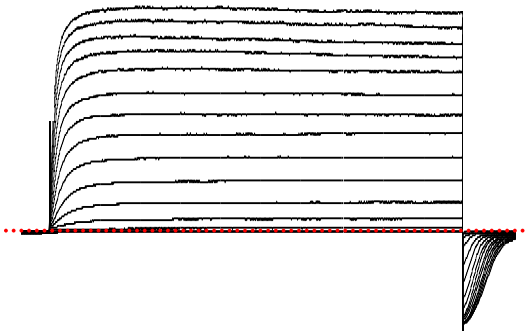

C. *Summary*

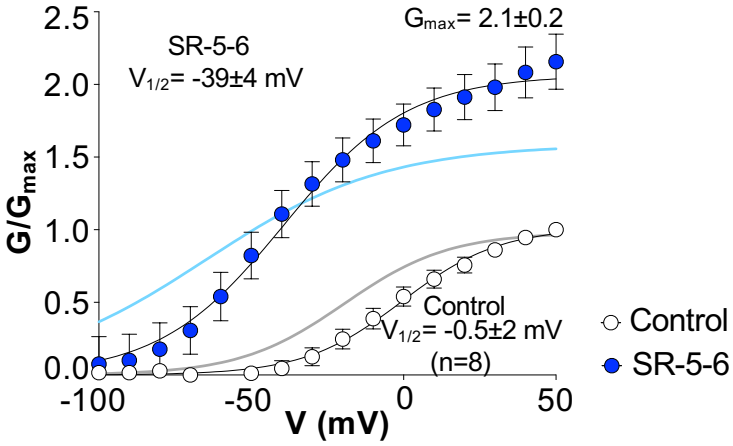

Figure 4.3: Effect of SR-5-6 on $K_v7.4$:$K_v7.3_{S6}$ channels. A) A typical family of currents obtained from $K_v7.4$:$K_v7.3_{S6}$ chimera channels expressed in HEK cells. Voltage clamp protocol as described in Figure 4.1. Dotted lines represent the zero current level. **B**) The effect of 10 μM SR-5-6 on currents from the same cell. **C**) Summary activation curves obtained by measuring tail currents in eight cells before (open circles) and during (blue circles) application of SR-5-6 (n=8). The continuous grey and light blue lines in the background represent the activation curves of control and the effect of the SR-5-6 on WT $K_v7.4$ channels respectively. The curves were fit with the Boltzmann equation.

A. *$K_v7.4$:$K_v7.3_{S5}$ control*

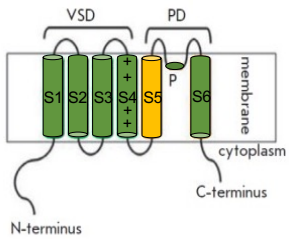

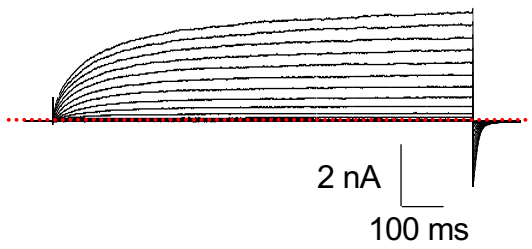

B. *SR-5-6 (10 μM) on $K_v7.4$:$K_v7.3_{S5}$*

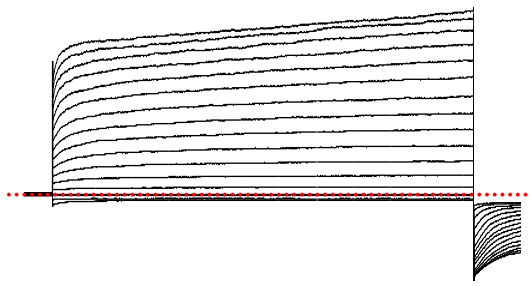

C. *Summary*

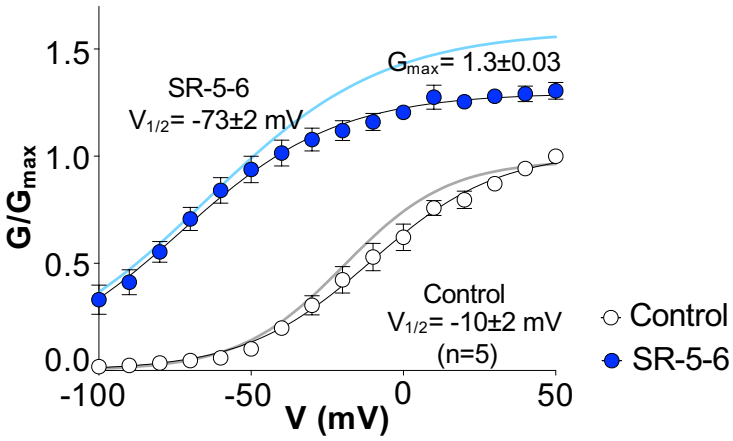

Figure 4.4: Effect of SR-5-6 on $K_v7.4$:$K_v7.3_{S5}$ channels. A) A typical family of currents obtained from $K_v7.4$:$K_v7.3_{S5}$ chimera channels expressed in HEK cells. Voltage clamp protocol as described in Figure 4.1. Dotted lines represent the zero current level. **B**) The effect of 10 μM SR-5-6 on currents from the same cell. **C**) Summary activation curves obtained by measuring tail currents in five cells before (open circles) and during (blue circles) application of SR-5-6 (n=5). The continuous grey and light blue lines in the background represent the activation curves of control and the effect of the SR-5-6 on WT $K_v7.4$ channels respectively. The curves were fit with the Boltzmann equation.

A. *$K_v7.4$:$K_v7.3_{S4}$ control*

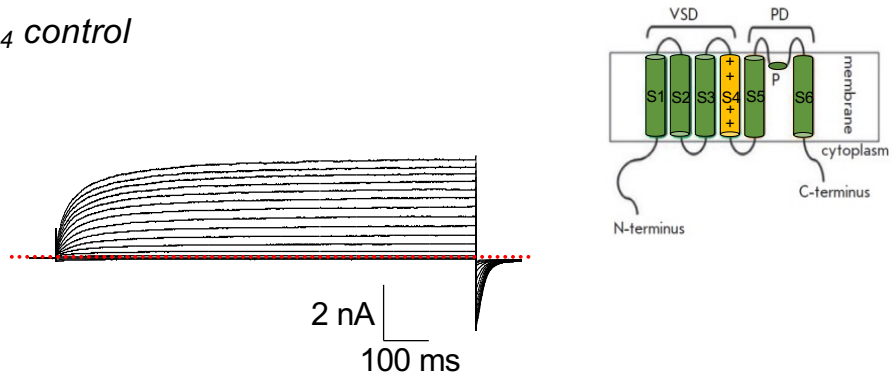

B. *SR-5-6 (10 μM) on $K_v7.4$:$K_v7.3_{S4}$*

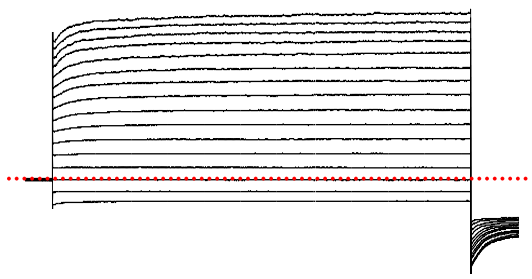

C. *Summary*

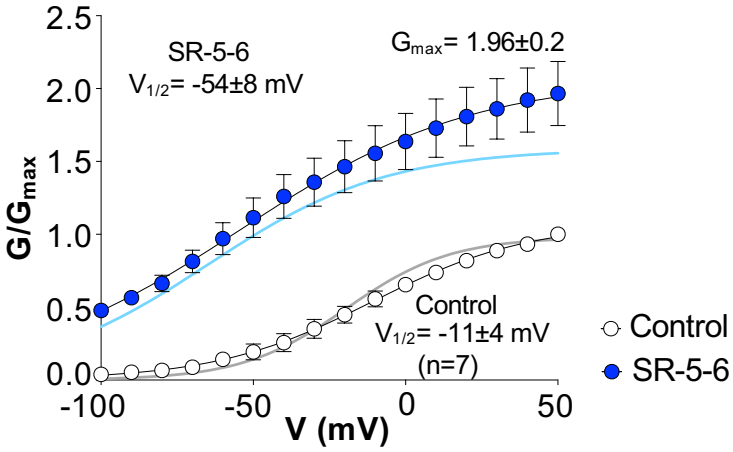

Figure 4.5: Effect of SR-5-6 on $K_v7.4$:$K_v7.3_{S4}$ channels. A) A typical family of currents obtained from $K_v7.4$:$K_v7.3_{S4}$ chimera channels expressed in HEK cells. Voltage clamp protocol as described in Figure 4.1. Dotted lines represent the zero current level. **B**) The effect of 10 μM SR-5-6 on currents from the same cell. **C**) Summary activation curves obtained by measuring tail currents in seven cells before (open circles) and during (blue circles) application of SR-5-6 (n=7). The continuous grey and light blue lines in the background represent the activation curves of control and the effect of the SR-5-6 on WT $K_v7.4$ channels respectively. The curves were fit with the Boltzmann equation.

A. *$K_v7.4$:$K_v7.3_{S3\text{-}S4L}$ control*

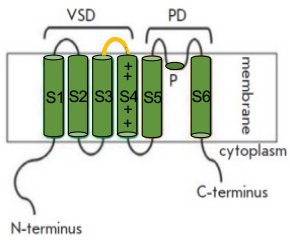

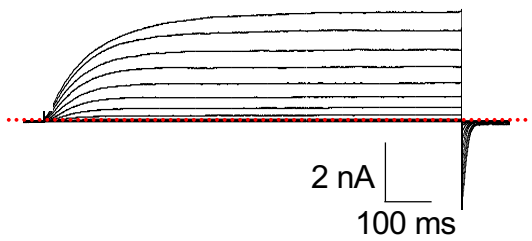

B. *SR-5-6 (10 μM) on $K_v7.4$:$K_v7.3_{S3\text{-}S4L}$*

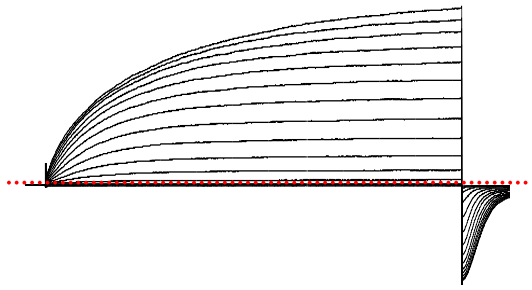

C. *Summary*

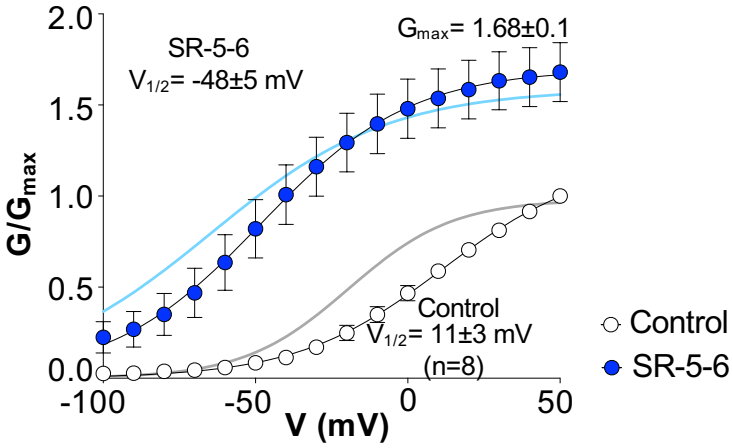

Figure 4.6: Effect of SR-5-6 on $K_v7.4$:$K_v7.3_{S3\text{-}S4L}$ channels. A) A typical family of currents obtained from $K_v7.4$:$K_v7.3_{S3\text{-}S4L}$ chimera channels expressed in HEK cells. Voltage clamp protocol as described in Figure 4.1. Dotted lines represent the zero current level. **B**) The effect of 10 μM SR-5-6 on currents from the same cell. **C**) Summary activation curves obtained by measuring tail currents in eight cells before (open circles) and during (blue circles) application of SR-5-6 (n=8). The continuous grey and light blue lines in the background represent the activation curves of control and the effect of the SR-5-6 on WT $K_v7.4$ channels respectively. The curves were fit with the Boltzmann equation.

A. *$K_v7.4$:$K_v7.3_{S1-S4}$ control*

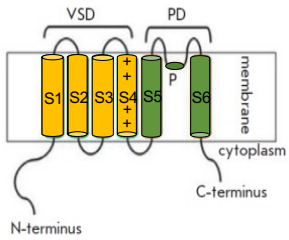

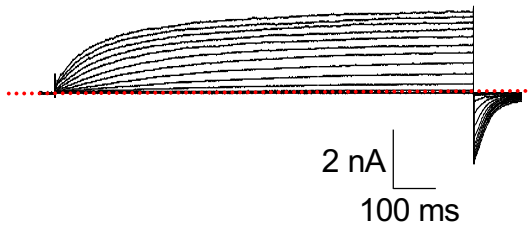

B. *SR-5-6 (10 μM) on $K_v7.4$:$K_v7.3_{S1-S4}$*

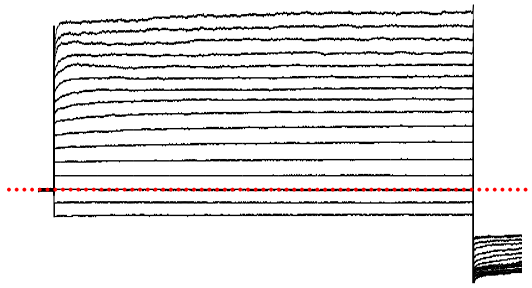

C. *Summary*

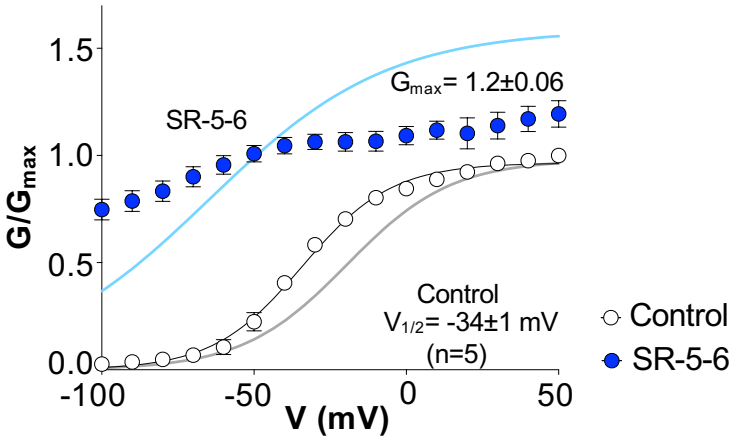

Figure 4.7: Effect of SR-5-6 on $K_v7.4$:$K_v7.3_{S1-S4}$ channels. A) A typical family of currents obtained from $K_v7.4$:$K_v7.3_{S1-S4}$ chimera channels expressed in HEK cells. Voltage clamp protocol as described in Figure 4.1. Dotted lines represent the zero current level. **B**) The effect of 10 μM SR-5-6 on currents from the same cell. **C**) Summary activation curves obtained by measuring tail currents in five cells before (open circles) and during (blue circles) application of SR-5-6 (n=5). The continuous grey and light blue lines in the background represent the activation curves of control and the effect of the SR-5-6 on WT $K_v7.4$ channels respectively. The curves were fit with the Boltzmann equation.

A. *$K_v7.4$:$K_v7.3_{C\text{-}terminus}$ control*

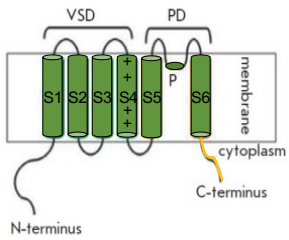

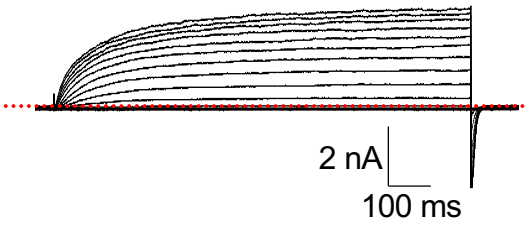

B. *SR-5-6 (10 μM) on $K_v7.4$:$K_v7.3_{C\text{-}terminus}$*

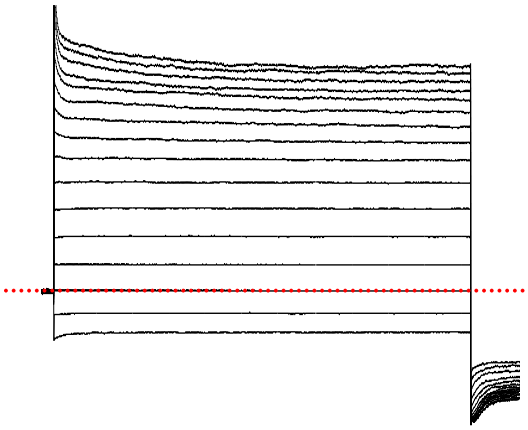

C. *Summary*

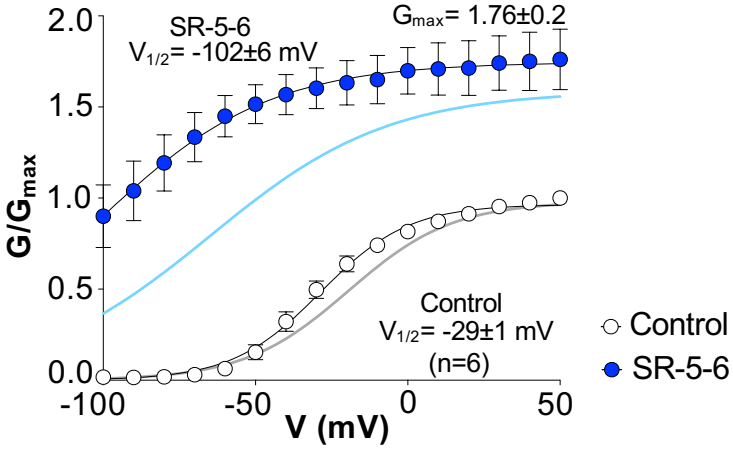

Figure 4.8: Effect of SR-5-6 on $K_v7.4$:$K_v7.3_{C\text{-}terminus}$ channels. A) A typical family of currents obtained from C-terminus chimera channels expressed in HEK cells. Voltage clamp protocol as described in Figure 4.1. Dotted lines represent the zero current level. **B**) The effect of 10 μM SR-5-6 on currents from the same cell. **C**) Summary activation curves obtained by measuring tail currents in six cells before (open circles) and during (blue circles) application of SR-5-6 (n=6). The continuous grey and light blue lines in the background represent the activation curves of control and the effect of the SR-5-6 on WT $K_v7.4$ channels respectively. The curves were fit with the Boltzmann equation.

A. *Effect of SR-5-6 (10 µM) on $\Delta V_{1/2}$ of $K_v7.4$ swap constructs*

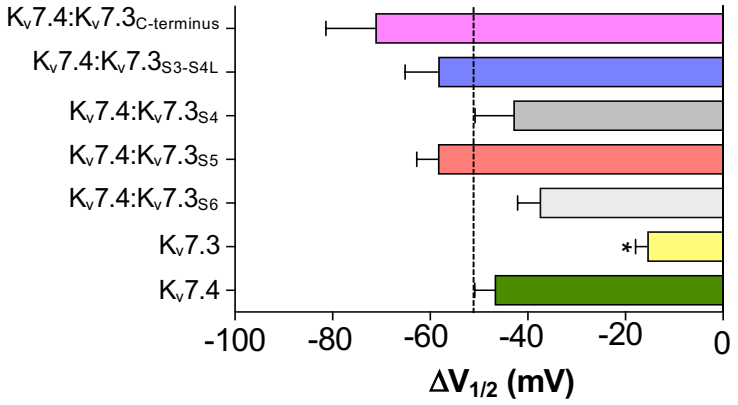

B. *Effect of SR-5-6 (10 µM) on G/G_{max} of $K_v7.4$ swap constructs*

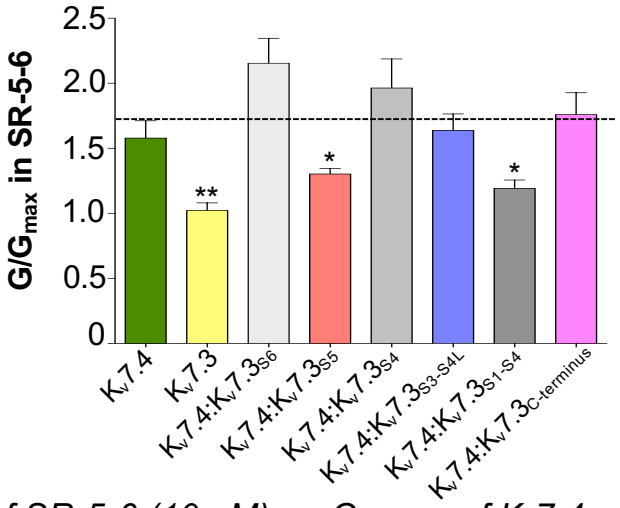

C. *Effect of SR-5-6 (10 µM) on $G_{-100\ mV}$ of $K_v7.4$ swap constructs*

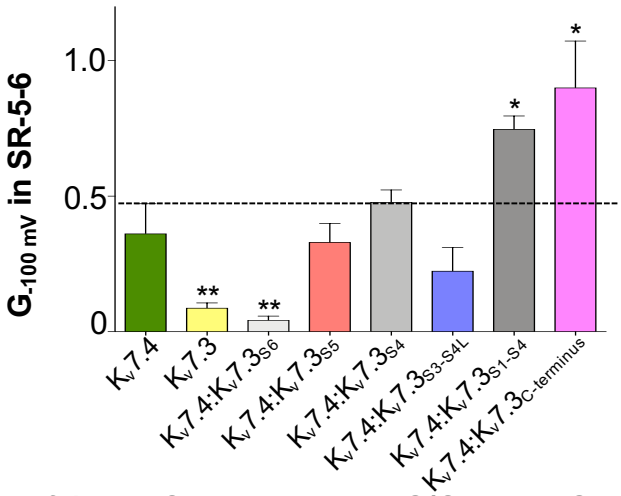

Figure 4.9: Effect of 10 µM SR-5-6 on $\Delta V_{1/2}$, G/G_{max} and $G_{-100\ mV}$ of $K_v7.4$ swap constructs. A) SR-5-6 mediated negative shift of the activation curve ($\Delta V_{1/2}$) on various constructs of $K_v7.4$ channels. A one-way ANOVA was performed with $K_v7.4$ as the control **B)** The effects of SR-5-6 on maximal conductance (G/G_{max}) of various constructs of $K_v7.4$ channels **C)** SR-5-6 mediated change in conductance (G) at -100 mV on different constructs of $K_v7.4$ channels. A Mann-Whitney, non-parametric test was used for G/G_{max} and $G_{-100\ mV}$ to compare $K_v7.4$ with other groups. *p<0.05, **p<0.01, ***p<0.001, ****p<0.0001.

A. *Effect of SR-5-6 (10 µM) on Tau activation (+50 mV) of K_v7.4 swap constructs*

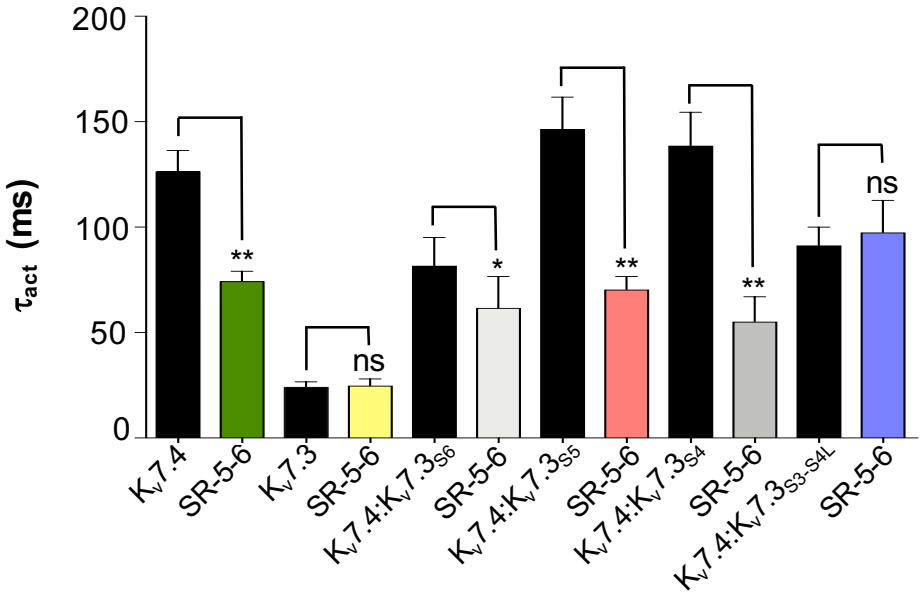

B. *Effect of SR-5-6 (10 µM) on Tau deactivation (-120 mV) of K_v7.4 swap constructs*

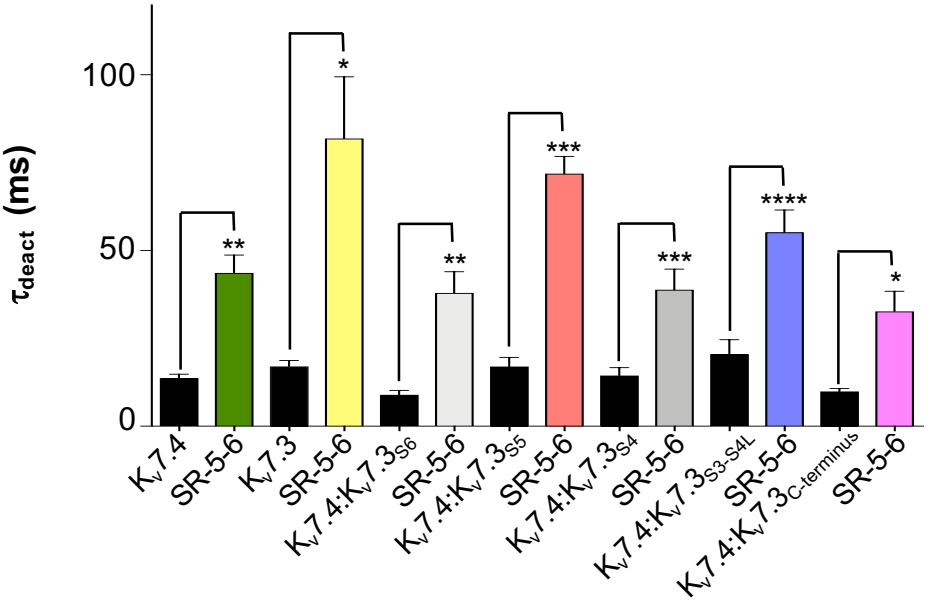

Figure 4.10: Effect of 10 µM SR-5-6 on time constant of activation (τ_{act}) and deactivation (τ_{deact}) of K_v7.4 swap constructs.
A) Time constant of activation analyzed from step to +50 mV **B)** Time constant of deactivation analyzed from stepping back to -120 mV from +50 mV. The black bars represent the control condition and the respective colored bars indicate the effect of SR-5-6 on the wildtype and mutant channels as labelled in the figure above. Paired t-tests, *p<0.05, **p<0.01, ***p<0.001, ****p<0.0001.

A. *Effect of SR-5-6 (10 µM) on $G_{-100\ mV}$ of $K_v7.4$ swap constructs*

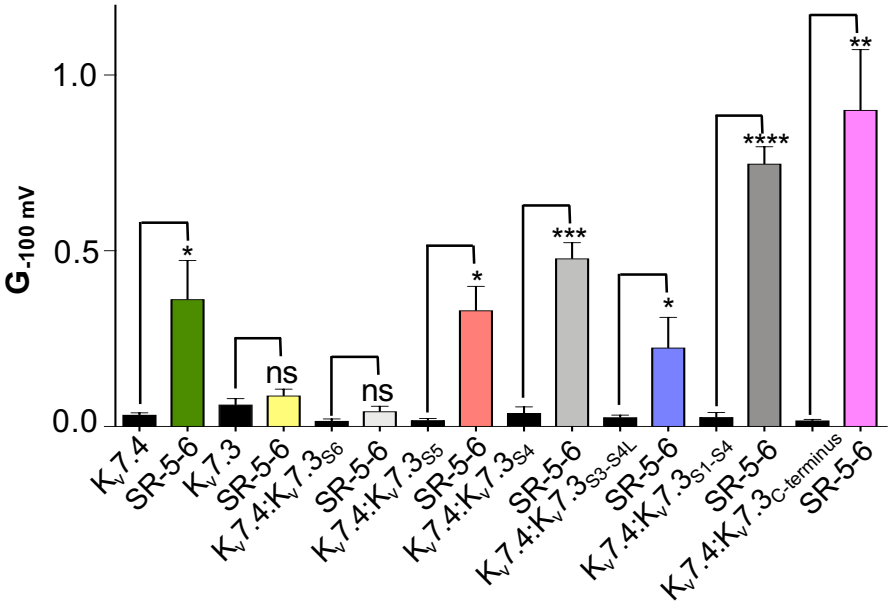

Figure 4.11: Effect of 10 µM SR-5-6 on $G_{-100\ mV}$ of $K_v7.4$ swap constructs. The above data depicts the change in conductance (G) at -100 mV in HEK cells expressing the wildtype and swap constructs. The black bars represent the control condition and the respective colored bars indicate the effect of SR-5-6 as labelled in the figure above. Paired t-tests, *p<0.05, **p<0.01, ***p<0.001, ****p<0.0001.

A. *V230A$_{(S4\text{-}S5L)}$ mutant control*

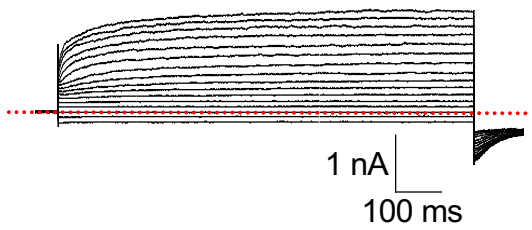

B. *SR-5-6 (10 μM) on V230A$_{(S4\text{-}S5L)}$ mutant*

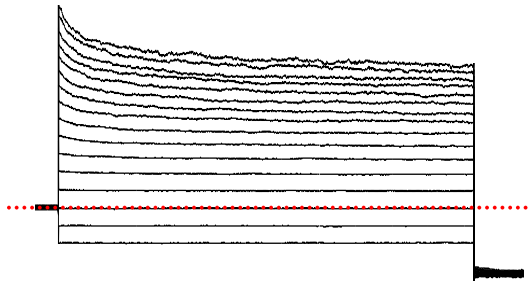

C. *Summary*

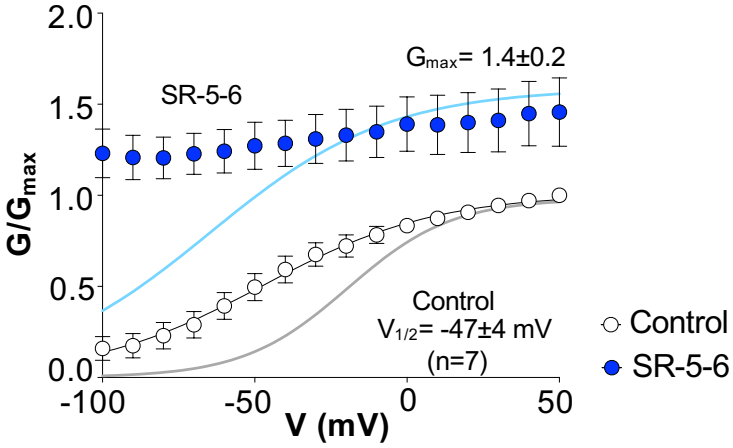

Figure 4.12: Effect of SR-5-6 on V230A$_{(S4\text{-}S5L)}$ mutant of K_v7.4 channels. A**) A typical family of currents obtained from V230A$_{(S4\text{-}S5L)}$ mutation of K_v7.4 channels expressed in HEK cells. Voltage clamp protocol as described in Figure 4.1. Dotted lines represent the zero current level. **B) The effect of 10 μM SR-5-6 on currents from the same cell. **C**) Summary activation curves obtained by measuring tail currents in seven cells before (open circles) and during (blue circles) application of SR-5-6 (n=7). The continuous grey and light blue lines in the background represent the activation curves of control and the effect of the SR-5-6 on WT K_v7.4 channels respectively. The curves were fit with the Boltzmann equation.

A. *V231I$_{(S4\text{-}S5L)}$ mutant control*

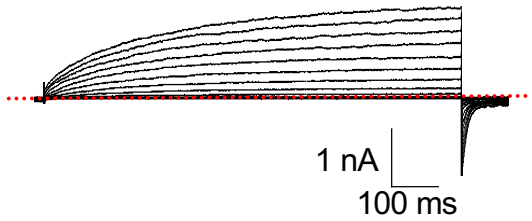

B. *SR-5-6 (10 μM) on V231I$_{(S4\text{-}S5L)}$ mutant*

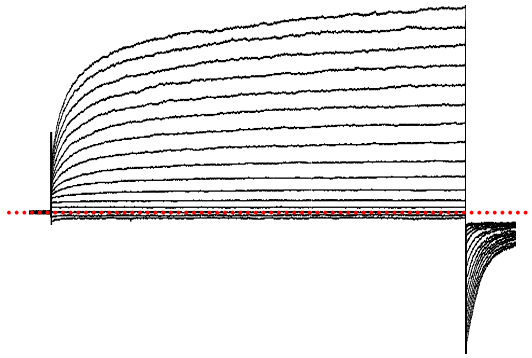

C. *Summary*

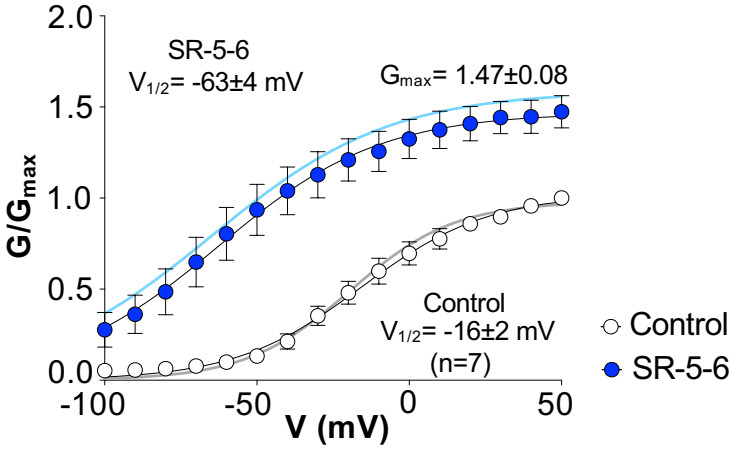

**Figure 4.13: Effect of SR-5-6 on V231I$_{(S4\text{-}S5L)}$ mutant of K$_v$7.4 channels. A**) A typical family of currents obtained from V231I$_{(S4\text{-}S5L)}$ mutation of K$_v$7.4 channels expressed in HEK cells. Voltage clamp protocol as described in Figure 4.1. Dotted lines represent the zero current level. **B**) The effect of 10 μM SR-5-6 on currents from the same cell. **C**) Summary activation curves obtained by measuring tail currents in seven cells before (open circles) and during (blue circles) application of SR-5-6 (n=7). The continuous grey and light blue lines in the background represent the activation curves of control and the effect of the SR-5-6 on WT K$_v$7.4 channels respectively. The curves were fit with the Boltzmann equation.

A. *Y232C$_{(S4\text{-}S5L)}$ mutant control*

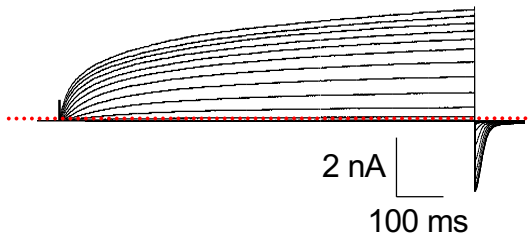

B. *SR-5-6 (10 μM) on Y232C$_{(S4\text{-}S5L)}$ mutant*

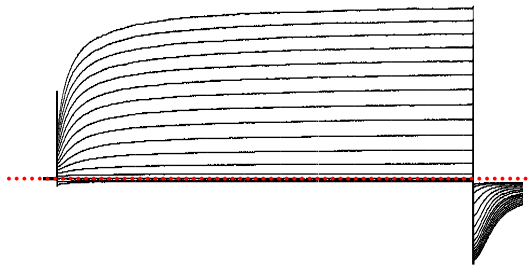

C. *Summary*

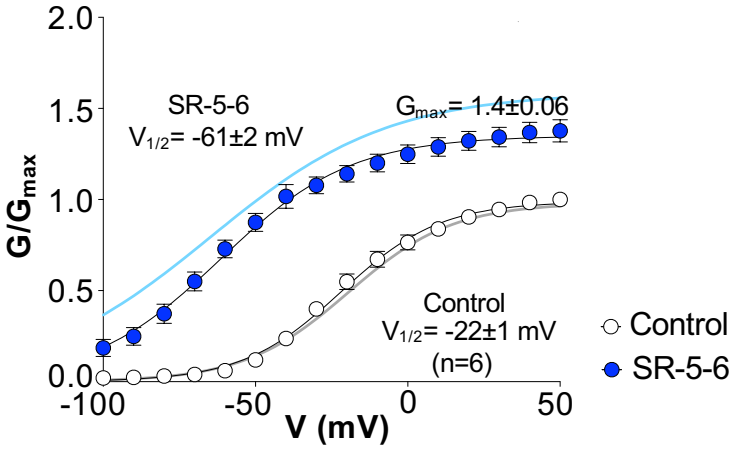

**Figure 4.14: Effect of SR-5-6 on Y232C$_{(S4\text{-}S5L)}$ mutant of K$_v$7.4 channels. A**) A typical family of currents obtained from Y232C$_{(S4\text{-}S5L)}$ mutation of K$_v$7.4 channels expressed in HEK cells. Voltage clamp protocol as described in Figure 4.1. Dotted lines represent the zero current level. **B**) The effect of 10 μM SR-5-6 on currents from the same cell. **C**) Summary activation curves obtained by measuring tail currents in six cells before (open circles) and during (blue circles) application of SR-5-6 (n=6). The continuous grey and light blue lines in the background represent the activation curves of control and the effect of the SR-5-6 on WT K$_v$7.4 channels respectively. The curves were fit with the Boltzmann equation.

A. *S265E$_{(PL)}$ mutant control*

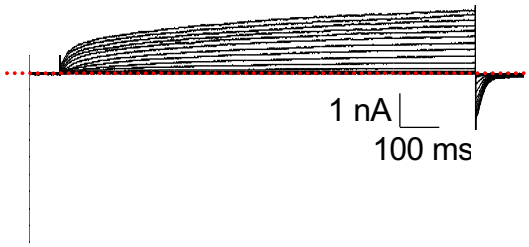

B. *SR-5-6 (10 μM) on S265E$_{(PL)}$ mutant*

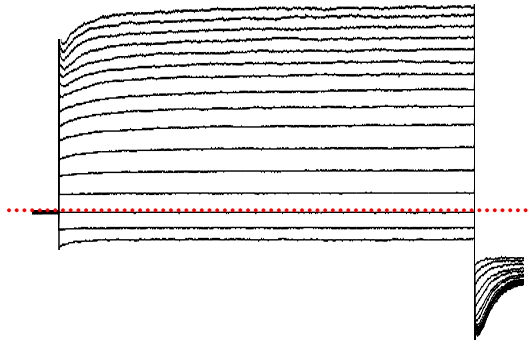

C. *Summary*

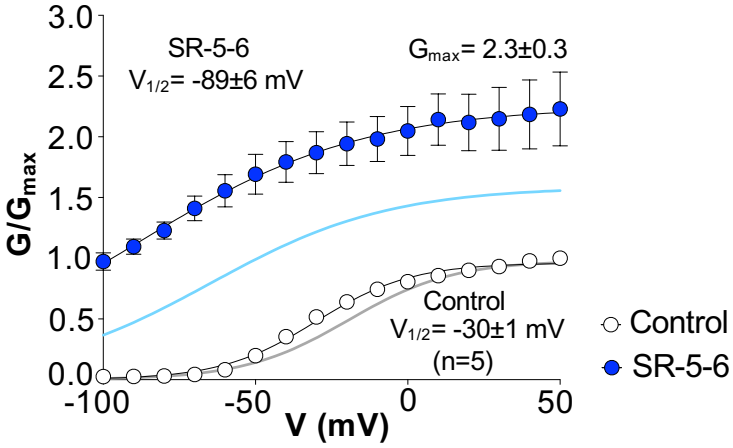

**Figure 4.15: Effect of SR-5-6 on S265E$_{(PL)}$ mutation of K$_v$7.4 channels. A**) A typical family of currents obtained from S265E$_{(PL)}$ mutation of K$_v$7.4 channels expressed in HEK cells. Voltage clamp protocol as described in Figure 4.1. Dotted lines represent the zero current level. **B**) The effect of 10 μM SR-5-6 on currents from the same cell. **C**) Summary activation curves obtained by measuring tail currents in five cells before (open circles) and during (blue circles) application of SR-5-6 (n=5). The continuous grey and light blue lines in the background represent the activation curves of control and the effect of the SR-5-6 on WT K$_v$7.4 channels respectively. The curves were fit with the Boltzmann equation.

A. *D266E$_{(PL)}$ mutant control*

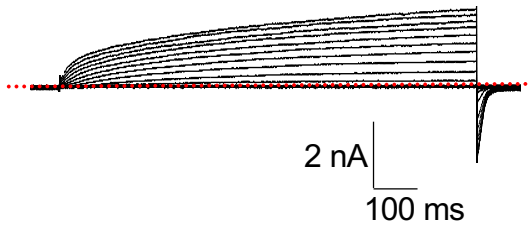

B. *SR-5-6 (10 μM) on D266E$_{(PL)}$ mutant*

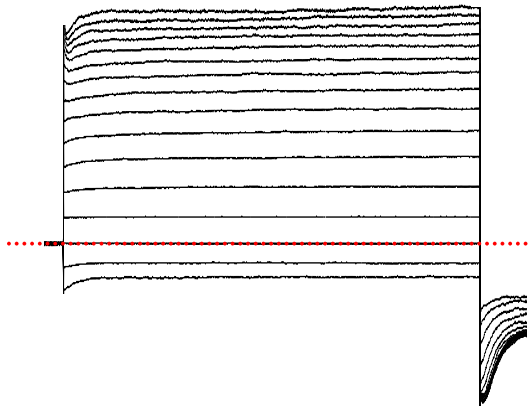

C. *Summary*

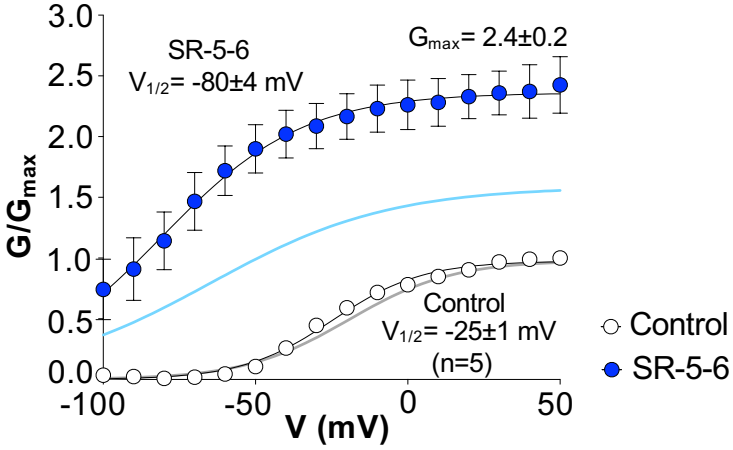

**Figure 4.16: Effect of SR-5-6 on D266E$_{(PL)}$ mutation of K$_v$7.4 channels. A**) A typical family of currents obtained from D266E$_{(PL)}$ mutation of K$_v$7.4 channels expressed in HEK cells. Voltage clamp protocol as described in Figure 4.1. Dotted lines represent the zero current level. **B**) The effect of 10 μM SR-5-6 on currents from the same cell. **C**) Summary activation curves obtained by measuring tail currents in five cells before (open circles) and during (blue circles) application of SR-5-6 (n=5). The continuous grey and light blue lines in the background represent the activation curves of control and the effect of the SR-5-6 on WT K$_v$7.4 channels respectively. The curves were fit with the Boltzmann equation.

A. *S268E$_{(PL)}$ mutant control*

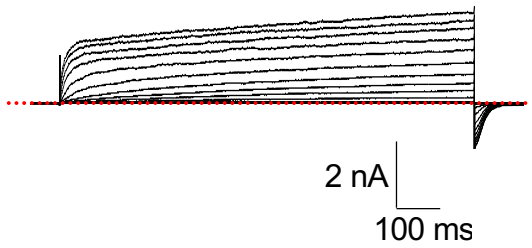

B. *SR-5-6 (10 μM) on S268E$_{(PL)}$ mutant*

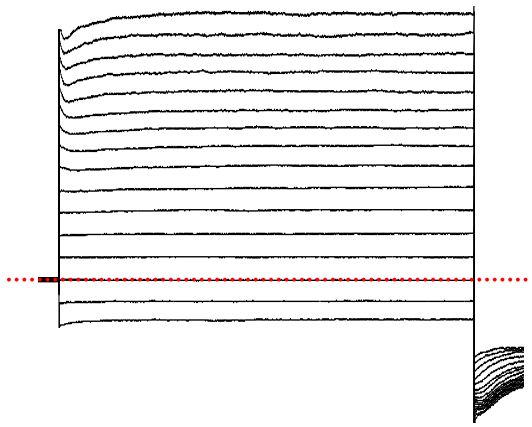

C. *Summary*

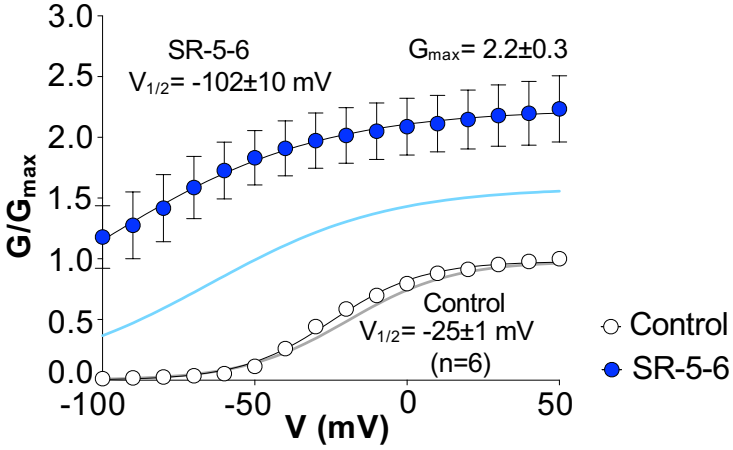

**Figure 4.17: Effect of SR-5-6 on S268E$_{(PL)}$ mutation of K$_v$7.4 channels. A**) A typical family of currents obtained from S268E$_{(PL)}$ mutation of K$_v$7.4 channels expressed in HEK cells. Voltage clamp protocol as described in Figure 4.1. Dotted lines represent the zero current level. **B**) The effect of 10 μM SR-5-6 on currents from the same cell. **C**) Summary activation curves obtained by measuring tail currents in six cells before (open circles) and during (blue circles) application of SR-5-6 (n=6). The continuous grey and light blue lines in the background represent the activation curves of control and the effect of the SR-5-6 on WT K$_v$7.4 channels respectively. The curves were fit with the Boltzmann equation.

A. *S269T$_{(PL)}$ mutant control*

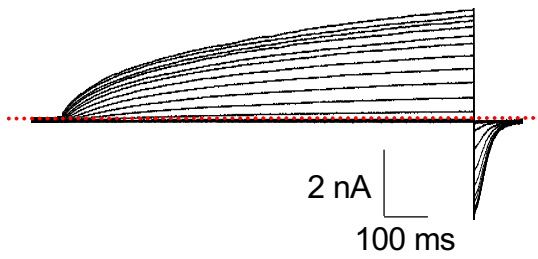

B. *SR-5-6 (10 μM) on S269T$_{(PL)}$ mutant*

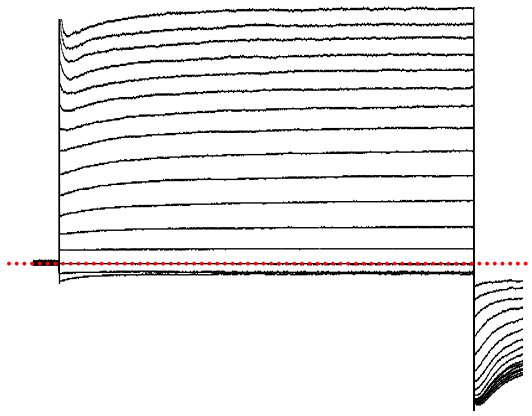

C. *Summary*

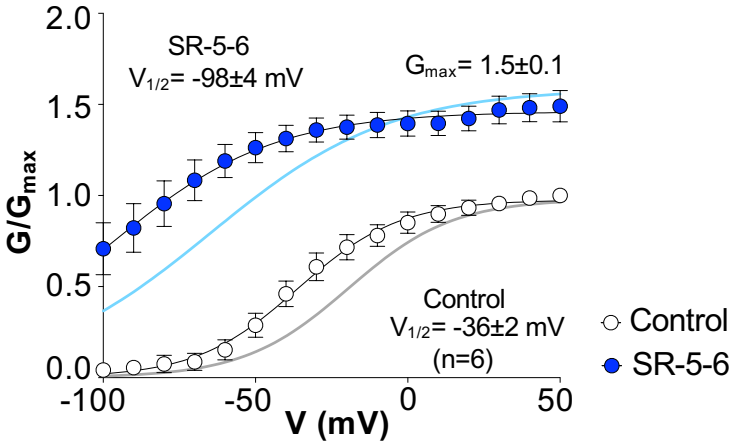

**Figure 4.18: Effect of SR-5-6 on S269T$_{(PL)}$ mutation of K$_v$7.4 channels. A**) A typical family of currents obtained from S269T$_{(PL)}$ mutation of K$_v$7.4 channels expressed in HEK cells. Voltage clamp protocol as described in Figure 4.1. Dotted lines represent the zero current level. **B**) The effect of 10 μM SR-5-6 on currents from the same cell. **C**) Summary activation curves obtained by measuring tail currents in six cells before (open circles) and during (blue circles) application of SR-5-6 (n=6). The continuous grey and light blue lines in the background represent the activation curves of control and the effect of the SR-5-6 on WT K$_v$7.4 channels respectively. The curves were fit with the Boltzmann equation.

A. *S273A$_{(PL)}$ mutant control*

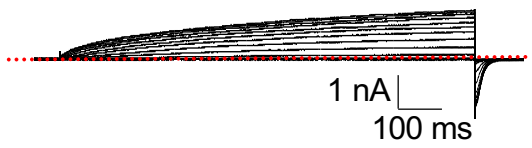

B. *SR-5-6 (10 μM) on S273A$_{(PL)}$ mutant*

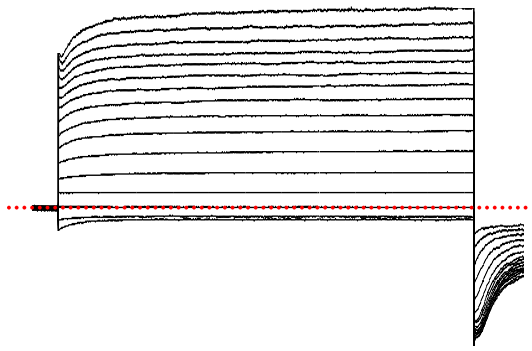

C. *Summary*

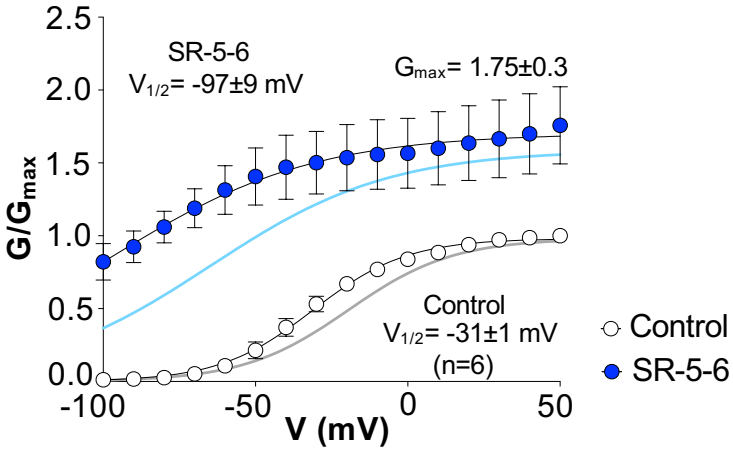

**Figure 4.19: Effect of SR-5-6 on S273A$_{(PL)}$ mutation of K$_v$7.4 channels. A**) A typical family of currents obtained from S273A$_{(PL)}$ mutation of K$_v$7.4 channels expressed in HEK cells. Voltage clamp protocol as described in Figure 4.1. Dotted lines represent the zero current level. **B**) The effect of 10 μM SR-5-6 on currents from the same cell. **C**) Summary activation curves obtained by measuring tail currents in six cells before (open circles) and during (blue circles) application of SR-5-6 (n=6). The continuous grey and light blue lines in the background represent the activation curves of control and the effect of the SR-5-6 on WT K$_v$7.4 channels respectively. The curves were fit with the Boltzmann equation.

A. *T278L & T282A$_{(PL)}$ mutant control*

B. *SR-5-6 (10 μM) on T278L & T282A$_{(PL)}$ mutant*

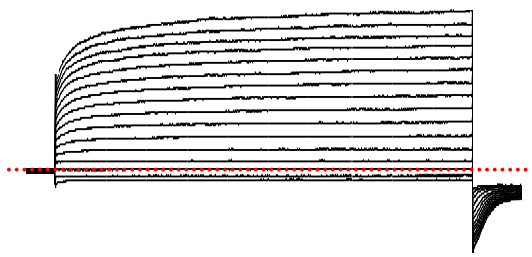

C. *Summary*

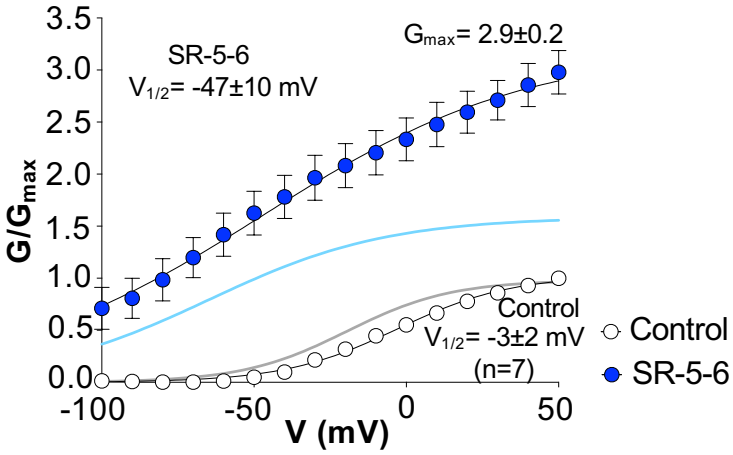

Figure 4.20: Effect of SR-5-6 on T278L & T282A$_{(PL)}$ mutation of K_v7.4 channels. A**) A typical family of currents obtained from T278L & T282A$_{(PL)}$ mutation of K_v7.4 channels expressed in HEK cells. Voltage clamp protocol as described in Figure 4.1. Dotted lines represent the zero current level. **B) The effect of 10 μM SR-5-6 on currents from the same cell. **C**) Summary activation curves obtained by measuring tail currents in seven cells before (open circles) and during (blue circles) application of SR-5-6 (n=7). The continuous grey and light blue lines in the background represent the activation curves of control and the effect of the SR-5-6 on WT K_v7.4 channels respectively. The curves were fit with the Boltzmann equation.

A. *Effect of SR-5-6 (10 μM) on $\Delta V_{1/2}$ of K_v7.4 mutants*

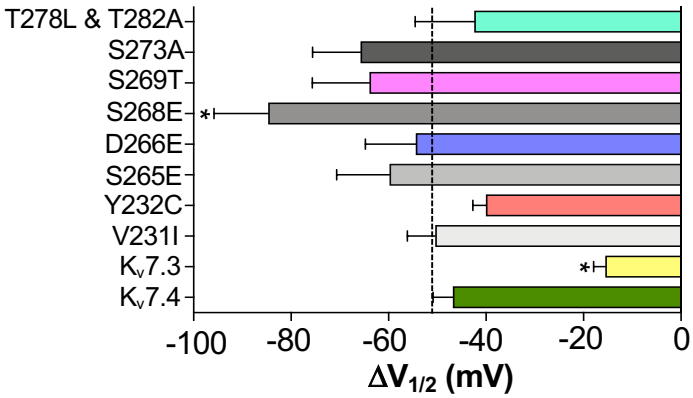

B. *Effect of SR-5-6 (10 μM) on G/G_{max} of K_v7.4 mutants*

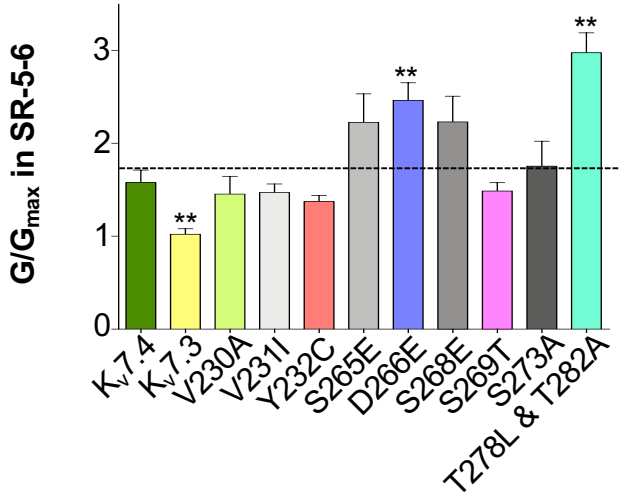

C. *Effect of SR-5-6 (10 μM) on $G_{-100\ mV}$ of K_v7.4 mutants*

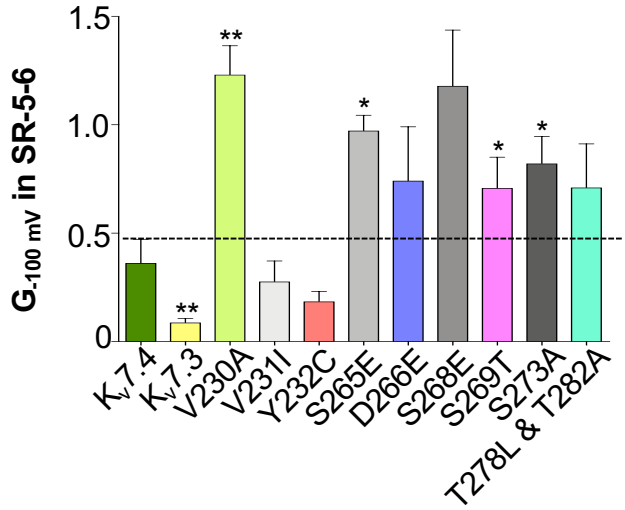

Figure 4.21: Effect of 10 μM SR-5-6 on $\Delta V_{1/2}$, G/G_{max} and $G_{-100\ mV}$ of K_v7.4 mutants. A) SR-5-6 mediated negative shift of the activation curve ($\Delta V_{1/2}$) on various mutants of K_v7.4 channels. A one-way ANOVA was performed with K_v7.4 as the control **B)** The effects of SR-5-6 on maximal conductance (G/G_{max}) of various mutants of K_v7.4 channels. **C)** SR-5-6 mediated change in $G_{-100\ mV}$ on mutants of K_v7.4 channels. A Mann-Whitney, non-parametric test was used for G/G_{max} and $G_{-100\ mV}$ to compare K_v7.4 with other groups. *p<0.05, **p<0.01, ***p<0.001, ****p<0.0001.

A. *Effect of SR-5-6 (10 µM) on $G_{-100\ mV}$ of $K_v7.4$ mutants*

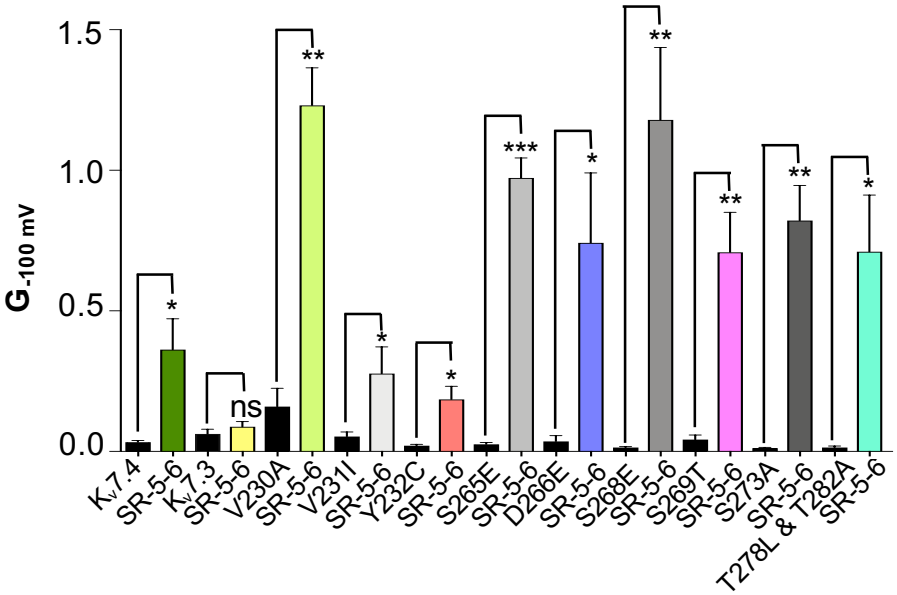

Figure 4.22: Effect of 10 µM SR-5-6 on $G_{-100\ mV}$ of $K_v7.4$ mutants.
The above data depicts the change in conductance (G) at -100 mV in HEK cells expressing the wildtype and the mutant channels. The black bars represent the control condition and the respective colored bars indicate the effect of SR-5-6 as labelled in the figure. Paired t-tests, *p<0.05, **p<0.01, ***p<0.001, ****p<0.0001.

Chapter 5

Involvement of PIP_2 and PIP_2 binding residues on the effects of SR-5-6 in $K_v7.4$

5.1 Introduction

Phosphatidylinositol-(4,5)-bisphosphate (PIP_2) is a phospholipid present in the inner leaflet of plasma membranes and is involved in the secondary messenger signalling pathways and modulation of ion channel function (Suh & Hille, 2008). In K_v7 channels, PIP_2 facilitates the coupling between the voltage-sensing domain and the pore domain (Zaydman *et al.,* 2013). At higher concentrations, PIP_2 has been shown to increase the open probability of homomeric and heteromeric $K_v7.2$-$K_v7.5$ channels, by stabilizing their open state (Li *et al.,* 2005). As shown previously (Figure 3.1C), SR-5-6 has three main effects on $K_v7.4$ channels, which are:

i) increased current conductance G/G_{max} (by ~60%);
ii) negatively shifted activation $V_{1/2}$ (~-50 mV) and;
iii) slowed deactivation (~30 ms).

Interestingly, PIP_2 when applied cytosolically, also slowed the deactivation kinetics and shifted the activation $V_{1/2}$ negatively in $K_v7.1$ channels (Loussouarn *et al.,* 2003; Choveau *et al.,* 2012). Given that SR-5-6 had quite similar effects to PIP_2 on K_v7 channels, it was important to test the hypothesis that SR-5-6 mediated its effects on $K_v7.4$ channels by mimicking the effect of PIP_2.

To investigate this hypothesis, the four complementary approaches listed below were taken, which form the main objectives of this chapter.

1. Examine the effects of PIP_2 depletion by co-expressing voltage sensor containing phosphatase (CiVSP) with WT $K_v7.4$ channels on the response to SR-5-6.
2. Establish the effect of inhibition of PIP_2 synthesis with wortmannin (phosphatidylinositol kinase inhibitor) on the response to SR-5-6 in $K_v7.4$ channels.
3. Investigate if the effects of SR-5-6 were altered when increasing the membrane PIP_2 concentration by using diC8-PIP_2.
4. Test if mutation of known PIP_2 binding residues reduced the effect of SR-5-6 in $K_v7.4$ channels.

5.2 Results

5.2.1 The effects of SR-5-6 on the control group WT $K_v7.4$ channels using the +60 mV protocol for 2 seconds

At first, the effects of SR-5-6 responses in WT $K_v7.4$ in absence of voltage-sensitive phosphatase CiVSP (VSP) was investigated using a longer duration (2s) voltage step protocol described below. This was a control group for the next set of experiments where the effects of PIP_2 depletion on the SR-5-6 responses by using VSP was examined. The protocol used was as follows - cells were held at -80 mV and then stepped from -100 mV to +60 mV in 10 mV increments for 2 seconds, before being repolarized back to -120 mV (Figure 5.1A inset). Given that the effects of SR-5-6 may depend on the activation state/configuration of the channel (Dudem, 2019), it was important to first establish if the drug effects were altered when cells were subjected to the 2s pulses, in the absence of the VSP. Panel A shows the typical control currents in absence of SR-5-6 and Panel B illustrates the typical stimulatory effects of SR-5-6 on these currents. The G-V curves derived from the tail currents in the absence (open circles) and presence of SR-5-6 (blue circles) illustrate that SR-5-6 increased G/G_{max} by a similar degree to the other protocol (to 1.5 ± 0.1) in presence of SR-5-6. These effects on G_{-100mV} (to 0.33 ± 0.05) and $\Delta V_{1/2}$ (-48 mV) were not significantly different to the effects shown in Figure 3.1C, with the shorter duration voltage steps (ns; unpaired t-test).

5.2.2 Co-expression of CiVSP with wildtype $K_v7.4$ reduced the effects of SR-5-6 on G/G_{max} and $G_{-100\ mV}$

After demonstrating the effects of SR-5-6 using the 2s pulse protocol described in the above section in the control group (WT $K_v7.4$ without VSP), the effects of SR-5-6 using the same protocol on HEK cells co-expressing VSP and WT $K_v7.4$ was next investigated. VSP is expressed in the membrane and cleaves PIP_2 when the cell is depolarized (Iwasaki *et al.,* 2008). In the experiments, WT $K_v7.4$ and VSP were co-transfected in a 1:6 ratio in HEK cells. Following patch rupture and cell dialysis, the cell was stepped repeatedly from -80 mV to +60 mV for 2s, every 10s for ~10 minutes, in an attempt to activate the VSP and deplete PIP_2. Cells were then subjected to the voltage protocol described in Section 5.2.1 and shown inset in Figure 5.1A. Figure 5.2A shows typical $K_v7.4$ currents recorded in

the absence of SR-5-6 and these showed slow activation and rapid deactivation kinetics. At potentials positive to +40 mV, it was noticed that the currents declined in amplitude approximately 600 ms into the pulse (see red trace Fig 5.2A), presumably as a consequence of depleting PIP_2 at these depolarized potentials. Once this protocol was completed, the cells were then repeatedly stepped to +60 mV during the application of SR-5-6 (10 μM). These steps to +60 mV were continued until the amplitude of the current reached a plateau (usually after 2-3 minutes). Once the effect of SR-5-6 had stabilized, another family of currents were generated using the protocol shown inset in Fig 5.1A. Panel B shows a typical recording of these currents in the presence of SR-5-6, where it was clear that at more positive potentials (>+20 mV), a sharp decline was observed in current amplitude during the depolarizing pulses, as shown in the coloured records in Figure 5.2B. The data from seven cells were summarized and the G-V curve from the tail currents was generated at -120 mV. The open circles show summary data in the absence of SR-5-6 and the blue symbols were recorded in the presence of SR-5-6. The background grey and blue solid lines indicate Boltzmann fits from WT $K_v7.4$ in the absence and presence of SR-5-6 respectively, using the same protocol as above, but without co-expression of the VSP. As seen in Figure 5.2C, a decrease in G/G_{max} was observed at +60 mV (0.49 ± 0.1) in presence of SR-5-6, compared to an increase to 1.5 ± 0.1 in WT $K_v7.4$ channels (n=7; $p<0.001$; Figure 5.2C and 5.3A). Also, the G_{-100mV} under these conditions only increased to 0.07 upon application of SR-5-6, which was significantly less than its effects on WT $K_v7.4$ channels, where it was 0.33 ± 0.05 ($p<0.05$; Figure 5.2C and 5.3B). Importantly, although SR-5-6 was able to shift the activation $V_{1/2}$, it was not possible to accurately quantify this effect, since the G-V relationship could not be fitted with a Boltzmann equation. Nevertheless, it could be concluded that depleting PIP_2 with a VSP led to a significant decrease in $G_{-100\ mV}$ and G/G_{max} in the presence of SR-5-6.

5.2.3 Examining the effects of SR-5-6 on the control group ($K_v7.4$ WT) using +60 mV prepulse protocol

Although the effects of SR-5-6 appeared reduced when PIP_2 was depleted with the VSP, it was a concern that the protocol described in Section 5.2.1 may not have completely depleted PIP_2 levels. To help address this concern, our protocol

was adapted to follow Zaydman *et al.,* (2013) and a two-step protocol was utilized as illustrated in Figure 5.4 (inset). In these experiments, cells were still repeatedly stepped to +60 mV for ~10 minutes, following break-in and dialysis. However, an additional 2 second depolarization was administered prior to each voltage step of the I-V. Figure 5.4 shows the effects of SR-5-6 in the control group (WT $K_v7.4$ without VSP). Panel A and B show the typical currents (red box) generated from the voltage steps in the absence and presence of SR-5-6 respectively. Panel C shows the G-V relationship derived from the tail currents, and as clearly seen, SR-5-6 (blue circles) enhanced the maximal conductance (G/G_{max}) to 1.52 ± 0.04 (n=6), which was very similar to that observed in the shorter protocol (Figure 3.1). The activation $V_{1/2}$ in SR-5-6 shifted from -29 ± 4 mV to -103 ± 4 mV, resulting in a $\Delta V_{1/2}$ of -76 ± 8 mV ($p<0.01$ when compared to $\Delta V_{1/2}$ effects on WT $K_v7.4$ with the shorter duration protocol; Figure 3.1). The conductance at very negative potentials ($G_{-100\ mV}$) also increased to 0.88 in SR-5-6, which was significantly more than what was observed with the shorter duration protocol ($p<0.05$; Figure 3.1).

5.2.4 The effects of SR-5-6 on $K_v7.4$ co-expressed with CiVSP using a prepulse protocol of +60 mV for 2 seconds

After establishing the effects of SR-5-6 using the two-step protocol in the control group described in the above section, the effects of the drug using the same protocol in HEK cells co-expressing VSP and WT $K_v7.4$ was then examined. Figure 5.5A shows the typical currents (red box) obtained in the absence of SR-5-6. When SR-5-6 was applied to the same cell (Figure 5.5B), it was noted that although the tail currents were slowed, their amplitude was barely increased compared to control. When the G-V curve was generated from these tail currents (Figure 5.5C), it was clear that SR-5-6 failed to increase G/G_{max} significantly (1 in control, compared to 0.95 ± 0.1 in SR-5-6; n=8). When it was compared with the effect of SR-5-6 on WT $K_v7.4$, using the same protocol, a significant reduction in G/G_{max} was found ($p<0.001$; Figure 5.5C and 5.6B). The background grey and blue lines in Figure 5.5C indicate the activation curves of WT $K_v7.4$ in the absence of VSP, using the same prepulse protocol. It is also important to note that the effect of SR-5-6 on $G_{-100\ mV}$ was also significantly reduced in the $K_v7.4$+VSP experiments when compared to control $K_v7.4$ channels (0.88 in $K_v7.4$ and 0.24 in

K_v7.4+VSP; p<0.001; Figure 5.6C). Similarly, the $\Delta V_{1/2}$ induced by SR-5-6 after PIP_2 depletion was only -38 ± 3 mV (n=8; Figure 5.5C) in this protocol, compared to -76 ± 8 mV in the control experiments, as shown in Figure 5.4 (p<0.01; unpaired t-test; Figure 5.6A). Taken together, these results suggested that PIP_2 depletion with CiVSP abolished the effects of SR-5-6 on G/G_{max}, and significantly reduced the effects on $\Delta V_{1/2}$ and $G_{-100\ mV}$.

5.2.5 The effects of SR-5-6, Wortmannin and SR-5-6+Wortmannin in K_v7.4 channels

To investigate PIP_2's role in the SR-5-6-mediated K_v7.4 channel activation further, wortmannin was next utilized, which has been shown to inhibit PIP_2 resynthesis in cells (Zhang *et al.,* 2003). K_v7.4 WT channels were overexpressed in HEK cells in these experiments, and currents were measured using the whole-cell patch configuration. In these experiments, the cells were held at -80 mV and 1 second voltage pulses were applied to the patch from -100mV to +50 mV with 10 mV increments (inset Fig 5.7A) to record steady-state currents before stepping back to -120 mV to generate tail currents. The experiment involved three different treatments on every single cell. Thus, a control I-V was first generated, followed by an I-V in 10 μM SR-5-6, then another I-V in 10 μM wortmannin, before a final set of currents were recorded in the presence of SR-5-6 and wortmannin together. Before recording each I-V, we applied each drug whilst repeatedly stepping to +40 mV to observe the 'wash in' effect of each compound and only when the effects of each treatment had reached a steady-state, as evidenced by overlapping traces, proceeded on to recording the corresponding I-V. The control currents from one such experiment are shown in Figure 5.7A and Figure 5.7B shows the typical currents in the presence of 10 μM SR-5-6. At all potentials, an increase in current amplitude, large tail currents, and delayed deactivation kinetics was observed (Figure 5.7B) in SR-5-6. After washout of this compound, 10 μM wortmannin was administered to the same cell, which reduced the amplitude of the currents (in wortmannin G/G_{max} = 0.93 ± 0.1; ns; when compared to control = 1; Figure 5.7E). Following the wortmannin treatment, SR-5-6 was reapplied in the continued presence of wortmannin to the same cell and recorded an I-V (Figure 5.7D). When compared to the control, the current amplitude

increased modestly at all potentials, and tail currents were larger and slower to deactivate. The activation curves for control (open circles), SR-5-6 (dark blue circles), wortmannin (orange circles), and SR-5-6+wortmannin (light blue circles) are shown in Figure 5.7E. Figure 5.8 summarizes the impact of these treatments on $\Delta V_{1/2}$, G/G_{max}, and $G_{-100\ mV}$. In the presence of SR-5-6, the $V_{1/2}$ significantly shifted from -21 ± 1 mV to -72 ± 5 mV resulting in a $\Delta V_{1/2}$ of -50 ± 5 mV in 8 similar experiments. The $V_{1/2}$ was -29 ± 2 mV after wortmannin administration, compared to -21 ± 1 mV in the absence of any drugs, thus resulting in a $\Delta V_{1/2}$ of -7 ± 2 mV in wortmannin when compared to control. The $V_{1/2}$ was -57 ± 7 mV when SR-5-6+wortmannin was added, resulting in $\Delta V_{1/2}$ of -36 ± 7 mV, which was not a significant reduction when compared to SR-5-6 alone (ns; Figure 5.8A). The G/G_{max} was 1.7 ± 0.1 in the presence of SR-5-6 and 0.93 ± 0.1 in the presence of wortmannin which was significantly less when compared to SR-5-6 ($p<0.0001$). The G/G_{max} was 1.1 ± 0.1 in the presence of SR-5-6+wortmannin, which was a significant reduction when compared to the effects of SR-5-6 alone ($n=8$; $p<0.01$; Figure 5.8B). In contrast, no significant change was found in $G_{-100\ mV}$ in SR-5-6 versus SR-5-6+wortmannin (Figure 5.8C). Taking all this information into account, it can be concluded that decreasing PIP_2 with wortmannin treatment significantly reduced the effects of SR-5-6 on G/G_{max}.

5.2.6 The SR-5-6 effects on $K_v7.4$ channels when diC8-PIP_2 is added intracellularly

Next, investigated if exogenous PIP_2 would enhance the effects of SR-5-6 by dialysing 200 μM diC8-PIP_2 into the cell via the pipette. This homolog of PIP_2 has shorter (dioctanoyl) chains and is more water-soluble (Suh & Hille, 2008). The currents were recorded as shown in Figure 5.9 using a whole-cell patch arrangement and the typical protocol described in section 5.2.5 (Figure 5.7A). At the start of the experiment, stepped repeatedly to +40 mV for ~12 minutes to allow diC8-PIP_2 to diffuse into the cell and to allow its effects to saturate. Figure 5.9A depicts a typical current record in the presence of diC8-PIP_2, prior to the application of SR-5-6. In control conditions, the currents appeared similar to WT $K_v7.4$ channels, although they activated more negatively (-34 ± 1 mV) than untreated $K_v7.4$ channels (grey continuous line, $V_{1/2}$ = -19 ± 1 mV; $p<0.01$;

unpaired t-test). The channels appeared to be constitutively active when SR-5-6 was present, as seen in Figure 5.9B and at potentials negative to -80 mV, large inward currents were noticed. In the presence of SR-5-6, the activation $V_{1/2}$ was -99 ± 6 mV, which was more negative than that observed in cells in absence of diC8-PIP_2 (blue solid line). As a result, the $\Delta V_{1/2}$ was -67 ± 7 mV, which was significantly more negative than without diC8-PIP_2 ($p<0.05$; unpaired t-test, Figure 5.10A). In the presence of diC8-PIP_2, SR-5-6 modestly increased the G/G_{max} to 1.7 ± 0.1 (n=11), but this was not significantly different from the effect of SR-5-6 in absence of diC8-PIP_2 (Figure 5.10B). Importantly, in the presence of SR-5-6, the conductance at -100 mV ($G_{-100\ mV}$) significantly increased to 0.87 compared to the effect of SR-5-6 in the absence of PIP_2 ($p<0.01$; Figure 5.10C). All of these findings showed that in the presence of diC8-PIP_2, SR-5-6 effects were enhanced.

5.2.7 The effects of SR-5-6, Wortmannin and SR-5-6+Wortmannin in $K_v7.4$ channels in presence of diC8-PIP_2

The combined effects of wortmannin and diC8-PIP_2 on SR-5-6 effects in $K_v7.4$ channels were then investigated. The goal of this set of experiments was to examine if wortmannin could possibly be having any non-specific effects. If this were the case, the exogenous PIP_2 effects should still be very obvious when the endogenous PIP_2 production was blocked. In Figure 5.11, WT $K_v7.4$ was overexpressed in HEK cells and the standard protocol described in Section 5.2.5 was used to record currents and throughout these recordings, the pipette solution contained 200 μM diC8-PIP_2. At the start of the experiment, dialysed diC8-PIP_2 into the cells whilst repeatedly stepping to +40 mV for ~12 minutes to allow diC8-PIP_2 to have its maximal effects. Figure 5.11A and B shows typical currents recorded following dialysis with diC8-PIP_2 before and during 10 μM SR-5-6 application, respectively. As expected, the current amplitude increased at all voltages (Figure 5.11B), G/G_{max} increased to 1.7 ± 0.2 in SR-5-6+diC8-PIP_2 (Figure 5.11E) and $V_{1/2}$ was shifted negatively to -97 ± 7 mV. When SR-5-6 was removed and 10 μM wortmannin administered extracellularly, the currents, in this experiment, appeared to be greater than in control, presumably because SR-5-6 was not fully washed out (Figure 5.11C). From the typical record shown in Figure

5.11C, wortmannin appeared to enhance the currents even at positive potentials even though that is not reflected in the summary data. However, this was not a consistent observation and in two experiments, currents were increased and in the other three cells, the currents were decreased. When these data were averaged, a small decrease in current amplitudes at positive potentials was observed, as evidenced by the G-V curve in Figure 5.11E (orange circles), where wortmannin reduced the G/G_{max} to 0.93 ± 0.1 (ns; when compared to control = 1; Figure 5.11E). When SR-5-6+wortmannin was applied in the presence of diC8-PIP_2 inward currents at potentials negative to -80 mV and an increase in tail current amplitude at negative potentials was observed, as illustrated in the summary G-V curve. However, at positive potentials, the current amplitude did not increase, since the G/G_{max} was 0.95 ± 0.1, which was significantly smaller than that in SR-5-6+diC8-PIP_2 alone ($p<0.05$; Figures 5.11C and 5.12B). The activation curves for control (open circles), SR-5-6 (dark blue circles), wortmannin (orange circles), and SR-5-6+wortmannin (light blue circles) are shown in Figure 5.11E. For this set of data, summarized the effects on $\Delta V_{1/2}$, G/G_{max}, and $G_{-100\ mV}$ in Figure 5.12 and also included data from the SR-5-6 and SR-5-6+wortmannin studies from Section 5.2.5 (Figure 5.8), to compare the effects of wortmannin in the presence and absence of diC8-PIP_2 on SR-5-6 response. When SR-5-6 was added in presence of diC8-PIP_2, the $\Delta V_{1/2}$ was -65 ± 8 mV and was not significantly altered in SR-5-6+wortmannin+diC8-PIP_2 (-53 ± 10 mV, Figure 5.12A). When SR-5-6+wortmannin+diC8-PIP_2 was compared to SR-5-6+diC8-PIP_2, the conductance at -100 mV ($G_{-100\ mV}$) did not significantly change either (Figure 5.12C) and the effect on G_{-100} mV was retained. However, the effect of SR-5-6 on G/G_{max} was certainly reduced by wortmannin even in the continued presence of diC8-PIP_2.

5.2.8 The effects of SR-5-6 on PIP_2 binding mutations in $K_v7.4$ channels

The next hypothesis tested was if SR-5-6 partially mediated its effects on K_v7 channels by either altering PIP_2 binding or perhaps accessing the same binding pockets in K_v7 channels. Hence, systematically investigated the effect of mutating a series of residues that have been implicated in PIP_2 binding, prior to examining their effects on SR-5-6. A number of studies have previously identified clusters of basic residues in the S2-S3 linker, the S4-S5 linker and the C-terminus region of

the channels as necessary PIP_2 binding residues (Park *et al.,* 2005; Hernandez *et al.,* 2008; Zaydman *et al.,* 2013; Tobelaim *et al.,* 2017), so the corresponding residues were mutated (shown in Figure 5.0 below) in $K_v7.4$ and the effects of SR-5-6 on these mutants were examined.

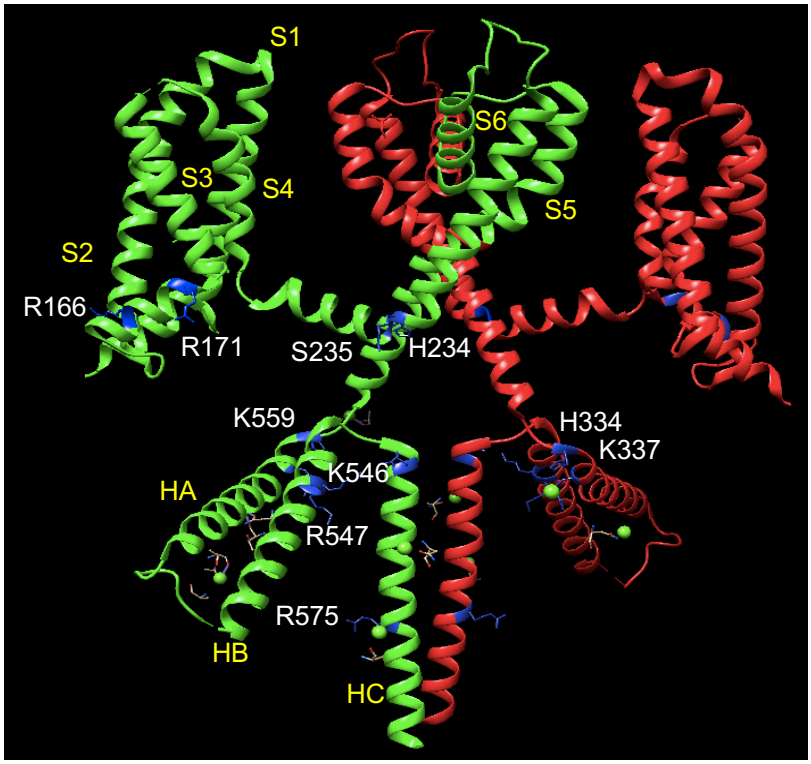

Figure 5.0: Structural location of PIP_2 binding residues. *Domain organization (side view) of two subunits in $K_v7.1$ coloured in green and red (adapted from Sun & MacKinnon, 2017). The residues represented in the diagram are the known PIP_2 binding residues that were investigated for the effects of SR-5-6 in $K_v7.4$ channels.*

5.2.8.1 Effect of SR-5-6 when PIP_2 binding residues in the VSD-PD interface were mutated

Zaydman *et al.,* (2013) found many lipid binding residues in the interface between the voltage-sensing domain and the pore domain and suggested that they were key PIP_2 binding residues. They utilised mutagenesis and homology modelling to identify several residues (R190, R195, H258, R259, H363, and R366) that could act as PIP_2 binding interaction sites in $K_v7.1$ channels. As Figure 5.0 suggests, these residues are located in the S2-S3 linker, the S4-S5 linker, the distal end of S6 and the C-terminus region of the protein. The Zaydman *et al.,* (2013) study reported a considerable drop (>50%) in the amplitude of whole-cell currents in a

number of these mutants, and this effect was attributed to a disruption in PIP_2 binding. Thereafter, the effects of SR-5-6 were investigated when the equivalent residues in $K_v7.4$ were neutralized.

The first mutation investigated in $K_v7.4$ was **R166A**, which corresponded to R190 in the S2-S3 linker region of the $K_v7.1$ channel. The mutant channels were expressed in HEK cells and examined using whole-cell recording with the voltage protocol detailed in Figure 5.7A. Figure 5.13A illustrates a family of currents obtained with the R166A mutant, which was remarkably similar to WT $K_v7.4$, under control conditions. As panel B suggests, application of 10 μM SR-5-6 to the same cell (Figure 5.13B) had a clear excitatory effect on the currents and large, slow deactivating tail currents were evoked upon repolarization to -120 mV. When the data from eleven cells was summarized and fitted with a Boltzmann equation, it was observed that SR-5-6 increased G/G_{max} from 1 to 1.46 ± 0.1 and this was not significantly different from its effect on WT $K_v7.4$ channels (n=11; Figure 5.13C and 5.25B). In the absence of SR-5-6, the activation $V_{1/2}$ was -30 ± 1 mV, but in the presence of SR-5-6, it was shifted to -80 ± 6 mV, resulting in a $\Delta V_{1/2}$ of -55 ± 5 mV, which was not significantly different compared to the effect on WT $K_v7.4$. Similarly, with the mutant, the conductance at -100 mV increased from 0.02 in control to 0.6 in SR-5-6, which was not substantially different from WT $K_v7.4$ channels. Based on these findings it was concluded that the effects of SR-5-6 were not significantly altered in $K_v7.4$ R166A mutant channels.

R171A in the S2-S3 linker region of $K_v7.4$ channels was the next mutation studied. In the Zaydman *et al.,* (2013) study, this residue corresponds to the PIP_2 binding residue R195. Figures 5.14A and 5.14B depict typical current records obtained with and without SR-5-6, respectively. In Figure 5.14A, the control currents began to activate at -70 mV. Figure 5.14B shows that SR-5-6 was just as effective on this mutant channel as it was on WT $K_v7.4$ channels. The summary activation curves from five cells under control (open circles) and when SR-5-6 (blue circles) was administered are shown in Figure 5.14C. The activation $V_{1/2}$ of the R171A $K_v7.4$ channel was -38 ± 1 mV, and when 10 μM SR-5-6 was applied, the activation curve shifted negatively to -99 ± 5 mV. As a result, the $V_{1/2}$ shift ($\Delta V_{1/2}$) was -61 ± 5 mV, which again was not substantially different from WT $K_v7.4$ channels. In addition, SR-5-6 increased the G/G_{max} from 1 to 1.5 ± 0.1 and

the conductance at 100 mV ($G_{-100\ mV}$) from 0.02 to 0.78 (n=5; Figures 5.14C, 5.25 & 5.26). Figure 5.14C shows that the effects of SR-5-6 were not minimized by R171A $K_v7.4$ mutant channels when compared to WT data (presented as solid grey and blue lines).

H234N in the S4-S5 linker region of $K_v7.4$ channels was one of the two PIP_2 binding residues investigated and when the mutant channels were expressed in HEK cells, they produced currents whose activation $V_{1/2}$ was -37 ± 1 mV (n=6; Figure 5.15C). This was significantly more negative than that of WT $K_v7.4$ under control conditions (-19 ± 2 mV; $p<0.001$; unpaired t-test; n=7). However, the current amplitude was substantially enhanced at all potentials when 10 μM SR-5-6 was applied to the same cell and at potentials negative to -80 mV, large inward currents were seen (Figure 5.15B). In the G-V summary data plotted from the tail currents at -120 mV, it was observed that although G/G_{max} increased from 1 to 1.4 ± 0.07 (n=6; ns than that observed with WT $K_v7.4$; Figure 5.15C & 5.25B). The $G_{-100\ mV}$ increased from 0.04 to 0.63 in the SR-5-6 (Figure 5.26) and was significantly more than that observed in WT $K_v7.4$ ($p<0.05$; Figure 5.25C). The activation $V_{1/2}$ was shifted negatively to -86 ± 8 mV in the presence of SR-5-6 (blue circles), which resulted in a $\Delta V_{1/2}$ of -49 ± 7 mV, which did not differ considerably from WT $K_v7.4$ channels (Figure 5.25A).

S235A, which corresponded to R259 in $K_v7.1$, was the other PIP_2 binding residue studied in the S4-S5 linker (Zaydman *et al.,* 2013). The S235A $K_v7.4$ channel also produced currents similar to the WT $K_v7.4$, as illustrated in Figure 5.16A. In the absence of SR-5-6, the activation $V_{1/2}$ for this mutant channel was -30 ± 1 mV. An increase in current amplitude was noticed at all potentials when 10 μM SR-5-6 was applied to the same cell. The tail currents were larger and decayed more slowly than the control currents (Figure 5.16B) and the G/G_{max} significantly increased to 3.3 ± 0.4 (n=7) in the presence of SR-5-6 ($p<0.01$; Figure 5.25B), as shown in Figure 5.16C from seven cells. The activation $V_{1/2}$ in the control (open circles) was -30 ± 1 mV, but in the presence of SR-5-6, it shifted negatively to -77 ± 8 mV, yielding in $\Delta V_{1/2}$ of -48 ± 8 mV which was not significantly different from WT $K_v7.4$ (Figure 5.25A). The conductance at -100 mV ($G_{-100\ mV}$) increased from 0.03 in control to 1.08 in SR-5-6, which was significantly greater than WT $K_v7.4$ ($p<0.01$; Figure 5.25B & 5.26). Overall, it was observed that the effects of

SR-5-6 on conductance were considerably enhanced in this mutant, not diminished.

The next residue looked into was **H334A** in $K_v7.4$. This residue is equivalent to H363 in $K_v7.1$, which has been linked to PIP_2 binding. As shown in Figure 5.17A, when the H334A channels were studied, they were enhanced in the presence of 10 μM SR-5-6 (Figure 5.17B) and large inward currents were seen at potentials negative to -80 mV. In this mutant channel, SR-5-6 increased the G/G_{max} to 3.1 ± 0.6 (n=5, Figure 5.17C) which was significantly greater than that in WT $K_v7.4$ channels ($p<0.05$; Figure 5.25B). The $V_{1/2}$ in control was 9 ± 9 mV (open circles), which was considerably right shifted compared to WT $K_v7.4$ channels (grey solid line). However, when SR-5-6 was applied, the activation $V_{1/2}$ was shifted to -24 ± 11 mV (blue circles). Thus, the mutant channel's $V_{1/2}$ shift ($\Delta V_{1/2}$) was -34 ± 1 mV, which was not statistically different from that of WT $K_v7.4$ channels (Figure 5.17C & 5.25A). An increase in $G_{-100\ mV}$ from 0.1 in control to 0.32 in the presence of SR-5-6 was observed with this mutant, which again was similar to WT $K_v7.4$, leading to conclude that mutation of the H334 residue in $K_v7.4$ failed to abolish the effects of SR-5-6 on $K_v7.4$ channels.

The **K337A** mutation, which is equivalent to the R366 residue in $K_v7.1$, is located near the C-terminus and has been linked to PIP_2 interactions in $K_v7.1$ channels (Zaydman *et al.,* 2013). Figures 5.18A and 5.18B illustrate typical currents measured in the absence and presence of SR-5-6. The control currents had an activation $V_{1/2}$ under control conditions of -18 ± 1 mV which was not significantly different to WT $K_v7.4$ (grey line, Figure 5.18C). Interestingly, as shown in Figure 5.18B, when SR-5-6 was applied, it had a huge effect and resulted in constitutively active channels. Thus, the G/G_{max} of this mutant was significantly increased by SR-5-6 to 2.9 ± 0.2, which was considerably higher than that of WT $K_v7.4$ channels (n=7; $p<0.001$; Figure 5.17C and 5.25B). Similarly, a large increase in $G_{-100\ mV}$ was noticed, which went from 0.04 in control to 2.05 in the presence of SR-5-6 (Figure 5.17C and 5.26, which was much larger than what was observed in WT $K_v7.4$ channels ($p<0.001$; Figure 5.25C). Therefore, when compared to the WT data presented as solid grey and blue lines in Figure 5.17C, it was clear that the putative PIP_2 binding mutant K337A in $K_v7.4$ greatly enhanced the effects of SR-5-6.

5.2.8.2 The effects of SR-5-6 on mutations linked to PIP_2 binding residues in the C-terminus inter-helix region

In 2008 Hernandez *et al*., produced one of the seminal works that helped identify the site of action and structural motif of PIP_2 binding to K_v7 channels. They utilized single channel recordings to demonstrate that three key residues (K452, R459, and R461) in the C-terminus inter-helix region of $K_v7.2$ acted as PIP_2 binding sites. According to their mutational and docking studies, these residues were essential for PIP_2 binding in $K_v7.2$, $K_v7.3$ and $K_v7.4$, but were absent in $K_v7.1$ channels (Hernandez *et al.,* 2008). The involvement of these carboxy-terminal residues was next examined by mutating the corresponding K452, R459, and R461 residues in $K_v7.4$ to alanine and testing the effects of SR-5-6 on these mutants.

The $K_v7.4$ **K481A** mutant, which corresponded to the K452 residue in $K_v7.2$, activated at potentials positive to -70 mV, as shown in Figure 5.19A. When 10 μM SR-5-6 was administered to the same cell (Figure 5.19B), the maximal conductance G/G_{max} increased to 1.7 ± 0.1 (n=5), which was not significantly greater than that observed in WT $K_v7.4$ channels, as demonstrated by the G-V curve in Figure 5.19C. The conductance at -100 mV increased from 0.03 in control to 0.68 in SR-5-6 which was significantly greater than that observed with SR-5-6 in the WT $K_v7.4$ channels ($p<0.05$; Figure 5.25C &5.26). The application of SR-5-6 also shifted the voltage-dependent activation from -12 ± 2 mV to -60 ± 5 mV, resulting in a $\Delta V_{1/2}$ of -46 ± 3 mV, but this change was not significantly different to WT $K_v7.4$. This data suggested that removal of the positive charge at position 481 in $K_v7.4$ failed to reduce the effect of SR-5-6.

When the **R488A** mutant was produced in $K_v7.4$, which corresponded to R459 in the C-terminus region of $K_v7.2$, it was found that the effects of SR-5-6 were clearly enhanced, rather than blocked, as illustrated in Figure 5.20B. The tail currents when normalized to the maximum and plotted from five cells fitted with the Boltzmann equation, yielded a control $V_{1/2}$ of -23 ± 1 mV before (ns vs WT $K_v7.4$) and -83 ± 8 mV during SR-5-6. As a result, the $\Delta V_{1/2}$ was -62 ± 12 mV, which was similar to that of WT $K_v7.4$ channels (ns; n=5; Figure 5.20C and 5.25A). The G/G_{max} increased to 2 ± 0.3 (n=5; Figure 5.20C) and it was not statistically significant when compared to WT $K_v7.4$ channels (1.58 ± 0.1; n=7; Figure 5.20C

and 5.25B). Although $G_{-100\ mV}$ increased from 0.02 to 0.8 in SR-5-6, it did not show significance when compared to WT $K_v7.4$ (ns; Figures 5.25C & 5.26). From the WT $K_v7.4$ activation curves (grey and blue lines), it was clear that in this mutant the SR-5-6 effects were enhanced rather than blocked.

The PIP_2 binding residue R461 in the inter-helix region of the $K_v7.2$ C-terminus was the next mutation looked into (Hernandez *et al.,* 2008). The equivalent charge neutralization mutation **R490A** was generated in $K_v7.4$ and the effects of SR-5-6 were evaluated, as shown in Figure 5.21. When SR-5-6 was added to the cell, a clear increase in current amplitude at all potentials was noticed. When the activation curves from the tail currents were constructed and summarized in the control (open circles) and SR-5-6 (blue circles), it was clear that SR-5-6 increased the G/G_{max} from 1 to 2.8 ± 0.4 (n=6; Figure 5.21C), which was significantly higher than the WT $K_v7.4$ channel ($p<0.05$; Figure 5.25B). The $V_{1/2}$ activation in control was -19 ± 2 mV, which was the same as in WT $K_v7.4$ channels (overlapped grey solid line). The $V_{1/2}$ shifted negatively to -63 ± 6 mV when SR-5-6 was applied, resulting in a shift in $V_{1/2}$ of 47 ± 6 mV, which was not significantly different from that found in WT $K_v7.4$ channels (Figure 5.25A). The conductance at -100 mV increased from 0.04 in the control to 0.48 in the presence of SR-5-6, which was similar to that seen in WT $K_v7.4$ channels (Figure 5.25C & 5.26). Consequently, it was clear that the R490A mutant channels also enhanced the effects of SR-5-6, rather than reducing them.

5.2.8.3 Investigating the effects of PIP_2 binding mutations K546N and R547A on response to SR-5-6 in $K_v7.4$ channels

A different PIP_2 binding region was then examined to assess the effects of SR-5-6 because the previous PIP_2 binding sites clearly did not minimize SR-5-6 effects. In their study, Tobelaim *et al.,* (2017) identified two residues (K526 and K527) in the helix-B region of the C-terminus of $K_v7.1$, as key locations for PIP_2 and calcified CaM binding that stabilized the open state of I_{Ks} channels. The K546N and R547A $K_v7.4$ mutant channels were generated, the corresponding residues in $K_v7.4$ and their effects were tested on the SR-5-6 response.

The **K546N** mutant currents shown in Figure 5.22A had an activation $V_{1/2}$ of -22 ± 1 mV (Figure 5.22C, open symbols), which overlapped with the WT $K_v7.4$ channels G-V curve (grey solid line). When 10 μM SR-5-6 was added it shifted

the $V_{1/2}$ to -61 ± 4 mV and the $\Delta V_{1/2}$ in the K546N mutant was -41 ± 3 mV (n=8; Figure 5.22C), neither of which were different to the responses observed in the WT $K_v7.4$ channel. Although the effect of SR-5-6 on G/G_{max} was reduced (1.4 ± 0.1, n=8; Figure 5.22C and 5.25B), it did not read significance when compared to the control. There also appeared to be a smaller change in the $G_{-100\ mV}$ (0.02 in control compared to 0.26 in SR-5-6) but this was not significantly different from WT $K_v7.4$ channels (Figure 5.25C and 5.26), suggesting that this mutant altered the effect of SR-5-6 on G/G_{max} and $G_{-100\ mV}$ rather modestly, but clearly didn't block it.

In the penultimate mutation, a **R547A** $K_v7.4$ construct was generated, which was equivalent to the K527 residue in $K_v7.1$. As Figure 5.23A suggests, the currents were similar to WT $K_v7.4$ channels in the absence of SR-5-6 and increased in amplitude at all potentials when 10 μM SR-5-6 was added (Figure 5.23B). As Figure 5.23C suggests, the control activation curve (open circles) yielded a $V_{1/2}$ of -22 ± 1 mV, whereas, in the presence of SR-5-6, it was -82 ± 9 mV. Thus, the $\Delta V_{1/2}$ for R547A mutant channels was -59 ± 11 mV (n=5; Figure 5.23C) which was similar to WT $K_v7.4$ channels (Figure 5.25A). However, like many of the PIP_2 binding mutations, G/G_{max} increased significantly from 1 to 2.1 ± 0.2 (n=5), compared to WT $K_v7.4$ ($p<0.05$; Figure 5.23C and 5.25B) and the conductance at -100 mV increased from 0.04 in control to 0.9 in SR-5-6, which was statistically different from that of the WT $K_v7.4$ channel ($p<0.05$; Figure 5.25C). These findings showed that the effects of SR-5-6 were again not blocked in $K_v7.4$ channels with the R547A mutation.

5.2.8.4 The effects of SR-5-6 on K559A $K_v7.4$ mutant channels

Park *et al.,* (2005) discovered a dysfunctional interaction between $K_v7.1$-KCNE1 and PIP_2 in their long QT-syndrome study. Residue R555 was proposed to be a key PIP_2 interaction site with $K_v7.1$ in the same study, and when it was altered, it impaired channel function. The effects of SR-5-6 were investigated by mutating the corresponding residue in $K_v7.4$ (**K559A**). This mutant channel generated currents that looked practically identical to WT $K_v7.4$ (Figure 5.24A). The current amplitude increased at all voltages when 10 μM SR-5-6 was administered, as illustrated in Figure 5.24B. When the data from ten cells was summarized in

Figure 5.24C, it was found that the control activation curve (open circles) was identical to that of WT $K_v7.4$ (grey solid line) and that the activation $V_{1/2}$ for this mutant in control was -19 ± 1 mV. The activation curve shifted to -65 ± 6 mV in the presence of 10 μM SR-5-6 (n=10; Figure 5.24C). As a result, the $\Delta V_{1/2}$ was -48 ± 6 mV, which was similar to what was seen in WT $K_v7.4$ channels (Figure 5.25A). G/G_{max} increased from 1 to 2.3 ± 0.1 (n=10), which was higher than WT $K_v7.4$ ($p<0.01$; Figure 5.25B). In the presence of SR-5-6, the $G_{-100\ mV}$ increased to 0.7 (Figure 5.26) but this was not statistically different from WT $K_v7.4$ channels (Figure 5.25C). Taken together, the findings suggested that the K559 residue was not essential for the excitatory effects of SR-5-6 on $K_v7.4$ channels.

5.3 Discussion

The aim of this chapter was to establish the role of PIP_2 in SR-5-6 mediated activation of $K_v7.4$ channels. The major conclusions from this chapter were as follows:

1. The effects of SR-5-6 on G/G_{max} was abolished in $K_v7.4$+VSP experiments.
2. The effect of SR-5-6 on $\Delta V_{1/2}$ and $G_{-100\ mV}$ was also significantly reduced when PIP_2 was depleted by co-expressing CiVSP with $K_v7.4$ WT channels.
3. Inhibition of PIP_2 synthesis with wortmannin significantly reduced the effects of SR-5-6 on G/G_{max} in $K_v7.4$ channels.
4. The increased levels of PIP_2 membrane concentration by using diC8-PIP_2 significantly increased the effects of SR-5-6 on $\Delta V_{1/2}$ and $G_{-100\ mV}$.
5. The application of diC8-PIP_2 and inhibition of PIP_2 synthesis via wortmannin simultaneously showed that wortmannin effects were specific and the reduction in G/G_{max} was indeed due to PIP_2 inhibitory effects by wortmannin in $K_v7.4$ channels.
6. The mutational study of known PIP_2 binding residues did not abolish the effect of SR-5-6 in any mutant channels.

In the initial results of this chapter, the effect of PIP_2 depletion on WT $K_v7.4$ channels was demonstrated, by co-expressing voltage-sensitive phosphatase (CiVSP) with them. A single step protocol was used initially to generate G-V (-100 mV to +60 mV for 2 seconds) and in the second set of experiments, a two-step protocol was used (prepulse to +60 mV for 2 seconds followed by stepping to the desired potential in the I-V for 500 ms) to maximally activate CiVSP, in order to study its effects on the SR-5-6 response. At positive potentials, when the CiVSP is presumably more effective, it was observed that SR-5-6 failed to enhance G/G_{max}. This effect resulted from a decline in current amplitude and was more obvious, at positive potentials, in presence of SR-5-6 than in the absence of the drug. It is known that PIP_2 is essential to stabilize the K_v7 channel open state leading to an increase in the current amplitude (Gamper & Shapiro, 2007; Logothetis *et al.,* 2015). Thus, when PIP_2 was depleted using the CiVSP, SR-5-6 clearly failed to enhance the current amplitude more so at positive potentials

(Figure 5.1 & 5.5). A shift in activation $V_{1/2}$ and also an increase in $G_{-100\ mV}$ was observed, but it was significantly reduced when compared to SR-5-6 effects in absence of CiVSP. Most importantly, the effect of SR-5-6 on G/G_{max} was completely abolished when PIP_2 was depleted using CiVSP. This suggested that depleting PIP_2 via CiVSP had an inhibiting effect on SR-5-6 response in $K_v7.4$ channels.

To further examine the role of PIP_2 in SR-5-6 response in $K_v7.4$ channels, the next approach taken was to deplete PIP_2 pharmacologically, using wortmannin. Zhang *et al.,* (2003) previously established that wortmannin at a concentration of 10 μM could effectively inhibit PIP_2 resynthesis and thus delay M-current recovery due to alterations in membrane PIP_2 levels. The same concentration of wortmannin was used and it was applied extracellularly to deplete PIP_2, prior to examining the effects of SR-5-6. In this set of experiments, any significant reduction in $\Delta V_{1/2}$ and $G_{-100\ mV}$ was not observed when the G-V curves in SR-5-6 alone to those obtained in SR-5-6 and wortmannin in the same cell were compared. However, there was a significant reduction in the G/G_{max}, in SR-5-6, when wortmannin was present, which supported the idea that the increase in G/G_{max} in $K_v7.4$ channels is PIP_2 dependent. Conversely, neither the $\Delta V_{1/2}$ nor change in $G_{-100\ mV}$ were significantly altered when PIP_2 replenishment was inhibited (Figure 5.7 & 5.8). However, many studies have confirmed the important role of PIP_2 in coupling the VSD to the PD in order to help stabilize the open state, increase current amplitude, slow deactivation kinetics and negatively shift the $V_{1/2}$ (Loussouarn *et al.,* 2003; Park *et al.,* 2005; Zaydman *et al.,* 2013; Choveau *et al.,* 2012 and Cui, 2016). The data on the SR-5-6 response demonstrated that the G/G_{max} effect was eliminated, suggesting that the stability of the open state and increase in current amplitude by SR-5-6 are probably reliant on PIP_2 levels, in some way. Overall, a considerable reduction was detected in the effect of SR-5-6 on G/G_{max} in $K_v7.4$ channels in both VSP and wortmannin experiments. As a result, it can be suggested that PIP_2 plays a key role in SR-5-6 response in $K_v7.4$ channel activation.

To assess the contribution of PIP_2 further, the effect of exogenous PIP_2 on SR-5-6 responses was next examined by the addition of 200 μM diC8-PIP_2 in the pipette solution. The purpose of this set of experiments was to see if the effects

of SR-5-6 were enhanced when exogenous PIP_2 was present. It has been reported by Loussouarn *et al.,* (2003) that exogenous PIP_2 treatment reduced $K_v7.1$/KCNE1 current rundown, shifted activation $V_{1/2}$ negatively (~30 mV) and slowed deactivation kinetics (~140 ms) (Loussouarn *et al.,* 2003). In the experiments on $K_v7.4$, when exogenous diC8-PIP_2 was added - i) it shifted activation $V_{1/2}$ by ~-15 mV, ii) slowed deactivation kinetics by ~30 ms, and iii) activated the channels more rapidly by ~45 ms when compared to control $K_v7.4$ currents. As shown in Chapter 3, SR-5-6 alone (Figure 3.1) had similar effects and slowed tail currents by ~30 ms, shifted $V_{1/2}$ by -50 mV and activation kinetics were accelerated by ~50 ms. Thus, diC8-PIP_2 and SR-5-6 had similar effects on activation and deactivation kinetics but SR-5-6 shifted the voltage dependence of the channel more negatively in $K_v7.4$ channels. When SR-5-6+diC8-PIP_2 was administered, a ~-70 mV shift in activation $V_{1/2}$ was seen, the deactivation of the channel was further slowed by ~40 ms and the activation kinetics was further enhanced by ~45 ms when compared to diC8-PIP_2. Also, SR-5-6+diC8-PIP_2 further amplified the effect on $G_{-100\ mV}$ when compared to only SR-5-6 by ~0.6 (Figure 5.9). All these data suggested that SR-5-6 effects were enhanced in the presence of exogenous diC8-PIP_2 in $K_v7.4$ channels. However, the G/G_{max} (1.7 ± 0.1) did not significantly increase when SR-5-6 to SR-5-6+diC8-PIP_2 effects were compared (Figure 5.9 & 5.10B). It is well established that PIP_2's primary function in K_v7 channels is to enhance the open probability of the channels (Li *et al.,* 2005). Hence, the unaltered G/G_{max} could be attributed to the open probability being saturated in presence of diC8-PIP_2 and it could not be further enhanced when SR-5-6+diC8-PIP_2 was administered. Taken together all these data, it can be said that exogenous diC8-PIP_2 further enhanced the effects of SR-5-6 on $K_v7.4$ channel activation and deactivation kinetics. But there was no significant enhancement on the conductance (G/G_{max}) of the channel by SR-5-6 in presence of diC8-PIP_2.

After determining the effects of wortmannin and diC8-PIP_2 on SR-5-6 responses separately, experiments were conducted in which both wortmannin and diC8-PIP_2 were administered at the same time. The objective of this set of experiments was to see if wortmannin had any non-specific effects. Wortmannin only inhibits the replenishment of the endogenous PIP_2 and should not have any effect on the levels of exogenous PIP_2 supplied. If this was the case, then exogenous diC8-

PIP_2 effects should still be apparent and it should enhance the SR-5-6 responses even when endogenous PIP_2 production was inhibited by wortmannin. It was observed that in the presence of wortmannin, the effect of SR-5-6 on G/G_{max} was abolished and was not restored, even when exogenous PIP_2 was supplied via the pipette. Although, in the presence of wortmannin, the effects of SR-5-6 on $G_{-100\ mV}$ and shift in $V_{1/2}$ were marginally reduced, the effects were rescued by the presence of diC8-PIP_2 (compare SR5-6+wortmannin effects in presence and absence of diC8-PIP_2 in Figure 5.12). This indicated that wortmannin somehow blocks SR-5-6 from increasing G/G_{max} even when endogenous PIP_2 levels were elevated in the presence of diC8-PIP_2. This could be possible by either i) wortmannin having an effect on the binding site of SR-5-6 in $K_v7.4$ channels and/or ii) PIP_2 depletion by wortmannin bringing about conformational changes that are only partially restored by the presence of diC8-PIP_2. The second possibility could be backed up by a recent study by Sun and MacKinnon (2020) where they showed that PIP_2 binding in the $K_v7.1_{EM}$-KCNE3-CaM structure brings about conformational changes in the pore loop and the ion conduction path that is involved in the opening and conduction of the channels (Sun & MacKinnon, 2020). Thus, it may be suggested that upon PIP_2 depletion via wortmannin, structural changes lead to the channel being non-conductive and the addition of a shorter-chain analog of PIP_2 (diC8-PIP_2) could not fully restore the channel back to its conductive state, thus reducing the SR-5-6 responses to G/G_{max}.

The next strategy used to investigate if PIP_2 played a role in mediating the effects of SR-5-6 was to mutate the cluster of basic residues which help bind PIP_2 in the S2-S3 linker, S4-S5 linker, and the C-terminus region of K_v7 channels (Loussouarn *et al.,* 2003; Park *et al.,* 2005; Hernandez *et al.,* 2008; Zaydman *et al.,* 2013; Choveau *et al.,* 2012, Cui J, 2016; Dvir *et al.,* 2014; Tobelaim *et al.,* 2017).

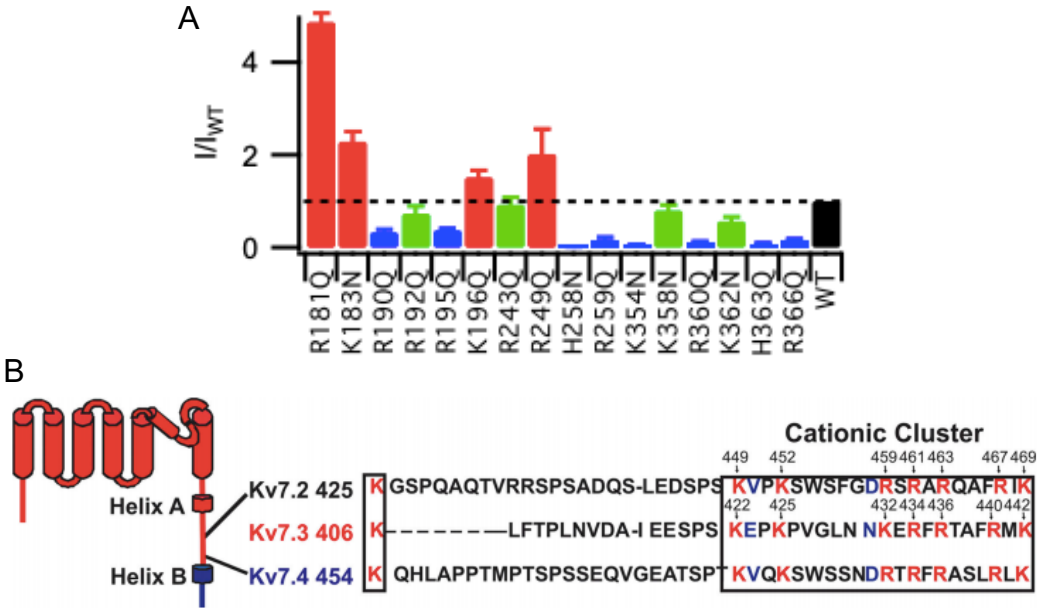

Figure 5.0A: PIP$_2$ binding mutations and residues in K$_v$7 channels. A) *Current amplitude at +20 mV normalized to WT (I/I$_{WT}$), Color code: blue, I/Iwt < 0.5; green, 0.5 < I/Iwt < 1; red, I/Iwt > 1.* ***B)*** *Alignment of the helix-A-B linker in K$_v$7.2-7.4 implicated in PIP$_2$ interactions in Hernandez et al., (2008) study (Adapted from Zaydman et al., 2013 and Hernandez et al., 2008).*

The first six PIP$_2$ binding mutations (Figure 5.13-5.18) came from the VSD-PD interface, which Zaydman *et al.,* (2013) identified as important PIP$_2$ binding sites. They identified sixteen basic residues at the VSD-PD interface that were highly conserved in K$_v$7 channels as key PIP$_2$ binding residues in K$_v$7.1 using site-directed mutagenesis and homology modelling. The R190Q, R195Q, H258N, R259Q, K354N, R360Q, H363Q, and R366Q mutants severely affected channel function and lowered current amplitude (blue bar graphs in Figure 5.0A$_A$). The S2-S3 linker, the S4-S5 linker, and the proximal terminus of the S6 helix all contained these residues. These residues are highly conserved among K$_v$7 channels (Figure 1.8A). Zaydman *et al.,* (2013) further demonstrated that these loss-of-current mutant channels retained VSD activation using voltage-clamp fluorometry. As a result, they determined that these mutations caused loss-of-current channels due to a decrease in coupling caused by PIP$_2$ unbinding that hindered pore-domain opening. No loss-of-current was seen in any of the mutant channels in K$_v$7.4 when the equivalent six residues were mutated (R166, R171, H234, S235, H334 and K337) and their response to SR-5-6 was evaluated (Figure 5.13-5.18). This was unexpected and the possible reasons for observing

currents in these equivalent mutations in $K_v7.4$ channels could be - i) may be more than one PIP_2 binding mutation was required to bring about the total loss of current in $K_v7.4$ channels, ii) the study by Zaydman *et al.,* (2013) was done on $K_v7.1$, but not on $K_v7.4$. Although sequence alignment showed conservation of the basic residues involved in PIP_2 binding across K_v7 channels, it is possible that the PIP_2 binding residues differ between $K_v7.1$ and $K_v7.4$ channels, and iii) with the exception of H234N, charge neutralizing mutations was performed in which the corresponding residues were altered to alanine, whereas Zaydman *et al.,* (2013) performed charge neutralizing mutations with glutamine. This could have played a role in defining the differences observed in $K_v7.1$ and $K_v7.4$ channels from a structural standpoint. Nonetheless, when these PIP_2 binding residues in $K_v7.4$ (shown in Figure 5.0) were mutated, it was observed that the effects of SR-5-6 were rarely reduced in the mutant channels, with the exception of a very modest decrease in G/G_{max} in R166A (S2-S3 linker) and H234N (S4-S5 linker; Figure 5.25B). In the S235A (S4-S5 linker) and K337A (C-terminus) mutant channels, however, a considerable increase in G/G_{max} and $G_{-100\ mV}$ was observed (Figure 5.25B & C).

Given that the proposed 'VSD-PD interface' PIP_2 mutations failed to abolish the effect of SR-5-6, next moved on to the proposed PIP_2 binding region in the C-terminus of K_v7 channels. Hernandez *et al.,* (2008) discovered a cluster of seven basic residues in the inter-helix region between helix A and helix B of the C-terminus in $K_v7.2$ using chimeric, docking, and mutational investigations as PIP_2 binding residues (Figure $5.0A_B$). Mutations in three of these seven residues, K452, R459, and R461 to negatively charged glutamate (E) in $K_v7.2$, led to a 50% reduction in open probability (P_o). Furthermore, the triple-charge reversal mutation KRR-EEE drastically lowered the channel's open probability (P_o) by 95%. Their study also discovered that charge neutralizing changes in these three residues had a significant impact on $K_v7.2$ channel open probability. However, when equivalent mutants in $K_v7.4$ were generated (K481, R488 and R490), any significant reduction in G/G_{max}, $\Delta V_{1/2}$ or $G_{-100\ mV}$ was not seen with any of these three mutant channels, suggesting that the PIP_2 binding residues in the inter helix region of the K_v7 channel's C-terminus aren't involved in the SR-5-6 effects in $K_v7.4$ channels.

K546N and R547A in $K_v7.4$'s helix B at the C-terminal end were next examined because the equivalent residues in $K_v7.1$, (K526 and K527) have been demonstrated to be important in PIP_2 and CaM binding and thus help to stabilize the $K_v7.1$ channel in the open state (Tobelaim *et al.,* 2017). When these residues in $K_v7.1$ were altered (K526N and K527N), the mutants had considerably lower PIP_2 binding than WT $K_v7.1$ (Tobelaim *et al.,* 2017). Tobelaim *et al.,* (2017) found that these mutant channels had a rightward shift in activation $V_{1/2}$ (30 ± 1 mV in K526N $K_v7.1$ mutant channels). When we mutated the corresponding residues in $K_v7.4$ (K546N and R547A) were mutated, a similar rightward shift in activation $V_{1/2}$ (Figure 5.22 & 5.23) was not observed when compared to the WT $K_v7.4$ channels (Figure 3.1C). A small drop in G/G_{max} and a small reduction in $G_{-100\ mV}$ was seen in K546N mutant channels when the effects of SR-5-6 were investigated (Figure 5.22 & 5.25). No abolishing effects of SR-5-6 response in R547A mutant channels was found (Figure 5.23 & 5.25).

Lastly, the K559A $K_v7.4$ mutant channel was generated since Park *et al.,* (2005) found that PIP_2 affinity was reduced in R555C mutant channels and that direct administration of PIP_2 recovered this mutant channel's loss of function. Park *et al.,* (2005) also demonstrated that the channel activity, in inside-out patch recordings, were likewise restored when a positive charge was reintroduced by application of methanethiosulfonate ethylammonium on the cytoplasmic face of the R555C mutant channel (Park *et al.,* 2005). It was possible to create a functioning channel by mutating the equivalent residue in $K_v7.4$ (K559A), but the effect of SR-5-6 on G/G_{max}, $\Delta V_{1/2}$, and $G_{-100\ mV}$ remained in this mutant (Figure 5.24 & 5.25). This supports the argument that, despite being conserved across the K_v7 family, known PIP_2 binding residues in $K_v7.1$ may not be involved in PIP_2 binding in $K_v7.4$ channels.

When the summary graphs were generated for the above mentioned mutations (Figure 5.25), it was observed that the SR-5-6 effects on $\Delta V_{1/2}$, G/G_{max}, and $G_{-100\ mV}$ were mostly enhanced in these mutants when compared to WT $K_v7.4$ channels. Only a modest reduction in G/G_{max} was seen in three mutant channels (R166A, H234N and K546N) but none of them completely abolished the effects of SR-5-6. None of the other mutant channels were able to diminish SR-5-6 effects in $K_v7.4$ channels. This suggested that SR-5-6 most likely does not mediate its effects through these known PIP_2 binding residues in $K_v7.4$.

In conclusion, the results from this chapter suggested that when PIP_2 was depleted with either VSP or wortmannin, the effect of SR-5-6 on G/G_{max} was either abolished or reduced significantly. Accordingly, intracellular diC8-PIP_2 enhanced the effects of SR-5-6 on $\Delta V_{1/2}$ and $G_{-100\ mV}$. Also, the known PIP_2 binding residues were not implicated in SR-5-6 mediated activation of $K_v7.4$ channels. Lastly, the loss of current PIP_2 binding mutations generating functional channels in $K_v7.4$ implicated that the PIP_2 binding residues may differ between $K_v7.1$ and $K_v7.4$ channels.

5.4 Future directions

Based on the results obtained in this and the previous chapters, it may be useful to carry out additional experimentation including:

1) Investigating PIP_2 depletion on L249A mutant channels, to test if this completely abolishes the effects of SR-5-6 on $\Delta V_{1/2}$ and G/G_{max} in $K_v7.4$ channels.

2) Using a fluorescent technique such as called FRET (Förster resonant energy transfer), to determine how effective PIP_2 depletion by VSP and wortmannin is.

3) Mutational and single channel studies to determine the precise binding residues for PIP_2 in $K_v7.4$ channels

4) Single-channel experiments investigating the effects of SR-5-6 on the open probability of K_v7 channel subtypes could give additional insights into the role of PIP_2 in SR-5-6 mediated K_v7 channel activation.

A. *K_V7.4 WT control*

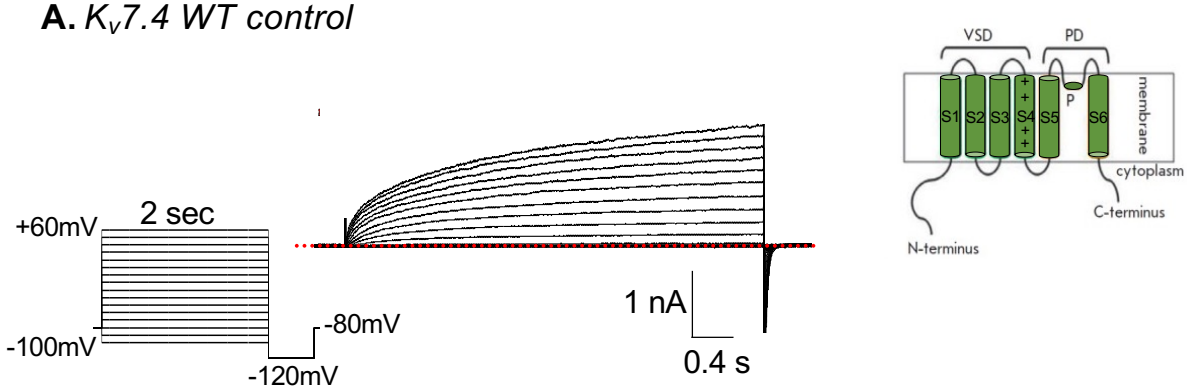

B. *SR-5-6 (10 μM) on K_V7.4 WT*

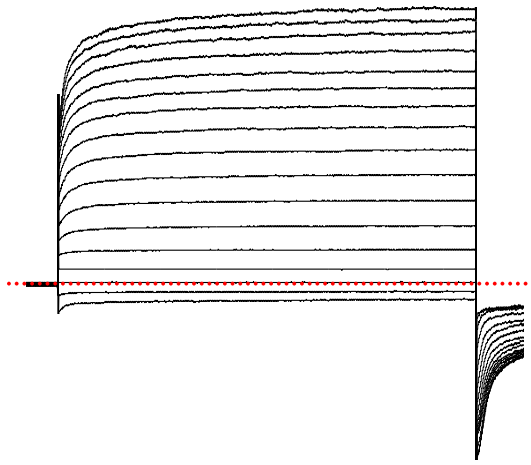

C. *Summary*

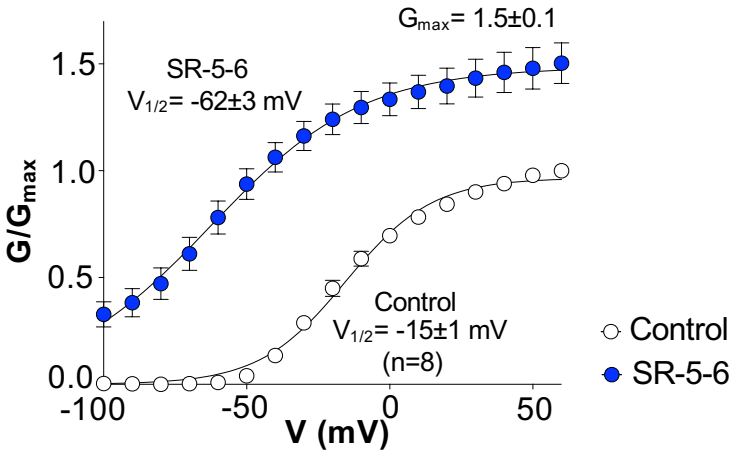

Figure 5.1: Effect of SR-5-6 on K_V7.4 WT channels; +60 mV, 2 sec protocol. **A**) A typical family of currents obtained from K_V7.4 WT channels expressed in HEK cells. Voltage clamp protocol as described in the inset. Dotted lines represent the zero current level. **B**) The effect of 10 μM SR-5-6 on currents from the same cell. **C**) Summary activation curves obtained by measuring tail currents in eight cells before (open circles) and during (blue circles) application of SR-5-6 (n=8). The curves were fit with the Boltzmann equation.

A. *K_v7.4 WT + VSP control*

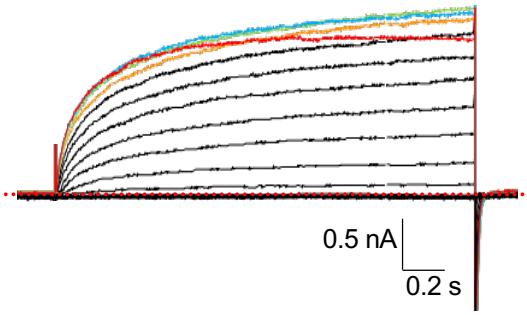

B. *SR-5-6 (10 μM) on K_v7.4 WT + VSP*

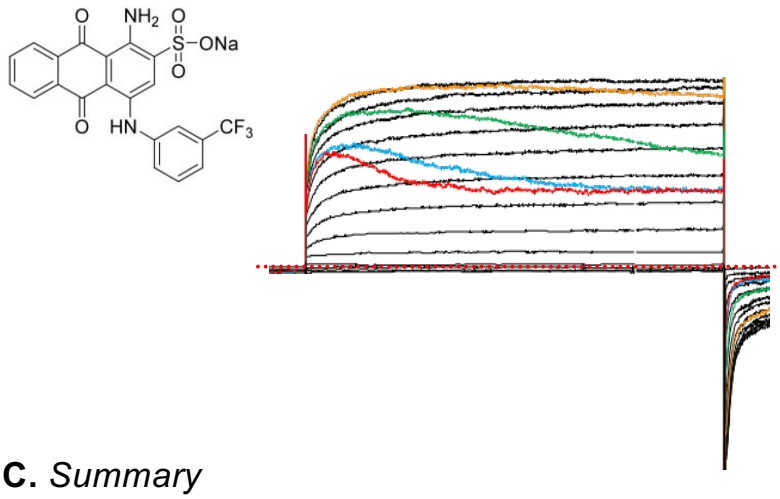

C. *Summary*

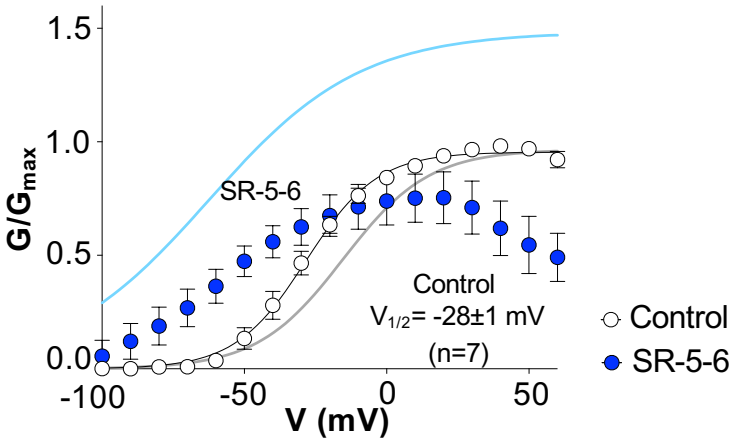

Figure 5.2: Effect of SR-5-6 on K_v7.4 WT + VSP channels; +60 mV, 2 sec protocol. A) A typical family of currents obtained from K_v7.4 WT + VSP channels expressed in HEK cells. Voltage clamp protocol as described in the Figure 5.1. Dotted lines represent the zero current level. **B**) The effect of 10 μM SR-5-6 on currents from the same cell. **C**) Summary activation curves obtained by measuring tail currents in seven cells before (open circles) and during (blue circles) application of SR-5-6 (n=7). The continuous grey and light blue lines in the background represent the activation curves of control and the effect of the SR-5-6 on WT K_v7.4 channels respectively. The curves were fit with the Boltzmann equation.

A. *Effect on G/G_{max} on $K_v7.4$ WT and $K_v7.4$ WT+VSP in SR-5-6*

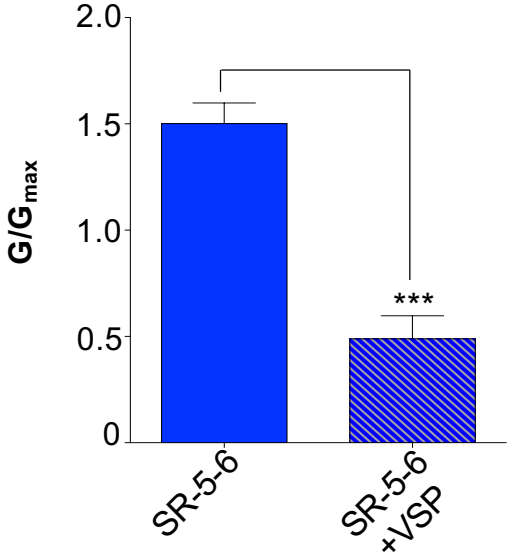

B. *Effect on $G_{-100\ mV}$ on $K_v7.4$ WT and $K_v7.4$ WT+VSP in SR-5-6*

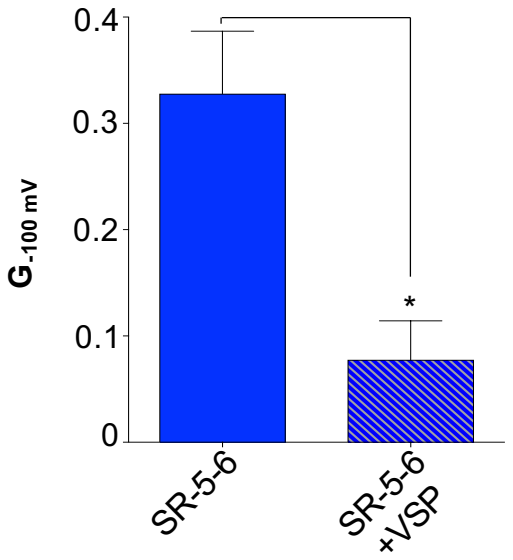

Figure 5.3: Effect of 10 μM SR-5-6 on G/G_{max} and $G_{-100\ mV}$ on $K_v7.4$ and $K_v7.4$+VSP using +60 mV, 2 sec protocol. A) The effects of SR-5-6 on maximal conductance (G/G_{max}) in $K_v7.4$ WT alone and when co-expressed with Ci-VSP. **B)** The effects on $G_{-100\ mV}$ in $K_v7.4$ WT and $K_v7.4$+VSP channels. A Mann-Whitney non-parametric test was used to compare SR-5-6+VSP group with SR-5-6. *p<0.05, **p<0.01, ***p<0.001, ****p<0.0001.

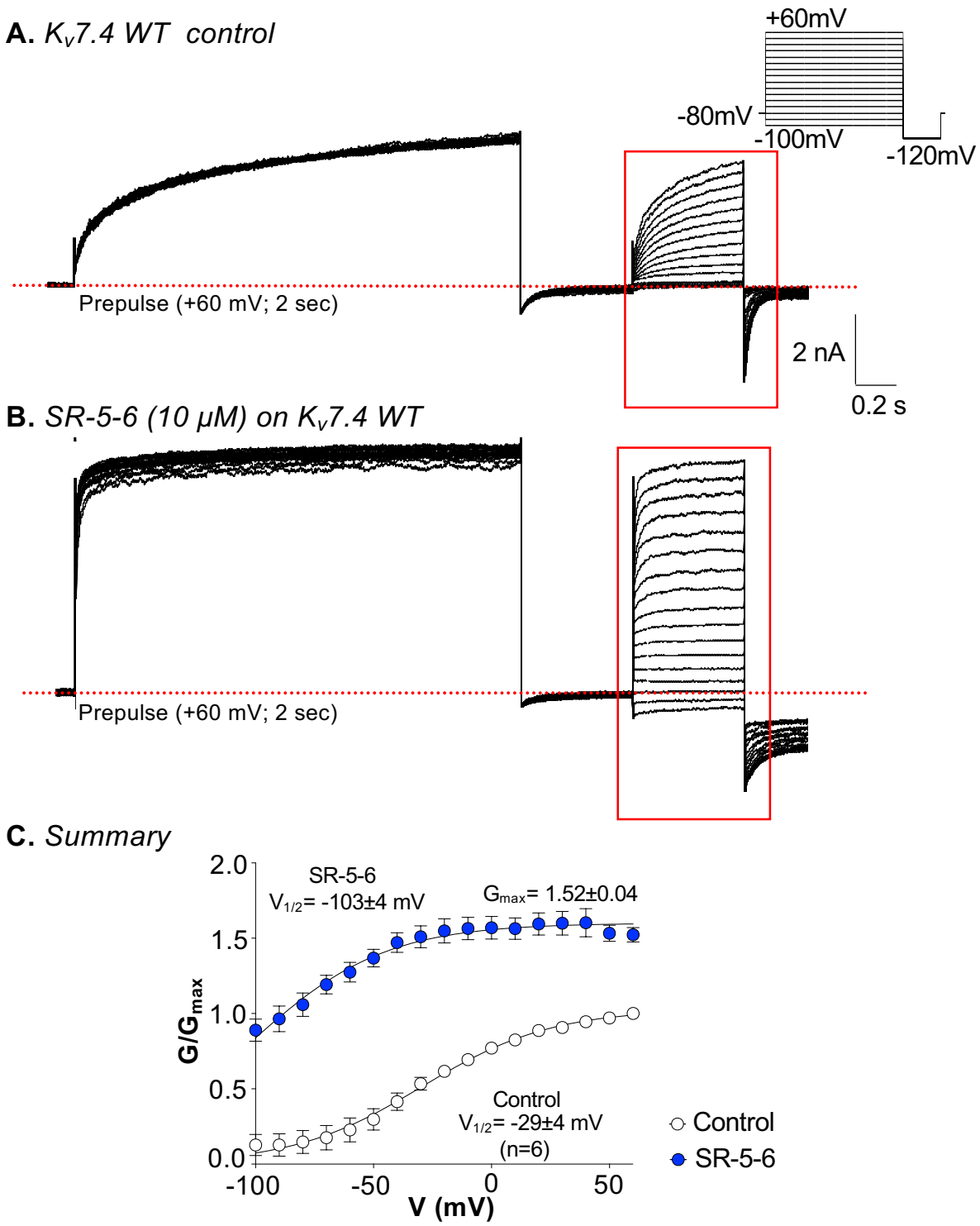

Figure 5.4: Effect of SR-5-6 on K_v7.4 WT channels; prepulse, +60 mV, 2 sec protocol. A) A typical family of currents obtained from K_v7.4 WT + VSP channels expressed in HEK cells. Voltage clamp protocol as described in the inset. Dotted lines represent the zero current level. **B**) The effect of 10 μM SR-5-6 on currents from the same cell. **C**) Summary activation curves obtained by measuring tail currents in six cells before (open circles) and during (blue circles) application of SR-5-6 (n=6). The curves were fit with the Boltzmann equation.

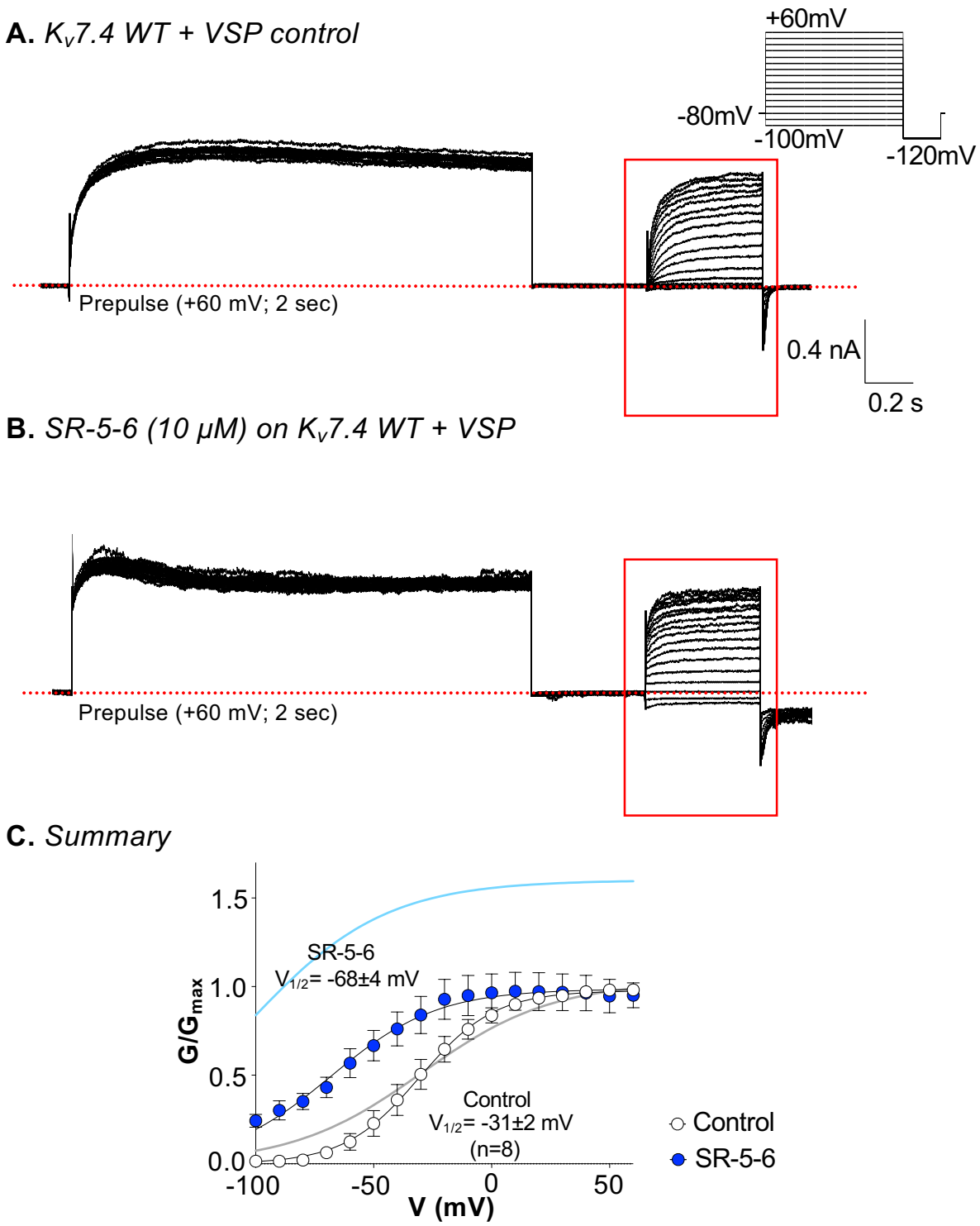

Figure 5.5: Effect of SR-5-6 on K_v7.4 WT + VSP channels; prepulse, +60 mV, 2 sec protocol. A) A typical family of currents obtained from K_v7.4 WT + VSP channels expressed in HEK cells. Voltage clamp protocol as described in the inset. Dotted lines represent the zero current level. **B**) The effect of 10 μM SR-5-6 on currents from the same cell. **C**) Summary activation curves obtained by measuring tail currents in eight cells before (open circles) and during (blue circles) application of SR-5-6 (n=8). The continuous grey and light blue lines in the background represent the activation curves of control and the effect of the SR-5-6 on WT K_v7.4 channels respectively. The curves were fit with the Boltzmann equation.

A. *Effect on $\Delta V_{1/2}$ on $K_v7.4$ WT and $K_v7.4$ WT+VSP in SR-5-6*

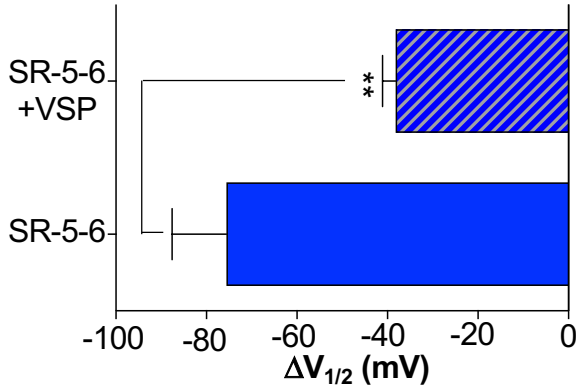

B. *Effect on G/G_{max} on $K_v7.4$ WT and $K_v7.4$ WT+VSP in SR-5-6*

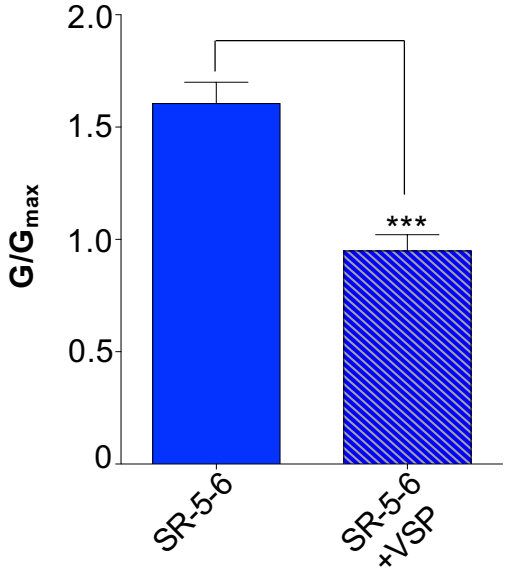

C. *Effect on $G_{-100\ mV}$ on $K_v7.4$ WT and $K_v7.4$ WT+VSP in SR-5-6*

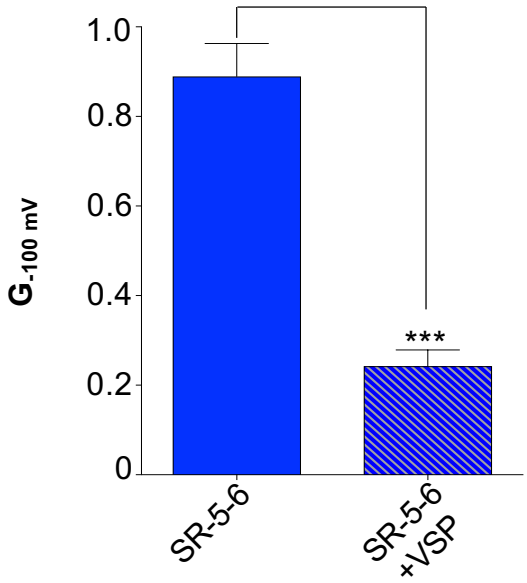

Figure 5.6: Effects of SR-5-6 on $\Delta V_{1/2}$, G/G_{max} and $G_{-100\ mV}$ on $K_v7.4$ and $K_v7.4$+VSP for the prepulse +60 mV, 2 sec protocol. A) Drug mediated negative shift of the activation curve ($\Delta V_{1/2}$). An unpaired t-test was used to compare SR-5-6+VSP with SR-5-6. **B)** The effects on maximal conductance (G/G_{max}). **C)** The effects on $G_{-100\ mV}$. A Mann-Whitney non-parametric test used to compare SR-5-6+VSP group with SR-5-6, no VSP group. *p<0.05, **p<0.01, ***p<0.001, ****p<0.0001.

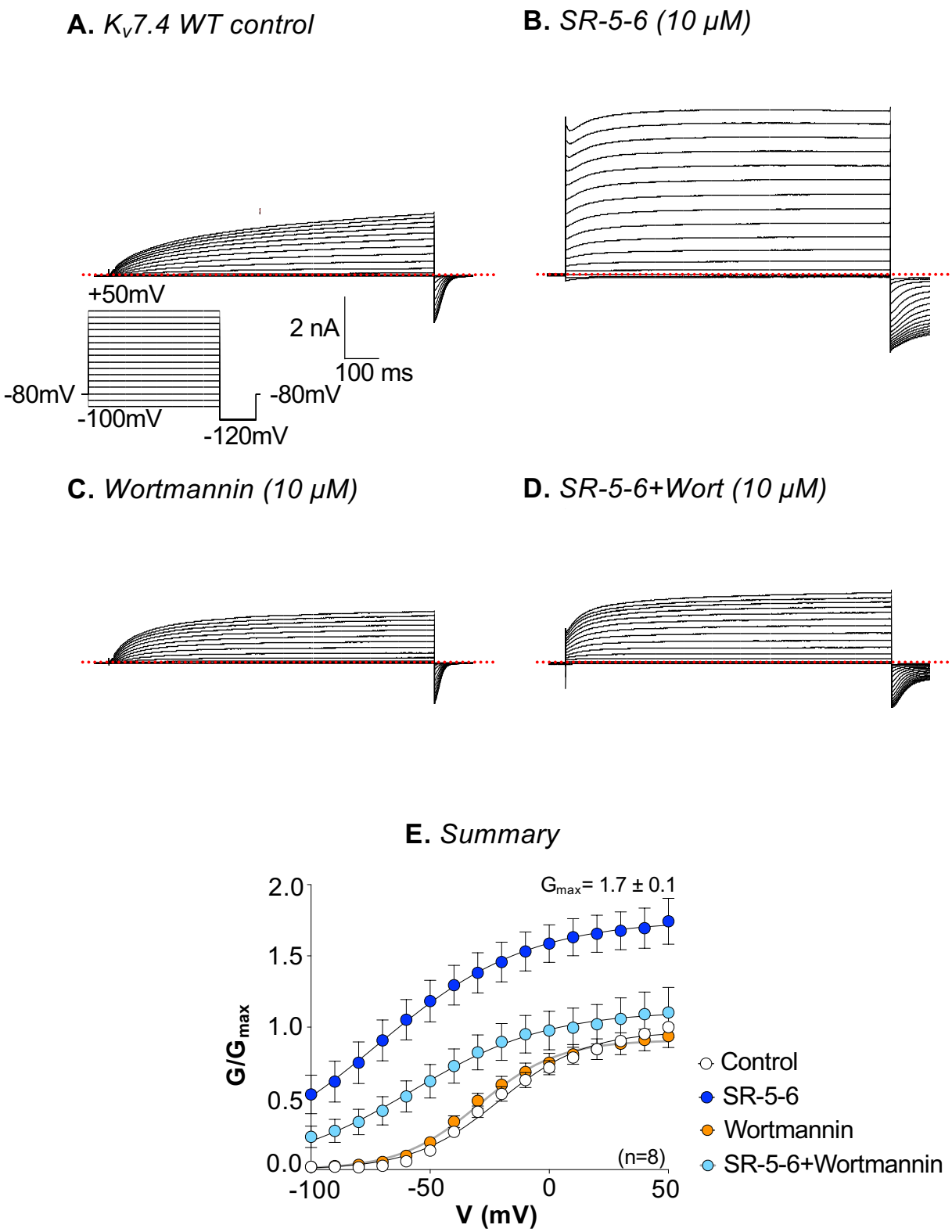

Figure 5.7: Effect of wortmannin, SR-5-6 on K_v7.4 WT channels. A) A typical family of currents obtained from K_v7.4 WT channels expressed in HEK cells. Voltage clamp protocol is described in the inset. Dotted lines represent the zero current level. **B**) The effect of 10 μM SR-5-6 on currents from the same cell. **C**) The effect of 10 μM wortmannin on currents on same cell. **D)** The effect of 10 μM wortmannin+SR-5-6 on currents from the same cell. **E)** Summary activation curves obtained by measuring tail currents in eight cells before (open circles) and during application of SR-5-6 (dark blue circles), wortmannin (orange circles) and wortmannin+SR-5-6 (light blue circles) (n=8). The curves were fit with the Boltzmann equation.

A. *Effect on $\Delta V_{1/2}$ on $K_v7.4$ WT in SR-5-6 and SR-5-6+Wortmannin*

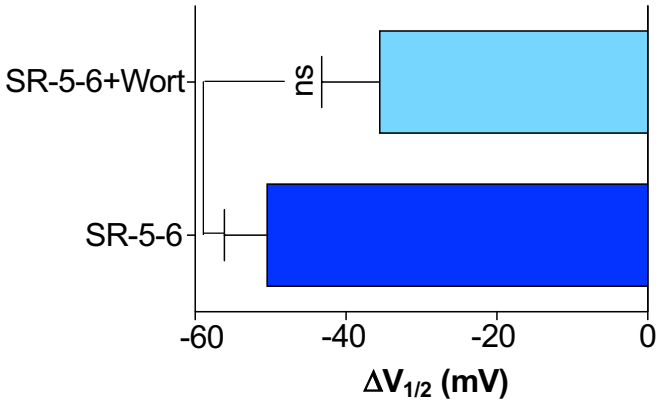

B. *Effect on G/G_{max} on $K_v7.4$ WT in SR-5-6 and SR-5-6+Wortmannin*

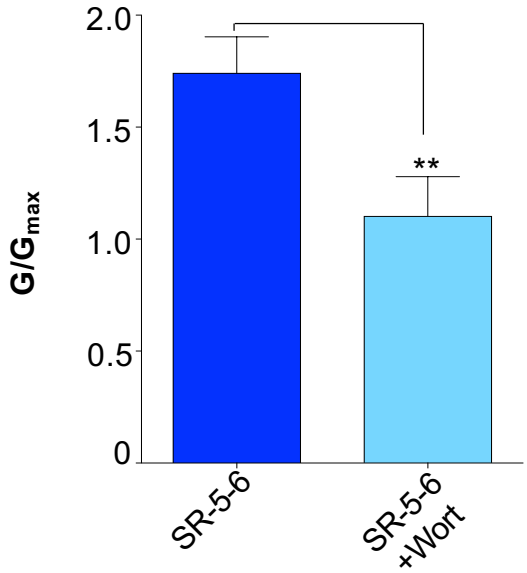

C. *Effect on $G_{-100\ mV}$ on $K_v7.4$ WT in SR-5-6 and SR-5-6+Wortmannin*

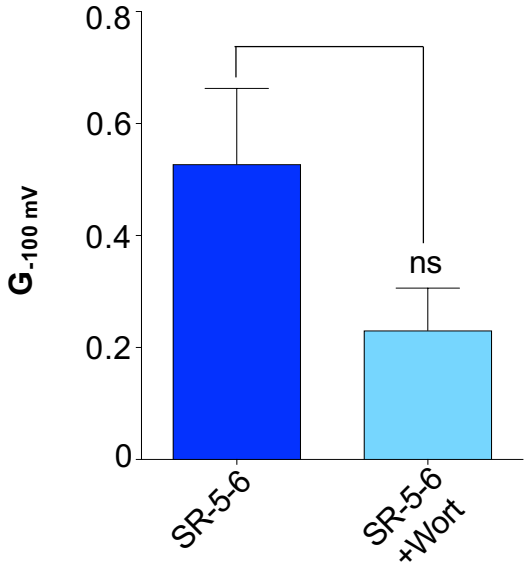

Figure 5.8: Summary graphs of effects on $\Delta V_{1/2}$, G/G_{max} and $G_{-100\ mV}$ on $K_v7.4$ WT in presence of SR-5-6, wortmannin and SR-5-6+wortmannin (n=8). A) Drug mediated negative shift of the activation curve ($\Delta V_{1/2}$). **B)** The effects on G/G_{max}. **C)** The effects on $G_{-100\ mV}$. A one-way ANOVA for $\Delta V_{1/2}$ and a Mann-Whitney non-parametric test for G/G_{max} and $G_{-100\ mV}$ was used to compare SR-5-6+Wort group with SR-5-6. *p<0.05, **p<0.01, ***p<0.001, ****p<0.0001.

A. *K_v7.4 WT control; 200 µM diC8-PIP$_2$*

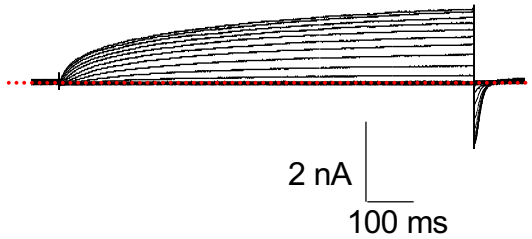

B. *SR-5-6 (10 µM); 200 µM diC8-PIP$_2$*

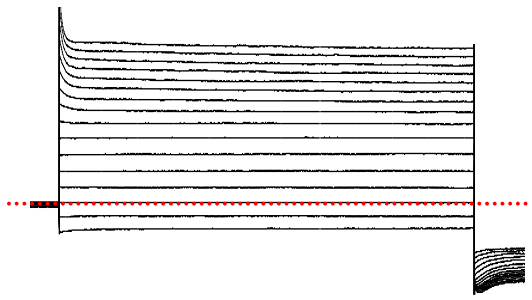

C. *Summary*

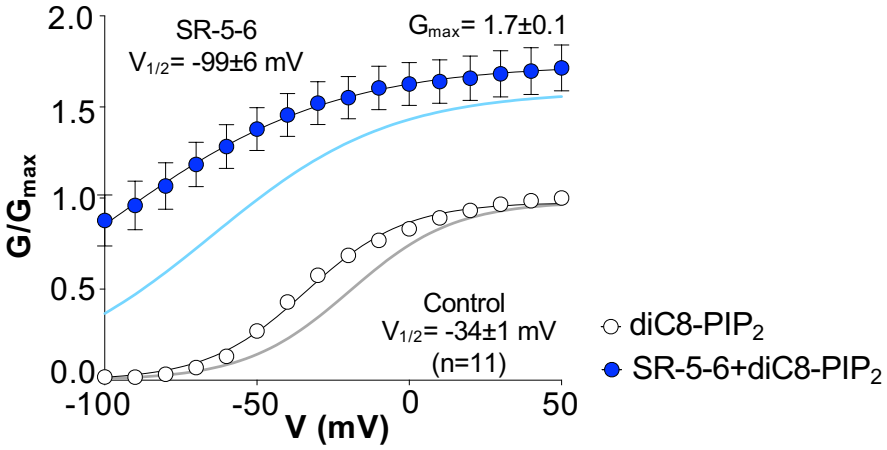

Figure 5.9: Effect of SR-5-6 on K_v7.4WT, 200 µM diC8-PIP$_2$. A) A typical family of currents obtained from wildtype K_v7.4 channels expressed in HEK cells in presence of 200 µM diC8-PIP$_2$. Voltage clamp protocol as described in Figure 5.7. Dotted lines represent the zero current level. **B**) The effect of 10 µM SR-5-6 on currents from the same cell. **C**) Summary activation curves obtained by measuring tail currents in eleven cells before (open circles) and during (blue circles) application of SR-5-6 (n=11). The continuous grey and light blue lines in the background represent the activation curves of control and the effect of the SR-5-6 on WT K_v7.4 channels respectively. The curves were fit with the Boltzmann equation.

A. *Effect on $\Delta V_{1/2}$ on $K_v7.4$ WT in SR-5-6 and SR-5-6+diC8-PIP$_2$*

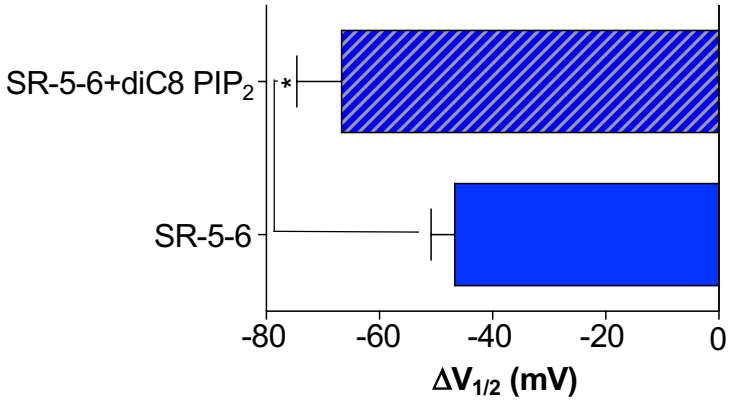

B. *Effect on G/G_{max} on $K_v7.4$ WT in SR-5-6 and SR-5-6+diC8-PIP$_2$*

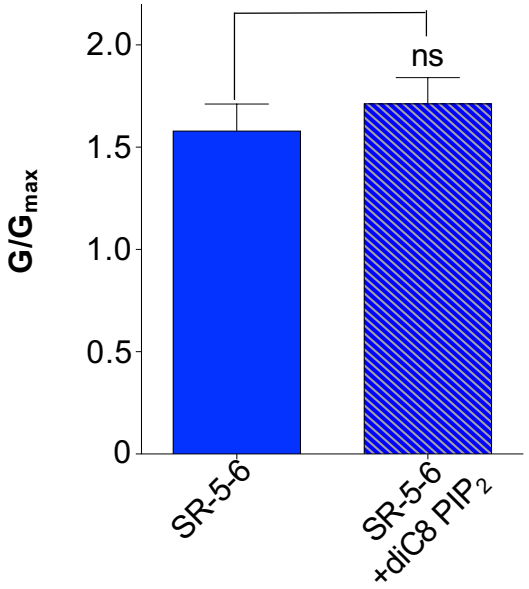

C. *Effect on $G_{-100\ mV}$ on $K_v7.4$ WT in SR-5-6 and SR-5-6+diC8-PIP$_2$*

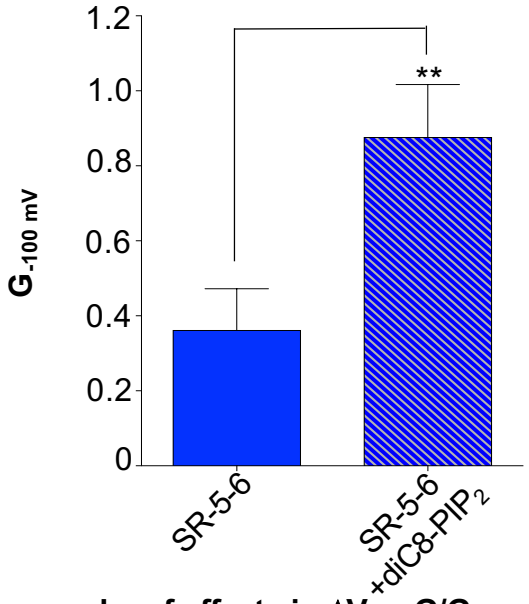

Figure 5.10: Summary graphs of effects in $\Delta V_{1/2}$, G/G_{max} and $G_{-100\ mV}$ on $K_v7.4$ and $K_v7.4$+diC8-PIP$_2$ (n=11). A) Drug mediated negative shift of the activation curve ($\Delta V_{1/2}$). **B)** The effects on maximal conductance (G/G_{max}). **C)** The effects on $G_{-100\ mV}$. An unpaired t-test for $\Delta V_{1/2}$ and a Mann-Whitney non-parametric test for G/G_{max} and $G_{-100\ mV}$ was used to compare SR-5-6+diC8-PIP$_2$ group with SR-5-6. *p<0.05, **p<0.01, ***p<0.001, ****p<0.0001.

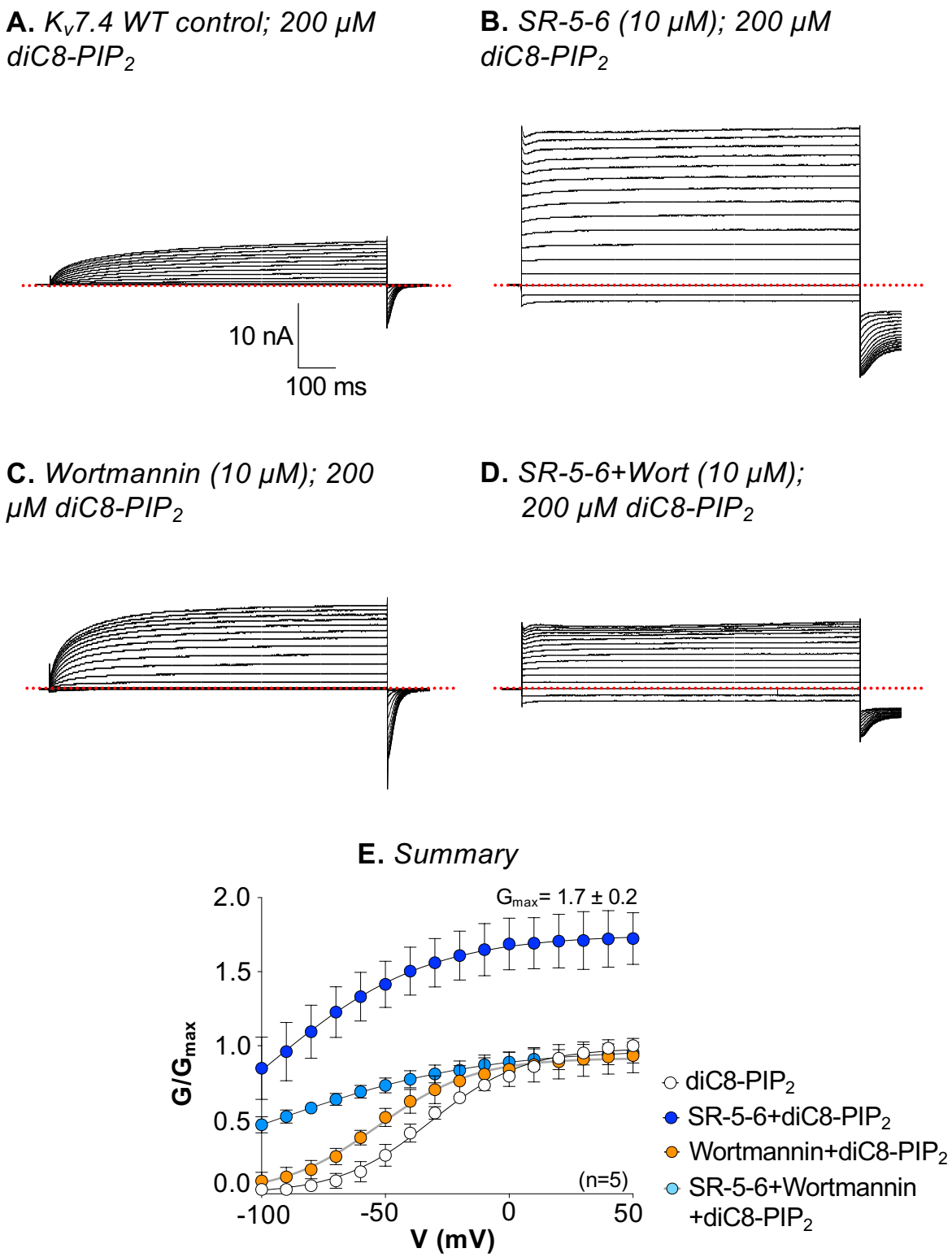

Figure 5.11: Effect of Wortmannin, SR-5-6 on K_v7.4 WT channels; 200 μM diC8-PIP$_2$. A) A typical family of currents obtained from K_v7.4 WT channels expressed in HEK cells in presence of 200 μM diC8-PIP$_2$. Voltage clamp protocol as described in Figure 5.7. Dotted lines represent the zero current level. **B**) The effect of 10 μM SR-5-6 on currents from the same cell. **C**) The effect of 10 μM wortmannin on currents on same cell. **D)** The effect of 10 μM wortmannin+SR-5-6 on currents from the same cell. **E)** Summary activation curves obtained by measuring tail currents in five cells before (open circles) and during application of SR-5-6 (dark blue circles), wortmannin (orange circles) and wortmannin+SR-5-6 (light blue circles) (n=5). The curves were fit with the Boltzmann equation.

A. *Effect on $\Delta V_{1/2}$ on $K_v7.4$ WT in SR-5-6 and SR-5-6+Wort*

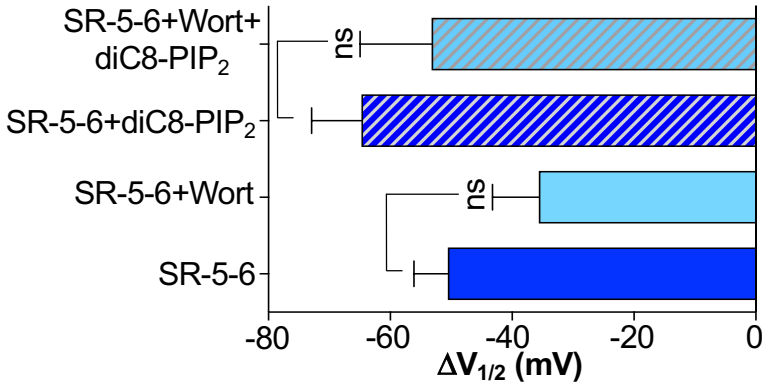

B. *Effect on G/G_{max} on $K_v7.4$ WT in SR-5-6 and SR-5-6+Wort*

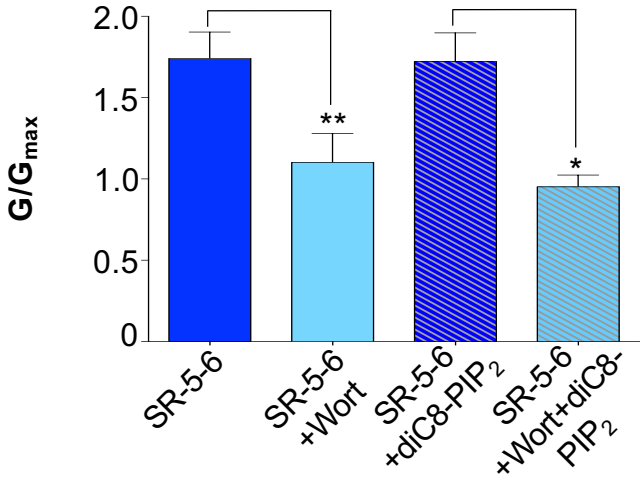

C. *Effect on $G_{-100\ mV}$ on $K_v7.4$ WT in SR-5-6 and SR-5-6+Wort*

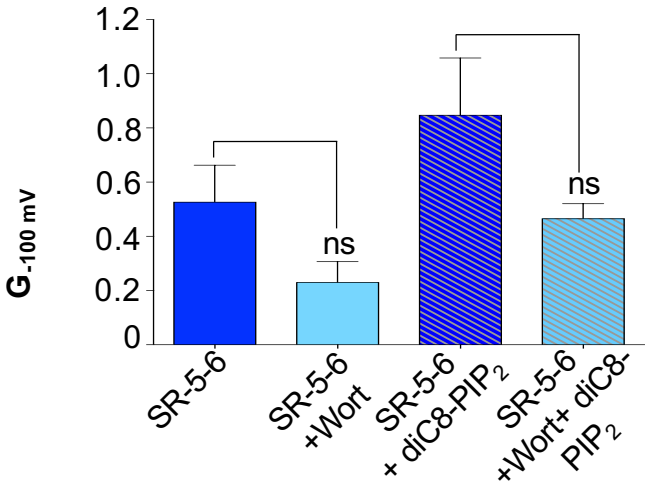

Figure 5.12: Summary graphs of effects on $\Delta V_{1/2}$, G/G_{max} and $G_{-100\ mV}$ on $K_v7.4$WT in SR-5-6, wortmannin and SR-5-6+wortmannin; in presence and absence of 200 µM diC8-PIP_2 (n=5). A) Drug mediated negative shift of the activation curve ($\Delta V_{1/2}$). **B)** The effects on maximal conductance (G/G_{max}). **C)** The effects on $G_{-100\ mV}$. A one-way ANOVA for $\Delta V_{1/2}$ and a Mann-Whitney non-parametric test for G/G_{max} and $G_{-100\ mV}$ was used to compare SR-5-6+Wort group with SR-5-6 in presence and absence of diC8-PIP_2. *p<0.05, **p<0.01, ***p<0.001, ****p<0.0001.

A. *R166A mutant control*

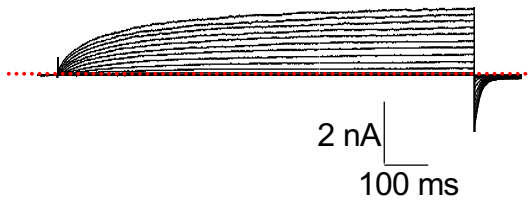

B. *SR-5-6 (10 μM) on R166A mutant*

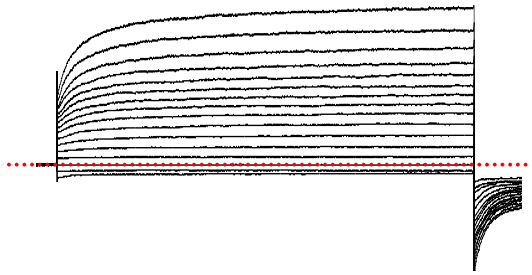

C. *Summary*

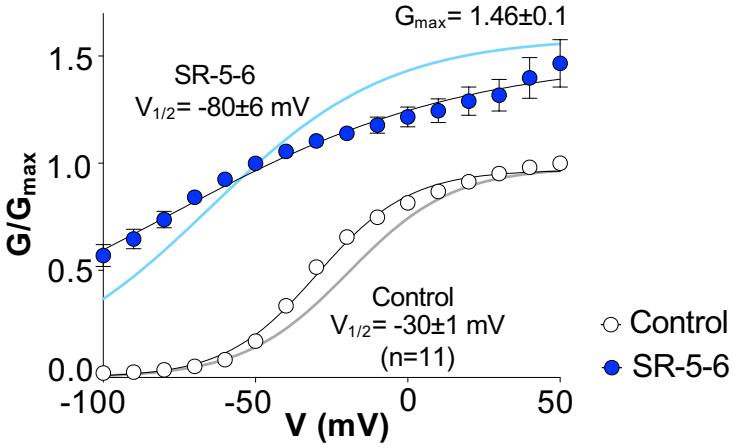

Figure 5.13: Effect of SR-5-6 on R166A mutation of K_v7.4 channels. A) A typical family of currents obtained from R166A mutation of K_v7.4 channels expressed in HEK cells. Voltage clamp protocol as described in Figure 5.7. Dotted lines represent the zero current level. **B**) The effect of 10 μM SR-5-6 on currents from the same cell. **C**) Summary activation curves obtained by measuring tail currents in eleven cells before (open circles) and during (blue circles) application of SR-5-6 (n=11). The continuous grey and light blue lines in the background represent the activation curves of control and the effect of the SR-5-6 on WT K_v7.4 channels respectively. The curves were fit with the Boltzmann equation.

A. *R171A mutant control*

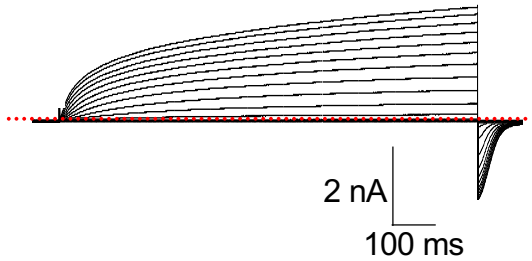

B. *SR-5-6 (10 μM) on R171A mutant*

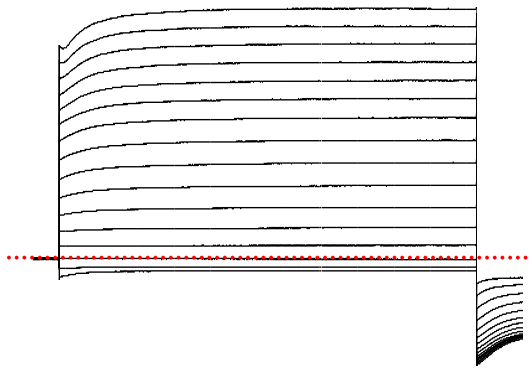

C. *Summary*

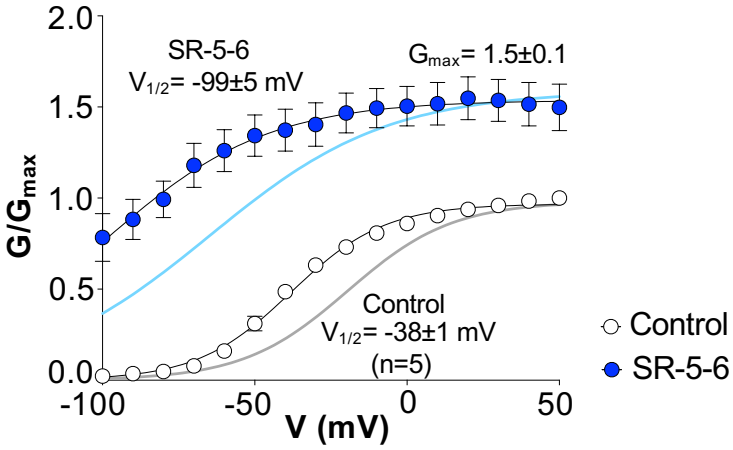

Figure 5.14: Effect of SR-5-6 on R171A mutation of K_v7.4 channels. A) A typical family of currents obtained from R171A mutation of K_v7.4 channels expressed in HEK cells. Voltage clamp protocol as described in Figure 5.7. Dotted lines represent the zero current level. **B**) The effect of 10 μM SR-5-6 on currents from the same cell. **C**) Summary activation curves obtained by measuring tail currents in five cells before (open circles) and during (blue circles) application of SR-5-6 (n=5). The continuous grey and light blue lines in the background represent the activation curves of control and the effect of the SR-5-6 on WT K_v7.4 channels respectively. The curves were fit with the Boltzmann equation.

A. *H234N mutant control*

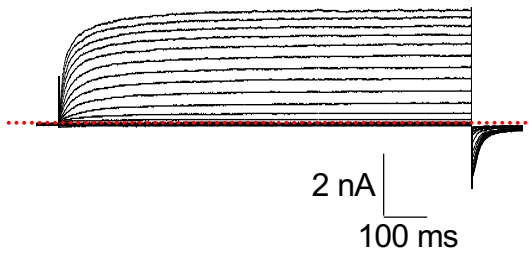

B. *SR-5-6 (10 μM) on H234N mutant*

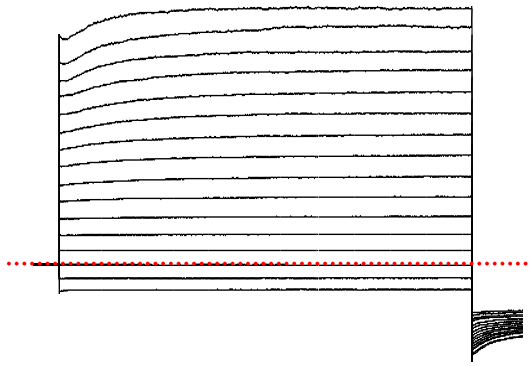

C. *Summary*

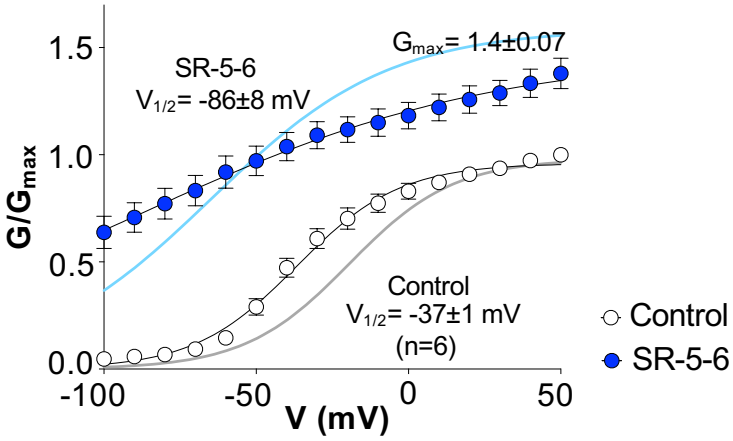

Figure 5.15: Effect of SR-5-6 on H234N mutation of K_v7.4 channels. A) A typical family of currents obtained from H234N mutation of K_v7.4 channels expressed in HEK cells. Voltage clamp protocol as described in Figure 5.7. Dotted lines represent the zero current level. **B**) The effect of 10 μM SR-5-6 on currents from the same cell. **C**) Summary activation curves obtained by measuring tail currents in six cells before (open circles) and during (blue circles) application of SR-5-6 (n=6). The continuous grey and light blue lines in the background represent the activation curves of control and the effect of the SR-5-6 on WT K_v7.4 channels respectively. The curves were fit with the Boltzmann equation.

A. *S235A mutant control*

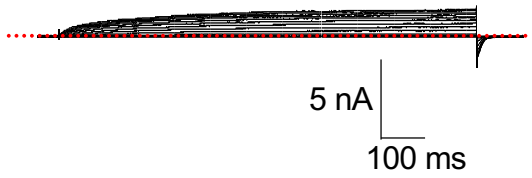

B. *SR-5-6 (10 μM) on S235A mutant*

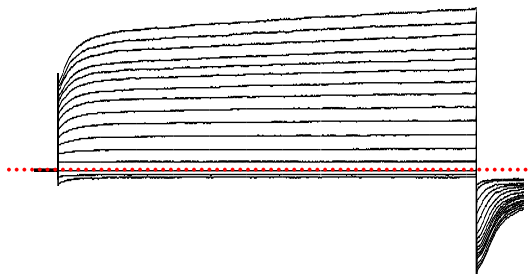

C. *Summary*

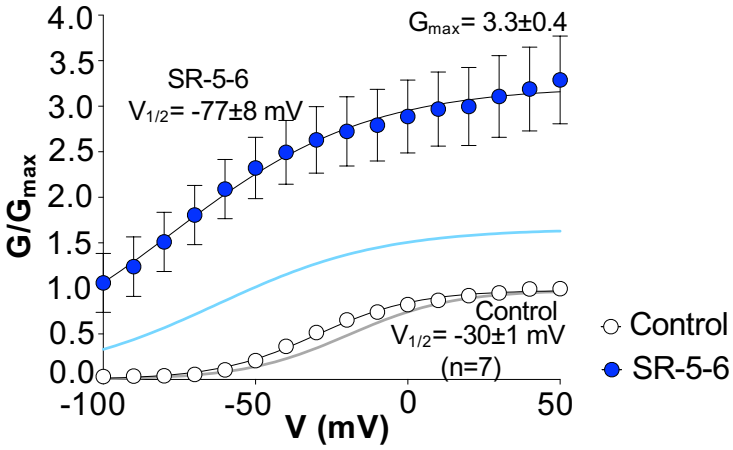

Figure 5.16: Effect of SR-5-6 on S235A mutation of K_v7.4 channels. A) A typical family of currents obtained from S235A mutation of K_v7.4 channels expressed in HEK cells. Voltage clamp protocol as described in Figure 5.7. Dotted lines represent the zero current level. **B**) The effect of 10 μM SR-5-6 on currents from the same cell. **C**) Summary activation curves obtained by measuring tail currents in seven cells before (open circles) and during (blue circles) application of SR-5-6 (n=7). The continuous grey and light blue lines in the background represent the activation curves of control and the effect of the SR-5-6 on WT K_v7.4 channels respectively. The curves were fit with the Boltzmann equation.

A. *H334A mutant control*

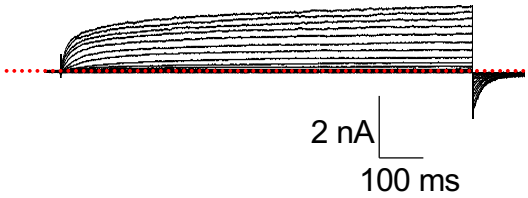

B. *SR-5-6 (10 μM) on H334A mutant*

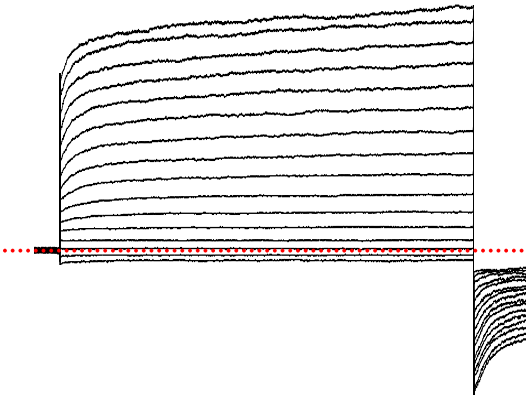

C. *Summary*

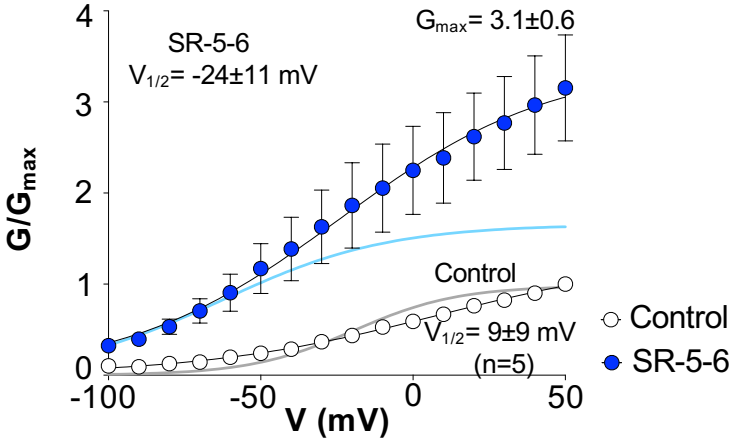

Figure 5.17: Effect of SR-5-6 on H334A mutation of K_v7.4 channels. A) A typical family of currents obtained from H334A mutation of K_v7.4 channels expressed in HEK cells. Voltage clamp protocol as described in Figure 5.7. Dotted lines represent the zero current level. **B**) The effect of 10 μM SR-5-6 on currents from the same cell. **C**) Summary activation curves obtained by measuring tail currents in five cells before (open circles) and during (blue circles) application of SR-5-6 (n=5). The continuous grey and light blue lines in the background represent the activation curves of control and the effect of the SR-5-6 on WT K_v7.4 channels respectively. The curves were fit with the Boltzmann equation.

A. *K337A mutant control*

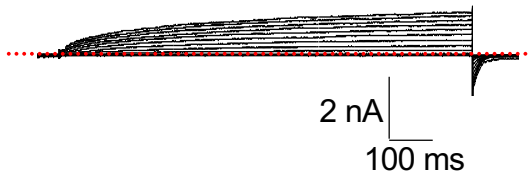

B. *SR-5-6 (10 μM) on K337A mutant*

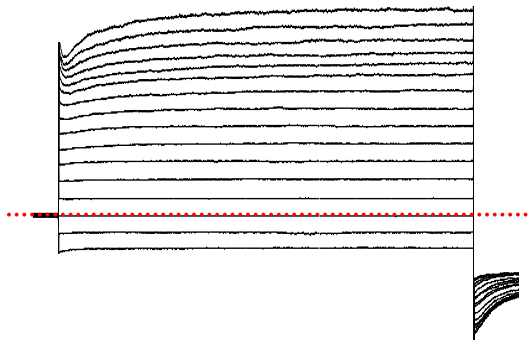

C. *Summary*

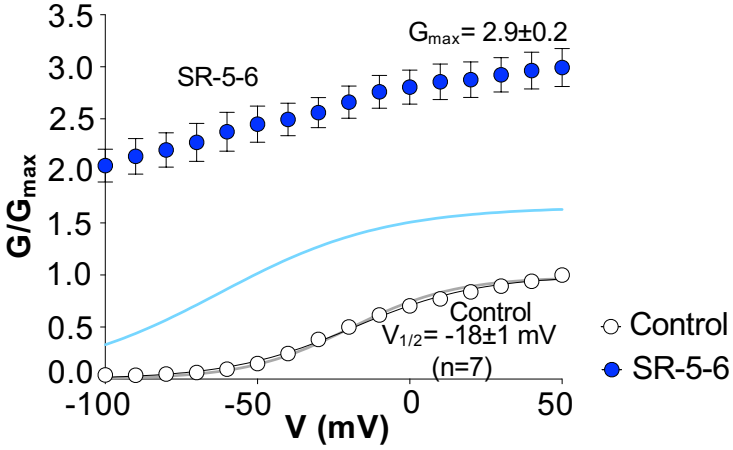

Figure 5.18: Effect of SR-5-6 on K337A mutation of K_v7.4 channels. A) A typical family of currents obtained from K337A mutation of K_v7.4 channels expressed in HEK cells. Voltage clamp protocol as described in Figure 5.7. Dotted lines represent the zero current level. **B**) The effect of 10 μM SR-5-6 on currents from the same cell. **C**) Summary activation curves obtained by measuring tail currents in seven cells before (open circles) and during (blue circles) application of SR-5-6 (n=7). The continuous grey and light blue lines in the background represent the activation curves of control and the effect of the SR-5-6 on WT K_v7.4 channels respectively. The curves were fit with the Boltzmann equation.

A. *K481A mutant control*

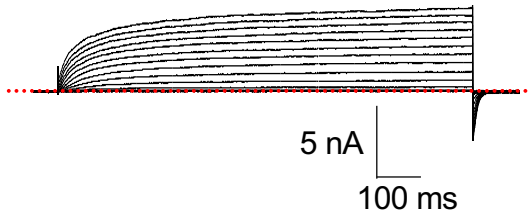

B. *SR-5-6 (10 μM) on K481A mutant*

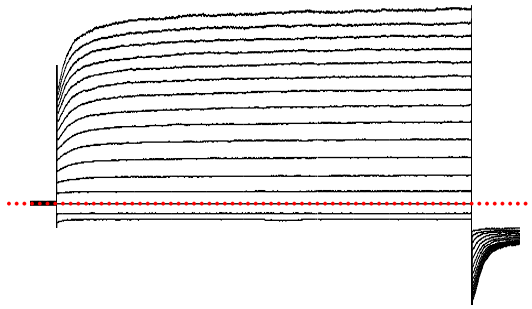

C. *Summary*

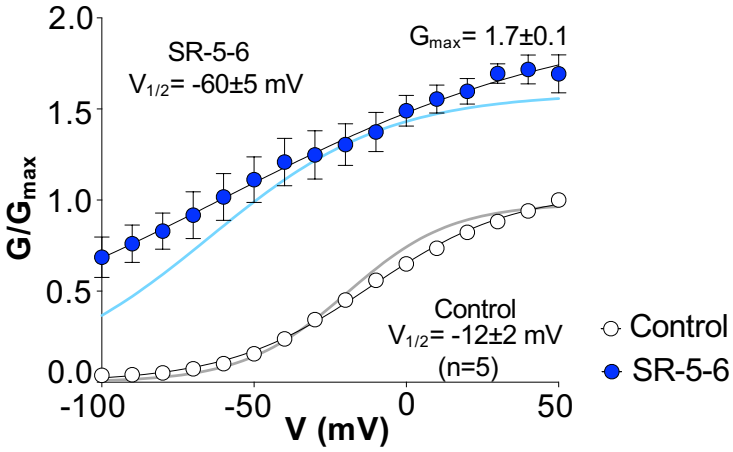

Figure 5.19: Effect of SR-5-6 on K481A mutation of K_v7.4 channels. A) A typical family of currents obtained from K481A mutation of K_v7.4 channels expressed in HEK cells. Voltage clamp protocol as described in Figure 5.7. Dotted lines represent the zero current level. **B**) The effect of 10 μM SR-5-6 on currents from the same cell. **C**) Summary activation curves obtained by measuring tail currents in five cells before (open circles) and during (blue circles) application of SR-5-6 (n=5). The continuous grey and light blue lines in the background represent the activation curves of control and the effect of the SR-5-6 on WT K_v7.4 channels respectively. The curves were fit with the Boltzmann equation.

A. *R488A mutant control*

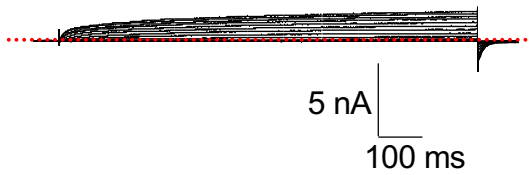

B. *SR-5-6 (10 μM) on R488A mutant*

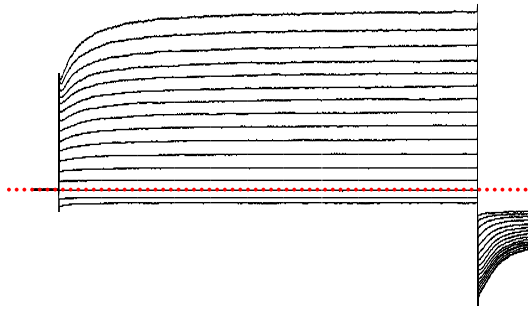

C. *Summary*

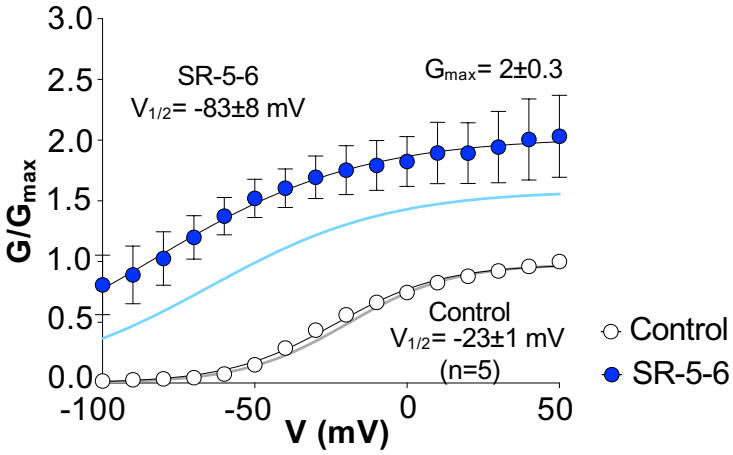

Figure 5.20: Effect of SR-5-6 on R488A mutation of K_v7.4 channels. A) A typical family of currents obtained from R488A mutation of K_v7.4 channels expressed in HEK cells. Voltage clamp protocol as described in Figure 5.7. Dotted lines represent the zero current level. **B**) The effect of 10 μM SR-5-6 on currents from the same cell. **C**) Summary activation curves obtained by measuring tail currents in five cells before (open circles) and during (blue circles) application of SR-5-6 (n=5). The continuous grey and light blue lines in the background represent the activation curves of control and the effect of the SR-5-6 on WT K_v7.4 channels respectively. The curves were fit with the Boltzmann equation.

A. *R490A mutant control*

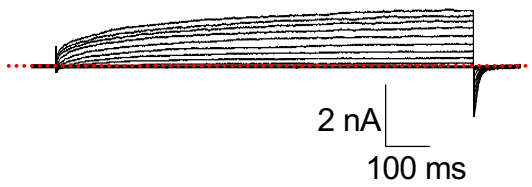

B. *SR-5-6 (10 μM) on R490A mutant*

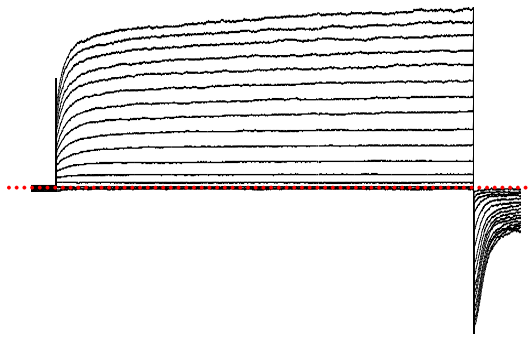

C. *Summary*

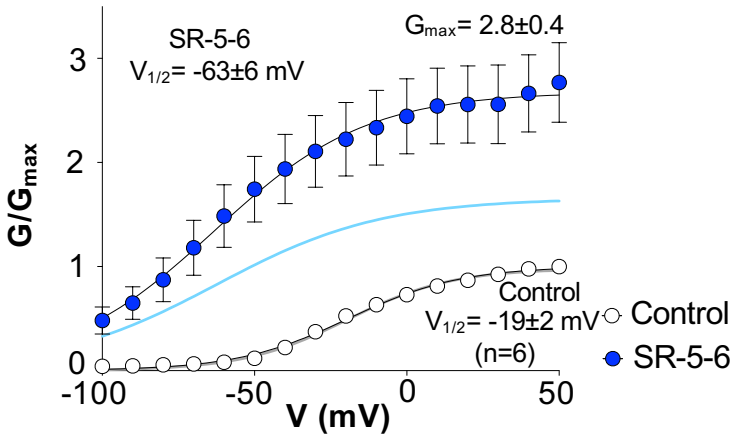

Figure 5.21: Effect of SR-5-6 on R490A mutation of K_v7.4 channels. A) A typical family of currents obtained from R490A mutation of K_v7.4 channels expressed in HEK cells. Voltage clamp protocol as described in Figure 5.7. Dotted lines represent the zero current level. **B**) The effect of 10 μM SR-5-6 on currents from the same cell. **C**) Summary activation curves obtained by measuring tail currents in six cells before (open circles) and during (blue circles) application of SR-5-6 (n=6). The continuous grey and light blue lines in the background represent the activation curves of control and the effect of the SR-5-6 on WT K_v7.4 channels respectively. The curves were fit with the Boltzmann equation.

A. *K546N mutant control*

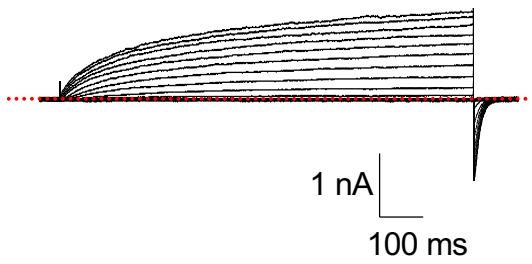

B. *SR-5-6 (10 μM) on K546N mutant*

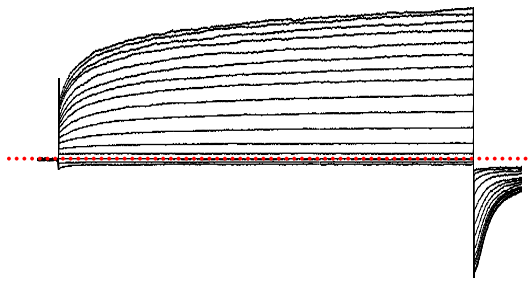

C. *Summary*

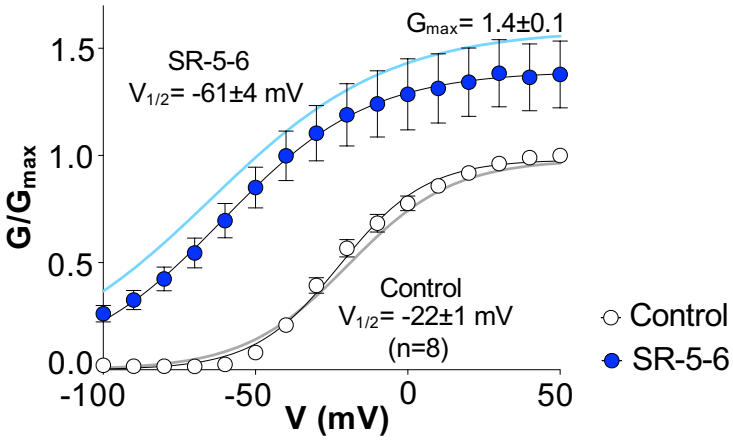

Figure 5.22: Effect of SR-5-6 on K546N mutation of K_v7.4 channels. A) A typical family of currents obtained from K546N mutation of K_v7.4 channels expressed in HEK cells. Voltage clamp protocol as described in Figure 5.7. Dotted lines represent the zero current level. **B**) The effect of 10 μM SR-5-6 on currents from the same cell. **C**) Summary activation curves obtained by measuring tail currents in eight cells before (open circles) and during (blue circles) application of SR-5-6 (n=8). The continuous grey and light blue lines in the background represent the activation curves of control and the effect of the SR-5-6 on WT K_v7.4 channels respectively. The curves were fit with the Boltzmann equation.

A. *R547A mutant control*

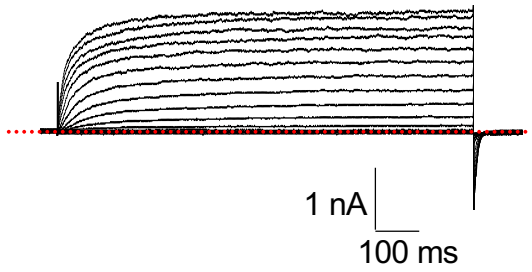

B. *SR-5-6 (10 μM) on R547A mutant*

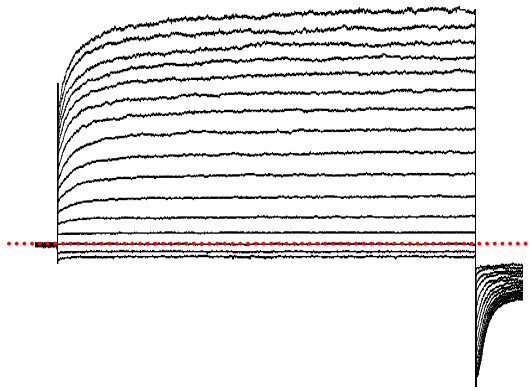

C. *Summary*

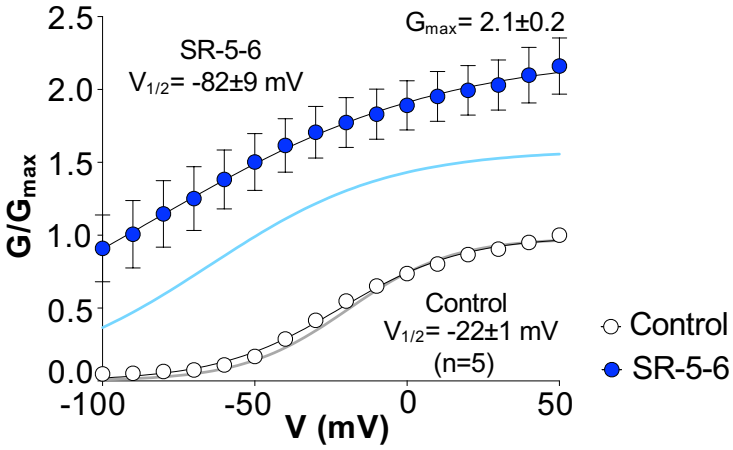

Figure 5.23: Effect of SR-5-6 on R547A mutation of K_v7.4 channels. A) A typical family of currents obtained from R547A mutation of K_v7.4 channels expressed in HEK cells. Voltage clamp protocol as described in Figure 5.7. Dotted lines represent the zero current level. **B**) The effect of 10 μM SR-5-6 on currents from the same cell. **C**) Summary activation curves obtained by measuring tail currents in five cells before (open circles) and during (blue circles) application of SR-5-6 (n=5). The continuous grey and light blue lines in the background represent the activation curves of control and the effect of the SR-5-6 on WT K_v7.4 channels respectively. The curves were fit with the Boltzmann equation.

A. *K559A mutant control*

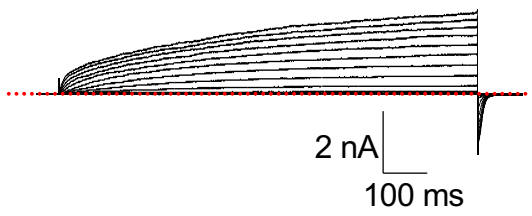

B. *SR-5-6 (10 μM) on K559A mutant*

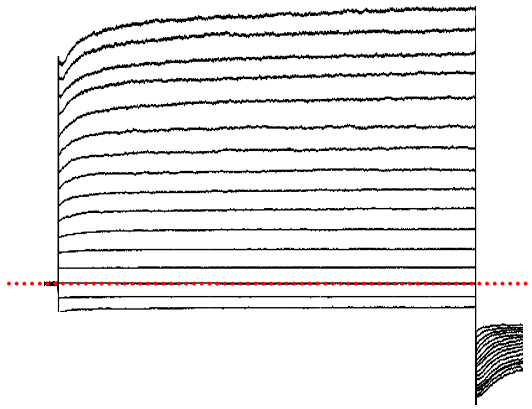

C. *Summary*

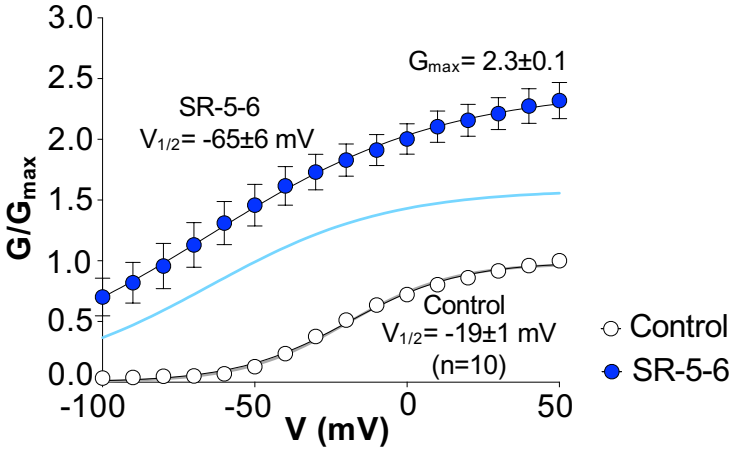

Figure 5.24: Effect of SR-5-6 on K559A mutation of K_v7.4 channels. A) A typical family of currents obtained from K559A mutation of K_v7.4 channels expressed in HEK cells. Voltage clamp protocol as described in Figure 5.7. Dotted lines represent the zero current level. **B**) The effect of 10 μM SR-5-6 on currents from the same cell. **C**) Summary activation curves obtained by measuring tail currents in ten cells before (open circles) and during (blue circles) application of SR-5-6 (n=10). The continuous grey and light blue lines in the background represent the activation curves of control and the effect of the SR-5-6 on WT K_v7.4 channels respectively. The curves were fit with the Boltzmann equation.

A. *Effect of SR-5-6 (10 μM) on $\Delta V_{1/2}$ of K_v7.4 mutants*

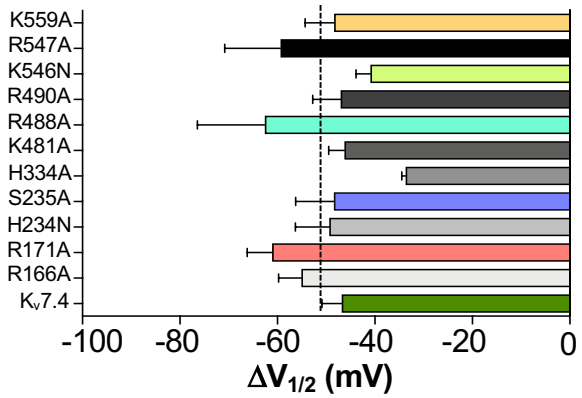

B. *Effect of SR-5-6 (10 μM) on G/G_{max} of K_v7.4 mutants*

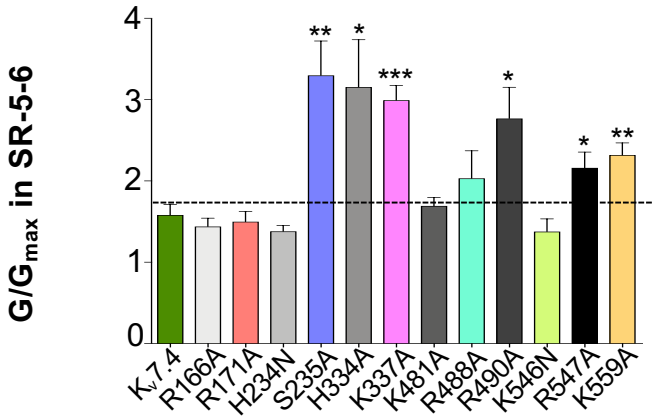

C. *Effect of SR-5-6 (10 μM) on $G_{-100\ mV}$ of K_v7.4 mutants*

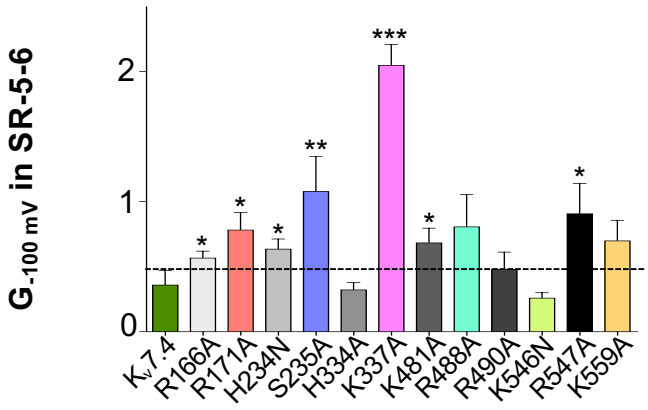

Figure 5.25: Effect of 10 μM SR-5-6 on $\Delta V_{1/2}$, G/G_{max} and $G_{-100\ mV}$ on K_v7.4 mutants. A) SR-5-6 mediated negative shift of the activation curve ($\Delta V_{1/2}$) on various mutants of K_v7.4 channels. A one-way ANOVA was performed with K_v7.4 as the control **B)** The effects of SR-5-6 on maximal conductance (G/G_{max}) of various mutants of K_v7.4 channels. **C)** SR-5-6 mediated change in conductance (G) at -100 mV on mutants of K_v7.4 channels. A Mann-Whitney non-parametric test was used to compare K_v7.4 with other groups. *p<0.05, **p<0.01, ***p<0.001, ****p<0.0001.

A. *Effect of SR-5-6 (10 µM) on $G_{-100\ mV}$ of $K_v7.4$ mutants*

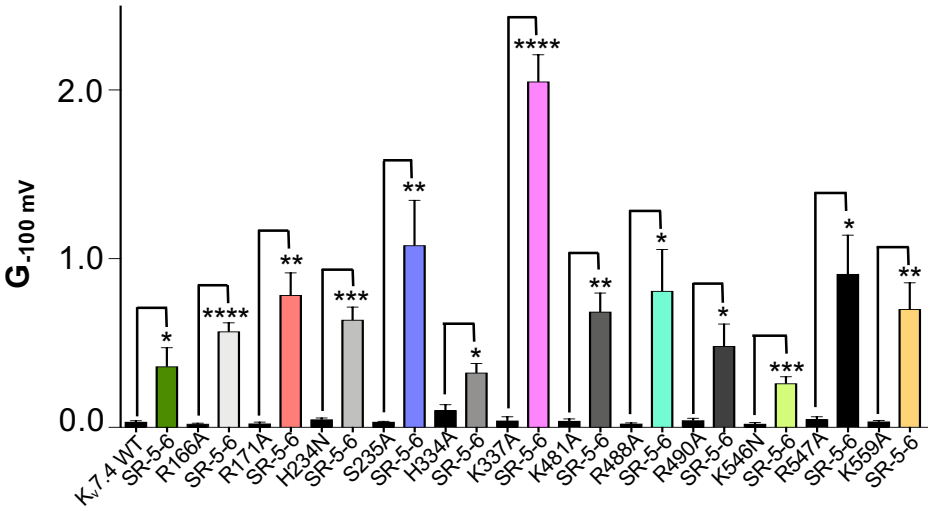

Figure 5.26: Effect of 10 µM SR-5-6 on $G_{-100\ mV}$ of $K_v7.4$ mutants.
The above data depicts the change in conductance (G) at -100 mV in HEK cells expressing the wildtype and the mutant channels. The black bars represent the control condition and the respective colored bars indicate the effect of SR-5-6 as labelled in the figure. Paired t-tests, *p<0.05, **p<0.01, ***p<0.001, ****p<0.0001.

6. General discussion

The results presented in this thesis attempted to use a combination of combinatorial cloning, mutagenesis, electrophysiology and pharmacology in an attempt to elucidate the drug-binding pocket(s) and molecular mechanism involved in SR-5-6 mediated activation of K_v7.4 channels.

K_v7 channels (K_v7.1-7.5) are found in a wide range of tissues, including the heart, CNS, and auditory pathways (Jentsch, 2000; Robbins, 2001; Jesperson *et al.,* 2005), vascular system (Ohya *et al.,* 2003; Yeung *et al.,* 2007; Mackie *et al.,* 2008), uterine smooth muscle cells (McCallum *et al.,* 2009), and pulmonary epithelium (Greenwood *et al.,* 2009). They've been explored extensively for treatment options for illnesses involving neuronal excitability and smooth muscle contractility (Lawson & McKay, 2006; Surti & Jan, 2005; Brueggemann *et al.,* 2012). There are more than a dozen K_v7 modulators available but their pharmacological uses are restricted either because the patients are resistant to them (Brodie & French 2000; Kwan & Brodie, 2010), or due to side effects which were caused by the lack of subtype specificity (Jankovic & Ilickovic, 2013). Therefore, there is a need for developing K_v7 channel activators that target distinct subtypes that could enable more targeted and tissue-specific medicinal development.

GoSlo-SR-5-6 had been developed and extensively investigated by our group (Roy *et al.,* 2014; Roy *et al.,* 2012). It was established as an activator of BK and K_v7 channels (Large *et al.,* 2015; Hannigan *et al.,* 2016; Zavaritskaya *et al.,* 2020). Among K_v7 channels, this drug was an efficacious activator of K_v7.1, K_v7.4, and K_v7.5 channels, but was much less effective on K_v7.2 and K_v7.3 channels (Zavaritskaya *et al.,* 2020). K_v7.4 channels were chosen as a convenient subtype to measure the effects of SR-5-6 and to quantify these effects by measuring changes in G/G_{max}, negative shifts in activation $V_{1/2}$ and increases in the conductance at -100 mV. K_v7.4 channels were also chosen to study these effects because this subtype expressed more robustly than other K_v7 channels.

In Chapter 3, the effects of SR-5-6 on the residues that have been shown previously to bind to known activators of K_v7 channels were investigated. Retigabine, like SR-5-6, is a well-studied K_v7 channel activator that shifted $V_{1/2}$ negatively, increased G/G_{max}, and slowed deactivation. At first, the residues that defined the retigabine binding pocket (L272, L314 and L338 in K_v7.3; Lange *et al.,* 2008) were investigated to see if they were involved in the SR-5-6 effect but

found that only one of these mutants had any effect on the response to this drug. Thus, the effect of SR-5-6 on $\Delta V_{1/2}$ was greatly reduced in L249A mutant channels (L272 in $K_v7.3$), although its effects on G/G_{max} remained. This result indicated that SR-5-6 could possibly mediate its two effects (shift in activation $V_{1/2}$ and increase in G/G_{max}) through two independent sites and that L249 in S5 helix could possibly be involved in SR-5-6 binding that brings about the hyperpolarizing shift in $K_v7.4$ channels. The involvement of two independent binding sites for K_v7 channels activators had already been demonstrated with zinc pyrithione (ZnPy) and polyunsaturated fatty acids (PUFA) (Xiong *et al.,* 2007; Liin *et al.,* 2018; Yazdi *et al.,* 2021). The effects of L281A mutant (L314 in $K_v7.3$) could not be determined as it yielded non-functional channels, however, L305A mutant channel (L338 in $K_v7.3$) did not reduce the effects of SR-5-6. Therefore, except for maybe L249A, SR-5-6 and retigabine do not appear to share any other common binding residues.

Subsequently, the contribution of other residues known to be involved in enhancing K_v7 channel currents in response to different compounds was investigated. For example, the cysteine modifying reagent N-ethylmaleimide (NEM) enhanced $K_v7.2$ channels (Li *et al.,* 2004). and a single mutation C519A in the C-terminus region is sufficient to abolish its effects. Perhaps, unsurprisingly any reduction in SR-5-6 effects was not seen when the identical residues were altered in $K_v7.4$. Similarly, the residues previously implicated in mediating the effects of the Icagen compounds were also ineffective at reducing the response to SR-5-6.

The residues which appear to contribute to polyunsaturated fatty acids (PUFAs) binding, when examined also failed to demonstrate their role in mediating the effects of SR-5-6. Previous studies had suggested that PUFA interacted with two distinct sites in S4 and S6 to increase G/G_{max} and shift $V_{1/2}$. The S4 helix's R218 and R221 were identified to play a role in the negative shift in $V_{1/2}$ in $K_v7.1$ (Liin *et al.,* 2015, 2018; Yazdi *et al.,* 2021), whereas K326 in the S6 helix of $K_v7.1$ channels was responsible for the rise in G_{max} (Liin *et al.,* 2018). In addition, Y268 in the S5 helix was also identified as a key PUFA binding residue necessary for fatty acid selectivity in K_v7 channels by Yazdi *et al.,* (2021). This was intriguing because as discussed earlier, L249A mutant channels reduced only one component of SR-5-6 effects indicating that SR-5-6 may have dual sites of action

on $K_v7.4$ channels. As a result, the PUFA binding mutants F254A and R297A in $K_v7.4$ corresponding to Y268 and K316 in $K_v7.1$ were examined which were said to be responsible for fatty acid selectivity and increase in G_{max} respectively. It was clear that the F254A mutant channel failed to reduce the effects of SR-5-6 on G/G_{max} or $\Delta V_{1/2}$. However, when the R297 residue was mutated to alanine, the channel appeared to be non-functional, as evidenced by the biophysical properties of currents, which were indistinguishable from endogenous K^+ currents. Nevertheless, the application of 10 μM SR-5-6 to this mutant did induce currents in the R297A construct, but only at very positive potentials. In contrast, 10 μM SR-5-6 had no effect on endogenous currents alone and suggests that the R297 residue was critical for channel function. It was assumed that this mutation shifts $K_v7.4$ activation very positively so that no obvious K_v7 currents were detected unless SR-5-6 was present.

Finally, investigated whether the effects of SR-5-6 differed when the VSD was locked in different states. In BK channels, three residues (L227A, S317R & I326A) were identified by Webb *et al.,* (2015) to abolish the effects of SR-5-6. The corresponding residues in $K_v7.4$ channels (L227, L313 and F322) were investigated by Dudem (2019). Interestingly, the F322A mutation alone reduced the effects of 10 μM SR-5-6 and consequently, Dudem (2019) investigated if a hydrophobic binding pocket for SR-5-6 was present in this region in $K_v7.4$. However, none of the mutations of residues in this pocket affected the response to SR-5-6 significantly. An alternative explanation of the effect of the F322A mutation was that it affected the pharmacology of the $K_v7.4$ channels, by locking the channels in a state where SR-5-6 binding was altered. Zaydman *et al*., (2014) had previously demonstrated that the F351A mutant in $K_v7.1$ (equivalent to F322A in $K_v7.4$) altered the coupling between the VSD and pore by preventing the channels from entering the intermediate open state. It is possible that this mutant locked the channels in a state where SR-5-6 binding was reduced since the equivalent mutant altered the pharmacology of $K_v7.1$ channels (Zaydman *et al*., 2014). Consequently, in the final section of this chapter, SR-5-6 effects on mutations were examined where the $K_v7.4$ channels remain locked in the closed, intermediate-open and activated-open states (Zaydman *et al*., 2014). An inspiration from Wu *et al.,* (2010) was taken and a series of mutants were created

that locked the channels in resting, partially active and fully active state. However, although each mutant was produced successfully, SR-5-6 still clearly activated all of these constructs, as evidenced by the increase in G/G_{max}. Unfortunately, the activation $V_{1/2}$ in any of these locked states could not be quantified. SR-5-6 had the greatest effect on increasing G/G_{max} when channels were locked in the resting state (E136R). The results of the state-dependent mutant studies taken together revealed that SR-5-6 can activate $K_v7.4$ channels regardless of the VSD activation state in which it was locked.

In Chapter 4, a chimeric approach was utilized to investigate the molecular determinants implicated in SR-5-6 actions in $K_v7.4$ channels, since it had been shown to be successful in finding drug binding sites by others (Schenzer *et al.,* 2005; Padilla *et al.,* 2009). Because SR-5-6 was a less effective activator of $K_v7.3$ channels than $K_v7.4$, this difference in efficacy was used to narrow down the search for the SR-5-6 binding site in $K_v7.4$ channels. Different transmembrane helices from the $K_v7.3$ channel were first swapped into the $K_v7.4$ background to create each swap construct. The impact of SR-5-6 on point mutations of residues was also evaluated that were non-conserved between $K_v7.3$ and $K_v7.4$ in swap regions that initially yielded non-functional proteins. The results from these experiments also suggested that SR-5-6 effectiveness was not considerably reduced in any of these swap constructs. Although the effect of SR-5-6 on G/G_{max} was marginally reduced in some constructs ($K_v7.4$:$K_v7.3_{S5}$ and $K_v7.4$:$K_v7.3_{S1\text{-}S4}$), no reduction in the effects on $\Delta V_{1/2}$ and $G_{-100\ mV}$ was observed in these swap constructs, indicating that these domains do not play a substantial role in SR-5-6 mediated action on the $K_v7.4$ channel. In the $K_v7.4$:$K_v7.3_{S6}$ channel, SR-5-6 did not significantly enhance the $G_{-100\ mV}$. However, this may be due to the fact that the $K_v7.4$:$K_v7.3_{S6}$ chimeric channels were activated at more positive potentials than WT $K_v7.4$, and therefore, SR-5-6 was also unable to activate the channels at very negative potentials.

The chimeric approach was very time and labour intensive and using this approach was thought to yield valuable information about the binding site of SR-5-6 in K_v7 channels. Although small reductions in G/G_{max} were observed, it was very clear that this approach did not pinpoint a drug binding site. This was very disappointing and it appears that a more fruitful approach would be to collaborate with structural biologists to either crystallize the channel or generate cryo-EM

structures in the absence and presence of SR-5-6. This is obviously a massive undertaking and currently, there are no cryo-EM resources available in the island of Ireland to go ahead with this approach.

In the final chapter, the role of PIP_2 in $K_v7.4$ channel activation by SR-5-6 was investigated. PIP_2 plays a key function in coupling between VSD and PD and stabilizing the open state of K_v7 channels (Zaydman *et al.,* 2013). When applied cytosolically, PIP_2 (Loussouarn *et al.,* 2003; Park *et al.,* 2005; Choveau *et al.,* 2012 and Cui, 2016) mimicked the effects of SR-5-6 as shown in the third chapter. Given that SR-5-6 and PIP_2 effects were similar, the effects of SR-5-6 by depleting membrane PIP_2 levels was first explored by co-expressing voltage-sensitive phosphatase (CiVSP) with WT $K_v7.4$ channels. A considerable reduction was observed in SR-5-6 responses in $\Delta V_{1/2}$ and $G_{-100\ mV}$ and ablation of the effect on G/G_{max} when PIP_2 was depleted via this voltage-sensitive phosphatase. The effects of SR-5-6 in the presence of wortmannin was also evaluated, and although the effects on $\Delta V_{1/2}$ and $G_{-100\ mV}$ were found to be reduced, they were not statistically significant. However, the rise in G/G_{max} was significantly reduced in SR-5-6 and wortmannin, confirming that the SR-5-6-mediated rise in G/G_{max} in $K_v7.4$ channels was likely PIP_2 dependent.

In the next approach, exogenous PIP_2 levels were increased using 200 μM diC8-PIP_2. As expected, it enhanced the effects of SR-5-6 on $\Delta V_{1/2}$ and $G_{-100\ mV}$ although the G/G_{max} did not appear to significantly increase. However, given that the major effect of PIP_2 is to increase the channel open probability (Li *et al.,* 2005), the exogenous diC8-PIP_2 may maximally enhance P_o and SR-5-6 may not have been able to increase this further.

In the final part of Chapter 5, mutagenesis was employed, in an attempt to modify known PIP_2 binding residues in $K_v7.4$ and evaluated the effects of SR-5-6 on these channels. However, none of the mutant channels were found to reduce the effects of SR-5-6 in $K_v7.4$ channels. This suggested that SR-5-6 effects were not mediated by the recognized PIP_2 binding residues in $K_v7.4$. Also, surprisingly, the mutations did not yield loss-of-current mutations as has been reported in other K_v7 channels (Zaydman *et al.,* 2013; Park *et al.,* 2005). This suggested that $K_v7.4$ may have different PIP_2 binding residues even though the sequence alignment revealed that the basic residues involved in PIP_2 binding were conserved in K_v7

channels (Zaydman *et al.,* 2013). Alternatively, it is possible that PIP_2 binding may be caused by numerous residues and the mutation of a single amino acid was insufficient to reduce its binding. This also possibly explains why SR-5-6 effects were not ablated in any of these mutants and perhaps suggests that other, as yet undetermined, residues may participate in PIP_2 binding in $K_v7.4$ channels. Combining the data from the three chapters, Table 6.1 (overleaf) summarizes the effects of SR-5-6 on all the mutations and swap constructs.

Mutations L249A, T278L/T282A$_{(PL)}$, H334A, and $K_v7.4$:$K_v7.3_{S6}$ shifted the activation $V_{1/2}$ toward more positive potentials than that observed in WT channels in the absence of SR-5-6. This indicated that the voltage dependence of the channels was altered when these mutations or swap constructs were incorporated into $K_v7.4$. It is important to note that these mutant residues are all situated in the pore domain, suggesting that they may play an important role in coupling between the voltage-sensing domain and the pore domain, which presumably explains why these mutants activated at more positive potentials than WT $K_v7.4$ channels. The findings that the pore domain is essential for the coupling between VSDs and pore domains of K_v7 channels has been confirmed by a number of studies (Lu *et al.,* 2001; Lu *et al.,* 2002; Barghaan & Bähring, 2009; Ferrer *et al.,* 2006; Long *et al.,* 2005; Payandeh *et al.,* 2011). Although $K_v7.4$:$K_v7.3_{S6}$, T278L/T282A$_{(PL)}$, and H334A shifted the activation $V_{1/2}$ to more positive potentials, SR-5-6 was still able to produce $\Delta V_{1/2}$ similar to WT $K_v7.4$. Interestingly, however, in the L249A mutant channels, SR-5-6 was only able to shift the $V_{1/2}$ by -7 mV, compared to -47 mV in the WT $K_v7.4$ channels (Table 6.1). In all the regions examined, $K_v7.4$:$K_v7.3_{S5}$ and $K_v7.4$:$K_v7.3_{S1-S4}$ domain swap constructs substantially reduced the effect of SR-5-6 on G/G_{max} (Table 6.1). It, therefore, appears that the voltage-sensing domains and the S5 helix of $K_v7.4$ may contribute to the increase in G/G_{max} observed in the presence of SR-5-6. The effects of SR-5-6 on $G_{-100\ mV}$ are similarly summarized in Table 6.1, where a clear reduction in $G_{-100\ mV}$ was observed in R297A, $K_v7.4$:$K_v7.3_{S6}$, $K_v7.4$: $K_v7.3_{S3-S4L}$ and Y232C. Thus, these results suggest that these residues and domains alter the channel properties in $K_v7.4$ channels, thereby preventing SR-5-6 from activating the channels at quite hyperpolarized potentials. Furthermore, the results from the C-terminal swap (Chapter 4) and the PIP_2-binding mutations (K337A, K481A, R488A, R490A, K546N, and K559A)

WT & Mutant channels	$V_{1/2}$ in mV		$\Delta V_{1/2}$	G/G_{max}	$G_{-100\ mV}$
	Control	SR-5-6		SR-5-6	SR-5-6
WT $K_v7.4$	-19 ± 2	-65 ± 5	-47 ± 4	1.58 ± 0.1	0.36
WT $K_v7.3$	-42 ± 1	-57 ± 2	-15 ± 2	1.02 ± 0.05	0.08
L249A	-3 ± 2	-8 ± 5	-7 ± 5	2.2 ± 0.1	0.1
L305A	-22 ± 2	-82 ± 7	-66 ± 11	1.9 ± 0.2	0.75
F174L	-28 ± 2	-75 ± 5	-49 ± 6	2.18 ± 0.2	0.64
A187P	-24 ± 3	-89 ± 5	-67 ± 10	1.8 ± 0.1	0.78
C519A	-29 ± 1	-91 ± 4	-61 ± 9	1.9 ± 0.2	0.87
F254A	-21 ± 2	-73 ± 5	-53 ± 7	1.58 ± 0.1	0.54
R297A	15 ± 3	-	-	1.5 ± 0.1	0.01
E136R	-	-	-	8.3 ± 1.4	3.6
E136R/R204E	-	-	-	1.8 ± 0.1	0.3
E136R/R207E	-	-	-	1.37 ± 0.1	1.0
E136R/R213E	-	-	-	1.56 ± 0.1	0.78
$K_v7.4:K_v7.3_{S6}$	-0.5 ± 2	-39 ± 4	-38 ± 4	2.1 ± 0.2	0.04
$K_v7.4:K_v7.3_{S5}$	-10 ± 2	-73 ± 2	-58 ± 4	1.3 ± 0.03	0.3
$K_v7.4:K_v7.3_{S4}$	-11 ± 4	-54 ± 8	-43 ± 8	1.96 ± 0.2	0.5
$K_v7.4:K_v7.3_{S3\text{-}S4L}$	11 ± 3	-48 ± 5	-58 ± 6	1.68 ± 0.1	0.2
$K_v7.4:K_v7.3_{S1\text{-}S4}$	-34 ± 1	-	-	1.2 ± 0.06	0.74
$K_v7.4:K_v7.3_{C\text{-}terminus}$	-29 ± 1	-102 ± 6	-71 ± 10	1.76 ± 0.2	0.9
$V230A_{(S4\text{-}S5L)}$	-47 ± 4	-	-	1.4 ± 0.2	1.2
$V231I_{(S4\text{-}S5L)}$	-16 ± 2	-63 ± 4	-50 ± 5	1.47 ± 0.08	0.27
$Y232C_{(S4\text{-}S5L)}$	-22 ± 1	-61 ± 2	-40 ± 2	1.4 ± 0.06	0.18
$S265E_{(PL)}$	-30 ± 1	-89 ± 6	-60 ± 9	2.3 ± 0.3	0.97
$D266E_{(PL)}$	-25 ± 1	-80 ± 4	-54 ± 10	2.4 ± 0.2	0.74
$S268E_{(PL)}$	-25 ± 1	-102 ± 9	-85 ± 11	2.2 ± 0.3	1.2
$S269T_{(PL)}$	-36 ± 2	-98 ± 4	-64 ± 10	1.5 ± 0.1	0.7
$S273A_{(PL)}$	-31 ± 1	-97 ± 9	-66 ± 9	1.75 ± 0.3	0.8
$T278L/T282A_{(PL)}$	-3 ± 2	-47 ± 10	-42 ± 11	2.9 ± 0.2	0.7
R166A	-30 ± 1	-80 ± 6	-55 ± 5	1.46 ± 0.1	0.6
R171A	-38 ± 1	-99 ± 5	-61 ± 5	1.5 ± 0.1	0.78
H234N	-37 ± 1	-86 ± 8	-49 ± 7	1.4 ± 0.07	0.63
S235A	-30 ± 1	-77 ± 8	-48 ± 8	3.3 ± 0.4	1.08
H334A	9 ± 9	-24 ± 11	-34 ± 1	3.1 ± 0.6	0.32
K337A	-18 ± 1	-	-	2.9 ± 0.2	2.05
K481A	-12 ± 2	-60 ± 5	-46 ± 3	1.7 ± 0.1	0.68
R488A	-23 ± 1	-83 ± 8	-62 ± 12	2 ± 0.3	0.8
R490A	-19 ± 2	-63 ± 6	-47 ± 6	2.8 ± 0.4	0.48
K546N	-22 ± 1	-61 ± 4	-41 ± 3	1.4 ± 0.1	0.26
R547A	-22 ± 1	-82 ± 9	-59 ± 11	2.1 ± 0.2	0.9
K559A	-19 ± 1	-65 ± 6	-48 ± 6	2.3 ± 0.1	0.7

Table 6.1: Summary of SR-5-6 effects on $K_v7.4$ mutant channels and domain swap constructs: *The effects on the activation $V_{1/2}$ in absence and presence of SR-5-6. The effects of SR-5-6 on maximal conductance (G_{max}) and $G_{-100\ mV}$ of $K_v7.4$ mutant channels and domain swap constructs.*

presented in Chapter 5, failed to alter the effects of SR-5-6. Interestingly, however, we did note that there was a significant rise in $G_{-100\ mV}$ in the $K_v7.4$:$K_v7.3_{C\text{-terminus}}$, K337A, K481A, R488A, R490A, K546N, and K559A mutant channels. This suggested that some of the C-terminal residues may be involved in controlling the activation of $K_v7.4$ channels at hyperpolarizing potentials.

In conclusion, this thesis established the role of L249 residue in the shift in activation $V_{1/2}$ in the excitatory effects of SR-5-6 in $K_v7.4$ channels. It also suggested that PIP_2 may be involved in the increase in G/G_{max} observed in the presence of SR-5-6 in $K_v7.4$ channels. Finally, the results with the PIP_2 'binding' mutants in $K_v7.4$ channels suggests that the PIP_2 binding residues could differ in $K_v7.4$ channels, but this will await confirmation when the relevant $K_v7.4$ structures are published.

Future directions:

It was very clear that the SR-5-6 binding site remains elusive and additional research is required to fully elucidate the mechanism of this drug in K_v7 channels. Future experiments could be directed at:

1) Resolving a cryo-EM structure of K_v7 channels in the absence and presence of SR-5-6 could be a worthwhile approach to locate the binding site of SR-5-6. In addition, a comparison of the structures in the SR-5-6 'bound' and 'unbound' states would allow the determination of the changes induced by drug binding in $K_v7.4$.

2) Investigating the effects of SR-5-6 on open probability (P_o) of K_v7 channel subtypes to establish if single-channel conductance is altered by SR-5-6. These single-channel electrophysiology experiments would also help to quantify if the effect of SR-5-6 on G/G_{max} is due entirely to an increase in open probability (P_o) or if an increase in unitary conductance also occurs.

3) Identifying the definitive PIP_2 binding residues in $K_v7.4$ channels. This could be achieved indirectly by using site-directed mutagenesis, homology modelling, patch clamping and voltage-clamp fluorometry. However, a more direct approach would be to use a cryo-EM approach to resolve the structure of $K_v7.4$ channels in the absence and presence of PIP_2.

7. References

Abbott, G. (2014). Biology of the KCNQ1 Potassium Channel. *New Journal of Science*, 2014, pp.1-26.

Abbott, G., 2012. KCNE2 and the K+channel. *Channels*, 6(1), pp.1-10.

Abbott, G., 2016. KCNE4 and KCNE5: K+ channel regulation and cardiac arrhythmogenesis. *Gene*, 593(2), pp.249-260.

Abbott, G., Sesti, F., Splawski, I., Buck, M., Lehmann, M., Timothy, K., Keating, M. and Goldstein, S. (1999). MiRP1 Forms I Kr Potassium Channels with HERG and Is Associated with Cardiac Arrhythmia. *Cell*, 97(2), pp.175-187.

Abitbol, I., Peretz, A., Lerche, C., Busch, A. and Attali, B. (1999). Stilbenes and fenamates rescue the loss of IKS channel function induced by an LQT5 mutation and other IKs mutants. *The EMBO Journal*, 18(15), pp.4137-4148.

Adams, P., Brown, D. and Constanti, A. (1982). M-currents and other potassium currents in bullfrog sympathetic neurones. *The Journal of Physiology*, 330(1), pp.537-572.

Addgene, protocols/subcloning [online] Available from: https://www.addgene.org/protocols/subcloning/

Aggarwal, S. and MacKinnon, R. (1996). Contribution of the S4 Segment to Gating Charge in the Shaker K+ Channel. *Neuron*, 16(6), pp.1169-1177.

Aiken, S., Lampe, B., Brown, B. and Murphy, P. (1995). Reduction of spike frequency adaptation and blockade of M-current in rat CA1 pyramidal neurones by linopirdine (DuP 996), a neurotransmitter release enhancer. *British Journal of Pharmacology*, 115(7), pp.1163-1168.

Aivar, P., Fernández-Orth, J., Gomis-Perez, C., Alberdi, A., Alaimo, A., Rodríguez, M., Giraldez, T., Miranda, P., Areso, P. and Villarroel, A. (2012).

Surface Expression and Subunit Specific Control of Steady Protein Levels by the K_v7.2 Helix A-B Linker. *PLoS ONE*, 7(10), p.e47263.

Alonso-Ron, C., de la Peña, P., Miranda, P., Domínguez, P. and Barros, F. (2008). Thermodynamic and Kinetic Properties of Amino-Terminal and S4-S5 Loop HERG Channel Mutants under Steady-State Conditions. *Biophysical Journal*, 94(10), pp.3893-3911.

Amato, G., Roeloffs, R., Rigdon, G., Antonio, B., Mersch, T., McNaughton-Smith, G., Wickenden, A., Fritch, P. and Suto, M. (2011). N-Pyridyl and Pyrimidine Benzamides as KCNQ2/Q3 Potassium Channel Openers for the Treatment of Epilepsy. *ACS Medicinal Chemistry Letters*, 2(6), pp.481-484.

Angelo, K., Jespersen, T., Grunnet, M., Nielsen, M., Klaerke, D. and Olesen, S. (2002). KCNE5 Induces Time- and Voltage-Dependent Modulation of the KCNQ1 Current. *Biophysical Journal*, 83(4), pp.1997-2006.

Ay, B., Prakash, Y., Pabelick, C. and Sieck, G. (2004). Store-operated Ca2+ entry in porcine airway smooth muscle. *American Journal of Physiology-Lung Cellular and Molecular Physiology*, 286(5), pp.L909-L917.

Backliwal, G., Hildinger, M., Chenuet, S., Wulhfard, S., De Jesus, M. and Wurm, F., 2008. Rational vector design and multi-pathway modulation of HEK 293E cells yield recombinant antibody titers exceeding 1 g/l by transient transfection under serum-free conditions. *Nucleic Acids Research*, 36(15), pp.e96-e96.

Bal, M., Zhang, J., Hernandez, C., Zaika, O. and Shapiro, M. (2010). Ca2+/Calmodulin Disrupts AKAP79/150 Interactions with KCNQ (M-Type) K+ Channels. *Journal of Neuroscience*, 30(6), pp.2311-2323.

Bal, M., Zhang, J., Zaika, O., Hernandez, C. and Shapiro, M. (2008). Homomeric and Heteromeric Assembly of KCNQ (K_v7) K+Channels Assayed by Total Internal Reflection Fluorescence/Fluorescence Resonance Energy Transfer and Patch Clamp Analysis. *Journal of Biological Chemistry*, 283(45), pp.30668-30676.

Baldi, L., Hacker, D., Adam, M. and Wurm, F., 2007. Recombinant protein production by large-scale transient gene expression in mammalian cells: state of the art and future perspectives. *Biotechnology Letters*, 29(5), pp.677-684.

Balijepalli, R., Delisle, B., Balijepalli, S., Foell, J., Slind, J., Kamp, T. and January, C., 2007. Kv11.1 (ERG1) K+Channels Localize in Cholesterol and Sphingolipid Enriched Membranes and Are Modulated by Membrane Cholesterol. *Channels*, 1(4), pp.263-272.

Barghaan, J. and Bähring, R. (2009). Dynamic Coupling of Voltage Sensor and Gate Involved in Closed-State Inactivation of Kv4.2 Channels. *Biophysical Journal*, 96(3), p.656a.

Barhanin, J., Lesage, F., Guillemare, E., Fink, M., Lazdunski, M. and Romey, G. (1996). KvLQT1 and IsK (minK) proteins associate to form the IKS cardiac potassium current. *Nature*, 384(6604), pp.78-80.

Barrese, V., Stott, J. and Greenwood, I., 2018. KCNQ-Encoded Potassium Channels as Therapeutic Targets. *Annual Review of Pharmacology and Toxicology*, 58(1), pp.625-648.

Beech, D., Muraki, K. and Flemming, R., 2004. Non-selective cationic channels of smooth muscle and the mammalian homologues ofDrosophilaTRP. *The Journal of Physiology*, 559(3), pp.685-706.

Bellini, G., Miceli, F., Soldovieri, MV., Miraglia del Giudice, E., Pascotto, A., Taglialatela, M. (2010). Benign familial neonatal seizures. *GeneReviews*, eds

Bellocq, C., van Ginneken, A., Bezzina, C., Alders, M., Escande, D., Mannens, M., Baró, I. and Wilde, A. (2004). Mutation in the KCNQ1 Gene Leading to the Short QT-Interval Syndrome. *Circulation*, 109(20), pp.2394-2397.

Bendahhou, S., Marionneau, C., Haurogne, K., Larroque, M., Derand, R., Szuts, V., Escande, D., Demolombe, S. and Barhanin, J. (2005). In vitro molecular

interactions and distribution of KCNE family with KCNQ1 in the human heart. *Cardiovascular Research*, 67(3), pp.529-538.

Benson, D., MacRae, C., Vesely, M., Walsh, E., Seidman, J., Seidman, C. and Satler, C., 1996. Missense Mutation in the Pore Region of HERG Causes Familial Long QT Syndrome. *Circulation*, 93(10), pp.1791-1795.

Bentzen, B., Schmitt, N., Calloe, K., Dalby Brown, W., Grunnet, M. and Olesen, S. (2006). The acrylamide (S)-1 differentially affects K_v7 (KCNQ) potassium channels. *Neuropharmacology*, 51(6), pp.1068-1077.

Bezanilla, F. (2002). Voltage Sensor Movements. *The Journal of General Physiology*, 120(4), pp.465-473.

Billington, C. and Penn, R. (2003). Signaling and regulation of G protein-coupled receptors in airway smooth muscle. *Respiratory Research*, 4(1).

Blom, S., Rottländer, M., Kehler, J., Bundgaard, C., Schmitt, N. and Jensen, H. (2014). From Pan-Reactive K_v7 Channel Opener to Subtype Selective Opener/Inhibitor by Addition of a Methyl Group. *PLoS ONE*, 9(6), p.e100209.

Blom, S., Schmitt, N. and Jensen, H. (2009). The Acrylamide (S)-2 As a Positive and Negative Modulator of K_v7 Channels Expressed in Xenopus laevis Oocytes. *PLoS ONE*, 4(12), p.e8251.

Blom, S., Schmitt, N. and Jensen, H. (2010). Differential Effects of ICA-27243 on Cloned K_v7 Channels. *Pharmacology*, 86(3), pp.174-181.

Bollin, F., Dechavanne, V. and Chevalet, L., 2011. Design of Experiment in CHO and HEK transient transfection condition optimization. *Protein Expression and Purification*, 78(1), pp.61-68.

Boulet, I., Labro, A., Raes, A. and Snyders, D. (2007). Role of the S6 C-terminus in KCNQ1 channel gating. *The Journal of Physiology*, 585(2), pp.325-337.

Bright, J. and Sansom, M. (2004). Kv channel S6 helix as a molecular switch: simulation studies. *IEE Proceedings - Nanobiotechnology*, 151(1), p.17.

Brodie, M. J., & French, J. A. (2000). Management of epilepsy in adolescents and adults. *The Lancet*, *356*(9226), 323–329.

Broomand, A., Männikkö, R., Larsson, H. and Elinder, F. (2003). Molecular Movement of the Voltage Sensor in a K Channel. *The Journal of General Physiology*, 122(6), pp.741-748.

Brown, D. and Adams, P. (1980). Muscarinic suppression of a novel voltage-sensitive K+ current in a vertebrate neurone. *Nature*, 283(5748), pp.673-676.

Brown, D. and Passmore, G., 2009. Neural KCNQ (Kv7) channels. *British Journal of Pharmacology*, 156(8), pp.1185-1195.

Brown, D., Hughes, S., Marsh, S. and Tinker, A. (2007). Regulation of M(K_v7.2/7.3) channels in neurons by PIP2 and products of PIP2hydrolysis: significance for receptor-mediated inhibition. *The Journal of Physiology*, 582(3), pp.917-925.

Brown, D., Selyanko, A., Hadley, J. and Tatulian, L. (2002). *Neurophysiology*, 34(2/3), pp.91-94.

Brueggemann, L., Cribbs, L. and Byron, K., 2019. Structural Determinants of Kv7.5 Potassium Channels That Confer Changes in Phosphatidylinositol 4,5-Bisphosphate (PIP2) Affinity and Signaling Sensitivities in Smooth Muscle Cells. *Molecular Pharmacology*, 97(3), pp.145-158.

Brueggemann, L., Cribbs, L., Schwartz, J., Wang, M., Kouta, A. and Byron, K. (2018). Mechanisms of PKA-Dependent Potentiation of K_v7.5 Channel Activity in Human Airway Smooth Muscle Cells. *International Journal of Molecular Sciences*, 19(8), p.2223.

Brueggemann, L., Haick, J., Cribbs, L. and Byron, K. (2014). Differential Activation of Vascular Smooth Muscle K_v7.4, K_v7.5, and K_v7.4/7.5 Channels by ML213 and ICA-069673. *Molecular Pharmacology*, 86(3), pp.330-341.

Brueggemann, L., Kakad, P., Love, R., Solway, J., Dowell, M., Cribbs, L. and Byron, K. (2012). K_v7 potassium channels in airway smooth muscle cells: signal transduction intermediates and pharmacological targets for bronchodilator therapy. *American Journal of Physiology-Lung Cellular and Molecular Physiology*, 302(1), pp.L120-L132.

Brueggemann, L., Mackie, A., Martin, J., Cribbs, L. and Byron, K. (2011). Diclofenac Distinguishes among Homomeric and Heteromeric Potassium Channels Composed of KCNQ4 and KCNQ5 Subunits. *Molecular Pharmacology*, 79(1), pp.10-23.

Brueggemann, L., Moran, C., Barakat, J., Yeh, J., Cribbs, L. and Byron, K. (2007). Vasopressin stimulates action potential firing by protein kinase C-dependent inhibition of KCNQ5 in A7r5 rat aortic smooth muscle cells. *American Journal of Physiology-Heart and Circulatory Physiology*, 292(3), pp.H1352-H1363.

Byron, K., Brueggemann, L., Kakad, P. and Haick, J. (2014). K_v7 (KCNQ) Potassium Channels and L-type Calcium Channels in the Regulation of Airway Diameter. *Calcium Signaling In Airway Smooth Muscle Cells*, pp.21-33.

Casis, O., Olesen, S. and Sanguinetti, M. (2006). Mechanism of Action of a Novel Human ether-a-go-go-Related Gene Channel Activator. *Molecular Pharmacology*, 69(2), pp.658-665.

Castaldo, P., del Giudice, E., Coppola, G., Pascotto, A., Annunziato, L. and Taglialatela, M. (2002). Benign Familial Neonatal Convulsions Caused by Altered Gating of KCNQ2/KCNQ3 Potassium Channels. *The Journal of Neuroscience*, 22(2), pp.RC199-RC199.

Catterall, W. (1986). Molecular Properties of Voltage-Sensitive Sodium Channels. *Annual Review of Biochemistry*, 55(1), pp.953-985.

Chadha, P., Zunke, F., Zhu, H., Davis, A., Jepps, T., Olesen, S., Cole, W., Moffatt, J. and Greenwood, I. (2012). Reduced KCNQ4-Encoded Voltage-Dependent Potassium Channel Activity Underlies Impaired β-Adrenoceptor–Mediated Relaxation of Renal Arteries in Hypertension. *Hypertension*, 59(4), pp.877-884.

Charlier, C., Singh, N., Ryan, S., Lewis, T., Reus, B., Leach, R. and Leppert, M. (1998). A pore mutation in a novel KQT-like potassium channel gene in an idiopathic epilepsy family. *Nature Genetics*, 18(1), pp.53-55.

Chen, J., Zou, A., Splawski, I., Keating, M. and Sanguinetti, M. (1999). Long QT Syndrome-associated Mutations in the Per-Arnt-Sim (PAS) Domain of HERG Potassium Channels Accelerate Channel Deactivation. *Journal of Biological Chemistry*, 274(15), pp.10113-10118.

Chen, L., Ge, Q., Tjin, G., Alkhouri, H., Deng, L., Brandsma, C., Adcock, I., Timens, W., Postma, D., Burgess, J., Black, J. and Oliver, B. (2014). Effects of cigarette smoke extract on human airway smooth muscle cells in COPD. *European Respiratory Journal*, 44(3), pp.634-646.

Chen, Y., Xu, S., Bendahhou, S., Wang, X., Wang, Y., Xu, W., Jin, H., Sun, H., Su, X., Zhuang, Q., Yang, Y., Li, Y., Liu, Y., Xu, H., Li, X., Ma, N., Mou, C., Chen, Z., Barhanin, J. and Huang, W. (2003). KCNQ1 gain-of-function mutation in familial atrial fibrillation. *ACC Current Journal Review*, 12(2), p.86.

Choveau, F., Abderemane-Ali, F., Coyan, F., Es-Salah-Lamoureux, Z., Baró, I. and Loussouarn, G. (2012). Opposite Effects of the S4–S5 Linker and PIP2 on Voltage-Gated Channel Function: KCNQ1/KCNE1 and Other Channels. *Frontiers in Pharmacology*, 3.

Choveau, F., De la Rosa, V., Bierbower, S., Hernandez, C. and Shapiro, M., 2018. Phosphatidylinositol 4,5-bisphosphate (PIP2) regulates KCNQ3 K+

channels by interacting with four cytoplasmic channel domains. *Journal of Biological Chemistry*, 293(50), pp.19411-19428.

Chung, H., Jan, Y. and Jan, L. (2006). Polarized axonal surface expression of neuronal KCNQ channels is mediated by multiple signals in the KCNQ2 and KCNQ3 C-terminal domains. *Proceedings of the National Academy of Sciences*, 103(23), pp.8870-8875.

Constanti, A. and Brown, D. (1981). M-currents in voltage-clamped mammalian sympathetic neurones. *Neuroscience Letters*, 24(3), pp.289-294.

Cui, J. (2016). Voltage-Dependent Gating: Novel Insights from KCNQ1 Channels. *Biophysical Journal*, 110(1), pp.14-25.

Dahimène, S., Alcoléa, S., Naud, P., Jourdon, P., Escande, D., Brasseur, R., Thomas, A., Baró, I. and Mérot, J. (2006). The N-Terminal Juxtamembranous Domain of KCNQ1 Is Critical for Channel Surface Expression. *Circulation Research*, 99(10), pp.1076-1083.

Dalton, A. and Barton, W., 2014. Over-expression of secreted proteins from mammalian cell lines. *Protein Science*, 23(5), pp.517-525.

de la Peña, P., Alonso-Ron, C., Machín, A., Fernández-Trillo, J., Carretero, L., Domínguez, P. and Barros, F. (2011). Demonstration of Physical Proximity between the N Terminus and the S4-S5 Linker of the Humanether-à-go-go-related Gene (hERG) Potassium Channel. *Journal of Biological Chemistry*, 286(21), pp.19065-19075.

Decher, N., Chen, J. and Sanguinetti, M., 2004. Voltage-dependent Gating of Hyperpolarization-activated, Cyclic Nucleotide-gated Pacemaker Channels. *Journal of Biological Chemistry*, 279(14), pp.13859-13865.

Dedek, K. and Waldegger, S. (2001). Colocalization of KCNQ1/KCNE channel subunits in the mouse gastrointestinal tract. *Pflugers Archiv European Journal of Physiology*, 442(6), pp.896-902.

Dedek, K., Kunath, B., Kananura, C., Reuner, U., Jentsch, T. and Steinlein, O. (2001a). Myokymia and neonatal epilepsy caused by a mutation in the voltage sensor of the KCNQ2 K+ channel. *Proceedings of the National Academy of Sciences*, 98(21), pp.12272-12277.

del Camino, D. and Yellen, G. (2001). Tight Steric Closure at the Intracellular Activation Gate of a Voltage-Gated K+ Channel. *Neuron*, 32(4), pp.649-656.

del Camino, D., Holmgren, M., Liu, Y. and Yellen, G. (2000). Blocker protection in the pore of a voltage-gated K+ channel and its structural implications. *Nature*, 403(6767), pp.321-325.

Delaney, E., Khanna, P., Tu, L., Robinson, J. and Deutsch, C., 2014. Determinants of pore folding in potassium channel biogenesis. *Proceedings of the National Academy of Sciences*, 111(12), pp.4620-4625.

Delemotte, L., Tarek, M., Klein, M., Amaral, C. and Treptow, W. (2011). Intermediate states of the Kv1.2 voltage sensor from atomistic molecular dynamics simulations. *Proceedings of the National Academy of Sciences*, 108(15), pp.6109-6114.

Delmas, P. and Brown, D. (2005). Pathways modulating neural KCNQ/M (K_v7) potassium channels. *Nature Reviews Neuroscience*, 6(11), pp.850-862.

Devaux, J., Kleopa, K., Cooper, E. and Scherer, S. (2004). KCNQ2 Is a Nodal K+ Channel. *Journal of Neuroscience*, 24(5), pp.1236-1244.

Dietrich, A., Chubanov, V., Kalwa, H., Rost, B. and Gudermann, T., 2006. Cation channels of the transient receptor potential superfamily: Their role in

physiological and pathophysiological processes of smooth muscle cells. *Pharmacology & Therapeutics*, 112(3), pp.744-760.

Diness, T., Hansen, R., Olesen, S. and Grunnet, M. (2006). Frequency-dependent modulation of KCNQ1 and HERG1 potassium channels. *Biochemical and Biophysical Research Communications*, 343(4), pp.1224-1233.

Ding, S., Ingleby, L., Ahern, C. and Horn, R. (2005). Investigating the Putative Glycine Hinge in Shaker Potassium Channel. *The Journal of General Physiology*, 126(3), pp.213-226.

Dodson, K. and Dominguez (2012). Genetics of hearing loss: focus on DFNA2. *The Application of Clinical Genetics*, p.97.

Doolan, G., Panchal, R., Fonnes, E., Clarke, A., Williams, D. and Petrou, S., 2002. Fatty acid augmentation of the cardiac slowly activating delayed rectifier current (I Ks) is conferred by hminK. *The FASEB Journal*, 16(12), pp.1662-1664.

Dudem, S., Sergeant, G., Thornbury, K. and Hollywood, M., 2021. Calcium-Activated K+ Channels (KCa) and Therapeutic Implications. *Pharmacology of Potassium Channels*, pp.379-416.

Dudem, S. (2019). Effects of the GoSlo-SR family of ion channel modulators on BK and K_v7 channels [unpublished]. PhD Thesis, Dublin City University.

Dupuis, D., Schrøder, R., Jespersen, T., Christensen, J., Christophersen, P., Jensen, B. and Olesen, S. (2002). Activation of KCNQ5 channels stably expressed in HEK293 cells by BMS-204352. *European Journal of Pharmacology*, 437(3), pp.129-137.

Dvir, M., Strulovich, R., Sachyani, D., Ben-Tal Cohen, I., Haitin, Y., Dessauer, C., Pongs, O., Kass, R., Hirsch, J. and Attali, B., 2014. Long QT mutations disrupt IKS regulation by PKA and PIP2 at the same KCNQ1 helix C-KCNE1 interface. *Journal of Cell Science*,.

E. Sander, S., Diwan, M., Raymond, R., N Nobrega, J. and Richter, A. (2016). Lower K_v7.5 Potassium Channel Subunit Expression in an Animal Model of Paroxysmal Dystonia. *CNS & Neurological Disorders - Drug Targets*, 15(1), pp.95-101.

Eckey, K., Wrobel, E., Strutz-Seebohm, N., Pott, L., Schmitt, N. and Seebohm, G., 2014. Novel Kv7.1-Phosphatidylinositol 4,5-Bisphosphate Interaction Sites Uncovered by Charge Neutralization Scanning. *Journal of Biological Chemistry*, 289(33), pp.22749-22758.

Etxeberria, A., Santana-Castro, I., Regalado, M., Aivar, P. and Villarroel, A. (2004). Three Mechanisms Underlie KCNQ2/3 Heteromeric Potassium M-Channel Potentiation. *Journal of Neuroscience*, 24(41), pp.9146-9152.

Ferrer, T., Rupp, J., Piper, D. and Tristani-Firouzi, M. (2006). The S4-S5 Linker Directly Couples Voltage Sensor Movement to the Activation Gate in the Human Ether-á-go-go-related Gene (hERG) K+Channel. *Journal of Biological Chemistry*, 281(18), pp.12858-12864.

Gajewski, C., Dagcan, A., Roux, B. and Deutsch, C., 2011. Biogenesis of the pore architecture of a voltage-gated potassium channel. *Proceedings of the National Academy of Sciences*, 108(8), pp.3240-3245.

Gamper, N. and Shapiro, M. (2003). Calmodulin Mediates Ca2+-dependent Modulation of M-type K+ Channels. *The Journal of General Physiology*, 122(1), pp.17-31.

Gamper, N. and Shapiro, M. (2007). Target-specific PIP2signalling: how might it work?. *The Journal of Physiology*, 582(3), pp.967-975.

Gamper, N., Li, Y. and Shapiro, M. (2005). Structural Requirements for Differential Sensitivity of KCNQ K+ Channels to Modulation by Ca2+/Calmodulin. *Molecular Biology of the Cell*, 16(8), pp.3538-3551.

Gamper, N., Stockand, J. and Shapiro, M. (2003a). Subunit-Specific Modulation of KCNQ Potassium Channels by Src Tyrosine Kinase. *The Journal of Neuroscience*, 23(1), pp.84-95.

Gandhi, C. and Isacoff, E. (2002). Molecular Models of Voltage Sensing. *The Journal of General Physiology*, 120(4), pp.455-463.

Gandhi, C., Clark, E., Loots, E., Pralle, A. and Isacoff, E. (2003). The Orientation and Molecular Movement of a K+ Channel Voltage-Sensing Domain. *Neuron*, 40(3), pp.515-525.

Gao, Z., Zhang, T., Wu, M., Xiong, Q., Sun, H., Zhang, Y., Zu, L., Wang, W. and Li, M. (2010). Isoform-specific Prolongation of K_v7 (KCNQ) Potassium Channel Opening Mediated by New Molecular Determinants for Drug-Channel Interactions. *Journal of Biological Chemistry*, 285(36), pp.28322-28332.

Gerlach, U. (2003). Blockers of the Slowly Delayed Rectifier Potassium IKs Channel: Potential Antiarrhythmic Agents. *Current Medicinal Chemistry-Cardiovascular & Hematological Agents*, 1(3), pp.243-252.

Gerlach, U., Brendel, J., Lang, H., Paulus, E., Weidmann, K., Brüggemann, A., Busch, A., Suessbrich, H., Bleich, M. and Greger, R. (2001). Synthesis and Activity of Novel and Selective IKs-Channel Blockers. *Journal of Medicinal Chemistry*, 44(23), pp.3831-3837.

Ghosh, S., Nunziato, D. and Pitt, G. (2006). KCNQ1 Assembly and Function Is Blocked by Long-QT Syndrome Mutations That Disrupt Interaction With Calmodulin. *Circulation Research*, 98(8), pp.1048-1054.

Gosling, M., Poll, C. and Li, S. (2005). TRP channels in airway smooth muscle as therapeutic targets. *Naunyn-Schmiedeberg's Archives of Pharmacology*, 371(4), pp.277-284.

Greenblatt, R., Blatt, Y. and Montai, M. (1985). The structure of the voltage-sensitive sodium channel. *FEBS Letters*, 193(2), pp.125-134.

Greenwood, I., Yeung, S., Hettiarachi, S., Andersson, M. and Baines, D. (2009). KCNQ-encoded channels regulate Na+ transport across H441 lung epithelial cells. *Pflügers Archiv - European Journal of Physiology*, 457(4), pp.785-794.

Grottesi, A., Domene, C., Hall, B. and Sansom, M. (2005). Conformational Dynamics of M2 Helices in KirBac Channels: Helix Flexibility in Relation to Gating via Molecular Dynamics Simulations†. *Biochemistry*, 44(44), pp.14586-14594.

Grunnet, M., Jespersen, T., Rasmussen, H., Ljungstrøm, T., Jorgensen, N., Olesen, S. and Klaerke, D. (2002). KCNE4 is an inhibitory subunit to the KCNQ1 channel. *The Journal of Physiology*, 542(1), pp.119-130.

Grunnet, M., Olesen, S., Klaerke, D. and Jespersen, T. (2005). hKCNE4 inhibits the hKCNQ1 potassium current without affecting the activation kinetics. *Biochemical and Biophysical Research Communications*, 328(4), pp.1146-1153.

Guy, H. and Seetharamulu, P. (1986). Molecular model of the action potential sodium channel. *Proceedings of the National Academy of Sciences*, 83(2), pp.508-512.

Hackos, D., Chang, T. and Swartz, K. (2002). Scanning the Intracellular S6 Activation Gate in the Shaker K+ Channel. *The Journal of General Physiology*, 119(6), pp.521-531.

Hadley, J., Noda, M., Selyanko, A., Wood, I., Abogadie, F. and Brown, D. (2000). Differential tetraethylammonium sensitivity of KCNQ1-4 potassium channels. *British Journal of Pharmacology*, 129(3), pp.413-415.

Hadley, J., Passmore, G., Tatulian, L., Al-Qatari, M., Ye, F., Wickenden, A. and Brown, D. (2003). Stoichiometry of Expressed KCNQ2/KCNQ3 Potassium Channels and Subunit Composition of Native Ganglionic M Channels Deduced from Block by Tetraethylammonium. *The Journal of Neuroscience*, 23(12), pp.5012-5019.

Haick, J. and Byron, K. (2016). Novel treatment strategies for smooth muscle disorders: Targeting K_v7 potassium channels. *Pharmacology & Therapeutics*, 165, pp.14-25.

Haitin, Y. and Attali, B. (2008). The C-terminus of K_v7 channels: a multifunctional module. *The Journal of Physiology*, 586(7), pp.1803-1810.

Hamill, O., Marty, A., Neher, E., Sakmann, B. and Sigworth, F. (1981). Improved patch-clamp techniques for high-resolution current recording from cells and cell-free membrane patches. *Pflügers Archiv - European Journal of Physiology*, 391(2), pp.85-100.

Hannigan, K., Large, R., Bradley, E., Hollywood, M., Sergeant, G., McHale, N. and Thornbury, K., 2016. Effect of a novel BKCa opener on BKCa currents and contractility of the rabbit corpus cavernosum. *American Journal of Physiology-Cell Physiology*, 310(4), pp.C284-C292.

Hansen, R., Diness, T., Christ, T., Demnitz, J., Ravens, U., Olesen, S. and Grunnet, M. (2006). Activation of Human ether-a-go-go-Related Gene Potassium Channels by the Diphenylurea 1,3-Bis-(2-hydroxy-5-trifluoromethyl-phenyl)-urea (NS1643). *Molecular Pharmacology*, 69(1), pp.266-277.

Heginbotham, L., Abramson, T. and MacKinnon, R. (1992). A functional connection between the pores of distantly related ion channels as revealed by mutant K+ channels. *Science*, 258(5085), pp.1152-1155.

Heitzmann, D. and Warth, R. (2007). No Potassium, No Acid: K+ Channels and Gastric Acid Secretion. *Physiology*, 22(5), pp.335-341.

Hernandez, C., Zaika, O. and Shapiro, M. (2008). A Carboxy-terminal Inter-Helix Linker As the Site of Phosphatidylinositol 4,5-Bisphosphate Action on K_v7 (M-type) K+ Channels. *The Journal of General Physiology*, 132(3), pp.361-381.

Hirota, N. and Martin, J. (2013). Mechanisms of Airway Remodeling. *Chest*, 144(3), pp.1026-1032.

Hirota, S., Helli, P. and Janssen, L. (2007). Ionic mechanisms and Ca2+ handling in airway smooth muscle. *European Respiratory Journal*, 30(1), pp.114-133.

Hodgkin, A. and Huxley, A., 1952. A quantitative description of membrane current and its application to conduction and excitation in nerve. *The Journal of Physiology*, 117(4), pp.500-544.

Hogg, J., Macklem, P. and Thurlbeck, W. (1968). Site and Nature of Airway Obstruction in Chronic Obstructive Lung Disease. *New England Journal of Medicine*, 278(25), pp.1355-1360.

Hogg, J., Chu, F., Utokaparch, S., Woods, R., Elliott, W., Buzatu, L., Cherniack, R., Rogers, R., Sciurba, F., Coxson, H. and Paré, P., 2004. The Nature of Small-Airway Obstruction in Chronic Obstructive Pulmonary Disease. *New England Journal of Medicine*, 350(26), pp.2645-2653.

Hoosien, M., Ellen Ahearn, M., Myerburg, R., Pham, T., Miller, T., Smets, M., Baumbach-Reardon, L., Young, M., Farooq, A. and Bishopric, N. (2013). Dysfunctional potassium channel subunit interaction as a novel mechanism of long QT syndrome. *Heart Rhythm*, 10(5), pp.728-737.

Horowitz, A., Menice, C., Laporte, R. and Morgan, K. (1996). Mechanisms of smooth muscle contraction. *Physiological Reviews*, 76(4), pp.967-1003.

Hoshi, N., Zhang, J., Omaki, M., Takeuchi, T., Yokoyama, S., Wanaverbecq, N., Langeberg, L., Yoneda, Y., Scott, J., Brown, D. and Higashida, H. (2003).

AKAP150 signaling complex promotes suppression of the M-current by muscarinic agonists. *Nature Neuroscience*, 6(6), pp.564-571.

Housley, G. and Ashmore, J. (1992). Ionic currents of outer hair cells isolated from the guinea-pig cochlea. *The Journal of Physiology*, 448(1), pp.73-98.

Howard, R., Clark, K., Holton, J. and Minor, D. (2007). Structural Insight into KCNQ (K_v7) Channel Assembly and Channelopathy. *Neuron*, 53(5), pp.663-675.

Howarth, P., Knox, A., Amrani, Y., Tliba, O., Panettieri, R. and Johnson, M. (2004). Synthetic responses in airway smooth muscle. *Journal of Allergy and Clinical Immunology*, 114(2), pp.S32-S50.

Huang, F., Chen, J., Lin, M., Keating, M. and Sanguinetti, M., 2001. Long-QT Syndrome-Associated Missense Mutations in the Pore Helix of the HERG Potassium Channel. *Circulation*, 104(9), pp.1071-1075.

Hughes, S., Marsh, S., Tinker, A. and Brown, D. (2007). PIP2-dependent inhibition of M-type ($K_v7.2/7.3$) potassium channels: direct on-line assessment of PIP2 depletion by Gq-coupled receptors in single living neurons. *Pflügers Archiv - European Journal of Physiology*, 455(1), pp.115-124.

Iannotti, F., Panza, E., Barrese, V., Viggiano, D., Soldovieri, M. and Taglialatela, M. (2010). Expression, Localization, and Pharmacological Role of K_v7 Potassium Channels in Skeletal Muscle Proliferation, Differentiation, and Survival after Myotoxic Insults. *Journal of Pharmacology and Experimental Therapeutics*, 332(3), pp.811-820.

Iwasaki, H., Murata, Y., Kim, Y., Hossain, M., Worby, C., Dixon, J., McCormack, T., Sasaki, T. and Okamura, Y., 2008. A voltage-sensing phosphatase, Ci-VSP, which shares sequence identity with PTEN, dephosphorylates phosphatidylinositol 4,5-bisphosphate. *Proceedings of the National Academy of Sciences*, 105(23), pp.7970-7975.

James, A. and Wenzel, S. (2007). Clinical relevance of airway remodelling in airway diseases. *European Respiratory Journal*, 30(1), pp.134-155.

Jankovic, S. and Ilickovic, I., 2013. The preclinical discovery and development of ezogabine for the treatment of epilepsy. *Expert Opinion on Drug Discovery*, 8(11), pp.1429-1437.

Janssen, L., 1997. T-type and L-type Ca2+ currents in canine bronchial smooth muscle: characterization and physiological roles. *American Journal of Physiology-Cell Physiology*, 272(6), pp.C1757-C1765.

Jensen, M., Jogini, V., Borhani, D., Leffler, A., Dror, R. and Shaw, D. (2012). Mechanism of Voltage Gating in Potassium Channels. *Science*, 336(6078), pp.229-233.

Jentsch, T. (2000). Neuronal KCNQ potassium channels:physiology and role in disease. *Nature Reviews Neuroscience*, 1(1), pp.21-30.

Jepps, T., Carr, G., Lundegaard, P., Olesen, S. and Greenwood, I. (2015). Fundamental role for the KCNE4 ancillary subunit in K_v7.4 regulation of arterial tone. *The Journal of Physiology*, 593(24), pp.5325-5340.

Jepps, T., Olesen, S., Greenwood, I. and Dalsgaard, T. (2016). Molecular and functional characterization of K_v7 channels in penile arteries and corpus cavernosum of healthy and metabolic syndrome rats. *British Journal of Pharmacology*, 173(9), pp.1478-1490.

Jespersen, T., B. Rasmussen, H., Grunnet, M., S. Jensen, H., Angelo, K., S. Dupuis, D., K. Vogel, L., K. Jorgensen, N., A. Klaerke, D. and Peter Olesen, S. (2004). Basolateral localisation of KCNQ1 potassium channels in MDCK cells: molecular identification of an N-terminal targeting motif. *Journal of Cell Science*, 117(19), pp.4517-4526.

Jespersen, T., Grunnet, M. and Olesen, S. (2005). The KCNQ1 Potassium Channel: From Gene to Physiological Function. *Physiology*, 20(6), pp.408-416.

Jiang, Y., Lee, A., Chen, J., Cadene, M., Chait, B. and MacKinnon, R. (2002). The open pore conformation of potassium channels. *Nature*, 417(6888), pp.523-526.

Jiang, Y., Lee, A., Chen, J., Ruta, V., Cadene, M., Chait, B. and MacKinnon, R. (2003). X-ray structure of a voltage-dependent K+ channel. *Nature*, 423(6935), pp.33-41.

Johnson, M. (1998). The β -Adrenoceptor. *American Journal of Respiratory and Critical Care Medicine*, 158(supplement_2), pp.S146-S153.

Jongbloed, R., Marcelis, C., Velter, C., Doevendans, P., Geraedts, J. and Smeets, H., 2002. DHPLC analysis of potassium ion channel genes in congenital long QT syndrome. *Human Mutation*, 20(5), pp.382-391.

Jonsson, A., Isomaa, B., Tuomi, T., Taneera, J., Salehi, A., Nilsson, P., Groop, L. and Lyssenko, V. (2009). A Variant in the KCNQ1 Gene Predicts Future Type 2 Diabetes and Mediates Impaired Insulin Secretion. *Diabetes*, 58(10), pp.2409-2413.

Jost, N., Papp, J. and Varró, A. (2007). Slow Delayed Rectifier Potassium Current (IKs) and the Repolarization Reserve. *Annals of Noninvasive Electrocardiology*, 12(1), pp.64-78.

Jost, N., Virág, L., Bitay, M., Takács, J., Lengyel, C., Biliczki, P., Nagy, Z., Bogáts, G., Lathrop, D., Papp, J. and Varró, A. (2005). Restricting Excessive Cardiac Action Potential and QT Prolongation. *Circulation*, 112(10), pp.1392-1399.

Kalappa, B., Soh, H., Duignan, K., Furuya, T., Edwards, S., Tzingounis, A. and Tzounopoulos, T. (2015). Potent KCNQ2/3-Specific Channel Activator

Suppresses In Vivo Epileptic Activity and Prevents the Development of Tinnitus. *Journal of Neuroscience*, 35(23), pp.8829-8842.

Kanda, V. and Abbott, G. (2012). KCNE Regulation of K+ Channel Trafficking – a Sisyphean Task?. *Frontiers in Physiology*, 3.

Kasimova, M., Zaydman, M., Cui, J. and Tarek, M., 2015. PIP2-dependent coupling is prominent in Kv7.1 due to weakened interactions between S4-S5 and S6. *Scientific Reports*, 5(1).

Kavanaugh, M., Varnum, M., Osborne, P., Christie, M., Busch, A., Adelman, J. and North, R., 1991. Interaction between tetraethylammonium and amino acid residues in the pore of cloned voltage-dependent potassium channels. *Journal of Biological Chemistry*, 266(12), pp.7583-7587.

Ke, Y., Hunter, M., Ng, C., Perry, M. and Vandenberg, J., 2014. Role of the Cytoplasmic N-terminal Cap and Per-Arnt-Sim (PAS) Domain in Trafficking and Stabilization of Kv11.1 Channels. *Journal of Biological Chemistry*, 289(20), pp.13782-13791.

Khanamiri, S., Soltysinska, E., Jepps, T., Bentzen, B., Chadha, P., Schmitt, N., Greenwood, I. and Olesen, S. (2013). Contribution of K v 7 Channels to Basal Coronary Flow and Active Response to Ischemia. *Hypertension*, 62(6), pp.1090-1097.

Kharkovets, T., Hardelin, J., Safieddine, S., Schweizer, M., El-Amraoui, A., Petit, C. and Jentsch, T. (2000). KCNQ4, a K+ channel mutated in a form of dominant deafness, is expressed in the inner ear and the central auditory pathway. *Proceedings of the National Academy of Sciences*, 97(8), pp.4333-4338.

Kimitsuki, T., Komune, N., Noda, T., Takaiwa, K., Ohashi, M. and Komune, S. (2010). Property of IK,n in inner hair cells isolated from guinea-pig cochlea. *Hearing Research*, 261(1-2), pp.57-62.

Kobayashi, H. and Libet, B. (1968). Generation of slow postsynaptic potentials without increases in ionic conductance. *Proceedings of the National Academy of Sciences*, 60(4), pp.1304-1311.

Krnjević, K., Pumain, R. and Renaud, L. (1971). The mechanism of excitation by acetylcholine in the cerebral cortex. *The Journal of Physiology*, 215(1), pp.247-268.

Kuba, K. and Koketsu, K. (1976). The muscarinic effects of acetylcholine on the action potential of bullfrog sympathetic ganglion cells. *The Japanese Journal of Physiology*, 26(6), pp.703-716.

Kubisch, C., Schroeder, B., Friedrich, T., Lütjohann, B., El-Amraoui, A., Marlin, S., Petit, C. and Jentsch, T. (1999). KCNQ4, a Novel Potassium Channel Expressed in Sensory Outer Hair Cells, Is Mutated in Dominant Deafness. *Cell*, 96(3), pp.437-446.

Kwan, P. and Brodie, M., 2010. Definition of refractory epilepsy: defining the indefinable?. *The Lancet Neurology*, 9(1), pp.27-29.

Labro, A., Raes, A., Bellens, I., Ottschytsch, N. and Snyders, D. (2003). Gating ofShaker-type Channels Requires the Flexibility of S6 Caused by Prolines. *Journal of Biological Chemistry*, 278(50), pp.50724-50731.

Lacroix, J., Pless, S., Maragliano, L., Campos, F., Galpin, J., Ahern, C., Roux, B. and Bezanilla, F. (2012). Intermediate state trapping of a voltage sensor. *The Journal of General Physiology*, 140(6), pp.635-652.

Lange, W., Geißendörfer, J., Schenzer, A., Grötzinger, J., Seebohm, G., Friedrich, T. and Schwake, M. (2008). Refinement of the Binding Site and Mode of Action of the Anticonvulsant Retigabine on KCNQ K+ Channels. *Molecular Pharmacology*, 75(2), pp.272-280.

Large, R., Kshatri, A., Webb, T., Roy, S., Akande, A., Bradley, E., Sergeant, G., Thornbury, K., McHale, N. and Hollywood, M., 2015. Effects of the novel BK (KCa1.1) channel opener GoSlo-SR-5-130 are dependent on the presence of BKβsubunits. *British Journal of Pharmacology*, 172(10), pp.2544-2556.

Larsson, H., Baker, O., Dhillon, D. and Isacoff, E. (1996). Transmembrane Movement of the Shaker K+ Channel S4. *Neuron*, 16(2), pp.387-397.

Lawson, K. and McKay, N. (2006). Modulation of Potassium Channels as a Therapeutic Approach. *Current Pharmaceutical Design*, 12(4), pp.459-470.

Lee, S., Banerjee, A. and MacKinnon, R. (2009). Two Separate Interfaces between the Voltage Sensor and Pore Are Required for the Function of Voltage-Dependent K+ Channels. *PLoS Biology*, 7(3), p.e1000047.

Lehman, A., Thouta, S., Mancini, G., Naidu, S., van Slegtenhorst, M., McWalter, K., Person, R., Mwenifumbo, J., Salvarinova, R., Guella, I., McKenzie, M., Datta, A., Connolly, M., Kalkhoran, S., Poburko, D., Friedman, J., Farrer, M., Demos, M., Desai, S. and Claydon, T. (2017). Loss-of-Function and Gain-of-Function Mutations in KCNQ5 Cause Intellectual Disability or Epileptic Encephalopathy. *The American Journal of Human Genetics*, 101(1), pp.65-74.

Lemtiri-Chlieh, F. and Ali, R., 2013. Characterization of Heterologously Expressed Transporter Genes by Patch- and Voltage-Clamp Methods: Application to Cyclic Nucleotide-Dependent Responses. *Cyclic Nucleotide Signaling in Plants*, pp.67-93.

Lerche, C., Bruhova, I., Lerche, H., Steinmeyer, K., Wei, A., Strutz-Seebohm, N., Lang, F., Busch, A., Zhorov, B. and Seebohm, G. (2007). Chromanol 293B Binding in KCNQ1 (K_v7.1) Channels Involves Electrostatic Interactions with a Potassium Ion in the Selectivity Filter. *Molecular Pharmacology*, 71(6), pp.1503-1511.

Lerche, C., Scherer, C., Seebohm, G., Derst, C., Wei, A., Busch, A. and Steinmeyer, K. (2000). Molecular Cloning and Functional Expression of KCNQ5, a Potassium Channel Subunit That May Contribute to Neuronal M-current Diversity. *Journal of Biological Chemistry*, 275(29), pp.22395-22400.

Li-Smerin, Y., Hackos, D. and Swartz, K. (2000). α-Helical Structural Elements within the Voltage-Sensing Domains of a K+ Channel. *The Journal of General Physiology*, 115(1), pp.33-50.

Li, P., Chen, X., Zhang, Q., Zheng, Y., Jiang, H., Yang, H. and Gao, Z. (2014). The Human Ether-A-Go-Go–Related Gene Activator NS1643 Enhances Epilepsy-Associated KCNQ Channels. *Journal of Pharmacology and Experimental Therapeutics*, 351(3), pp.596-604.

Li, P., Chen, Z., Xu, H., Sun, H., Li, H., Liu, H., Yang, H., Gao, Z., Jiang, H. and Li, M. (2013). The gating charge pathway of an epilepsy-associated potassium channel accommodates chemical ligands. *Cell Research*, 23(9), pp.1106-1118.

Li, Y., Gamper, N. and Shapiro, M. (2004). Single-Channel Analysis of KCNQ K+ Channels Reveals the Mechanism of Augmentation by a Cysteine-Modifying Reagent. *Journal of Neuroscience*, 24(22), pp.5079-5090.

Li, Y., Hilgemann, D. and Shapiro, M. (2005). Regulation of K_v7 (KCNQ) K+ Channel Open Probability by Phosphatidylinositol 4,5-Bisphosphate. *Journal of Neuroscience*, 25(43), pp.9825-9835.

Li, Y., Langlais, P., Gamper, N., Liu, F. and Shapiro, M. (2004a). Dual Phosphorylations Underlie Modulation of Unitary KCNQ K+Channels by Src Tyrosine Kinase. *Journal of Biological Chemistry*, 279(44), pp.45399-45407.

Li, Y., Um, S. and Mcdonald, T. (2006). Voltage-Gated Potassium Channels: Regulation by Accessory Subunits. *The Neuroscientist*, 12(3), pp.199-210.

Li, Y., Zaydman, M., Wu, D., Shi, J., Guan, M., Virgin-Downey, B. and Cui, J. (2011). KCNE1 enhances phosphatidylinositol 4,5-bisphosphate (PIP2) sensitivity of IKs to modulate channel activity. *Proceedings of the National Academy of Sciences*, 108(22), pp.9095-9100.

Liin, S., Larsson, J., Barro-Soria, R., Bentzen, B. and Larsson, H., 2016. Fatty acid analogue N-arachidonoyl taurine restores function of IKs channels with diverse long QT mutations. *eLife*, 5.

Liin, S., Silverå Ejneby, M., Barro-Soria, R., Skarsfeldt, M., Larsson, J., Starck Härlin, F., Parkkari, T., Bentzen, B., Schmitt, N., Larsson, H. and Elinder, F., 2015. Polyunsaturated fatty acid analogs act antiarrhythmically on the cardiac IKs channel. *Proceedings of the National Academy of Sciences*, 112(18), pp.5714-5719.

Liin, S., Yazdi, S., Ramentol, R., Barro-Soria, R. and Larsson, H., 2018. Mechanisms Underlying the Dual Effect of Polyunsaturated Fatty Acid Analogs on Kv7.1. *Cell Reports*, 24(11), pp.2908-2918.

Liu, XS. and Xu, YJ. (2005) Potassium channels in airway smooth muscle and airway hyperreactivity in asthma. *Chin Med J (Engl)* 118, pp.574-580.

Liu, Y., Holmgren, M., Jurman, M. and Yellen, G. (1997). Gated Access to the Pore of a Voltage-Dependent K+ Channel. *Neuron*, 19(1), pp.175-184.

Logothetis, D., Petrou, V., Zhang, M., Mahajan, R., Meng, X., Adney, S., Cui, M. and Baki, L., 2015. Phosphoinositide Control of Membrane Protein Function: A Frontier Led by Studies on Ion Channels. *Annual Review of Physiology*, 77(1), pp.81-104.

Long, S., Campbell, E. and MacKinnon, R. (2005). Crystal Structure of a Mammalian Voltage-Dependent Shaker Family K+ Channel. *Science*, 309(5736), pp.897-903.

Long, S., Campbell, E. and Mackinnon, R. (2005a). Voltage Sensor of Kv1.2: Structural Basis of Electromechanical Coupling. *Science*, 309(5736), pp.903-908.

Long, S., Tao, X., Campbell, E. and MacKinnon, R. (2007). Atomic structure of a voltage-dependent K+ channel in a lipid membrane-like environment. *Nature*, 450(7168), pp.376-382.

Loussouarn, G., Park, K., Bellocq, C., Baro, I., Charpentier, F. and Escande, D. (2003). Phosphatidylinositol-4,5-bisphosphate, PIP2, controls KCNQ1/KCNE1 voltage-gated potassium channels: a functional homology between voltage-gated and inward rectifier K+ channels. *The EMBO Journal*, 22(20), pp.5412-5421.

Lu, Z., Klem, A. and Ramu, Y. (2001). Ion conduction pore is conserved among potassium channels. *Nature*, 413(6858), pp.809-813.

Lu, Z., Klem, A. and Ramu, Y. (2002). Coupling between Voltage Sensors and Activation Gate in Voltage-gated K+ Channels. *The Journal of General Physiology*, 120(5), pp.663-676.

Mackie, A., Brueggemann, L., Henderson, K., Shiels, A., Cribbs, L., Scrogin, K. and Byron, K. (2008). Vascular KCNQ Potassium Channels as Novel Targets for the Control of Mesenteric Artery Constriction by Vasopressin, Based on Studies in Single Cells, Pressurized Arteries, and in Vivo Measurements of Mesenteric Vascular Resistance. *Journal of Pharmacology and Experimental Therapeutics*, 325(2), pp.475-483.

Maljevic, S., Lerche, C., Seebohm, G., Alekov, A., Busch, A. and Lerche, H. (2003). Rapid Report. *The Journal of Physiology*, 548(2), pp.353-360.

Manderfield, L. and George, A. (2008). KCNE4 can co-associate with the IKs (KCNQ1-KCNE1) channel complex. *FEBS Journal*, 275(6), pp.1336-1349.

Manderfield, L., Daniels, M., Vanoye, C. and George Jr, A. (2009). KCNE4 domains required for inhibition of KCNQ1. *The Journal of Physiology*, 587(2), pp.303-314.

Mani, B., Robakowski, C., Brueggemann, L., Cribbs, L., Tripathi, A., Majetschak, M. and Byron, K. (2016). K_v7.5 Potassium Channel Subunits Are the Primary Targets for PKA-Dependent Enhancement of Vascular Smooth Muscle K_v7 Currents. *Molecular Pharmacology*, 89(3), pp.323-334.

Marrion, NV. (1997). Control of M-current. *Annu Rev Physiol*, 59:483-504.

Martire, M., Castaldo, P., D'Amico, M., Preziosi, P., Annunziato, L. and Taglialatela, M. (2004). M Channels Containing KCNQ2 Subunits Modulate Norepinephrine, Aspartate, and GABA Release from Hippocampal Nerve Terminals. *Journal of Neuroscience*, 24(3), pp.592-597.

Marx, S., Kurokawa, J., Reiken, S., Motoike, H., D'Armiento, J., Marks, A. and Kass, R. (2002). Requirement of a Macromolecular Signaling Complex for beta Adrenergic Receptor Modulation of the KCNQ1-KCNE1 Potassium Channel. *Science*, 295(5554), pp.496-499.

Mazhari, R., Nuss, H., Armoundas, A., Winslow, R. and Marbán, E. (2002). Ectopic expression of KCNE3 accelerates cardiac repolarization and abbreviates the QT interval. *Journal of Clinical Investigation*, 109(8), pp.1083-1090.

McCallum, L., Greenwood, I. and Tribe, R. (2009). Expression and function of K_v7 channels in murine myometrium throughout oestrous cycle. *Pflügers Archiv - European Journal of Physiology*, 457(5), pp.1111-1120.

McCrossan, Z. and Abbott, G. (2004). The MinK-related peptides. *Neuropharmacology*, 47(6), pp.787-821.

Melman, Y., Domènech, A., de la Luna, S. and McDonald, T. (2000). Structural Determinants of KvLQT1 Control by the KCNE Family of Proteins. *Journal of Biological Chemistry*, 276(9), pp.6439-6444.

Melman, Y., Um, S., Krumerman, A., Kagan, A. and McDonald, T. (2004). KCNE1 Binds to the KCNQ1 Pore to Regulate Potassium Channel Activity. *Neuron*, 42(6), pp.927-937.

Miceli, F., Cilio, M., Taglialatela, M. and Bezanilla, F. (2009). Gating currents from neuronal $K_v7.4$ Channels: General features and correlation with the ionic conductance. *Channels*, 3(4), pp.277-286.

Neher, E., & Sakmann, B. (1976). Single-channel currents recorded from membrane of denervated frog muscle fibres. *Nature*, *260*(5554), 799–802.

Nickolson, V., William Tam, S., Myers, M. and Cook, L. (1990). DuP 996 (3,3-bis(4-pyrindinylmethyl)-1-phenylindolin-2-one) enhances the stimulus-induced release of acetylcholine from rat brain in vitro and in vivo. *Drug Development Research*, 19(3), pp.285-300.

Noda, M., Ikeda, T., Suzuki, H., Takeshima, H., Takahashi, T., Kuno, M. and Numa, S. (1986). Expression of functional sodium channels from cloned cDNA. *Nature*, 322(6082), pp.826-828.

Noda, M., Shimizu, S., Tanabe, T., Takai, T., Kayano, T., Ikeda, T., Takahashi, H., Nakayama, H., Kanaoka, Y., Minamino, N., Kangawa, K., Matsuo, H., Raftery, M., Hirose, T., Inayama, S., Hayashida, H., Miyata, T. and Numa, S. (1984). Primary structure of Electrophorus electricus sodium channel deduced from cDNA sequence. *Nature*, 312(5990), pp.121-127.

Ogden D, Stanfield P (1994) Patch clamp techniques for single channel and whole-cell recording. In: Ogden D (ed) Microelectrode techniques: the Plymouth workshop handbook, 2nd edn. The Company of Biologists, Cambridge, pp 53-78

Ohya, S., Sergeant, G., Greenwood, I. and Horowitz, B. (2003). Molecular Variants of KCNQ Channels Expressed in Murine Portal Vein Myocytes. *Circulation Research*, 92(9), pp.1016-1023.

Ooi, A., Wong, A., Esau, L., Lemtiri-Chlieh, F. and Gehring, C., 2016. A Guide to Transient Expression of Membrane Proteins in HEK-293 Cells for Functional Characterization. *Frontiers in Physiology*, 7.

Osteen, J., Gonzalez, C., Sampson, K., Iyer, V., Rebolledo, S., Larsson, H. and Kass, R. (2010). KCNE1 alters the voltage sensor movements necessary to open the KCNQ1 channel gate. *Proceedings of the National Academy of Sciences*, 107(52), pp.22710-22715.

Osteen, J., Sampson, K. and Kass, R. (2010). The cardiac IKs channel, complex indeed. *Proceedings of the National Academy of Sciences*, 107(44), pp.18751-18752.

Padilla, K., Wickenden, A., Gerlach, A. and McCormack, K. (2009). The KCNQ2/3 selective channel opener ICA-27243 binds to a novel voltage-sensor domain site. *Neuroscience Letters*, 465(2), pp.138-142.

Panaghie, G. and Abbott, G. (2007). The Role of S4 Charges in Voltage-dependent and Voltage-independent KCNQ1 Potassium Channel Complexes. *The Journal of General Physiology*, 129(2), pp.121-133.

Panaghie, G., Tai, K. and Abbott, G. (2006). Interaction of KCNE subunits with the KCNQ1 K+channel pore. *The Journal of Physiology*, 570(3), pp.455-467.

Papazian, D., Shao, X., Seoh, S., Mock, A., Huang, Y. and Wainstock, D. (1995). Electrostatic interactions of S4 voltage sensor in shaker K+ channel. *Neuron*, 14(6), pp.1293-1301.

Park, K., Piron, J., Dahimene, S., Mérot, J., Baró, I., Escande, D. and Loussouarn, G., 2005. Impaired KCNQ1–KCNE1 and Phosphatidylinositol-4,5-

Bisphosphate Interaction Underlies the Long QT Syndrome. *Circulation Research*, 96(7), pp.730-739.

Patoine, D., Hasibu, I., Pilote, S., Champagne, J., Drolet, B. and Simard, C. (2011). A Novel KCNQ1 Variant (L203P) Associated with Torsades de Pointes–Related Syncope in a Steinert Syndrome Patient. *Canadian Journal of Cardiology*, 27(2), pp.263.e5-263.e12.

Payandeh, J., Scheuer, T., Zheng, N. and Catterall, W. (2011). The crystal structure of a voltage-gated sodium channel. *Nature*, 475(7356), pp.353-358.

Penn, R. and Benovic, J. (2008). Regulation of Heterotrimeric G Protein Signaling in Airway Smooth Muscle. *Proceedings of the American Thoracic Society*, 5(1), pp.47-57.

Peretz, A., Degani-Katzav, N., Nachman, R., Uziyel, Y., Gibor, G., Shabat, D. and Attali, B. (2005). Meclofenamic Acid and Diclofenac, Novel Templates of KCNQ2/Q3 Potassium Channel Openers, Depress Cortical Neuron Activity and Exhibit Anticonvulsant Properties. *Molecular Pharmacology*, 67(4), pp.1053-1066.

Peretz, A., Degani-Katzav, N., Talmon, M., Danieli, E., Gopin, A., Malka, E., Nachman, R., Raz, A., Shabat, D. and Attali, B. (2007). A Tale of Switched Functions: From Cyclooxygenase Inhibition to M-Channel Modulation in New Diphenylamine Derivatives. *PLoS ONE*, 2(12), p.e1332.

Peretz, A., Pell, L., Gofman, Y., Haitin, Y., Shamgar, L., Patrich, E., Kornilov, P., Gourgy-Hacohen, O., Ben-Tal, N. and Attali, B. (2010). Targeting the voltage sensor of $K_v7.2$ voltage-gated K+ channels with a new gating-modifier. *Proceedings of the National Academy of Sciences*, 107(35), pp.15637-15642.

Peretz, A., Sheinin, A., Yue, C., Degani-Katzav, N., Gibor, G., Nachman, R., Gopin, A., Tam, E., Shabat, D., Yaari, Y. and Attali, B. (2007). Pre- and

Postsynaptic Activation of M-Channels By a Novel Opener Dampens Neuronal Firing and Transmitter Release. *Journal of Neurophysiology*, 97(1), pp.283-295.

Perez-Zoghbi, J., Karner, C., Ito, S., Shepherd, M., Alrashdan, Y. and Sanderson, M. (2009). Ion channel regulation of intracellular calcium and airway smooth muscle function. *Pulmonary Pharmacology & Therapeutics*, 22(5), pp.388-397.

Peroz, D., Rodriguez, N., Choveau, F., Baró, I., Mérot, J. and Loussouarn, G. (2008). $K_v7.1$ (KCNQ1) properties and channelopathies. *The Journal of Physiology*, 586(7), pp.1785-1789.

Piccini, M., Vitelli, F., Seri, M., Galietta, L., Moran, O., Bulfone, A., Banfi, S., Pober, B. and Renieri, A. (1999). KCNE1-like Gene Is Deleted in AMME Contiguous Gene Syndrome: Identification and Characterization of the Human and Mouse Homologs. *Genomics*, 60(3), pp.251-257.

Plouin, P. (1994). Benign familial neonatal convulsions. In:Idiopathic Generalized Epilepsies: Clinical, Experimental and Genetic Aspects, eds Malafosse, A., Hirsch, E., Marescaux, C., Broglin, D., Bernasconi, R, *London: John Libbey*, p. 39-44.

Ponce, A., Castillo, A., Hinojosa, L., Martinez-Rendon, J. and Cereijido, M., 2018. The expression of endogenous voltage-gated potassium channels in HEK293 cells is affected by culture conditions. *Physiological Reports*, 6(8), p.e13663.

Prole, D. and Yellen, G. (2006). Reversal of HCN Channel Voltage Dependence via Bridging of the S4–S5 Linker and Post-S6. *The Journal of General Physiology*, 128(3), pp.273-282.

Rennie, K. and Correia, M. (1994). Potassium currents in mammalian and avian isolated type I semicircular canal hair cells. *Journal of Neurophysiology*, 71(1), pp.317-329.

Robbins, J. (2001). KCNQ potassium channels: physiology, pathophysiology, and pharmacology. *Pharmacology & Therapeutics*, 90(1), pp.1-19.

Roche, J., Westenbroek, R., Sorom, A., Hille, B., Mackie, K. and Shapiro, M. (2002). Antibodies and a cysteine-modifying reagent show correspondence of M current in neurons to KCNQ2 and KCNQ3 K+channels. *British Journal of Pharmacology*, 137(8), pp.1173-1186.

Roepke, T., King, E., Reyna-Neyra, A., Paroder, M., Purtell, K., Koba, W., Fine, E., Lerner, D., Carrasco, N. and Abbott, G. (2009). Kcne2 deletion uncovers its crucial role in thyroid hormone biosynthesis. *Nature Medicine*, 15(10), pp.1186-1194.

Romey, G., Attali, B., Chouabe, C., Abitbol, I., Guillemare, E., Barhanin, J. and Lazdunski, M. (1997). Molecular Mechanism and Functional Significance of the MinK Control of the KvLQT1 Channel Activity. *Journal of Biological Chemistry*, 272(27), pp.16713-16716.

Rostock, A., Tober, C., Rundfeldt, C., Bartsch, R., Engel, J., Polymeropoulos, E., Kutscher, B., Löscher, W., Hönack, D., White, H. and Wolf, H., 1996. D-23129: a new anticonvulsant with a broad spectrum activity in animal models of epileptic seizures. *Epilepsy Research*, 23(3), pp.211-223.

Roura-Ferrer, M., Solé, L., Martínez-Mármol, R., Villalonga, N. and Felipe, A. (2008). Skeletal muscle K_v7 (KCNQ) channels in myoblast differentiation and proliferation. *Biochemical and Biophysical Research Communications*, 369(4), pp.1094-1097.

Roy, S., Large, R., Akande, A., Kshatri, A., Webb, T., Domene, C., Sergeant, G., McHale, N., Thornbury, K. and Hollywood, M. (2014). Development of GoSlo-SR-5-69, a potent activator of large conductance Ca2+-activated K+ (BK) channels. *European Journal of Medicinal Chemistry*, 75, pp.426-437.

Roy, S., Morayo Akande, A., Large, R., Webb, T., Camarasu, C., Sergeant, G., McHale, N., Thornbury, K. and Hollywood, M. (2012). Structure-Activity Relationships of a Novel Group of Large-Conductance Ca2+-Activated K+(BK) Channel Modulators: The GoSlo-SR Family. *ChemMedChem*, 7(10), pp.1763-1769.

Rundfeldt, C. (1997). The new anticonvulsant retigabine (D-23129) acts as an opener of K+ channels in neuronal cells. *European Journal of Pharmacology*, 336(2-3), pp.243-249.

Rundfeldt, C. and Netzer, R. (2011). Investigations into the Mechanism of Action of the New Anticonvulsant Retigabine - Interaction with GABAergic and glutamatergic neurotransmission and with voltage gated ion channels. *Arzneimittelforschung*, 50(12), pp.1063-1070.

Salata, J., Jurkiewicz, N., Wang, J., Evans, B., Orme, H. and Sanguinetti, M. (1998). A Novel Benzodiazepine that Activates Cardiac Slow Delayed Rectifier K+ Currents. *Molecular Pharmacology*, 54(1), pp.220-230.

Sanderson, M., Delmotte, P., Bai, Y. and Perez-Zogbhi, J. (2008). Regulation of Airway Smooth Muscle Cell Contractility by Ca2+ Signaling and Sensitivity. *Proceedings of the American Thoracic Society*, 5(1), pp.23-31.

Sanguinetti, M. and Jurkiewicz, N. (1990). Two components of cardiac delayed rectifier K+ current. Differential sensitivity to block by class III antiarrhythmic agents. *The Journal of General Physiology*, 96(1), pp.195-215.

Sanguinetti, M., Curran, M., Zou, A., Shen, J., Specter, P., Atkinson, D. and Keating, M. (1996). Coassembly of KVLQT1 and minK (IsK) proteins to form cardiac IKS potassium channel. *Nature*, 384(6604), pp.80-83.

Schenzer, A., Friedrich, T., Pusch, M., Saftig, P., Jentsch, T., Grotzinger, J. and Schwake, M. (2005). Molecular Determinants of KCNQ (K_v7) K+ Channel

Sensitivity to the Anticonvulsant Retigabine. *Journal of Neuroscience*, 25(20), pp.5051-5060.

Schmitt, N., Schwarz, M., Peretz, A., Abitbol, I., Attali, B. and Pongs, O. (2000). A recessive C-terminal Jervell and Lange-Nielsen mutation of the KCNQ1 channel impairs subunit assembly. *The EMBO Journal*, 19(3), pp.332-340.

Schnee ME, Brown BS. 1998. Selectivity of linopirdine (DuP 996), a neurotransmitter release enhancer, in blocking voltage-dependent and calcium-activated potassium currents in hippocampal neurons. *J Pharmacol Exp Ther* 286: pp. 709–717.

Schroeder, B., Hechenberger, M., Weinreich, F., Kubisch, C. and Jentsch, T. (2000a). KCNQ5, a Novel Potassium Channel Broadly Expressed in Brain, Mediates M-type Currents. *Journal of Biological Chemistry*, 275(31), pp.24089-24095.

Schroeder, B., Waldegger, S., Fehr, S., Bleich, M., Warth, R., Greger, R. and Jentsch, T. (2000). A constitutively open potassium channel formed by KCNQ1 and KCNE3. *Nature*, 403(6766), pp.196-199.

Schubert ML (2010). Gastric secretion. *Curr Opin Gastroenterol* 26: pp. 598-603.

Schwake, M., Athanasiadu, D., Beimgraben, C., Blanz, J., Beck, C., Jentsch, T., Saftig, P. and Friedrich, T. (2006). Structural Determinants of M-Type KCNQ (K_v7) K+ Channel Assembly. *Journal of Neuroscience*, 26(14), pp.3757-3766.

Schwake, M., Jentsch, T. and Friedrich, T. (2003). A carboxy-terminal domain determines the subunit specificity of KCNQ K + channel assembly. *EMBO reports*, 4(1), pp.76-81.

Schwartz, P., Priori, S., Bloise, R., Napolitano, C., Ronchetti, E., Piccinini, A., Goj, C., Breithardt, G., Schulze-Bahr, E., Wedekind, H. and Nastoli, J., 2001.

Molecular diagnosis in a child with sudden infant death syndrome. *The Lancet*, 358(9290), pp.1342-1343.

Schwarz, J., Glassmeier, G., Cooper, E., Kao, T., Nodera, H., Tabuena, D., Kaji, R. and Bostock, H. (2006). KCNQ channels mediateIKs, a slow K+current regulating excitability in the rat node of Ranvier. *The Journal of Physiology*, 573(1), pp.17-34.

Scichilone, N., Battaglia, S., Sala, A. and Bellia, V., 2006. Clinical implications of airway hyper-responsiveness in COPD. *International Journal of COPD*, 1(1), pp.49-60.

Seebohm, G., Pusch, M., Chen, J. and Sanguinetti, M. (2003). Pharmacological Activation of Normal and Arrhythmia-Associated Mutant KCNQ1 Potassium Channels. *Circulation Research*, 93(10), pp.941-947.

Seebohm, G., Sanguinetti, M. and Pusch, M. (2003a). Tight coupling of rubidium conductance and inactivation in human KCNQ1 potassium channels. *The Journal of Physiology*, 552(2), pp.369-378.

Seebohm, G., Strutz-Seebohm, N., Ureche, O., Baltaev, R., Lampert, A., Kornichuk, G., Kamiya, K., Wuttke, T., Lerche, H., Sanguinetti, M. and Lang, F. (2006). Differential Roles of S6 Domain Hinges in the Gating of KCNQ Potassium Channels. *Biophysical Journal*, 90(6), pp.2235-2244.

Seebohm, G., Westenskow, P., Lang, F. and Sanguinetti, M. (2005). Mutation of colocalized residues of the pore helix and transmembrane segments S5 and S6 disrupt deactivation and modify inactivation of KCNQ1 K+channels. *The Journal of Physiology*, 563(2), pp.359-368.

Seoh, S., Sigg, D., Papazian, D. and Bezanilla, F. (1996). Voltage-Sensing Residues in the S2 and S4 Segments of the Shaker K+ Channel. *Neuron*, 16(6), pp.1159-1167.

Shamgar, L., Ma, L., Schmitt, N., Haitin, Y., Peretz, A., Wiener, R., Hirsch, J., Pongs, O. and Attali, B. (2006). Calmodulin Is Essential for Cardiac I KS Channel Gating and Assembly. *Circulation Research*, 98(8), pp.1055-1063.

Shapiro, M., Roche, J., Kaftan, E., Cruzblanca, H., Mackie, K. and Hille, B., 2000. Reconstitution of Muscarinic Modulation of the KCNQ2/KCNQ3 K+Channels That Underlie the Neuronal M Current. *The Journal of Neuroscience*, 20(5), pp.1710-1721.

Sihn, C., Kim, H., Woltz, R., Yarov-Yarovoy, V., Yang, P., Xu, J., Clancy, C., Zhang, X., Chiamvimonvat, N. and Yamoah, E., 2016. Mechanisms of Calmodulin Regulation of Different Isoforms of Kv7.4 K+ Channels. *Journal of Biological Chemistry*, 291(5), pp.2499-2509.

Silva, J., Pan, H., Wu, D., Nekouzadeh, A., Decker, K., Cui, J., Baker, N., Sept, D. and Rudy, Y. (2009). A multiscale model linking ion-channel molecular dynamics and electrostatics to the cardiac action potential. *Proceedings of the National Academy of Sciences*, 106(27), pp.11102-11106.

Singh, N., Charlier, C., Stauffer, D., DuPont, B., Leach, R., Melis, R., Ronen, G., Bjerre, I., Quattlebaum, T., Murphy, J., McHarg, M., Gagnon, D., Rosales, T., Peiffer, A., Anderson, V. and Leppert, M. (1998). A novel potassium channel gene, KCNQ2, is mutated in an inherited epilepsy of newborns. *Nature Genetics*, 18(1), pp.25-29.

Smith, J., Vanoye, C., George, A., Meiler, J. and Sanders, C. (2007). Structural Models for the KCNQ1 Voltage-Gated Potassium Channel†. *Biochemistry*, 46(49), pp.14141-14152.

Smith, RJH., Hildebrand, M. (2008). DFNA2 nonsyndromic hearing loss. In:*GeneReviews*, eds Pagon, RA., Bird, TD., Dolan, CR., Stephens, K. Seattle, WA: University of Washington, Seattle, 1993-2021

Soh, H., Pant, R., LoTurco, J. and Tzingounis, A. (2014). Conditional Deletions of Epilepsy-Associated KCNQ2 and KCNQ3 Channels from Cerebral Cortex Cause Differential Effects on Neuronal Excitability. *Journal of Neuroscience*, 34(15), pp.5311-5321.

Soldovieri, M., Cilio, M., Miceli, F., Bellini, G., Miraglia del Giudice, E., Castaldo, P., Hernandez, C., Shapiro, M., Pascotto, A., Annunziato, L. and Taglialatela, M. (2007). Atypical Gating Of M-Type Potassium Channels Conferred by Mutations in Uncharged Residues in the S4 Region of KCNQ2 Causing Benign Familial Neonatal Convulsions. *Journal of Neuroscience*, 27(18), pp.4919-4928.

Soldovieri, M., Miceli, F. and Taglialatela, M. (2011). Driving With No Brakes: Molecular Pathophysiology of K_v7 Potassium Channels. *Physiology*, 26(5), pp.365-376.

Somlyo, A. and Somlyo, A. (1994). Signal transduction and regulation in smooth muscle. *Nature*, 372(6503), pp.231-236.

Somlyo, A. and Somlyo, A. (1998). From pharmacomechanical coupling to G-proteins and myosin phosphatase. *Acta Physiologica Scandinavica*, 164(4), pp.437-448.

Somlyo, A. and Somlyo, A. (2000). Signal transduction by G-proteins, Rho-kinase and protein phosphatase to smooth muscle and non-muscle myosin II. *The Journal of Physiology*, 522(2), pp.177-185.

Somlyo, A., Wu, X., Walker, L. and Somlyo, A. (1999). Pharmacomechanical coupling: the role of calcium, G-proteins, kinases and phosphatases. *Reviews of Physiology Biochemistry and Pharmacology, Volume 134*, pp.201-234.

Splawski, I., Shen, J., Timothy, K., Lehmann, M., Priori, S., Robinson, J., Moss, A., Schwartz, P., Towbin, J., Vincent, G. and Keating, M., 2000. Spectrum of Mutations in Long-QT Syndrome Genes. *Circulation*, 102(10), pp.1178-1185.

Splawski, I., Tristani-Firouzi, M., Lehmann, M., Sanguinetti, M. and Keating, M. (1997). Mutations in the hminK gene cause long QT syndrome and suppress lKs function. *Nature Genetics*, 17(3), pp.338-340.

Stott, J., Jepps, T. and Greenwood, I. (2014). K_v7 potassium channels: a new therapeutic target in smooth muscle disorders. *Drug Discovery Today*, 19(4), pp.413-424.

Strutz-Seebohm, N., Henrion, U., Schmitt, N., Schulze-Bahr, E. and Seebohm, G., 2013. A Common Structural Component for β-Subunit Mediated Modulation of Slow Inactivation in Different K_V Channels. *Cellular Physiology and Biochemistry*, 31(6), pp.968-980.

Strutz-Seebohm, N., Seebohm, G., Fedorenko, O., Baltaev, R., Engel, J., Knirsch, M. and Lang, F. (2006). Functional Coassembly of KCNQ4 with KCNE-ß- Subunits in Xenopus Oocytes. *Cellular Physiology and Biochemistry*, 18(1-3), pp.57-66.

Suh, B. and Hille, B. (2005). Regulation of ion channels by phosphatidylinositol 4,5-bisphosphate. *Current Opinion in Neurobiology*, 15(3), pp.370-378.

Suh, B. and Hille, B. (2008). PIP2Is a Necessary Cofactor for Ion Channel Function:Howand Why?. *Annual Review of Biophysics*, 37(1), pp.175-195.

Sun, J. and MacKinnon, R. (2017). Cryo-EM Structure of a KCNQ1/CaM Complex Reveals Insights into Congenital Long QT Syndrome. *Cell*, 169(6), pp.1042-1050.e9.

Sun, J. and MacKinnon, R., 2020. Structural Basis of Human KCNQ1 Modulation and Gating. *Cell*, 180(2), pp.340-347.e9.

Surti, T.S. and Jan, L.Y. (2005) A potassium channel, the M-channel, as a therapeutic target. *Curr. Opin. Investig. Drugs* 6, pp.704–711

Svalø, J., Hansen, H., Rønn, L., Sheykhzade, M., Munro, G. and Rode, F., 2011. Kv7 Positive Modulators Reduce Detrusor Overactivity and Increase Bladder Capacity in Rats. *Basic & Clinical Pharmacology & Toxicology*, 110(2), pp.145-153.

Takumi, T., Ohkubo, H. and Nakanishi, S. (1988). Cloning of a membrane protein that induces a slow voltage-gated potassium current. *Science*, 242(4881), pp.1042-1045.

Tao, X., Lee, A., Limapichat, W., Dougherty, D. and MacKinnon, R. (2010). A Gating Charge Transfer Center in Voltage Sensors. *Science*, 328(5974), pp.67-73.

Tatulian, L. and Brown, D. (2003). Effect of the KCNQ potassium channel opener retigabine on single KCNQ2/3 channels expressed in CHO cells. *The Journal of Physiology*, 549(1), pp.57-63.

Tatulian, L., Delmas, P., Abogadie, F. and Brown, D. (2001). Activation of Expressed KCNQ Potassium Currents and Native Neuronal M-Type Potassium Currents by the Anti-Convulsant Drug Retigabine. *The Journal of Neuroscience*, 21(15), pp.5535-5545.

Telezhkin, V., Thomas, A., Harmer, S., Tinker, A. and Brown, D. (2013). A basic residue in the proximal C-terminus is necessary for efficient activation of the M-channel subunit $K_v7.2$ by PI(4,5)P2. *Pflügers Archiv - European Journal of Physiology*, 465(7), pp.945-953.

Tester, D., Will, M., Haglund, C. and Ackerman, M., 2005. Compendium of cardiac channel mutations in 541 consecutive unrelated patients referred for long QT syndrome genetic testing. *Heart Rhythm*, 2(5), pp.507-517.

Thomas, P. and Smart, T., 2005. HEK293 cell line: A vehicle for the expression of recombinant proteins. *Journal of Pharmacological and Toxicological Methods*, 51(3), pp.187-200.

Thomas, A., Harmer, S., Khambra, T. and Tinker, A., 2011. Characterization of a Binding Site for Anionic Phospholipids on KCNQ1. *Journal of Biological Chemistry*, 286(3), pp.2088-2100.

Thornbury, K., Sergeant, G., McHale, N., Roy, S., Hollywood, M. Anthraquinone compounds and their uses, US 9877940 B2, *United States Patent and Trademark Office*, 30 January 2018.

Tinel, N., Dichot, S., Borsotto, M., Lazdunski, M. and Barhanin, J. (2000). KCNE2 confers background current characteristics to the cardiac KCNQ1 potassium channel. *The EMBO Journal*, 19(23), pp.6326-6330.

Tiwari-Woodruff, S., Schulteis, C., Mock, A. and Papazian, D. (1997). Electrostatic interactions between transmembrane segments mediate folding of Shaker K+ channel subunits. *Biophysical Journal*, 72(4), pp.1489-1500.

Tobelaim, W., Dvir, M., Lebel, G., Cui, M., Buki, T., Peretz, A., Marom, M., Haitin, Y., Logothetis, D., Hirsch, J. and Attali, B. (2017). Ca2+-Calmodulin and PIP2 interactions at the proximal C-terminus of K_V7 channels. *Channels*, 11(6), pp.686-695.

Towart, R., Linders, J., Hermans, A., Rohrbacher, J., van der Linde, H., Ercken, M., Cik, M., Roevens, P., Teisman, A. and Gallacher, D. (2009). Blockade of the IKs potassium channel: An overlooked cardiovascular liability in drug safety screening?. *Journal of Pharmacological and Toxicological Methods*, 60(1), pp.1-10.

Tran, B., Ji, Z., Xu, M., Tsuchida, T. and Cooper, E., 2020. Two KCNQ2 Encephalopathy Variants in the Calmodulin-Binding Helix A Exhibit Dominant-Negative Effects and Altered PIP2 Interaction. *Frontiers in Physiology*, 11.

Tristani-Firouzi, M. and Sanguinetti, M. (1998). Voltage-dependent inactivation of the human K+channel KvLQT1 is eliminated by association with minimal K+channel (minK) subunits. *The Journal of Physiology*, 510(1), pp.37-45.

Tristani-Firouzi, M., Chen, J. and Sanguinetti, M., 2002. Interactions between S4-S5 Linker and S6 Transmembrane Domain Modulate Gating of HERG K+ Channels. *Journal of Biological Chemistry*, 277(21), pp.18994-19000.

Unoki, H., Takahashi, A., Kawaguchi, T., Hara, K., Horikoshi, M., Andersen, G., Ng, D., Holmkvist, J., Borch-Johnsen, K., Jørgensen, T., Sandbæk, A., Lauritzen, T., Hansen, T., Nurbaya, S., Tsunoda, T., Kubo, M., Babazono, T., Hirose, H., Hayashi, M., Iwamoto, Y., Kashiwagi, A., Kaku, K., Kawamori, R., Tai, E., Pedersen, O., Kamatani, N., Kadowaki, T., Kikkawa, R., Nakamura, Y. and Maeda, S. (2008). SNPs in KCNQ1 are associated with susceptibility to type 2 diabetes in East Asian and European populations. *Nature Genetics*, 40(9), pp.1098-1102.

Vatta, M. and Towbin, J. (2006). Mutations in KCNE1 in long QT syndrome (LQTS): Insights into mechanism of LQTS and drug sensitivity?. *Heart Rhythm*, 3(9), pp.1041-1042.

Wang, C., Lamothe, S., Wang, A., Yang, R. and Kurata, H. (2018). Pore- and voltage sensor–targeted KCNQ openers have distinct state-dependent actions. *The Journal of General Physiology*, 150(12), pp.1722-1734.

Wang, H., Pan, Z., Shi, W., S. Brown, B., S. Wymore, R., S. Cohen, I., E. Dixon, J. and McKinnon, D. (1998). KCNQ2 and KCNQ3 Potassium Channel Subunits: Molecular Correlates of the M-Channel. *Science*, 282(5395), pp.1890-1893.

Wang, HS., Brown, BS., McKinnon, D., Cohen, IS. (2001). Molecular basis for differential sensitivity of KCNQ and I(Ks) channels to the cognitive enhancer XE991. Mol *Pharmacol* 57: pp.1218-1223

Wang, Q., Curran, M., Splawski, I., Burn, T., Millholland, J., VanRaay, T., Shen, J., Timothy, K., Vincent, G., de Jager, T., Schwartz, P., Towbin, J., Moss, A., Atkinson, D., Landes, G., Connors, T. and Keating, M. (1996). Positional cloning of a novel potassium channel gene: KVLQT1 mutations cause cardiac arrhythmias. *Nature Genetics*, 12(1), pp.17-23.

Wang, Z., Tristani-Firouzi, M., Xu, Q., Lin, M., Keating, M. and Sanguinetti, M. (1999). Functional Effects of Mutations in KvLQT1 that Cause Long QT Syndrome. *Journal of Cardiovascular Electrophysiology*, 10(6), pp.817-826.

Webb, T., Kshatri, A., Large, R., Akande, A., Roy, S., Sergeant, G., McHale, N., Thornbury, K. and Hollywood, M., 2015. Molecular mechanisms underlying the effect of the novel BK channel opener GoSlo: Involvement of the S4/S5 linker and the S6 segment. *Proceedings of the National Academy of Sciences*, 112(7), pp.2064-2069.

Webster, S., del Camino, D., Dekker, J. and Yellen, G. (2004). Intracellular gate opening in Shaker K+ channels defined by high-affinity metal bridges. *Nature*, 428(6985), pp.864-868.

Weight, F. and Votava, J. (1970). Slow Synaptic Excitation in Sympathetic Ganglion Cells: Evidence for Synaptic Inactivation of Potassium Conductance. *Science*, 170(3959), pp.755-758.

Wen, H. and Levitan, I. (2002). Calmodulin Is an Auxiliary Subunit of KCNQ2/3 Potassium Channels. *The Journal of Neuroscience*, 22(18), pp.7991-8001.

Wickenden, A., Krajewski, J., London, B., Wagoner, P., Wilson, W., Clark, S., Roeloffs, R., McNaughton-Smith, G. and Rigdon, G. (2008). N-(6-Chloro-pyridin-3-yl)-3,4-difluoro-benzamide (ICA-27243): A Novel, Selective KCNQ2/Q3 Potassium Channel Activator. *Molecular Pharmacology*, 73(3), pp.977-986.

Wickenden, A., Zou, A., Wagoner, P. and Jegla, T. (2001). Characterization of KCNQ5/Q3 potassium channels expressed in mammalian cells. *British Journal of Pharmacology*, 132(2), pp.381-384.

Wladyka, C. and Kunze, D. (2006). KCNQ/M-currents contribute to the resting membrane potential in rat visceral sensory neurons. *The Journal of Physiology*, 575(1), pp.175-189.

Woolcock, A., Anderson, S., Peat, J., Du Toit, J., Zhang, Y., Smith, C. and Salome, C. (1991). Characteristics of Bronchial Hyperresponsiveness in Chronic Obstructive Pulmonary Disease and in Asthma. *American Review of Respiratory Disease*, 143(6), pp.1438-1443.

Wu, D., Delaloye, K., Zaydman, M., Nekouzadeh, A., Rudy, Y. and Cui, J. (2010). State-dependent electrostatic interactions of S4 arginines with E1 in S2 during K_v7.1 activation. *The Journal of General Physiology*, 135(6), pp.595-606.

Wurm, F., 2004. Production of recombinant protein therapeutics in cultivated mammalian cells. *Nature Biotechnology*, 22(11), pp.1393-1398

Wuttke, T., Seebohm, G., Bail, S., Maljevic, S. and Lerche, H. (2005). The New Anticonvulsant Retigabine Favors Voltage-Dependent Opening of the K_v7.2 (KCNQ2) Channel by Binding to Its Activation Gate. *Molecular Pharmacology*, 67(4), pp.1009-1017.

Xia, Y., Chu, W., Qi, Q. and Xun, L. (2015). New insights into the QuikChangeTM process guide the use of Phusion DNA polymerase for site-directed mutagenesis. *Nucleic Acids Research*, 43(2), pp.e12-e12.

Xiong, Q., Gao, Z., Wang, W. and Li, M. (2008). Activation of K_v7 (KCNQ) voltage-gated potassium channels by synthetic compounds. *Trends in Pharmacological Sciences*, 29(2), pp.99-107.

Xiong, Q., Sun, H. and Li, M. (2007). Zinc pyrithione-mediated activation of voltage-gated KCNQ potassium channels rescues epileptogenic mutants. *Nature Chemical Biology*, 3(5), pp.287-296.

Xu, Q., Chang, A., Tolia, A. and Minor, D. (2013). Structure of a Ca2+/CaM:K_v7.4 (KCNQ4) B-Helix Complex Provides Insight into M Current Modulation. *Journal of Molecular Biology*, 425(2), pp.378-394.

Yamakage, M., Chen, X., Tsujiguchi, N., Kamada, Y. and Namiki, A., 2001. Different Inhibitory Effects of Volatile Anesthetics on T- and L-type Voltage-dependent Ca2+Channels in Porcine Tracheal and Bronchial Smooth Muscles. *Anesthesiology*, 94(4), pp.683-693.

Yan, F., Gao, H., Zhao, H., Bhatia, M. and Zeng, Y. (2018). Roles of airway smooth muscle dysfunction in chronic obstructive pulmonary disease. *Journal of Translational Medicine*, 16(1).

Yang, W., Levesque, P., Little, W., Conder, M., Ramakrishnan, P., Neubauer, M. and Blanar, M. (1998). Functional Expression of Two KvLQT1-related Potassium Channels Responsible for an Inherited Idiopathic Epilepsy. *Journal of Biological Chemistry*, 273(31), pp.19419-19423.

Yazdi, S., Nikesjö, J., Miranda, W., Corradi, V., Tieleman, D., Noskov, S., Larsson, H. and Liin, S., 2021. Identification of PUFA interaction sites on the cardiac potassium channel KCNQ1. *Journal of General Physiology*, 153(6).

Yellen, G. (1998). The moving parts of voltage-gated ion channels. *Quarterly Reviews of Biophysics*, 31(3), pp.239-295.

Yeung, S., Lange, W., Schwake, M. and Greenwood, I. (2008). Expression profile and characterisation of a truncated KCNQ5 splice variant. *Biochemical and Biophysical Research Communications*, 371(4), pp.741-746.

Yeung, S., Pucovský, V., Moffatt, J., Saldanha, L., Schwake, M., Ohya, S. and Greenwood, I. (2007). Molecular expression and pharmacological identification of a role for K_v7 channels in murine vascular reactivity. *British Journal of Pharmacology*, 151(6), pp.758-770.

Yu, H.; Wu, M.; Townsend, S. D.; Zou, B.; Long, S.; Daniels, J. S.; McManus, O. B.; Li, M.; Lindsley, C. W.; Hopkins, C. R. (2011) Discovery, synthesis, and structure−activity relationship of a series of N-arylbicyclo[2.2.1]heptane-2-

carboxamides: characterization of ML213 as a novel KCNQ2 and KCNQ4 potassium channel opener. *ACS Chem. Neurosci*, 2, pp.572−577.

Yus-Nájera, E., Santana-Castro, I. and Villarroel, A. (2002). The Identification and Characterization of a Noncontinuous Calmodulin-binding Site in Noninactivating Voltage-dependent KCNQ Potassium Channels. *Journal of Biological Chemistry*, 277(32), pp.28545-28553.

Zaczek, R., Chrovat. R.J., Saye, J.A., Pierdomenico, M.E., Maciag, C.M., Logue, A.R., Fisher, B.B., Rominger, D.H., Earl, R.A. (1998). Two new potent neurotransmitter release enhancers, 10,10-bis(4-pyridinylmethyl)-9(10H)-anthracenone and 10,10-bis(2-fluoro-4-pyridinylmethyl)-9(10H)-anthracenone: comparison to linopirdine. *J Pharmacol Exp Ther,* 285, pp.724-730

Zaika, O., Hernandez, C., Bal, M., Tolstykh, G. and Shapiro, M. (2008). Determinants within the Turret and Pore-Loop Domains of KCNQ3K+ Channels Governing Functional Activity. *Biophysical Journal*, 95(11), pp.5121-5137.

Zavaritskaya, O., Dudem, S., Ma, D., Rabab, K., Albrecht, S., Tsvetkov, D., Kassmann, M., Thornbury, K., Mladenov, M., Kammermeier, C., Sergeant, G., Mullins, N., Wouappi, O., Wurm, H., Kannt, A., Gollasch, M., Hollywood, M. and Schubert, R. (2020). Vasodilation of rat skeletal muscle arteries by the novel BK channel opener GoSlo is mediated by the simultaneous activation of BK and K v 7 channels. *British Journal of Pharmacology*, 177(5), pp.1164-1186.

Zaydman, M., Kasimova, M., McFarland, K., Beller, Z., Hou, P., Kinser, H., Liang, H., Zhang, G., Shi, J., Tarek, M. and Cui, J. (2014). Domain–domain interactions determine the gating, permeation, pharmacology, and subunit modulation of the IKs ion channel. *eLife*, 3.

Zaydman, M., Silva, J., Delaloye, K., Li, Y., Liang, H., Larsson, H., Shi, J. and Cui, J. (2013). K_v7.1 ion channels require a lipid to couple voltage sensing to pore opening. *Proceedings of the National Academy of Sciences*, 110(32), pp.13180-13185.

Zhang, A. and Li, P., 2006. Vascular physiology of a Ca2+mobilizing second messenger - cyclic ADP - ribose. *Journal of Cellular and Molecular Medicine*, 10(2), pp.407-422.

Zhang, H., Craciun, L., Mirshahi, T., Rohács, T., Lopes, C., Jin, T. and Logothetis, D. (2003). PIP2 Activates KCNQ Channels, and Its Hydrolysis Underlies Receptor-Mediated Inhibition of M Currents. *Neuron*, 37(6), pp.963-975.

Zhang, L., Sato, Y., Hessa, T., von Heijne, G., Lee, J., Kodama, I., Sakaguchi, M. and Uozumi, N. (2007). Contribution of hydrophobic and electrostatic interactions to the membrane integration of the Shaker K+ channel voltage sensor domain. *Proceedings of the National Academy of Sciences*, 104(20), pp.8263-8268.

Zhang, X., An, H., Li, J., Zhang, Y., Liu, Y., Jia, Z., Zhang, W., Chu, L. and Zhang, H., 2016. Selective activation of vascular Kv7.4/Kv7.5 K+channels by fasudil contributes to its vasorelaxant effect. *British Journal of Pharmacology*, 173(24), pp.3480-3491.

Zhang, Y., Chu, X., Liu, L., Zhang, N., Guo, H., Yang, F., Liu, Z., Dong, Y., Bao, Y., Zhang, X. and Zhang, J. (2016a). Tannic acid activates the K_v7.4 and K_v7.3/7.5 K+channels expressed in HEK293 cells and reduces tension in the rat mesenteric arteries. *Journal of Pharmacy and Pharmacology*, 68(4), pp.494-502.

Zhong, X., Harhun, M., Olesen, S., Ohya, S., Moffatt, J., Cole, W. and Greenwood, I. (2010). Participation ofKCNQ(K_v7) potassium channels in myogenic control of cerebral arterial diameter. *The Journal of Physiology*, 588(17), pp.3277-3293.